LIÈGE université
Gembloux
Agro-Bio Tech

Improving jujube fruit yield estimation by assimilating a remotely sensed leaf area index into the WOFOST model

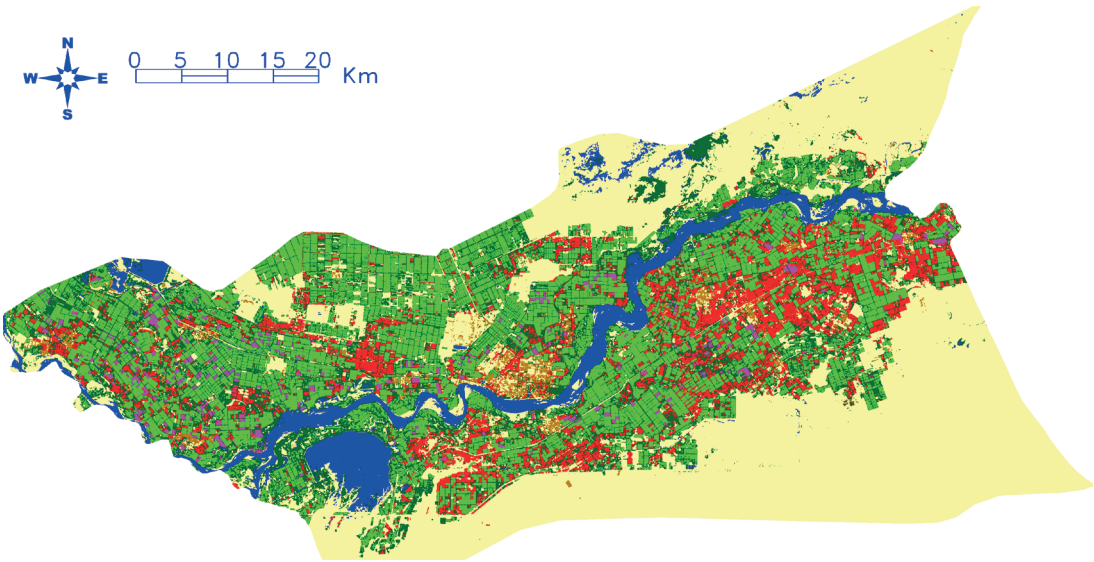

TIECHENG BAI

2020

COMMUNAUTÉ FRANÇAISE DE BELGIQUE

UNIVERSITÉ DE LIÈGE – GEMBLOUX AGRO-BIO TECH

Improving jujube fruit yield estimation by assimilating a remotely sensed leaf area index into the WOFOST model

Tiecheng Bai

Dissertation originale présentée en vue de l'obtention du grade de docteur en sciences agronomiques et ingénierie biologique

Promoteurs : Prof. Benoît Mercatoris & Prof. Youqi Chen

2020

Résumé

Tiecheng Bai (2020). Amélioration de l'estimation du rendement en fruits du jujube en assimilant l'indice de surface foliaire télédétecté dans le modèle WOFOST (thèse de doctorat).

Gembloux Agro-Bio Tech, Liège Université, Gembloux, Belgique.

182 pages, 49 figures, 19 tableaux

Résumé: Jujube a d'importantes valeurs nutritionnelles et médicales et est l'un des fruits séchés les plus précieux de Chine. À mesure que la superficie plantée augmente, la surveillance de la croissance et du rendement du jujube sur le terrain avant la récolte permet aux agriculteurs d'améliorer la prise de décisions en matière de gestion des cultures, telles que l'irrigation, la fertilisation, la taille et la sélection de la densité de plantation. Les méthodes de télédétection et d'assimilation ont été largement utilisées pour le suivi de la croissance et l'évaluation du rendement des cultures annuelles. L'utilisation de méthodes d'assimilation pour estimer le rendement des cultures fruitières, en particulier des jujubes, a suscité jusqu'à présent peu de recherche et de développement. L'objectif principal de la thèse est d'exploiter pleinement les avantages d'un modèle de croissance de culture et de la technologie de télédétection afin d'améliorer la précision de l'estimation du rendement en jujubes. La première innovation consiste à introduire une durée phénologique dans le modèle de régression par télédétection afin d'améliorer la précision de l'estimation du rendement par télédétection. La deuxième innovation consiste à développer et à évaluer des méthodes d'assimilation par télédétection afin de quantifier et de réduire l'incertitude des principaux paramètres d'entrée dans les simulations de croissance de jujubes, en mettant l'accent sur la réduction de l'incertitude liée à l'âge des arbres et à la densité de plantation, améliorant ainsi l'estimation du rendement à l'échelle du verger.

Premièrement, les performances du modèle WOFOST (World Food STudies) dans la simulation de la croissance des arbres fruitiers de jujubes ont été évaluées dans des conditions de production potentielle (en l'absence de stress hydrique ou de nutriment). Le modèle a été établi et validé à l'aide de données recueillies lors d'expériences sur le terrain effectuées au cours de trois saisons de croissance. Pour la simulation en mode potentiel, la dynamique de croissance simulée des feuilles, des tiges, des fruits, de la biomasse totale et de l'indice de surface foliaire (LAI) correspond bien aux valeurs mesurées, montrant des valeurs de RMSE (erreur quadratique moyenne) de 0,14, 0,33, 0,37, 0,62 t ha^{-1} et 0,19 m^2 m^{-2} et R^2 (coefficient de détermination) de 0,95, 0,98, 0,99, 0,99 et 0,95, respectivement. Les erreurs validées de –2, –3 et –3 jours ont été détectées à différents stades de développement phénologique correspondant à l'émergence, à la floraison et à la maturité. Afin d'estimer les rendements de jujubes d'âge différents, le poids des nouveaux organes à chaque saison de croissance (bourgeons et racines initiaux) a été introduit en tant que poids sec total initial (TDWI), calculé en tant que valeurs moyennes des arbres de même âge. Les résultats ont montré que le R^2 et le RMSE de l'estimation du rendement à l'échelle du champ étaient

respectivement de 0,22 et 1,07 (16,3%) t ha^{-1} pour 2016, de 0,04 et 1,33 (17,2%) t ha^{-1} pour 2017. Le modèle proposé peut fournir une stratégie fondamentale pour simuler la croissance d'autres arbres fruitiers. Il convient de noter que la méthode de définition du TDWI pour les jujubes du même âge reste incertaine, ce qui se traduit par une précision du modèle légèrement inférieure.

Deuxièmement, les méthodes de régression par télédétection sont encore largement utilisées pour l'estimation du rendement des cultures. Des recherches antérieures ont confirmé la corrélation entre les rendements des cultures et les informations phénologiques. La période de calcul fiable du rendement en jujubes sur la base de l'indice de végétation par télédétection a été choisie. Une approche utilisant la longueur des périodes phénologiques pour améliorer les estimations par télédétection de la variabilité interannuelle des rendements a été explorée et testée. On a constaté que le meilleur moment pour estimer le rendement des jujubes était pendant la période de remplissage des fruits, montrant un coefficient de corrélation (R^2) plus élevé entre les indices de végétation (VI) et les rendements. Les VIs moyens pour la 14ème quinzaine (du 16 au 31 juillet) et la 15ème quinzaine (du 1er au 15 août) représentent la meilleure performance pour l'estimation du rendement, avec une valeur de R^2 la plus élevée de 0,74 pour le NDVI (indice de végétation par différence normalisée), 0,61 pour le SAVI (indice de végétation ajusté au sol), 0,46 pour le NDWI (indice de différence normalisé de l'eau) et 0,44 pour le EVI (indice de végétation amélioré). Le potentiel d'utilisation de Landsat-NDVI pour l'estimation du rendement en jujubes, combiné à la longueur phénologique, a été prouvé sur la base de 181 observations de vergers de jujubes individuels, montrant un R^2 validé de 0,64 et une RMSE de 0,73 (11,1%) t ha^{-1} pour 2016, 0,71 et 0,73 (9,5%) t ha^{-1} pour 2017, respectivement.

Troisièmement, cette étude présente l'assimilation d'une seule valeur de LAI, dérivée des observations satellitaires Landsat à un stade proche du développement végétatif maximum, dans un modèle WOFOST calibré afin d'améliorer l'estimation du rendement des arbres fruitiers à jujubes à l'échelle du verger. L'assimilation après forçage a amélioré la précision de l'estimation du rendement par rapport à la simulation sans assimilation, affichant un R^2 de 0,62 et un RMSE de 0,74 (11,3%) t ha^{-1} pour 2016, et un R^2 de 0,59 et un RMSE de 0,87 (11,3%) t ha^{-1} pour 2017.

Finalement, la principale contribution de cette étude consista au développement d'un algorithme SUBPLEX permettant d'assimiler, dans un modèle WOFOST calibré, une série temporelle de valeurs de LAI détectées à distance pour quatre stades de croissance clés. La précision de l'estimation de cet algorithme a été comparée à celle d'une assimilation basée sur un filtre de Kalman (EnKF) largement utilisé en assimilation de données. Les résultats ont montré que les assimilations SUBPLEX et EnKF amélioraient considérablement les performances d'estimation du rendement par rapport à une simulation sans assimilation. Le SUBPLEX (R^2 = 0,78, RMSE = 0,64 (8,3%) t ha^{-1} et RPD = 2,13) a également montré une précision d'estimation du rendement légèrement supérieure à celle de l'assimilation EnKF (R^2 = 0,66, RMSE = 0,79 (10,2%) t ha^{-1} et RPD = 1,73). L'étude a fourni un nouveau schéma d'assimilation basé sur l'algorithme SUBPLEX pour utiliser des données de télédétection et un modèle de croissance des cultures pour améliorer les estimations de rendement des cultures fruitières à l'échelle du champ.

En résumé, les méthodes de régression par télédétection et de simulation de la croissance des cultures peuvent être améliorées et plusieurs méthodes d'estimation du rendement proposées dans la thèse ont donné de bons résultats. Les méthodes de forçage sont un choix approprié lorsque seules les images de télédétection du plus grand stade de développement sont disponibles. Les méthodes de régression par télédétection peuvent être recommandées lorsque deux images satellites des principaux stades de développement sont disponibles et appliquées uniquement à des zones spécifiques. Les méthodes EnKF et SUBPLEX sont fortement recommandées lorsque plusieurs images de télédétection, de l'émergence à la maturité, sont disponibles. La méthode SUBPLEX présente généralement de meilleures performances et une meilleure stabilité, car la précision de la méthode EnKF dépend de la précision du temps phénologique. On pense que la méthode d'assimilation sera également la méthode d'estimation du rendement des cultures la plus prometteuse à l'avenir en raison d'un bon mécanisme.

Mots-clés: Télédétection, Modèle de croissance des cultures, Assimilation, Longueur phénologique, Estimation du rendement

Abstract

Tiecheng Bai (2020). Improving jujube fruit yield estimation by assimilating a remotely sensed leaf area index into the WOFOST model (PhD thesis).

Gembloux Agro-Bio Tech, Liège University, Gembloux, Belgium.

182 pages, 49 figures, 19 tables

Abstract: Jujube fruit has important nutritional and medicinal qualities and is one of the most economically valuable fruits in China. Field-scale jujube fruit yield estimation using site-specific techniques can provide indicators of the reasons for yield gaps, which could be promising to better understand spatial yield variation in jujube orchards, thereby analysing the possible causes to improve fruit orchard management decision-making. Both remote sensing and assimilation methods have been widely used for yield assessments of annual crops. There are few reports focusing on the use of assimilation methods to estimate yields for fruit crops, especially jujube trees. The main goal of this thesis is to make full use of the advantages of crop growth models and remote sensing technology to improve the accuracy of jujube fruit yield estimation. The first aim is to introduce phenological length into the yield regression model, based on a remotely sensed vegetation index, to enhance the accuracy of yield estimation. The second aim is to develop and evaluate remote sensing assimilation methods to reduce the uncertainty of key input parameters or state variables in the jujube growth simulation process, thereby improving yield estimation at the field scale for local jujube orchards.

Firstly, the performance of the calibrated WOFOST (World Food Studies) model was evaluated by simulating jujube fruit tree growth in potential mode. The model was calibrated and validated using data collected in field experiments performed in three growth seasons. The validated errors of –2, –3, and –3 days were detected in different phenological development stages corresponding to emergence, flowering, and maturity. Simulated growth dynamics of leaves, stems, fruits, total biomass, and leaf area index (LAI) agreed well with measured values, showing R^2 (coefficient of determination) values of 0.95, 0.98, 0.99, 0.99, and 0.95, and RMSE (root mean square error) values of 0.14, 0.33, 0.37, 0.62 t ha^{-1} and 0.19 m^2 m^{-2}, respectively. In order to estimate the yields of jujube orchards of different ages, the weight of initial new organs in each growing season (new buds and roots) was introduced as the initial total crop dry weight (TDWI), which was set as an average value for orchards of the same age. The R^2 and RMSE of the field-scale yield estimation for 181 orchards were 0.22 and 1.07 t ha^{-1} (16.3%) for 2016, 0.04 and 1.33 t ha^{-1} (17.2%) for 2017, respectively. Although the calibrated WOFOST model can provide a fundamental strategy for simulating the growth of jujube fruit trees, there may still be some uncertainty in the method of setting the fixed TDWI for the same aged jujube orchards, resulting in a slightly low estimation accuracy.

Secondly, this thesis evaluated the yield estimation performance of regression methods based on remotely sensed vegetation indices that are widely used for crop

yield estimation. An approach that used the phenological length to improve remotely sensed estimates of inter-annual variability for yields was explored and tested. The optimal time for determining jujube yield estimation was during the fruit filling period, which showed higher R^2 between vegetation indices (VIs) and fruit yields. The average VIs from 16 July to 15 August represented the best performance for yield estimation, with an average R^2 value of 0.75 for NDVI (Normalized Difference Vegetation Index), 0.61 for SAVI (Soil-adjusted Vegetation Index), 0.47 for NDWI (Normalized Difference Water Index), and 0.44 for EVI (Enhanced Vegetation Index), respectively. The potential of using Landsat-NDVI for jujube yield estimation, combined with the phenological length, was proved based on observed fruit yields of 181 jujube orchards, showing a validated R^2 of 0.64 and RMSE of 0.73 t ha^{-1} (11.1%) for 2016, 0.71 and 0.73 t ha^{-1} (9.5%) for 2017, respectively.

Thirdly, this study presented an attempt to assimilate a single LAI at near to maximum vegetative development stage, derived from Landsat satellite data, into a calibrated WOFOST model to improve fruit yield estimation at the field scale. The assimilation after forcing LAI improved the yield estimation performance compared with the unassimilated simulation, showing a R^2 of 0.62 and RMSE of 0.74 t ha^{-1} (11.3%) for 2016, and R^2 of 0.59 and RMSE of 0.87 t ha^{-1} (11.3%) for 2017, respectively.

Finally, the main contribution of this study was to develop a SUBPLEX algorithm to assimilate a time series of remotely sensed LAI during the main growth stages into the calibrated WOFOST model, and compared the yield estimation accuracy of the SUBPLEX algorithm with a widely used Ensemble Kalman Filter (EnKF) assimilation. The results showed that both SUBPLEX and EnKF assimilations significantly improved yield estimation performance compared with the un-assimilated simulation. The SUBPLEX (R^2 = 0.78, RMSE = 0.64 t ha^{-1} (8.3%) and RPD (Standard Deviation (SD)/RMSE) = 2.13) also showed slightly better yield estimation accuracy compared with EnKF assimilation (R^2 = 0.66, RMSE = 0.79 t ha^{-1} (10.2%) and RPD = 1.73). The study provides a new assimilation scheme based on a SUBPLEX algorithm to employ remotely sensed data and a crop growth model to improve field-scale jujube fruit yield estimates.

In summary, this thesis highlighted that the proposed forcing method is a suitable choice when only one remote sensing image is available at near to the maximum vegetative developmental stage. Remote sensing regression methods can be recommended when two satellite images of the fruit filling stage are available and applied only to specific areas. The EnKF and SUBPLEX methods are highly recommended when multiple remote sensing images from emergence to maturity are available. The SUBPLEX method usually exhibited better performance and stability because the accuracy of the EnKF method depended on whether the phenological time was clear. The assimilation methods may be the most promising fruit crop yield estimation methods to use in the future due to their good mechanism.

Keywords: Jujube, remote sensing, crop growth model, assimilation, phenology length, yield estimation

Acknowledgments

Four years of doctoral life is fleeting. I am grateful to Liège University and the Chinese Academy of Agricultural Sciences for giving me four years of study and research experience, which is the most valuable asset in my life.

First of all, I sincerely thank my supervisors, Professors Benoit Mercatoris and Youqi Chen. They not only provided valuable advice for my PhD project research, but also helped me to explore and live in Belgium. Because of their help and understanding, have I gained more opportunities to learn and communicate with excellent scientists. I would also like to thank you for your efforts and contributions in reviewing and revising the articles.

I would like to express my sincere gratitude to my PhD committee members, Professors Hélène Soyeurt and Vincent Leemans. They provided a lot of wonderful comments for my doctoral training, experimental design, data analysis calculations, and doctoral thesis. Thank you also for your thoughtful attention to my life in Belgium.

Thirdly, many thanks to my team's core members Nannan Zhang, Chaoyang Li, Hongbin Meng, and Tao Wang, and my master students Shanggui Wang and Wenbo Meng. They helped me complete the field experiment design, project execution, regional data surveys, parameter measurements, and data processing and analysis.

Thanks to Professor de Wit of Wageningen University. Although we have not met, many thanks for your careful answers to my questions through exchanges during the jujube growth simulation and data assimilation research.

I would like to thank the National Natural Science Foundation of China for funding two research projects for my doctoral research. In addition, I am very grateful to the China Scholarship Council for providing me with a year of funding to study and live in Belgium.

Finally, I would like to thank my parents and wife. They take care of my dear daughter and run the family attentively. Because of your considerate care, I have more time to study and work. Thanks to my lovely daughter, your smile is the power and hope of my advancement.

Table of content

List of Figures

List of Tables

Abbreviations

AMAXTB	Maximum Leaf CO_2 Assimilation Rate as a Function of Development Stage of the Crop (kg ha^{-1} hr^{-1}; −).
CVL	Conversion Efficiency of Assimilates into Leaf (kg kg^{-1}).
CVO	Conversion Efficiency of Assimilates into Storage Organ (kg kg^{-1}).
CVR	Conversion Efficiency of Assimilates into Root (kg kg^{-1}).
CVS	Conversion Efficiency of Assimilates into Stem (kg kg^{-1}).
DTSMTB	Daily Increase in Thermal Time as Function of Average Temperature (°C d^{-1}).
DVS	Development Stage of Crop
EFFTB	Initial Light-Use Efficiency of CO_2 Assimilation of Single Leaves as Function of Daily Temperature ((kg ha^{-1} hr^{-1})/(J M^{-2} S^{-1}); °C)
EVI	Enhanced Vegetation Index.
FLTB	Fraction of Above Ground Dry Matter Increase Partitioned to Leaves as a Function of Development Stage (kg kg^{-1}; −).
FOTB	Fraction of Above Ground Dry Matter Increase Partitioned to Storage Organs as a Function of Development Stage (kg kg^{-1}; −).
FRTB	Fraction of Total Dry Matter Increase Partitioned to Roots as a Function of Development Stage (kg kg^{-1}; −).
FSTB	Fraction of Above Ground Dry Matter Increase Partitioned to Stems as a Function of Development Stage (kg kg^{-1}; −).
KDIFTB	Extinction Coefficient for Diffuse Visible Light as Function of Development Stage (−).
LAI	Leaf Area Index (ha ha^{-1}).
LAIEM	Leaf Area Index at Emergence (ha ha^{-1}).
MAE	Mean Absolute Error.
MBE	Mean Bias Error.
NDWI	Normalized Difference Water Index
NDVI	Normalized Difference Vegetation Index
NRMSE	Normalized RMSE
Q10	Relative Change in Respiration Rate Per 10 °C Temperature Change.
R^2	Coefficient of Determination.
RBE	Relative Bias Error.
RDRSTB	Relative Death Rate of Stems as a Function of Development Stage (kg kg^{-1} d^{-1}; −)
RGRLAI	Maximum Relative Increase in LAI (ha ha^{-1} d^{-1}).
RMSE	Root Mean Square Error.
RPD	Standard Deviation (SD)/RMSE
SAVI	Soil-Adjusted Vegetation Index.
SLATB	Specific Leaf Area as a Function of Development Stage (ha kg^{-1}; −)
SM	Soil Moisture Content
SPAN	Life Span of Leaves Growing at 35 °C (Days)
TAGP	Dry Weight of Total Aboveground Production (kg ha^{-1})

TABSE	Lower Threshold Temperature for Ageing Of Leaves (°C)
TBASEM	Lower Threshold Temperature for Emergence (°C)
TEFFMX	Maximum Effective Temperature for Emergence (°C)
TDWI	Initial Total Crop Dry Weight (kg ha^{-1})
TSUM1	Thermal Time from Emergence to Anthesis (°C d^{-1})
TSUM2	Thermal Time from Anthesis to Maturity (°C d^{-1})
TSUMEM	Thermal Time from Sowing to Emergence (°C d^{-1})
TM	(Landsat) Thematic Mapper
TMPFTB	Reduction Factor of AMAX as Function of Average Temperature (°C)
VI	Vegetation Index
WLV	Dry Weight of Living Leaves (kg ha^{-1})
WOFOST	World FOod STudies.
WSO	Dry Weight of Living Storage Organs (kg ha^{-1})
WST	Dry Weight of Living Stems (kg ha^{-1})

Chapter 1

Introduction

1. Context and motivation

Jujube, *Zizyphus jujuba* Miller, is a small deciduous tree of the Rhamnaceae family from China. The jujube tree is mainly planted in orchards in the subtropical and tropical regions of Asia, with a history of more than 4000 years. Its fruit, commonly called jujube, red date, or Chinese date, is popular in China due to its high nutritional value. The jujube fruit is rich in components such as carbohydrates, reducing sugars, vitamin C, soluble and insoluble fibre, protein, mineral and phenolic compounds, which can be used as food, food additives, and flavourings. Jujube fruit is also well known in China for its significant medicinal value. It has been used in traditional medicines as an analeptic, palliative, and antibechic compound for thousands of years (Li et al., 2007). In addition, it is considered as a medical supplement that is used in tonic medicine and health supplements for blood nourishment and sedation (Gao et al., 2013). In 2017, the global amount of jujube fruit produced in the world was about 8.52 million tons, representing a market of 9.68 billion U.S. dollars (Zhiyan Consulting Group., 2018). China is the main country producing jujube fruit, accounting for 97% of the world's production (Zhiyan Consulting Group, 2018). In China, jujube trees are mainly cultivated and produced in Shandong, Hebei, Shanxi, Shaanxi, Henan provinces and Xinjiang Uygur Autonomous Region (Figure 1–1). Xinjiang accounted for almost 49% of the Chinese jujube production in 2018 (Figure 1–2), and significantly contributes to jujube fruit supply in terms of quantity and quality. Xinjiang has become the largest jujube planting base in China because of its abundant light and thermal resources, such as long periods of sunshine, strong radiation, high accumulated temperatures, and large temperature difference (Li., 2016).

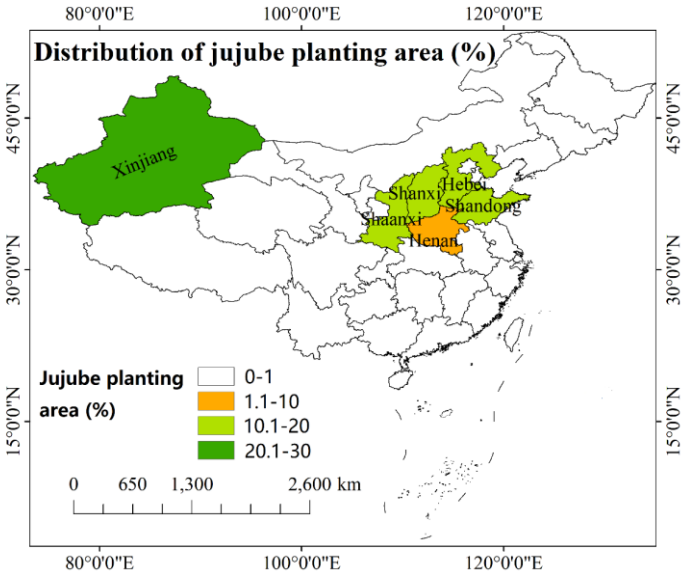

Figure 1–1: Major jujube planting regions in China.

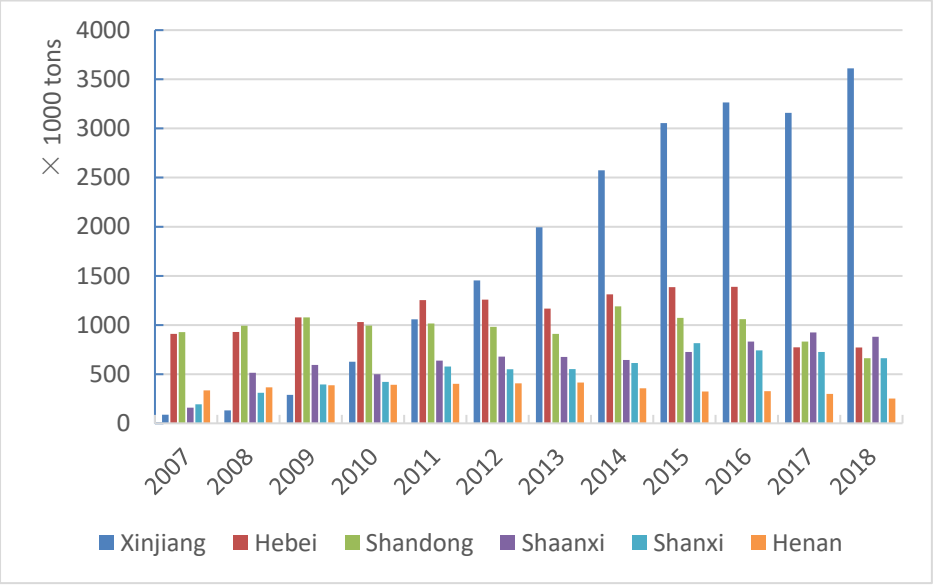

Figure 1–2: Statistics of jujube production in China's major provinces from 2007 to 2018 (data from National Bureau of Statistics of China).

The price of jujube has fluctuated significantly in recent years. From 2000 to 2018, the purchase price of Chinese jujube showed first a rising trend and then fell (Figure 1−3). From 2000 to 2005, the purchase price of jujube was relatively stable. From 2006 to 2011, the purchase price showed rapid growth, from 6,448 CNY ton^{-1} in 2006 to 35,251 CNY ton^{-1} in 2011. The main reason for the increase in the jujube fruit price is that production could not meet the demand, which was driven by the government's encouragement and support (Li, 2016). From 2011 to 2018, the price showed a large downward trend. The main reason for the sharp fall after 2011 is that the production was much greater than the demand. Due to the skyrocketing price of jujube in the early period, farmers planted more jujube trees to increase the planting area. At the same time, the jujube trees planted in Xinjiang in the early stage of 2011 gradually entered the fruiting period, so the production of jujube increased rapidly; the state of oversupply became more and more intense, resulting in the decline in jujube prices. The rapid decline in the purchase price will inevitably affect the income of fruit farmers, and even the sustainable development of the jujube industry. The contribution of jujube production amounts to the calculated market price is large, reaching almost 20% (Li, 2016). Therefore, assessing jujube yield before harvest could also benefit government agencies who formulate strategies to regulate the price of jujube fruit and promote the stable development of the jujube industry.

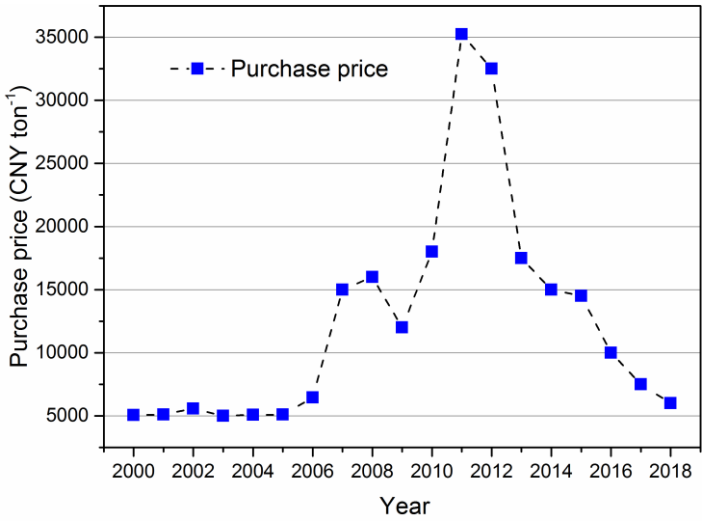

Figure 1−3: Purchase price of jujube fruit from 2000 to 2018. (Zhiyan Consulting Group, 2018)

In addition, the variability of planting area and yield distribution in different areas is large in Xinjiang. This is particularly the case in Xinjiang Region which showed a large spatial variability of yield across its agro-ecological zones from 2015 to 2017, as depicted in Figure 1–4, ranging from 1.06 to 6.76 t ha^{-1} (Data from Xinjiang Statistical Yearbook). This is due to several factors such as soil properties, climate, pruning, irrigation, and fertilization management.

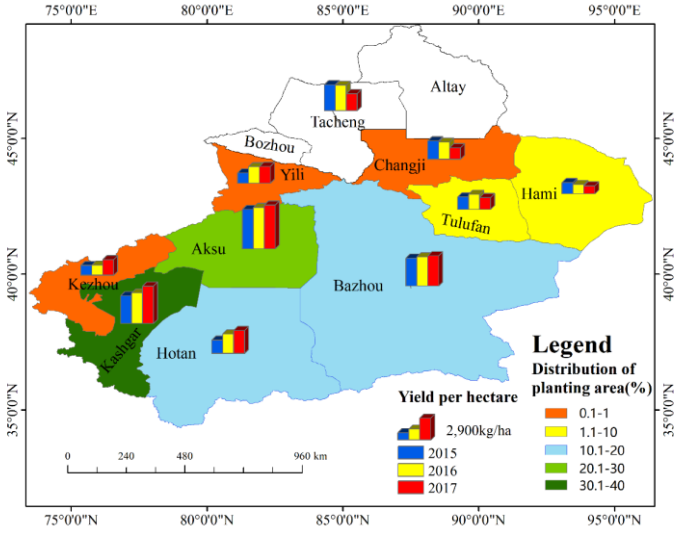

Figure 1−4: Average jujube yield of the main agro-ecological zones in Xinjiang.

The spatial distribution of yield is beneficial for exploring the reasons of yield gaps (Oliver, 2010). Crop yield estimation at the field scale could be promising to better understand spatial yield variation at a local (country) scale, thereby analysing the possible causes, such as climatic conditions, soil properties, irrigation, and fertilization management, to improve yield management decision-making (Schulthess et al., 2013). Therefore, field-scale jujube fruit yield estimation could help managers to make orchard management decisions and policies. Field or local-scale yield estimations are also the basis of regional-scale assessments, which could contribute to the analysis and forecast of jujube prices and policy decisions, to some extent.

Very few reports exist on the estimation of jujube fruit yield at field, local (country), regional, or national scales. Most research efforts on jujube orchards have been performed on the effects of irrigation, fertilization, pruning, and photosynthesis on the growth process and the annual yield based on field experiments. Existing research confirms that Regulated Deficit Irrigation (RDI) technique promotes the growth of jujube trees and improves fruit quality and water use efficiency (Cui et al., 2008; Cui et al., 2009b; Qiang et al., 2015). The maturity period is considered to be the best phenological period to achieve water deficit irrigation of jujube trees (Galindo et al., 2016). Pruning affects transpiration (Wei et al., 2014), water consumption (Zhang et al., 2013), water use efficiency (Chen et al., 2016a), and yield of jujube trees (Jin et al., 2018a). In addition, some studies have also reported the effects of soil management on soil water content and available nutrients (Wang et al., 2015, 2016), coupling effects of water and fertilizer management on yield, water, and nitrogen use efficiency (Dai et al., 2019; Wang et al., 2018), spatial variability of soil chemical properties (Bai and Wang, 2011), the relationship between stable carbon isotope discrimination and water use efficiency (Cui et al., 2009a), influences of environmental factors on leaf morphology (Li et al., 2015), and the effect of root pruning on competitive ability. It is worth noting that there is a high correlation between leaf area index (LAI) and yield. Yield first increases with the increase of LAI, but when it exceeds a certain critical value, the yield shows a downward trend (Yang et al., 2012). Because a higher leaf area index can intercept and utilize more light energy, the photosynthetic products and yield are usually higher. However, an excessively high leaf area index will reduce the light energy entering the canopy. The leaves in the canopy cannot photosynthesize to produce organic matter, but consume nutrients, resulting in a decrease in yield.

For yield estimation of other fruit tree crops, most research has focused on field and sub-field scales. The data used includes visible light cameras, ground spectrometers, drone and Landsat satellite images. However, most methods still depend on conventional techniques based, for instance, on agro-meteorological models and empirical statistical regressions between spectral vegetation indices and in-field measured yields (Anastasiou et al., 2018; Bonilla et al., 2015; Sepulcre-Cantó et al., 2007; Sun et al., 2017; Ye et al., 2008a, 2008b). Some studies have also used image processing (Aggelopoulou et al., 2011; Zhou et al., 2012b), and machine learning algorithms (Rahman et al., 2018; Ye et al., 2006). One of the main drawbacks of such empirical approaches is that they are validated for specific cultivars, growth stages, or certain geographical regions. Such an approach suffers from a lack of mechanistic

descriptions (Huang et al., 2015a). In contrast, cropping system modelling based on mathematical descriptions of key physical and physiological processes is considered to be a mature technology (Holzworth et al., 2014) which is widely applied in yield estimation, precision farming, and improves understanding of crop responses in field trials (Asseng et al., 2013; de Wit et al., 2019a; Ewert et al., 2015). Such modelling better considers the complex interactions between plant, weather, soil, and agricultural practices (de Wit et al., 2019a). However, factors affecting yield, such as soil characteristics, canopy state variables, and the spatial distribution of meteorological data, often lead to uncertainty in key input parameters or simulation process, which can lead to large errors in crop yield estimation when using crop models (Jin et al., 2018b). There are obvious advantages and disadvantages to remote sensing-based and crop modelling methods. Data assimilation (DA) technology provides a formal and easy-to-understand method that combines crop model simulation with remote sensing observations in order to reduce the uncertainty of model input parameters and simulation processes, thereby improving yield estimation accuracy (Huang et al., 2015b; Huang et al., 2019).

Assimilation methods have, however, been developed mostly for annual crops such as winter wheat, rice, and maize. Few studies have focused on perennial fruit trees, and in particular on jujube fruit crops. The yield of perennial jujube crops sharply varies with tree age and planting densities because of the evolution of branches, canopy width, tree height, and leaf area index (He et al., 2010). These factors may cause uncertainties of input parameters when a crop model is employed to estimate jujube fruit yield. Figure 1–5 shows an increase in the rate of total production that was significantly higher than that of the planting area until 2017, which may be because tree age plays a decisive role in the yield of jujube trees (Xinjiang Statistical Yearbook). Therefore, when implementing the assimilation method to evaluate the yield of jujube fruits, the uncertainty of the initial input parameters caused by the tree age may need to be considered.

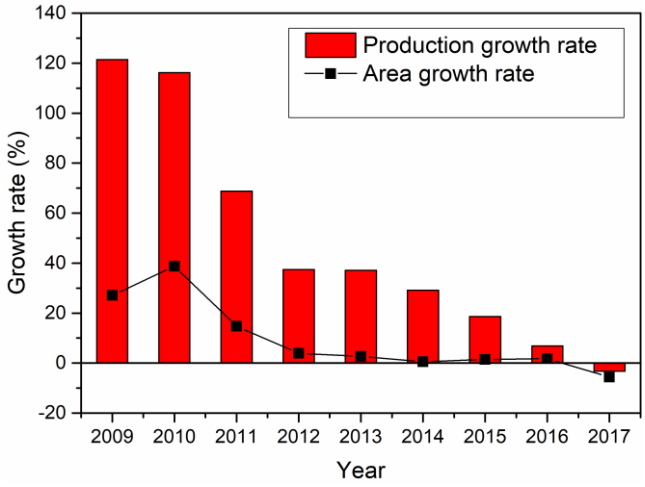

Figure 1–5: Growth rates of jujube planting area and production amounts in Xinjiang

In summary, the three methods for evaluating yield, including crop growth models, remote sensing, and assimilation-based methods, all have some application limitations. This thesis aims to develop methods combining crop growth modelling and remotely sensed observations to accurately estimate the field-scale jujube fruit yield. For this purpose, a crop growth model is first calibrated for perennial crop systems taking into account the tree age and the planting density. Two approaches are then considered. One approach is based on the integration of simulated phenological data within a remote sensing-based yield regression. Another approach, known to be more promising, consists in assimilating remotely sensed data within the calibrated crop growth model. These proposed methods have been calibrated and validated over the sub-region (181 orchards) of Alaer City in China.

2. Review of crop yield estimation methods

2.1. Crop growth modelling methods

2.1.1. Yield estimation based on crop models

Most crop models are based on physiological and ecological principles using mathematical representation of processes such as crop phenology development, photosynthetic production, organ establishment, and yield formation (van Diepen et al., 1989). The mathematical descriptions of crop modelling systems quantify crop development processes influenced by climate, soil, and management conditions (de Wit et al., 2019a). Such models have been considered as mature for yield estimation (Holzworth et al., 2014). Over the past decades, several crop models have been developed such as WOFOST (World Food Studies) (van Diepen et al., 1989), DSSAT (Decision Support System for Agrotechnology Transfer) (Jones et al., 2003), EPIC (Environmental Policy Integrated Climate) (Wang et al., 2013), STICS (*Simulateur Multidisciplinaire pour les Cultures Standard*) (Brisson et al., 2003), APSIM (Agricultural Production Systems Simulator) (Holzworth et al., 2014), SWAP (Soil, Water, Atmosphere, and Plant) (Kroes et al., 2017), AquaCrop (a crop-water productivity model) (Hsiao et al., 2009; Raes et al., 2009; Steduto et al., 2009), and CropSyst (Cropping Systems Simulation Model) (Stöckle et al., 2003). These models have been specially developed for different crops and purposes, with their own characteristics. They have been widely applied for assessments of regional crop yield and climate change impacts on yield (Tebaldi and Knutti, 2007; Reidsma et al., 2009; van Bussel et al., 2011; Supit et al., 2012; Van Walsum and Supit, 2012), crop growth monitoring (Ma et al., 2008), production potential assessment (Chauhan, 2010), crop ecosystem process research (Jongschaap, 2007; Mollier et al., 2008; Ceglar et al., 2011), production management (Guerra et al., 2007; Saseendran et al., 2007; García-Vila and Fereres, 2012; McNider et al., 2015; Zhou et al., 2012a), and a crop model-centred decision-making support system (Tittonell et al., 2010).

Crop growth models are based on equations to estimate the rate of biomass production as a function of resources such as carbon dioxide, solar radiation, and water. The methods driving crop models mainly include carbon-driven (WOFOST), radiation-driven (EPIC and STICS), and water-driven (CropSyst and AquaCrop)

modules (Todorovic et al., 2009a). Among them, WOFOST is a mechanistic model that explains crop growth on the basis of phenological development, CO_2-assimilation, transpiration, respiration, and how these processes are influenced by environmental conditions (de Wit et al., 2019a). It has been developed for the quantitative analysis of growth and the production of annual field crops, and has been thoroughly tested for 25 years in several studies on the effect of climate change on yields (Alexandrov and Eitzinger, 2005; Kroes and Supit, 2011; Reidsma et al., 2009; Supit et al., 2010; Van Walsum and Supit, 2012; Kassie et al., 2015; Blanco et al., 2017; Gilardelli et al., 2018; Pirttioja et al., 2019), regional yield forecasting (de Wit et al., 2010; Jones et al., 2003; Supit, 1997; de Wit et al., 2008; Bussay et al., 2015; Ogutu et al., 2018; Ceglar et al., 2019), crop yield analysis (Dobermann et al., 2000; Rötter and Van Keulen, 1997), and the inter-comparison of different irrigation and soil conditions (Confalonieri et al., 2009; Eitzinger et al., 2004; Rötter and Van Keulen, 1997; Todorovic et al., 2009b). It has also been optimized and validated by countless researchers all over the world and used for many new crops over a large range of climatic and management conditions (de Wit et al., 2019a). WOFOST can be applied using either potential production where crop growth is determined by irradiation, temperature, and plant characteristics only, or using a water-limited production where crop growth is limited by water use (van Diepen et al., 1989). The potential production represents the upper limit of absolute yield for a particular crop under specific weather conditions, which depends on the response of the crop to temperature and solar radiation during the growing season. In practice, this upper limit can only be achieved by high-input fertilizers, irrigation, and thorough pest and weed control (de Wit et al., 2019b). In addition, crops should not be damaged by wind, hail, and frost. Therefore, potential yields depend only on crop variety, date of seeding, and weather data. The water-limited production considers the effect of soil moisture deficits on crop growth, and the corresponding yield represents the maximum yield that can be obtained under rain-fed conditions (de Wit et al., 2019b). Crop modelling is mainly developed in the literature for annual crops including spring barley, cotton, maize, millet, potato, rice, sorghum, soybean, sugar beet, sweet potato, and winter wheat. Few studies have focused on perennial fruit trees. Regarding fruit tree crop simulations, studies have presented a biophysical simulation of fruit growth based on a biophysical representation of water and dry material transport (Fishman and Génard, 1998), a computer-based model simulating peach growth (L-PEACH) (Lopez et al., 2010), simulating the effect of orchard management on fruit number and size (Lescourret et al., 1999), transpiration and light interception (Green et al., 2003), and simulation of tree development using mixed stochastic and biomechanical models (Costes et al., 2008). However, the above fruit tree growth models are missing some mechanisms for fruit crop growth and development. Whether the WOFOST model has the potential to simulate the growth of perennial jujube tree crops is an interesting research subject to explore. There are some differences in physiological characteristics between perennial jujube trees and annual crops, such as tree age, tree shape, and planting density, which need to be properly considered during the simulation process.

2.1.2. Description of WOFOST model

In order to better understand the framework and the main processes considered in

such a crop growth model, WOFOST is briefly described in this section. This model is the main pillar of the proposed research work. As aforementioned, WOFOST is a mechanistic model that explains crop growth on the basis of underlying processes, such as phenological development, leaf development, light interception, CO_2-assimilation, transpiration, respiration, partitioning of assimilates into different organs, and dry matter formation. It also explains how these processes are influenced by environmental conditions. The soil module is not strictly included within the WOFOST model, except for root growth by considering different water balance approaches (de Wit et al., 2019a). A schematic diagram of the links between model components in WOFOST is shown in Figure 1–6.

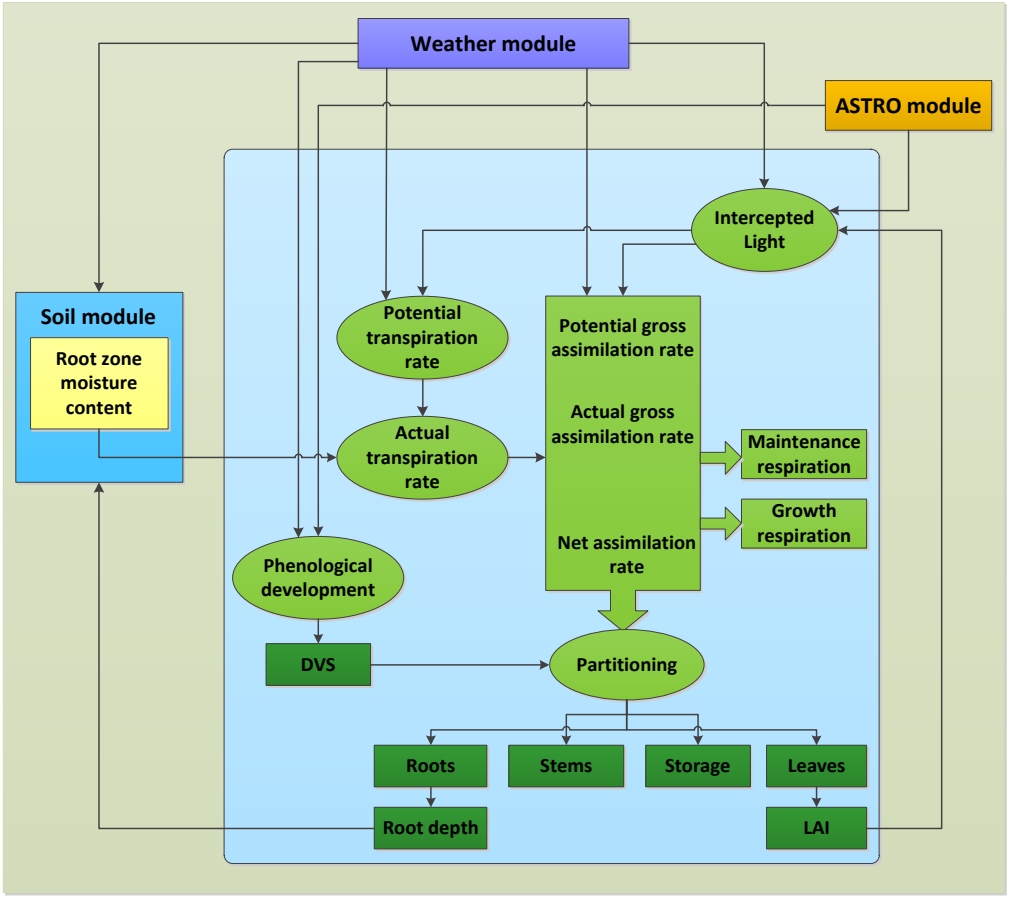

Figure 1–6: Schematic overview of the major processes implemented in WOFOST and their linkages (de Wit et al., 2019a). DVS: Development stages. LAI: Leaf Area Index.

WOFOST describes the basic physiological processes of crops from emergence to flowering according to crop characteristics and environmental conditions. Weather and ASTRO modules determine the intercepted light and phenological development

stages. The model simulates the dry matter accumulation of the plants under the influence of solar radiation, temperature, precipitation, and crop characteristics in a day's step. The basis of dry matter production is the total assimilation rate of the canopy, which is calculated from the absorbed solar radiant energy and the leaf area of the crop canopy. A part of the assimilation product (carbohydrates) is consumed to maintain respiration, the rest is converted to structural dry matter, and some dry matter is consumed by growth respiration during the conversion process. The dry matter produced is distributed in roots, stems, leaves, and storage organs. The partition coefficient varies with developmental stage. A brief overview of the important processes is expressed below, and specific mathematical descriptions and details can be referenced to existing studies (such as Supit et al., 1994; de Wit et al., 2019a, b).

a) Phenological development

WOFOST uses a development stage variable (DVS) to express the physiological age of the crop, with DVS = 0 at emergence, DVS = 1 at flowering, and DVS = 2 at physiological maturity for most annual crops. The model relies on an accumulation method to simulate the developmental period. Hence, crop growth and development stages can be regarded as a function of effective accumulated temperature. The daily effective accumulated temperature depends on the lower limit and the upper limit of temperature. The crop development stops when the daily average temperature is lower than the lower limit. When the average temperature is higher than the upper limit temperature, the crop development rate is no longer accelerated. These temperature limits depend on the crop characteristics.

b) CO_2 assimilation

The production and distribution of daily assimilates is the most detailed part of the model, obtained by integrating the instantaneous assimilation rate of the canopy in one day, which is calculated from the absorbed radiation and photosynthesis response. The WOFOST model distinguishes the following steps for daily dry matter production, including the total instantaneous gross CO_2 assimilation, the total daily gross CO_2 assimilation rate, and the actual daily gross photosynthesis rate. The total instantaneous gross canopy CO_2 assimilation rate is calculated by integrating across the canopy depth (3-point Gaussian integration method). Then, the total daily gross CO_2 assimilation rate of the whole canopy can be obtained by integration over time. In addition, suboptimum temperatures, leaf stomata closure, and nutrient deficiencies can also cause a decrease in assimilation rates (de Wit et al., 2019b).

c) Respiration

Crop respiration processes can be divided into maintenance respiration that is used to maintain vital functions, and growth respiration when assimilates are converted into plant structural material. Maintenance respiration provides living organisms with the energy to maintain their biochemical and physiological status. The amount of protein, and minerals present in biomass as well as the metabolic activity of the crop can be used to estimate the maintenance respiration costs, depending on the ambient temperature. For growth respiration, WOFOST uses conversion efficiency factors instead of calculations.

d) Transpiration and evaporation

The Penman approach is used to calculate the potential evapotranspiration from bare soil, water, and crop surfaces (de Wit and Wolf, 2010). The potential transpiration is the loss of water from a field crop that completely covers the soil and obtains the best water supply from the soil (de Wit et al., 2019b). For most crops, the actual transpiration of the crop is equal to the potential evapotranspiration multiplied by the correction factor for light interception and the degree of water stress.

e) Crop growth

The crop growth mainly includes dry matter partitioning between leaves, stems, roots, and storage organs. The senescence of leaves is also taken into account. The remaining photosynthetic products after respiration consumption are distributed to leaves, stems, roots, and storage organs in a certain proportion that is calculated by field measured data. Dry matter distribution is related to the phenological development stage.

Green leaf area is a decisive factor in light absorption and canopy photosynthesis. Under ideal conditions, light intensity and temperature are the main environmental factors that affect leaf unfolding. The leaf area growth in the model is described in two stages. In the early stages, the leaf area increases exponentially with the temperature. When leaf area is extended to be affected by assimilated supply, leaf area growth is mainly related to leaf weight growth and leaf area under different development stages. The model also considers the effect of leaf physiological ageing on death rate.

The calculation process of leaf ageing is more complicated. Ageing refers to the process by which a leaf loses its ability to complete a basic physiological and ecological process and loses its biomass. The calculation of leaf ageing is set after the leaf has completed its life process. Water stress and mutual shading may accelerate the rate of leaf ageing death. The model distinguishes the ageing of leaves into physiological ageing, ageing caused by water stress, and ageing caused by mutual shading. The weight of the dead leaves is subtracted from the oldest leaves set.

The WOFOST model assumes that the death rate of the stored organ is equal to zero. The death rates of stems and roots are considered as a function of the development stage variable.

f) Soil moisture balance

Water shortage is very common during the actual growth of crops. When the soil moisture supply is insufficient, the stomatal resistance of the leaves increases, causing the actual transpiration rate and the photosynthesis rate to decrease, thereby affecting crop growth and final yield. To determine the time and intensity of water stress, the crop model simulates the daily soil moisture content through the soil water balance equation to estimate the crop water stress coefficient.

The WOFOST model is mainly run in two modes: potential and water-limited production. We calibrated the WOFOST model for potential mode, considering two reasons. The first reason is that the water-limited production of the WOFOST model

expresses the maximum yield under rain-fed conditions, with no yield losses caused by other factors (de Wit et al., 2019b).

2.2. Remote sensing-based methods

Yield estimation is one of the earliest directions for agricultural remote sensing technology applications. Remote sensing has been used for crop yield assessment and mapping for over three decades (Bolton and Friedl, 2013). For this purpose, different programmes have been developed at regional, national and international levels, such as GIEWS (Global Information and Early Warning System) from the FAO (Food and Agriculture Organization) of the United Nations, FEWS NET (the Famine Early Warning Systems Network) from USAID (the United States Agency for International Development), MARS (Monitoring Agriculture with Remote Sensing) from the European Commission (EC), CropWatch from China, and USDA-FAS (United States Department of Agriculture-Foreign Agricultural Service) (Fritz et al., 2019). In addition, a Group on Earth Observations (GEO) initiative launched the GEOGLAM (GEO Global Agricultural Monitoring) project, which hopes that the global agricultural monitoring community will share information internationally for Agricultural Market Information System (AMIS) and Early Warning, covering approximately 95% of the world's croplands. In addition, the World Food Programme Seasonal Monitor has been in operation since 2014 (Fritz et al., 2019). The Joint Research Centre (JRC) of the European Commission (EC) announced the Anomaly Hot Spots of Agricultural Production (ASAP) system in June 2017 (Rembold et al., 2019). Among them, the MCYFS (MARS Crop Yield Forecasting System) project focuses on providing early yield forecasting for key European crops. This project combines remote sensing, agro-meteorological data, and biophysical models (Baruth et al., 2004). The University of Maryland has established a global crop growth monitoring operational system as part of a decision support system of the US Foreign Agricultural Service (Becker-Reshef et al., 2010). The US Space Agency, the Pakistan Space and Upper Atmosphere Research Commission (SUPARCO), and the Food and Agriculture Organization (FAO) have jointly developed a regional framework system that uses satellite data to obtain crop yields and agricultural statistics for wheat and other crop production with a monthly bulletins (SUPARCO Crop Situation and Forecast). In China, the Ministry of Agriculture have implemented a national project which established remote sensing crop monitoring business operation systems suitable for the national conditions in order to estimate production (Chen et al., 2016b). The first monitoring targets included wheat, corn, and cotton, and this was gradually expanded to rice, soybean, and other crops. Recently, Beijing Normal University and the National Bureau of Statistics have proposed a system for estimating the area and yields of food crops in the main grain-producing areas of the country (Chen et al., 2016b).

Remote sensing-based yield estimation relies on reflectance and SAR information to express the factors influencing the process of crop growth. In the last 10–15 years, new satellite data have become available, such as optical remote sensing data with medium and high spatial and temporal resolution (Sentinel-2, Landsat 8, RapidEye, WorldView-2, SPOT-6, GeoEye-1, Huanjing-1, Gaofen-1, etc.) and radar satellite

data (ENVISAT, Sentinel-1, ALOS, ALOS-2, RADARSAT-2, TERRASAR-X, COSMO, etc.). They provide more timely and reliable data for crop growth monitoring and yield estimation (Jin et al., 2018b).

For larger scales, such as regional, crop yield is estimated by means of satellite imaging systems with rather low and medium spatial resolution. Recently, an increasing number of remote sensing-based studies have been performed for yield forecasting on annual crop systems, using satellite data from the Moderate Resolution Imaging Spectroradiometer (MODIS) (Bolton and Friedl, 2013; Dempewolf et al., 2014; Kouadio et al., 2014; Becker-Reshef et al., 2010; Ren et al., 2008; Victoria et al., 2012). The advantages of this Earth-observing system are its high-frequency acquisitions (daily) and its superior spectral resolution (36 bands). However, the available spatial resolutions, namely 250 m, 500 m, or 1000 m depending on the spectral band, are relatively low for field-scale or local yield monitoring (Bolton and Friedl, 2013). At the field scale, satellite data with high and medium-high spatial resolution, such as Sentinel-2, Landsat 8, and WorldView-2, and aircraft or unmanned aerial vehicles (UAV) are more suitable for crop yield assessment (Chen et al., 2016b).

Fruit tree crops differ from annual crops and usually grow in specific areas, which usually requires remote sensing data with medium or high spatial resolution for fruit crop yield estimation. Vegetation indices obtained from Landsat Thematic Mapper (TM), WorldView-3, and ASTER satellite data have shown promising yield predictors for grapes (Anastasiou et al., 2018; Sun et al., 2017), mangoes (Rahman et al., 2018), and olives (Sepulcre-Cantó et al., 2007). Airborne and UAV remote sensing monitoring systems have also demonstrated appreciable performance for grapes and citrus (Bonilla et al., 2015; Ye et al., 2006, 2008a, b).

The empirical methods based on VIs are still widely used for crop yield estimation due to their operability and simplicity of use (Piekarczyk, 2015). The main vegetation indices used for yield assessment are the Normalized Difference Vegetation Index (NDVI) (Asseng et al., 2013; de la Casa et al., 2018; Dempewolf et al., 2014; Funk and Budde, 2009; Mkhabela et al., 2005; Panda et al., 2010; Yu and Shang, 2018), Enhanced Vegetation Index (EVI) (Kouadio et al., 2014; Son et al., 2014), Normalized Difference Water Index (NDWI) (Bolton and Friedl, 2013), Soil-adjusted Vegetation Index (SAVI) (Panda et al., 2010), and Green NDVI (GNDVI) (Jurečka et al., 2018). Among these indices, NDVI remains the most widely used index for yield estimation for fruit tree crops, such as table grapes (Anastasiou et al., 2018; Sun et al., 2017), mangoes (Rahman et al., 2018), grapes (Bonilla et al., 2015), and citrus (Ye et al., 2008a). In addition, biophysical variables, such as LAI derived from the inversion of a radiative transfer model or an empirical relationship can be also related to yields. Note that both empirical statistical models and radiative transfer models such as PROSAIL (PROSPECT and SAIL radiative transfer models) can be used to obtain these biophysical variables.

To enhance empirical methods, some studies have also shown that correlations between VIs and yields could strongly vary during a growing season (Bognár et al., 2017; Brian et al., 2011; Dempewolf et al., 2014; Rojas, 2007; Salazar et al., 2007; Wall et al., 2008). The crop phenology can obviously also change from one year to

another. As a consequence, a fixed calendar for VI acquisition may not be optimal for accurate crop yield estimation (Bolton and Friedl, 2013; Dempewolf et al., 2014, Brian et al., 2011). To overcome this issue, several studies have taken into consideration phenological information, a time series of VIs, ground-based ancillary data, or surface parameters to adjust VIs to optimize the empirical estimation models (Bolton and Friedl, 2013; Funk and Budde, 2009; Holzman et al., 2014, Prasad et al., 2006; Reynolds et al., 2000; Rojas, 2007; Sakamoto et al., 2013; Wang et al., 2014).

However, even if they are improved by integrating phenological information, empirical methods based on VIs often lack the in-depth understanding of crop yield mechanisms, and the space and time scalability for various applications is not robust (Chen et al., 2016b). In order to account for the photosynthetic process, semi-empirical methods have been developed using light use efficiency models to estimate the above-ground dry matter weight (DM) of crops. For yield estimation at the regional level, remote sensing information can be used for parameter inversion (Bastiaanssen and Ali, 2003; Moriondo et al., 2007). The net primary productivity of vegetation is then expressed by the product of the absorbed photosynthetically active radiation and the light energy use. This physical approach has the advantage of involving a limited number of input variables to achieve good estimation accuracy (Bastiaanssen and Ali, 2003).

In summary, for fruit tree crops, the use of medium or high spatial resolution satellite data for yield estimation is a suitable choice. However, it is challenging to generate a time series of vegetation indices because satellites usually have a long revisit period and images are susceptible to meteorological factors such as clouds and rain (Huang et al. 2015b), such as Landsat 8 with its 30 m resolution. Of course, Sentinel-2 has a shorter revisit cycle with 5 days. Under the condition that the remote sensing observation data is limited, integrating some auxiliary information will be beneficial to the accuracy of the yield estimation. Usually, higher average temperature results in a shorter growth period and lower yield (de Wit and Wolf, 2010). The longer growth duration, especially the long fruit filling period (from flowering to maturity), usually results in higher yields in the case of good water and fertilizer management and no pests and diseases. Hochheim et al. (1998) also found that inter-annual differences in crop phenology across Census Agricultural Regions (CARs) normally varied by 2–3 weeks and therefore required consideration when integrating data over time. Bolton and Friedl (2013) confirmed that integrating information related to crop phenology derived from MODIS could significantly improve modelling performance within and across years. Therefore, remote sensing-based crop yield estimation models might considerably benefit from combining the length of crop phenology growth periods, which presents a valuable research avenue for limited Landsat 8 data or other moderate and high spatial resolution remote sensing data.

2.3. Assimilation methods

The use of crop growth models at large scales usually suffers from the spatial heterogeneities of input parameters such as soil properties (soil moisture, field capacity, etc.), canopy state variables (LAI, biomass, etc.), thereby leading to large errors in yield estimation (Jin et al., 2018b). In addition, empirical methods based on

remote sensing data for yield assessment lack some consideration of crop growth mechanisms. It is difficult to explain the factors affecting yield formation, and these methods rely on a large amount of ground observation data. In order to improve the accuracy of yield estimation, methods combining remote sensing data and crop growth models have recently emerged, taking advantage of spatially continuous remotely sensed information and physiological mechanisms of crop growth models (de Wit et al., 2012; Jin et al., 2018b).

In recent years, crop growth models have been combined with expert systems, decision support systems, and 3S technologies (Remote Sensing, Geographical Information System, and Global Positioning System) to achieve advanced crop simulation and yield estimation. It is an important development direction to try to solve the problems of regional applicability and versatility of crop modelling, scale problems, application fields, and mechanism and application improvements (de Wit et al., 2019a).

Remote sensing can provide key information about meteorology, vegetation, and soil conditions for crop growth simulation in large areas. Initial input parameters, state variables, and soil properties can be observed over large areas, such as phenology information (Zhou et al., 2019), LAI (Fang et al., 2008; Jiang et al., 2014; Nearing et al., 2012; Yao et al., 2015), biomass (Jin et al., 2015), leaf nitrogen accumulation (Huang et al., 2013), evapotranspiration (Bastiaanssen and Ali, 2003; Huang et al., 2015a), and soil moisture (Chakrabarti et al., 2014; Ines et al., 2013). These canopy and soil state variables can be integrated into crop growth modelling to improve the simulation results. In the last 15 years, in addition to the frequently used MODIS satellite data, more new satellite data have become available, such as optical remote sensing data with medium and high spatial resolution (Sentinel-2, Landsat 8, RapidEye, WorldView-2, SPOT-6, GeoEye-1, Huanjing-1, Gaofen-1, etc.) and radar satellite data (ENVISAT, Sentinel-1, ALOS, ALOS-2, RADARSAT-2, TERRASAR-X, COSMO, etc.).

The method of combining remote sensing information within crop growth models is called data assimilation. In general, the purpose of assimilation methods is to integrate spatial and temporal state variables obtained from remote sensing methods to optimize input parameters or state variables of crop models (Jin et al., 2018b). The assimilation methods that have been extensively studied and used include forcing methods, updating (sequential), and calibration (variational) methods. A brief description of these data assimilation methods is shown in Figure 1–7.

Forcing methods (Figure 1–7a) use the remotely sensed data to directly replace state variables into the models. Several studies have suggested forcing the LAI variable at specific periods in order to improve simulated LAI, above-ground biomass (AGB), yield, and transpiration accuracy (Hadria et al., 2006; Thorp et al., 2010; Schneider, 2003; Yao et al., 2015; Tripathy et al., 2013). Flowering dates deduced from remote sensing data have been used to improve the simulated wheat yield of the ROTASK model (Jongschaap and Schouten, 2005). Remotely sensed interception efficiency index and FAPAR (Fraction of Absorbed Photosynthetically Active Radiation) have

been forced into the MOSICAS model to estimate yields of sugar beet and sugarcane, respectively (Morel et al., 2012, 2014).

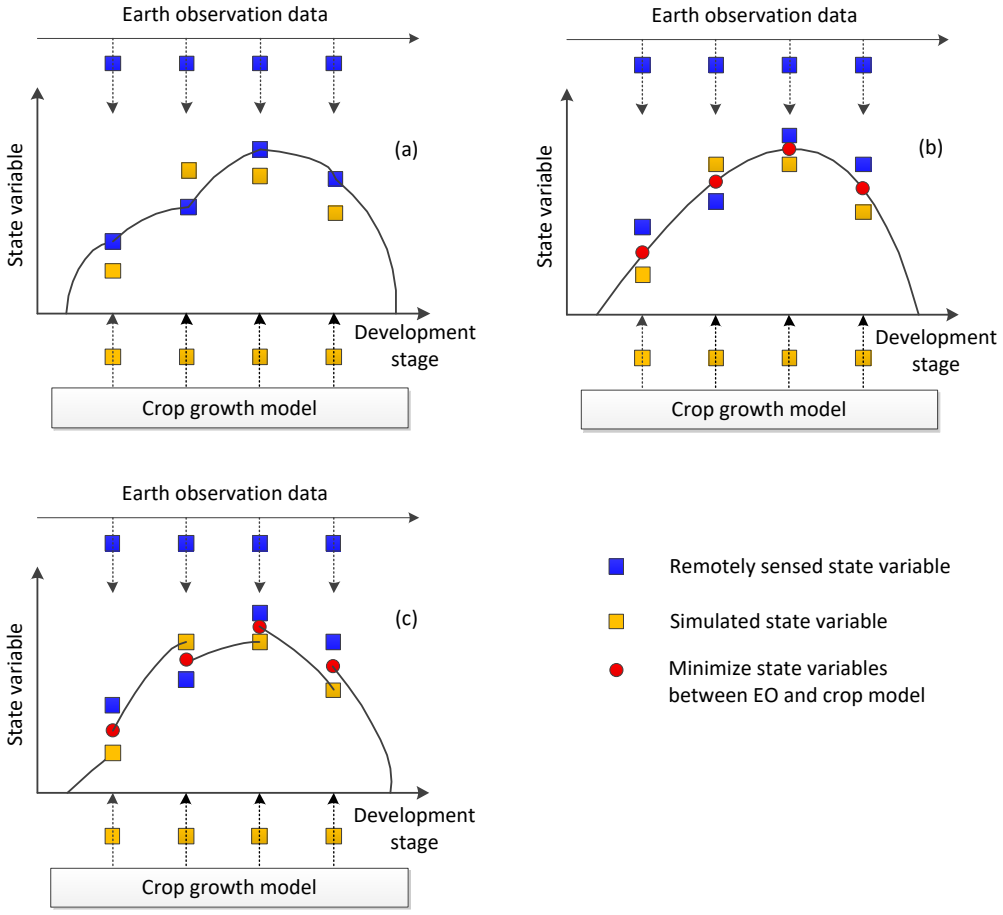

Figure 1–7: Schematic representation of three assimilation methods: (a) Forcing method, (b) calibration method, (c) updating method (Jin et al., 2018b).

Calibration methods (Figure 1–7b) usually employ specific algorithms to adjust initial input parameters for optimal agreement between the remotely sensed state variables and simulated values from the crop model. They take all the available observations during the main growth season and attempt to fit the model to the observations by minimizing a cost function, thereby optimizing the initial parameters of crop models. Maximum Likelihood Solution (MLS) (Dente et al., 2008), Simplex Search Algorithm (SSA) (Ma et al., 2013), Least Squares Method (LSM) (Zhao et al., 2013), Powell's Conjugate Direction Method (PCDM) (Fang et al., 2011), Shuffled Complex Evolution (SCE-UA) (Huang et al., 2015a), Three-Dimensional Variational Data Assimilation (3DVAR) (Lorenc et al., 2000), Four-Dimensional Variational

Data Assimilation (4DVAR) (Rawlins et al., 2007), Very Fast Annealing Algorithm (VFSA) (Dong et al., 2013), and Particle Swarm Optimization Algorithm (PSO) (Wang et al., 2014; Liu et al., 2015) are the main calibration methods described in the literature. These methods consider only the spatial heterogeneities of the initial conditions of the model parameters without taking into account their time evolution. Therefore, for practical applications, the assimilation accuracy of such methods often depends on the quality of the remote observations.

Updating methods (Figure 1–7c) directly correct the state variables of a modelling system when an observation becomes available. The magnitude of the state update then depends on the uncertainty in both the modelling and observed state variables (Huang et al., 2019). Examples of updating (sequential) approaches are the Ensemble Kalman Filter (EnKF) (Bolten et al., 2010; Chakrabarti et al., 2014; Cheng et al., 2018; Curnel et al., 2011; de Wit and van Diepen, 2007; Huang et al., 2016; Ines et al., 2013; Li et al., 2014; Ma et al., 2013; Nearing et al., 2012; Pauwels et al., 2007; Wang et al., 2013; Wu et al., 2012; Xie et al., 2017; Zhao et al., 2013; Zhu et al., 2013), Particle Filter (PF) (Jiang et al., 2014), Constant Gain Kalman Filter (CGKF) (Chen et al., 2018; Vazifedoust et al., 2009), and Ensemble Square Root Filter (EnSRF) (Huang et al., 2013; Mishra et al., 2015). For the state variables of sequential methods, LAI is also a widely used state variable, followed by soil moisture content (SM). The reported studies also show that the EnKF algorithm has been adopted by more researchers to improve assimilation accuracy.

These assimilation methods have their own advantages and disadvantages. The forcing method is relatively easy to implement, but the method is highly dependent on the accuracy of remotely sensed state variables and whether the state variables of the simulation and observation are consistent in phenological time. If there is a large error between the simulated and remote sensing observed phenology time, the forcing method may make the simulation results of the model worse (Jin et al. 2018b). The calibration and update methods have greater flexibility; however, minimization errors from remotely sensed data are brought into the crop model when the assimilation process is carried out. Phenology information has an important impact on the assimilation accuracy of the update method. Assimilation of erroneous phenological information not only decreases accuracy, but can also lead to worse simulation results (Curnel et al., 2011). In theory, the calibration method is superior to the forcing and update methods, because the calibration method can reduce the accumulation and diffusion of remote sensing data errors during the assimilation process (Jin et al., 2018b). However, this method usually requires a large number of optimization iterations and more computation time, especially for remote sensing data with a high spatial resolution (Jin et al., 2018b).

The widely used 4DVAR and EnKF methods are typical representations of variational and sequential assimilation methods, respectively. EnKF continuously updates a new set of input parameters at each observation point. If the state variable error statistic of remote sensing is a Gaussian distribution, the EnKF method can be considered as the preferred assimilation method because most crop growth models are nonlinear (Huang et al., 2019). EnKF requires the most expensive calculation and measurement uncertainty (Jin et al., 2018b). In addition, the assimilation accuracy and

efficiency of this method are susceptible to phenological shifts (Curnel et al. 2011). If the phenology information is uncertain, the variational method is usually superior to the sequential method (Jin et al., 2018b). The small disadvantage of the variational method is that it requires a large number of optimization iterations. The SUBPLEX method is based on the Nelder–Mead simplex algorithm (NMS), which determines an improved set of subspaces and then uses NMS to search each subspace (Rowan, 1990). For most applications, SUBPLEX shows higher computational efficiency for the unconstrained optimization of general multivariate functions than the simplex searching or forcing method (Jonsén, 2009). In principle, SUBPLEX is one of the calibration methods, and calculates a set of optimal input parameters based on the error of observed (satellite) and simulated state variables. In addition, the SUBPLEX method can divide the observation points into several lower-dimensional vectors, thereby improving computational efficiency. More importantly, for objective functions affected by remote sensing observed error, the measurement replication option of SUBPLEX can be used to avoid convergence to a false minimum (Rowan, 1990). Therefore, we can suppose that the SUBPLEX algorithm has the potential to be applied to the assimilation of remote sensing and crop growth models. The potential of the EnKF and SUBPLEX assimilation methods for jujube fruit yield estimation is worthy of further study and exploration.

3. Objectives and outline of this research

The main purpose of this thesis is to improve the accuracy of field-scale fruit yield estimation based on the WOFOST model and remote sensing assimilation method, which in turn helps managers to better analyse variation in yield and its possible causes to improve orchard management and agriculture decision-making for small agro-ecological areas or large farms. To accomplish this goal, the following specific objectives are addressed:

i. To calibrate input parameters of the WOFOST model for jujube tree growth simulation and assess its performance.
ii. To integrate the jujube phenology derived from the WOFOST model into a remote sensing-based yield estimation method.
iii. To force remotely sensed LAI into the calibrated WOFOST model to improve the field-scale jujube fruit yield estimation.
iv. To develop a new assimilation strategy based on a SUBPLEX algorithm to assimilate a time series of remotely sensed LAI into the calibrated WOFOST model to improve the fruit yield estimates of jujube trees, and compare the accuracy of assimilation with the widely used EnKF method.

This thesis compiles a series of four scientific articles published in international peer-reviewed journals. The outline of this thesis is as follows:

Chapter 1 introduces the research context, its motivations, and the specific objectives of the thesis. The framework of the manuscript is briefly described. This chapter reviews the current methods for final crop yield estimation, including crop growth models, remote sensing-based regressions, and assimilation methods. This chapter also compares the advantages and disadvantages of these methods to support

the aims of the proposed methods.

Chapter 2 describes the research material and strategy. The research experiments at the field scale and the yield data collected at the regional scale are detailed. This two-scale data set will be common for each method proposed in the core chapters of the manuscript, namely Chapters 3 to 6. For the sake of completeness, the jujube tree phenology and the conventional management of jujube orchards are summarized. Finally, the global research methodology is presented.

Chapter 3 expresses the WOFOST model calibration and validation on the field experiments for jujube tree and fruit growth simulation. The performance of the WOFOST model in estimating the final jujube fruit yield at the orchard scale is evaluated for different planting densities and ages.

Chapter 4 discusses the integration of a phenological time into a regression based on a remotely sensed vegetation index to estimate the final fruit yield of the jujube crop. An approach using a model-based phenological length is explored to improve the remotely sensed estimate of jujube fruit yield. The proposed approach is compared with a conventional cross-validation method to confirm the importance of phenological considerations for yield estimation.

Chapter 5 presents an improvement of the final fruit yield estimation of jujube crops by assimilating a single LAI measurement from Landsat satellite data into the calibrated WOFOST model by means of a forcing approach. The performances of the model with different remotely sensed LAI forcing times are compared.

Chapter 6 establishes a new assimilation strategy based on the SUBPLEX algorithm to improve the field-scale jujube fruit yield estimates. The developments rely on the integration of remotely sensed LAI at key growth stages into the calibrated WOFOST model, and this original approach is compared with the conventional EnKF assimilation method.

Chapter 7 concludes the research work, and compares and discusses the advantages and limitations of the proposed methods. Finally, the main findings and the perspectives for further work are highlighted.

4. Reference

Alexandrov, V.A., Eitzinger, J., 2005. The Potential Effect of Climate Change and Elevated Air Carbon Dioxide on Agricultural Crop Production in Central and Southeastern Europe. J. Crop Improv. 13, 291–331. https://doi.org/10.1300/j411v13n01_14

Aggelopoulou, A.D., Bochtis, D., Fountas, S., Swain, K.C., Gemtos, T.A., Nanos, G.D., 2011. Yield prediction in apple orchards based on image processing. Precis. Agric. 12, 448–456. https://doi.org/10.1007/s11119-010-9187-0

Anastasiou, E., Balafoutis, A., Darra, N., Psiroukis, V., Biniari, A., Xanthopoulos, G., Fountas, S., 2018. Satellite and Proximal Sensing to Estimate the Yield and Quality of Table Grapes. Agriculture 8, 94. https://doi.org/10.3390/agriculture8070094

Asseng, S., Ewert, F., Rosenzweig, C., Jones, J.W., Hatfield, J.L., Ruane, A.C., Boote, K.J., Thorburn, P.J., Rötter, R.P., Cammarano, D., Brisson, N., Basso, B., Martre, P., Aggarwal, P.K., Angulo, C., Bertuzzi, P., Biernath, C., Challinor, A.J., Doltra, J., Gayler,

S., Goldberg, R., Grant, R., Heng, L., Hooker, J., Hunt, L.A., Ingwersen, J., Izaurralde, R.C., Kersebaum, K.C., Müller, C., Naresh Kumar, S., Nendel, C., O'Leary, G., Olesen, J.E., Osborne, T.M., Palosuo, T., Priesack, E., Ripoche, D., Semenov, M.A., Shcherbak, I., Steduto, P., Stöckle, C., Stratonovitch, P., Streck, T., Supit, I., Tao, F., Travasso, M., Waha, K., Wallach, D., White, J.W., Williams, J.R., Wolf, J., 2013. Uncertainty in simulating wheat yields under climate change. Nat. Clim. Chang. 3, 827–832. https://doi.org/10.1038/nclimate1916

Bai, Y., Wang, Y., 2011. Spatial variability of soil chemical properties in a jujube slope on the loess plateau of China. Soil Sci. 176, 550–558. https://doi.org/10.1097/SS.0b013e3182285cfd

Baruth, B., Royer, A., Klisch, A., Genovese, G., Development, R., 2004. the Use of Remote Sensing Within the Mars Crop Yield Monitoring System of the European Commission. Int. Arch. Photogramm. Remote Sens. Spat. Inf. Sci. 37, 935–940.

Bastiaanssen, W.G.M., Ali, S., 2003. A new crop yield forecasting model based on satellite measurements applied across the Indus Basin, Pakistan. Agric. Ecosyst. Environ. 94, 321–340. https://doi.org/10.1016/S0167-8809(02)00034-8

Becker-Reshef, I., Justice, C., Sullivan, M., Vermote, E., Tucker, C., Anyamba, A., Small, J., Pak, E., Masuoka, E., Schmaltz, J., Hansen, M., Pittman, K., Birkett, C., Williams, D., Reynolds, C., Doorn, B., 2010. Monitoring Global Croplands with Coarse Resolution Earth Observations: The Global Agriculture Monitoring (GLAM) Project. Remote Sens. 2, 1589–1609. https://doi.org/10.3390/rs2061589

Blanco, M., Ramos, F., Van Doorslaer, B., Martínez, P., Fumagalli, D., Ceglar, A., Fernández, F.J., 2017. Climate change impacts on EU agriculture: A regionalized perspective taking into account market-driven adjustments. Agric. Syst. 156, 52–66. https://doi.org/10.1016/ j.agsy.2017.05.013

Bognár, P., Kern, A., Pásztor, S., Lichtenberger, J., Koronczay, D., Ferencz, C., 2017. Yield estimation and forecasting for winter wheat in Hungary using time series of modis data. Int. J. Remote Sens. 38, 3394–3414. https://doi.org/10.1080/01431161.2017.1295482

Bolten, J.D., Crow, W.T., Jackson, T.J., Zhan, X., Reynolds, C.A., 2010. Evaluating the Utility of Remotely Sensed Soil Moisture Retrievals for Operational Agricultural Drought Monitoring. IEEE J. Sel. Top. Appl. Earth Obs. Remote Sens. 3, 57–66. https://doi.org/10.1109/JSTARS.2009.2037163

Bolton, D.K., Friedl, M.A., 2013. Forecasting crop yield using remotely sensed vegetation indices and crop phenology metrics. Agric. For. Meteorol. 173, 74–84. https://doi.org/10.1016/j.agrformet.2013.01.007

Bonilla, I., De Toda, F.M., Martínez-Casasnovas, J.A., 2015. Vine vigor, yield and grape quality assessment by airborne remote sensing over three years: Analysis of unexpected relationships in cv. Tempranillo. Spanish J. Agric. Res. 13, 1–8. https://doi.org/10.5424/sjar/2015132-7809

Brian McConkey, P.B., Lafond, G.P., Moulin, A., Pelcat, Y., 2011. Optimal time for remote sensing to relate to crop grain yield on the Canadian prairies. Can. J. Plant Sci. 84, 97–103. https://doi.org/10.4141/p03-070

Brisson, N., Gary, C., Justes, E., Roche, R., Mary, B., Ripoche, D., Zimmer, D., Sierra, J., Bertuzzi, P., Burger, P., Bussière, F., Cabidoche, Y.M., Cellier, P., Debaeke, P., Gaudillère, J.P., Hénault, C., Maraux, F., Seguin, B., Sinoquet, H., 2003. An overview

of the crop model STICS, in: European Journal of Agronomy. pp. 309–332. https://doi.org/10.1016/S1161-0301(02)00110-7

Bussay, A., van der Velde, M., Fumagalli, D., Seguini, L., 2015. Improving operational maize yield forecasting in Hungary. Agric. Syst. 141, 94–106. https://doi.org/10.1016/j.agsy.2015.10.001

Ceglar, A., Črepinšek, Z., Kajfež-Bogataj, L., Pogačar, T., 2011. The simulation of phenological development in dynamic crop model: The Bayesian comparison of different methods. Agric. For. Meteorol. 151, 101–115. https://doi.org/10.1016/j.agrformet.2010.09.007

Ceglar, A., van der Wijngaart, R., de Wit, A., Lecerf, R., Boogaard, H., Seguini, L., van den Berg, M., Toreti, A., Zampieri, M., Fumagalli, D., Baruth, B., 2019. Improving WOFOST model to simulate winter wheat phenology in Europe: Evaluation and effects on yield. Agric. Syst. 168, 168–180. https://doi.org/10.1016/j.agsy.2018.05.002

Costes, E., Smith, C., Renton, M., Guédon, Y., Prusinkiewicz, P., Godin, C., 2008. MAppleT: Simulation of apple tree development using mixed stochastic and biomechanical models. Funct. Plant Biol. 35, 936–950. https://doi.org/10.1071/FP08081

Chakrabarti, S., Bongiovanni, T., Judge, J., Zotarelli, L., Bayer, C., 2014. Assimilation of SMOS soil moisture for quantifying drought impacts on crop yield in agricultural regions. IEEE J. Sel. Top. Appl. Earth Obs. Remote Sens. 7, 3867–3879. https://doi.org/10.1109/JSTARS.2014.2315999

Chauhan, Y.S., 2010. Potential productivity and water requirements of maize-peanut rotations in Australian semi-arid tropical environments-A crop simulation study. Agric. Water Manag. 97, 457–464. https://doi.org/10.1016/j.agwat.2009.11.005

Chen, D., Wang, Y., Wang, X., Nie, Z., Gao, Z., Zhang, L., 2016a. Effects of branch removal on water use of rain-fed jujube (Ziziphus jujuba Mill.) plantations in Chinese semiarid Loess Plateau region. Agric. Water Manag. 178, 258–270. https://doi.org/10.1016/j.agwat.2016.10.010

Chen, Y.; Zhang, Z.; Tao, F.,2018. Improving regional winter wheat yield estimation through assimilation of phenology and leaf area index from remote sensing data. Eur. J. Agron. 2018, 101, 163–173.

Cheng, Z.; Meng, J.; Qiao, Y.; Wang, Y.; Dong, W.; Han, Y. Preliminary study of soil available nutrient simulation using a modified WOFOST model and time-series remote sensing observations. Remote Sens. 2018, 10. https://doi.org/10.3390/rs10010064

Chen, Z., Ren, J., Tang, H., Shi, Y., Leng, P., Liu, J., Wang, L., Wu, W., Yao, Y., Hasiyuya, 2016b. Progress and perspectives on agricultural remote sensing research and applications in China. Yaogan Xuebao/Journal Remote Sens. 20, 748–767. https://doi.org/10.11834/jrs.20166214. (in Chinese with English abstract)

Confalonieri, R., Acutis, M., Bellocchi, G., Donatelli, M., 2009. Multi-metric evaluation of the models WARM, CropSyst, and WOFOST for rice. Ecol. Modell. 220, 1395–1410. https://doi.org/10.1016/j.ecolmodel.2009.02.017

Cui, N., Du, T., Kang, S., Li, F., Hu, X., Wang, M., Li, Z., 2009a. Relationship between stable carbon isotope discrimination and water use efficiency under regulated deficit irrigation of pear-jujube tree. Agric. Water Manag. 96, 1615–1622. https://doi.org/10.1016/j.agwat.2009.06.009

Cui, N., Du, T., Kang, S., Li, F., Zhang, J., Wang, M., Li, Z., 2008. Regulated deficit irrigation improved fruit quality and water use efficiency of pear-jujube trees. Agric. Water Manag. 95, 489–497. https://doi.org/10.1016/j.agwat.2007.11.007

Cui, N., Du, T., Li, F., Tong, L., Kang, S., Wang, M., Liu, X., Li, Z., 2009b. Response of vegetative growth and fruit development to regulated deficit irrigation at different growth stages of pear-jujube tree. Agric. Water Manag. 96, 1237–1246. https://doi.org/10.1016/j.agwat.2009.03.015

Curnel, Y., de Wit, A.J.W., Duveiller, G., Defourny, P., 2011. Potential performances of remotely sensed LAI assimilation in WOFOST model based on an OSS Experiment. Agric. For. Meteorol. 151, 1843–1855. https://doi.org/10.1016/j.agrformet.2011.08.002

Dai, Z., Fei, L., Huang, D., Zeng, J., Chen, L., Cai, Y., 2019. Coupling effects of irrigation and nitrogen levels on yield, water and nitrogen use efficiency of surge-root irrigated jujube in a semiarid region. Agric. Water Manag. 213, 146–154. https://doi.org/10.1016/j.agwat.2018.09.035

de la Casa, A., Ovando, G., Bressanini, L., Martínez, J., Díaz, G., Miranda, C., 2018. Soybean crop coverage estimation from NDVI images with different spatial resolution to evaluate yield variability in a plot. ISPRS J. Photogramm. Remote Sens. 146, 531–547. https://doi.org/10.1016/j.isprsjprs.2018.10.018

de Wit, A., Baruth, B., Boogaard, H., Van Diepen, K., Van Kraalingen, D., Micale, F., Te Roller, J., Supit, I., Van Den Wijngaart, R., 2010. Using ERA-INTERIM for regional crop yield forecasting in Europe. Clim. Res. 44, 41–53. https://doi.org/10.3354/cr00872

de Wit, A., Boogaard, H., Fumagalli, D., Janssen, S., Knapen, R., van Kraalingen, D., Supit, I., van der Wijngaart, R., van Diepen, K., 2019a. 25 years of the WOFOST cropping systems model. Agric. Syst. 168, 154–167. https://doi.org/10.1016/j.agsy.2018.06.018

de Wit, A., Boogaard, H., and Supit I. 2019b. System description of the WOFOST 7.2. cropping system model. Wageningen Environmental Research. September, 2019

de Wit, A., Duveiller, G., Defourny, P., 2012. Estimating regional winter wheat yield with WOFOST through the assimilation of green area index retrieved from MODIS observations. Agric. For. Meteorol. 164, 39–52. https://doi.org/10.1016/j.agrformet.2012.04.011

de Wit, A.J.W., van Diepen, C.A., 2008. Crop growth modelling and crop yield forecasting using satellite-derived meteorological inputs. Int. J. Appl. Earth Obs. Geoinf. 10, 414–425. https://doi.org/10.1016/j.jag.2007.10.004

de Wit, A.J.W., van Diepen, C.A., 2007. Crop model data assimilation with the Ensemble Kalman filter for improving regional crop yield forecasts. Agric. For. Meteorol. 146, 38–56. https://doi.org/10.1016/j.agrformet.2007.05.004

de Wit, A., Wolf, J. , 2010, Calibration of WOFOST crop growth simulation model for use within CGMS. 2010, 1–38.

Dempewolf, J., Adusei, B., Becker-Reshef, I., Hansen, M., Potapov, P., Khan, A., Barker, B., 2014. Wheat yield forecasting for Punjab Province from vegetation index time series and historic crop statistics. Remote Sens. 6, 9653–9675. https://doi.org/10.3390/rs6109653

Dente, L., Satalino, G., Mattia, F., Rinaldi, M., 2008. Assimilation of leaf area index derived from ASAR and MERIS data into CERES-Wheat model to map wheat yield. Remote Sens. Environ. 112, 1395–1407. https://doi.org/10.1016/j.rse.2007.05.023

Dobermann, A., Dawe, D., Roetter, R.P., Cassman, K.G., 2000. Reversal of rice yield decline in a long-term continuous cropping experiment. Agron. J. 92, 633–643. https://doi.org/10.2134/agronj2000.924633x

Dong, Y., Zhao, C., Yang, G., Chen, L., Wang, J., Feng, H., 2013. Integrating a very fast simulated annealing optimization algorithm for crop leaf area index variational assimilation. Math. Comput. Model. 58, 877–885. https://doi.org/10.1016/j.mcm.2012.12.013

Eitzinger, J., Trnka, M., Hösch, J., Žalud, Z., Dubrovský, M., 2004. Comparison of CERES, WOFOST and SWAP models in simulating soil water content during growing season under different soil conditions. Ecol. Modell. 171, 223–246. https://doi.org/10.1016/j.ecolmodel.2003.08.012

Ewert, F., Rötter, R.P., Bindi, M., Webber, H., Trnka, M., Kersebaum, K.C., Olesen, J.E., van Ittersum, M.K., Janssen, S., Rivington, M., Semenov, M.A., Wallach, D., Porter, J.R., Stewart, D., Verhagen, J., Gaiser, T., Palosuo, T., Tao, F., Nendel, C., Roggero, P.P., Bartošová, L., Asseng, S., 2015. Crop modelling for integrated assessment of risk to food production from climate change. Environ. Model. Softw. 72, 287–303. https://doi.org/10.1016/j.envsoft.2014.12.003

Fang, H., Liang, S., Hoogenboom, G., 2011. Integration of MODIS LAI and vegetation index products with the CSM-CERES-Maize model for corn yield estimation. Int. J. Remote Sens. 32, 1039–1065. https://doi.org/10.1080/01431160903505310

Fang, H., Liang, S., Hoogenboom, G., Teasdale, J., Cavigelli, M., 2008. Corn-yield estimation through assimilation of remotely sensed data into the CSM-CERES-Maize model. Int. J. Remote Sens. 29, 3011–3032. https://doi.org/10.1080/01431160701408386

Fishman, S., Génard, M., 1998. A biophysical model of fruit growth: Simulation of seasonal and diurnal dynamics of mass. Plant, Cell Environ. 21, 739–752. https://doi.org/10.1046/j.1365-3040.1998.00322.x

Fritz, S., See, L., Bayas, J.C.L., Waldner, F., Jacques, D., Becker-Reshef, I., Whitcraft, A., Baruth, B., Bonifacio, R., Crutchfield, J., Rembold, F., Rojas, O., Schucknecht, A., Van der Velde, M., Verdin, J., Wu, B., Yan, N., You, L., Gilliams, S., Mücher, S., Tetrault, R., Moorthy, I., McCallum, I., 2019. A comparison of global agricultural monitoring systems and current gaps. Agric. Syst. 168, 258–272. https://doi.org/10.1016/j.agsy.2018.05.010

Funk, C., Budde, M.E., 2009. Phenologically-tuned MODIS NDVI-based production anomaly estimates for Zimbabwe. Remote Sens. Environ. 113, 115–125. https://doi.org/10.1016/j.rse.2008.08.015

Galindo, A., Cruz, Z.N., Rodríguez, P., Collado-González, J., Corell, M., Memmi, H., Moreno, F., Moriana, A., Torrecillas, A., Pérez-López, D., 2016. Jujube fruit water relations at fruit maturation in response to water deficits. Agric. Water Manag. 164, 110–117. https://doi.org/10.1016/j.agwat.2015.08.024

Gao, Q.H., Wu, C. Sen, Wang, M., 2013. The Jujube (Ziziphus Jujuba Mill.) fruit: A Review of current knowledge of fruit composition and health benefits. J. Agric. Food Chem. 61, 3351–3363. https://doi.org/10.1021/jf4007032

García-Vila, M., Fereres, E., 2012. Combining the simulation crop model AquaCrop with an economic model for the optimization of irrigation management at farm level. Eur. J. Agron. 36, 21–31. https://doi.org/10.1016/j.eja.2011.08.003

Gilardelli, C., Confalonieri, R., Cappelli, G.A., Bellocchi, G., 2018. Sensitivity of WOFOST-based modelling solutions to crop parameters under climate change. Ecol. Modell. 368, 1–14. https://doi.org/10.1016/j.ecolmodel.2017.11.003

Green, S., McNaughton, K., Wünsche, J.N., Clothier, B., 2003. Modeling Light Interception and Transpiration of Apple Tree Canopies, in: Agronomy Journal. pp. 1380–1387. https://doi.org/10.2134/agronj2003.1380

Guerra, L.C., Garcia y Garcia, A., Hook, J.E., Harrison, K.A., Thomas, D.L., Stooksbury, D.E., Hoogenboom, G., 2007. Irrigation water use estimates based on crop simulation models and kriging. Agric. Water Manag. 89, 199–207. https://doi.org/10.1016/j.agwat.2007.01.010

Hadria, R., Duchemin, B., Lahrouni, A., Khabba, S., Er-Raki, S., Dedieu, G., Chehbouni, A.G., Olioso, A., 2006. Monitoring of irrigated wheat in a semi-arid climate using crop modelling and remote sensing data: Impact of satellite revisit time frequency. Int. J. Remote Sens. 27, 1093–1117. https://doi.org/10.1080/01431160500382980

He T. 2010. Study on the configuration and light distribution characteristics in slope-land jujube plantation of north Shaanxi, Yangling. (in Chinese with English abstract)

Hochheim, K.P.; Barber, D.G., 1998. Spring wheat yield estimation for western canada using NOAA NDVI Data. Can. J. Remote Sens. 1998, 24, 17–27. https://doi.org/10.1080/07038992.1998.10874687

Holzman, M.E., Rivas, R., Piccolo, M.C., 2014. Estimating soil moisture and the relationship with crop yield using surface temperature and vegetation index. Int. J. Appl. Earth Obs. Geoinf. 28, 181–192. https://doi.org/10.1016/j.jag.2013.12.006

Holzworth, D.P., Snow, V., Janssen, S., Athanasiadis, I.N., Donatelli, M., Hoogenboom, G., White, J.W., Thorburn, P., 2014. Agricultural production systems modelling and software: Current status and future prospects. Environ. Model. Softw. 72. https://doi.org/10.1016/j.envsoft.2014.12.013

Hsiao, T.C., Heng, L., Steduto, P., Rojas-Lara, B., Raes, D., Fereres, E., 2009. Aquacrop-The FAO crop model to simulate yield response to water: III. Parameterization and testing for maize. Agron. J. 101, 448–459. https://doi.org/10.2134/agronj2008.0218s.

Huang, J., Gómez-Dans, J.L., Huang, H., Ma, H., Wu, Q., Lewis, P.E., Liang, S., Chen, Z., Xue, J.H., Wu, Y., Zhao, F., Wang, J., Xie, X., 2019. Assimilation of remote sensing into crop growth models: Current status and perspectives. Agric. For. Meteorol. 276–277, 107609. https://doi.org/10.1016/j.agrformet.2019.06.008

Huang, J., Ma, H., Su, W., Zhang, X., Huang, Y., Fan, J., Wu, W., 2015a. Jointly Assimilating MODIS LAI and ET Products into the SWAP Model for Winter Wheat Yield Estimation. IEEE J. Sel. Top. Appl. Earth Obs. Remote Sens. 8, 4060–4071. https://doi.org/10.1109/JSTARS.2015.2403135

Huang, J.; Sedano, F.; Huang, Y.; Ma, H.; Li, X.; Liang, S.; Tian, L.; Zhang, X.; Fan, J.; Wu, W.,2016. Assimilating a synthetic Kalman filter leaf area index series into the WOFOST model to improve regional winter wheat yield estimation. Agric. For. Meteorol. 2016, 216, 188–202.

Huang, J., Tian, L., Liang, S., Ma, H., Becker-Reshef, I., Huang, Y., Su, W., Zhang, X., Zhu, D., Wu, W., 2015b. Improving winter wheat yield estimation by assimilation of the leaf area index from Landsat TM and MODIS data into the WOFOST model. Agric. For. Meteorol. 204, 106–121. https://doi.org/10.1016/j.agrformet.2015.02.001

Huang, Y., Zhu, Y., Li, W., Cao, W., Tian, Y., 2013. Assimilating Remotely Sensed Information with the WheatGrow Model Based on the Ensemble Square Root Filter forImproving Regional Wheat Yield Forecasts. Plant Prod. Sci. 16, 352–364. https://doi.org/10.1626/pps.16.352

Ines, A.V.M., Das, N.N., Hansen, J.W., Njoku, E.G., 2013. Assimilation of remotely sensed soil moisture and vegetation with a crop simulation model for maize yield prediction. Remote Sens. Environ. 138, 149–164. https://doi.org/10.1016/j.rse.2013.07.018

Jiang, Z., Chen, Z., Chen, J., Liu, J., Ren, J., Li, Z., Sun, L., Li, H., 2014. Application of crop model data assimilation with a particle filter for estimating regional winter wheat yields. IEEE J. Sel. Top. Appl. Earth Obs. Remote Sens. 7, 4422–4431. https://doi.org/10.1109/JSTARS.2014.2316012

Jin, S., Wang, Y., Shi, L., Guo, X., Zhang, J., 2018a. Effects of pruning and mulching measures on annual soil moisture, yield, and water use efficiency in jujube (Ziziphus jujube Mill.) plantations. Glob. Ecol. Conserv. 15. https://doi.org/10.1016/j.gecco.2018.e00406

Jin, X., Kumar, L., Li, Z., Feng, H., Xu, X., Yang, G., Wang, J., 2018b. A review of data assimilation of remote sensing and crop models. Eur. J. Agron. https://doi.org/10.1016/j.eja.2017.11.002

Jin, X., Yang, G., Xu, X., Yang, H., Feng, H., Li, Z., Shen, J., Zhao, C., Lan, Y., 2015. Combined multi-temporal optical and radar parameters for estimating LAI and biomass in winter wheat using HJ and RADARSAR-2 data. Remote Sens. 7, 13251–13272. https://doi.org/10.3390/rs71013251

Jones, J.W., Hoogenboom, G., Porter, C.H., Boote, K.J., Batchelor, W.D., Hunt, L.A., Wilkens, P.W., Singh, U., Gijsman, A.J., Ritchie, J.T., 2003. The DSSAT cropping system model, in: European Journal of Agronomy. pp. 235–265. https://doi.org/10.1016/S1161-0301(02)00107-7

Jongschaap, R.E.E., 2007. Sensitivity of a crop growth simulation model to variation in LAI and canopy nitrogen used for run-time calibration. Ecol. Modell. 200, 89–98. https://doi.org/10.1016/j.ecolmodel.2006.07.015

Jongschaap, R.E.E., Schouten, L.S.M., 2005. Predicting wheat production at regional scale by integration of remote sensing data with a simulation model. Agron. Sustain. Dev. 25, 481–489. https://doi.org/10.1051/agro:2005048

Jonsén, P., Isaksson, E., Sundin, K.G., Oldenburg, M., 2009. Identification of lumped parameter automotive crash models for bumper system development. Int. J. Crashworthiness 14, 533–541. https://doi.org/10.1080/13588260902837262

Jurečka, F., Lukas, V., Hlavinka, P., Semerádová, D., Žalud, Z., Trnka, M., 2018. Estimating crop yields at the field level using landsat and modis products. Acta Univ. Agric. Silvic. Mendelianae Brun. 66, 1141–1150. https://doi.org/10.11118/actaun201866051141

K. R. Thorp, D. J. Hunsaker, A. N. French, 2010. Assimilating Leaf Area Index Estimates from Remote Sensing into the Simulations of a Cropping Systems Model. Trans. ASABE 53, 251–262. https://doi.org/10.13031/2013.29490

Kassie, B.T., Asseng, S., Rotter, R.P., Hengsdijk, H., Ruane, A.C., Van Ittersum, M.K., 2015. Exploring climate change impacts and adaptation options for maize production in the Central Rift Valley of Ethiopia using different climate change scenarios and crop models. Clim. Change 129, 145–158. https://doi.org/10.1007/s10584-014-1322-x

Kouadio, L., Newlands, N.K., Davidson, A., Zhang, Y., Chipanshi, A., 2014. Assessing the performance of MODIS NDVI and EVI for seasonal crop yield forecasting at the ecodistrict scale. Remote Sens. 6, 10193–10214. https://doi.org/10.3390/rs61010193

Kroes, J.G., Supit, I., 2011. Impact analysis of drought, water excess and salinity on grass production in The Netherlands using historical and future climate data. Agric. Ecosyst. Environ. 144, 370–381. https://doi.org/10.1016/j.agee.2011.09.008

Kroes, J.G., van Dam, J.C., Bartholomeus, R.P., Groenendijk, P., Heinen, M., Hendriks, R.F.A., Mulder, H.M., Supit, I., van Walsum, P.E.V., 2017. SWAP version 4. https://doi.org/10.18174/416321

Lescourret, F., Blecher, N., Habib, R., Chadoeuf, J., Agostini, D., Pailly, O., Vaissière, B., Poggi, I., 1999. Development of a simulation model for studying kiwi fruit orchard management. Agric. Syst. 59, 215–239. https://doi.org/10.1016/S0308-521X(99)00006-2

Li, F. 2016. Research on the price formation mechanism of Jujube, China. Ph.d thesis. (In Chinese with english abstract)

Li, J.W., Fan, L.P., Ding, S.D., Ding, X.L., 2007. Nutritional composition of five cultivars of chinese jujube. Food Chem. 103, 454–460. https://doi.org/10.1016/j.foodchem.2006.08.016

Li, Xiaopeng, Li, Y., Zhang, Z., Li, Xingang, 2015. Influences of environmental factors on leaf morphology of Chinese jujubes. PLoS One 10. https://doi.org/10.1371/journal.pone.0127825

Li, Y., Zhou, Q., Zhou, J., Zhang, G., Chen, C., Wang, J., 2014. Assimilating remote sensing information into a coupled hydrology-crop growth model to estimate regional maize yield in arid regions. Ecol. Modell. 291, 15–27. https://doi.org/10.1016/j.ecolmodel.2014.07.013

Liu, F., Liu, X., Zhao, L., Ding, C., Jiang, J., Wu, L., 2015. The Dynamic Assessment Model for Monitoring Cadmium Stress Levels in Rice Based on the Assimilation of Remote Sensing and the WOFOST Model. IEEE J. Sel. Top. Appl. Earth Obs. Remote Sens. 8, 1330–1338. https://doi.org/10.1109/JSTARS.2014.2371058

Lopez, G., Favreau, R.R., Smith, C., Dejong, T.M., 2010. L-PEACH: A computer-based model to understand how peach trees grow. Horttechnology 20, 983–990. https://doi.org/10.21273/HORTSCI.20.6.983

Lorenc, A.C., Ballard, S.P., Bell, R.S., Ingleby, N.B., Andrews, P.L.F., Barker, D.M., Bray, J.R., Clayton, A.M., Dalby, T., Li, D., Payne, T.J., Saunders, F.W., 2000. The Met. Office global three-dimensional variational data assimilation scheme. Q. J. R. Meteorol. Soc. 126, 2991–3012. https://doi.org/10.1256/smsqj.57001

Ma, Y., Wang, S., Li, Z., Hou, Y., Zhuang, L., He, Y., Wang, F., 2008. Monitoring winter wheat growth in North China by combining a crop model and remote sensing data. Int. J. Appl. Earth Obs. Geoinf. 10, 426–437. https://doi.org/10.1016/j.jag.2007.09.002

Ma, G., Huang, J., Wu, W., Fan, J., Zou, J., Wu, S., 2013. Assimilation of MODIS-LAI into the WOFOST model for forecasting regional winter wheat yield. Math. Comput. Model. 58, 634–643. https://doi.org/10.1016/j.mcm.2011.10.038

McNider, R.T., Handyside, C., Doty, K., Ellenburg, W.L., Cruise, J.F., Christy, J.R., Moss, D., Sharda, V., Hoogenboom, G., Caldwell, P., 2015. An integrated crop and hydrologic

modelling system to estimate hydrologic impacts of crop irrigation demands. Environ. Model. Softw. 72, 341–355. https://doi.org/10.1016/j.envsoft.2014.10.009

Mkhabela, Manasah S., Mkhabela, Milton S., Mashinini, N.N., 2005. Early maize yield forecasting in the four agro-ecological regions of Swaziland using NDVI data derived from NOAA's-AVHRR. Agric. For. Meteorol. 129, 1–9. https://doi.org/10.1016/j.agrformet.2004.12.006

Mishra, A.K.; Ines, A.V.M.; Das, N.N.; Prakash Khedun, C.; Singh, V.P.; Sivakumar, B.; Hansen, J.W. Anatomy of a local-scale drought: Application of assimilated remote sensing products, crop model, and statistical methods to an agricultural drought study. J. Hydrol. 2015, 526, 15–29.

Mollier, A., De Willigen, P., Heinen, M., Morel, C., Schneider, A., Pellerin, S., 2008. A two-dimensional simulation model of phosphorus uptake including crop growth and P-response. Ecol. Modell. 210, 453–464. https://doi.org/10.1016/j.ecolmodel.2007.08.008

Morel, J., Bégué, A., Todoroff, P., Martiné, J.F., Lebourgeois, V., Petit, M., 2014. Coupling a sugarcane crop model with the remotely sensed time series of fIPAR to optimise the yield estimation. Eur. J. Agron. 61, 60–68. https://doi.org/10.1016/j.eja.2014.08.004

Morel, J., Martiné, J.-F., Bégué, A., Todoroff, P., Petit, M., 2012. A comparison of two coupling methods for improving a sugarcane model yield estimation with a NDVI-derived variable, in: Remote Sensing for Agriculture, Ecosystems, and Hydrology XIV. p. 85310E. https://doi.org/10.1117/12.975688

Moriondo, M., Maselli, F., Bindi, M., 2007. A simple model of regional wheat yield based on NDVI data. Eur. J. Agron. 26, 266–274. https://doi.org/10.1016/j.eja.2006.10.007

Nearing, G.S., Crow, W.T., Thorp, K.R., Moran, M.S., Reichle, R.H., Gupta, H. V., 2012. Assimilating remote sensing observations of leaf area index and soil moisture for wheat yield estimates: An observing system simulation experiment. Water Resour. Res. 48. https://doi.org/10.1029/2011WR011420

Oliver. M. A. Geostatistical Applications for Precision Agriculture, 2010. Geostatistical Applications for Precision Agriculture. https://doi.org/10.1007/978-90-481-9133-8

Ogutu, G.E.O., Franssen, W.H.P., Supit, I., Omondi, P., Hutjes, R.W.A., 2018. Probabilistic maize yield prediction over East Africa using dynamic ensemble seasonal climate forecasts. Agric. For. Meteorol. 250–251, 243–261. https://doi.org/10.1016/j.agrformet.2017.12.256

Panda, S.S., Ames, D.P., Panigrahi, S., 2010. Application of vegetation indices for agricultural crop yield prediction using neural network techniques. Remote Sens. 2, 673–696. https://doi.org/10.3390/rs2030673

Pauwels, V.R.N.; Verhoest, N.E.C.; De Lannoy, G.J.M.; Guissard, V.; Lucau, C.; Defourny, P.,2007. Optimization of a coupled hydrology-crop growth model through the assimilation of observed soil moisture and leaf area index values using an ensemble Kalman filter. Water Resour. Res. 2007, 43.

Piekarczyk, J., 2015. Application of Remote Sensing in Agriculture. Geoinformatica Pol. 13. https://doi.org/10.2478/gein-2014-0007

Pirttioja, N., Palosuo, T., Fronzek, S., Räisänen, J., Rötter, R.P., Carter, T.R., 2019. Using impact response surfaces to analyse the likelihood of impacts on crop yield under probabilistic climate change. Agric. For. Meteorol. 264, 213–224. https://doi.org/10.1016/j.agrformet.2018.10.006

Prasad, A.K., Chai, L., Singh, R.P., Kafatos, M., 2006. Crop yield estimation model for Iowa using remote sensing and surface parameters. Int. J. Appl. Earth Obs. Geoinf. 8, 26–33. https://doi.org/10.1016/j.jag.2005.06.002

Qiang, M., Fei, L., Liu, Y., 2015. Regulated deficit irrigation promoting growth and increasing fruit yield of jujube trees. Nongye Gongcheng Xuebao/Transactions Chinese Soc. Agric. Eng. 31, 91–96. https://doi.org/10.11975/j.issn.1002-6819.2015.19.013

Raes, D., Steduto, P., Hsiao, T.C., Fereres, E., 2009. Aquacrop-The FAO crop model to simulate yield response to water: II. main algorithms and software description. Agron. J. 101, 438–447. https://doi.org/10.2134/agronj2008.0140s

Rahman, M.M., Robson, A., Bristow, M., 2018. Exploring the potential of high resolution worldview-3 Imagery for estimating yield of mango. Remote Sens. 10. https://doi.org/10.3390/rs10121866

Rawlins, F., Ballard, S.P., Bovis, K.J., Clayton, A.M., Li, D., Inverarity, G.W., Lorenc, A.C., Payne, T.J., 2007. The met office global four-dimensional variational data assimilation scheme. Q. J. R. Meteorol. Soc. 133, 347–362. https://doi.org/10.1002/qj.32

Reidsma, P., Ewert, F., Boogaard, H., Diepen, K. van, 2009. Regional crop modelling in Europe: The impact of climatic conditions and farm characteristics on maize yields. Agric. Syst. 100, 51–60. https://doi.org/10.1016/j.agsy.2008.12.009

Rembold, F., Meroni, M., Urbano, F., Csak, G., Kerdiles, H., Perez-Hoyos, A., Lemoine, G., Leo, O., Negre, T., 2019. ASAP: A new global early warning system to detect anomaly hot spots of agricultural production for food security analysis. Agric. Syst. 168, 247–257. https://doi.org/10.1016/j.agsy.2018.07.002

Ren, J., Chen, Z., Zhou, Q., Tang, H., 2008. Regional yield estimation for winter wheat with MODIS-NDVI data in Shandong, China. Int. J. Appl. Earth Obs. Geoinf. 10, 403–413. https://doi.org/10.1016/j.jag.2007.11.003

Reynolds, C.A., Yitayew, M., Slack, D.C., Hutchinson, C.F., Huete, A., Petersen, M.S., 2000. Estimating crop yields and production by integrating the FAO Crop Specific Water Balance model with real-time satellite data and ground-based ancillary data. Int. J. Remote Sens. 21, 3487–3508. https://doi.org/10.1080/014311600750037516

Rojas, O., 2007. Operational maize yield model development and validation based on remote sensing and agro-meteorological data in Kenya. Int. J. Remote Sens. 28, 3775–3793. https://doi.org/10.1080/01431160601075608

Rowan, T.H., 1990. Functional stability analysis of numerical algorithms. Ph.D. thesis.

Rötter, R., Van Keulen, H., 1997. Variations in yield response to fertilizer application in the tropics: II. Risks and opportunities for smallholders cultivating maize on Kenya's arable land. Agric. Syst. 53, 69–95. https://doi.org/10.1016/S0308-521X(96)00037-6

Sakamoto, T., Gitelson, A.A., Arkebauer, T.J., 2013. MODIS-based corn grain yield estimation model incorporating crop phenology information. Remote Sens. Environ. 131, 215–231. https://doi.org/10.1016/j.rse.2012.12.017

Salazar, L., Kogan, F., Roytman, L., 2007. Use of remote sensing data for estimation of winter wheat yield in the United States. Int. J. Remote Sens. 28, 3795–3811. https://doi.org/10.1080/01431160601050395

Saseendran, S.A., Ma, L., Malone, R., Heilman, P., Ahuja, L.R., Kanwar, R.S., Karlen, D.L., Hoogenboom, G., 2007. Simulating management effects on crop production, tile

drainage, and water quality using RZWQM-DSSAT. Geoderma 140, 297–309. https://doi.org/10.1016/j.geoderma.2007.04.013

Schneider, K., 2003. Assimilating remote sensing data into a land-surface process model. Int. J. Remote Sens. 24, 2959–2980. https://doi.org/10.1080/01431160210154803

Schulthess, U., Timsina, J., Herrera, J.M., McDonald, A., 2013. Mapping field-scale yield gaps for maize: An example from Bangladesh. F. Crop. Res. 143, 151–156. https://doi.org/10.1016/j.fcr.2012.11.004

Sepulcre-Cantó, G., Zarco-Tejada, P.J., Jiménez-Muñoz, J.C., Sobrino, J.A., Soriano, M.A., Fereres, E., Vega, V., Pastor, M., 2007. Monitoring yield and fruit quality parameters in open-canopy tree crops under water stress. Implications for ASTER. Remote Sens. Environ. 107, 455–470. https://doi.org/10.1016/j.rse.2006.09.014

Son, N.T., Chen, C.F., Chen, C.R., Minh, V.Q., Trung, N.H., 2014. A comparative analysis of multitemporal MODIS EVI and NDVI data for large-scale rice yield estimation. Agric. For. Meteorol. 197, 52–64. https://doi.org/10.1016/j.agrformet.2014.06.007

Steduto, P., Hsiao, T.C., Raes, D., Fereres, E., 2009. Aquacrop-the FAO crop model to simulate yield response to water: I. concepts and underlying principles. Agron. J. 101, 426–437. https://doi.org/10.2134/agronj2008.0139s

Stöckle, C.O., Donatelli, M., Nelson, R., 2003. CropSyst, a cropping systems simulation model, in: European Journal of Agronomy. pp. 289–307. https://doi.org/10.1016/S1161-0301(02)00109-0

Sun, L., Gao, F., Anderson, M.C., Kustas, W.P., Alsina, M.M., Sanchez, L., Sams, B., McKee, L., Dulaney, W., White, W.A., Alfieri, J.G., Prueger, J.H., Melton, F., Post, K., 2017. Daily mapping of 30 m LAI and NDVI for grape yield prediction in California vineyards. Remote Sens. 9. https://doi.org/10.3390/rs9040317

Supit, I., Hooyer, A.A., Van Diepen, C.A., 1994. System description of the WOFOST 6.0 crop simulation model implemented in the CGMS Vol. 1: Theory and algorithms. EUR publication 15956. Agric. Ser. Luxemb.

Supit, I., 1997. Predicting national wheat yields using a crop simulation and trend models. Agric. For. Meteorol. 88, 199–214. https://doi.org/10.1016/S0168-1923(97)00037-3

Supit, I., van Diepen, C.A., de Wit, A.J.W., Kabat, P., Baruth, B., Ludwig, F., 2010. Recent changes in the climatic yield potential of various crops in Europe. Agric. Syst. 103, 683–694. https://doi.org/10.1016/j.agsy.2010.08.009

Supit, I., van Diepen, C.A., de Wit, A.J.W., Wolf, J., Kabat, P., Baruth, B., Ludwig, F., 2012. Assessing climate change effects on European crop yields using the Crop Growth Monitoring System and a weather generator. Agric. For. Meteorol. 164, 96–111. https://doi.org/10.1016/j.agrformet.2012.05.005

Tebaldi, C., Knutti, R., 2007. The use of the multi-model ensemble in probabilistic climate projections. Philos. Trans. R. Soc. A Math. Phys. Eng. Sci. 2053–2075. https://doi.org/10.1098/rsta.2007.2076

Tittonell, P., Corbeels, M., van Wijk, M.T., Giller, K.E., 2010. FIELD-A summary simulation model of the soil-crop system to analyse long-term resource interactions and use efficiencies at farm scale. Eur. J. Agron. 32, 10–21. https://doi.org/10.1016/j.eja.2009.05.008

Todorovic, M., Albrizio, R., Zivotic, L., Abi Saab, M.T., Stöckle, C., Steduto, P., 2009a. Assessment of aquacrop, cropsyst, and WOFOST models in the simulation of

sunflower growth under different water regimes. Agron. J. 101, 509–521. https://doi.org/10.2134/agronj2008.0166s

Todorovic, M., Albrizio, R., Zivotic, L., Abi Saab, M.T., Stöckle, C., Steduto, P., 2009b. Assessment of aquacrop, cropsyst, and WOFOST models in the simulation of sunfl ower growth under different water regimes. Agron. J. 101, 509–521. https://doi.org/10.2134/agronj2008.0166s

Tripathy, R., Chaudhari, K.N., Mukherjee, J., Ray, S.S., Patel, N.K., Panigrahy, S., Singh Parihar, J., 2013. Forecasting wheat yield in Punjab state of India by combining crop simulation model WOFOST and remotely sensed inputs. Remote Sens. Lett. 4, 19–28. https://doi.org/10.1080/2150704X.2012.683117

Vazifedoust, M.; van Dam, J.C.; Bastiaanssen, W.G.M.; Feddes, R.A. Assimilation of satellite data into agrohydrological models to improve crop yield forecasts. Int. J. Remote Sens. 2009, 30, 2523–2545. https://doi.org/10.1080/01431160802552769

van Bussel, L.G.J., Müller, C., van Keulen, H., Ewert, F., Leffelaar, P.A., 2011. The effect of temporal aggregation of weather input data on crop growth models' results. Agric. For. Meteorol. 151, 607–619. https://doi.org/10.1016/j.agrformet.2011.01.007

van Diepen, C.A., Wolf, J., van Keulen, H., Rappoldt, C., 1989. WOFOST: a simulation model of crop production. Soil Use Manag. 5, 16–24. https://doi.org/10.1111/j.1475-2743.1989.tb00755.x

Van Walsum, P.E.V., Supit, I., 2012. Influence of ecohydrologic feedbacks from simulated crop growth on integrated regional hydrologic simulations under climate scenarios. Hydrol. Earth Syst. Sci. 16, 1577–1593. https://doi.org/10.5194/hess-16-1577-2012

Victoria, D. de C., da Paz, A.R., Coutinho, A.C., Kastens, J., Brown, J.C., 2012. Cropland area estimates using Modis NDVI time series in the state of Mato Grosso, Brazil. Pesqui. Agropecu. Bras. 47, 1270–1278. https://doi.org/10.1590/S0100-204X2012000900012

Wall, L., Larocque, D., Léger, P.M., 2008. The early explanatory power of NDVI in crop yield modelling. Int. J. Remote Sens. 29, 2211–2225. https://doi.org/10.1080/01431160701395252

Wang, H., Zhu, Y., Li, W., Cao, W., Tian, Y., 2014. Integrating remotely sensed leaf area index and leaf nitrogen accumulation with RiceGrow model based on particle swarm optimization algorithm for rice grain yield assessment. J. Appl. Remote Sens. 8, 083674. https://doi.org/10.1117/1.JRS.8.083674

Wang, J., Huang, J., Wu, P., Zhao, X., Gao, X., Dumlao, M., Si, B.C., 2015. Effects of soil managements on surface runoff and soil water content in jujube orchard under simulated rainfalls. Catena 135, 193–201. https://doi.org/10.1016/j.catena.2015.07.025

Wang, J., Huang, J., Zhao, X., Wu, P., Horwath, W.R., Li, H., Jing, Z., Chen, X., 2016. Simulated Study on Effects of Ground Managements on Soil Water and Available Nutrients in Jujube Orchards. L. Degrad. Dev. 27, 35–42. https://doi.org/10.1002/ldr.2334

Wang, J.; Li, X.; Lu, L.; Fang, F. Estimating near future regional corn yields by integrating multi-source observations into a crop growth model. Eur. J. Agron. 2013, 49, 126–140. https://doi.org/10.1016/j.eja.2013.03.005

Wang, M., Tao, F.L., Shi, W.J., 2014. Corn yield forecasting in northeast china using remotely sensed spectral indices and crop phenology metrics. J. Integr. Agric. 13, 1538–1545. https://doi.org/10.1016/S2095-3119(14)60817-0

Wang, Z., Bian, Q., Zhang, J., Zhou, B., 2018. Optimized water and fertilizer management of Mature Jujube in Xinjiang arid area using drip irrigation. Water (Switzerland) 10. https://doi.org/10.3390/w10101467

Wei, X., Chen, D., Liu, S., Wang, X., Gao, Z., Wang, Y., 2014. Effect of trim on jujube transpiration in loess hilly region. Nongye Jixie Xuebao/Transactions Chinese Soc. Agric. Mach. 45. https://doi.org/10.6041/j.issn.1000-1298.2014.12.029

Wu, S.; Huang, J.; Liu, X.; Fan, J.; Ma, G.; Zou, J., 2012. Assimilating MODIS-LAI into crop growth model with EnKF to predict regional crop yield. In Proceedings of the IFIP Advances in Information and Communication Technology; 2012; Vol. 370 AICT, pp. 410–418. https://doi.org/10.1016/j.ecolmodel.2013.08.016

Xie, Y.; Wang, P.; Bai, X.; Khan, J.; Zhang, S.; Li, L.; Wang, L., 2017. Assimilation of the leaf area index and vegetation temperature condition index for winter wheat yield estimation using Landsat imagery and the CERES-Wheat model. Agric. For. Meteorol. 2017, 246, 194–206. https://doi.org/10.1016/j.agrformet.2017.06.015

Yang, W., Gao, J., Xu, C., 2012. The correlation analysis of leaf area index and yield of red jujube. Xinjiang Agricultural Sciences, 49, 1397-1400. (In Chinese with English abstract)

Yao, F., Tang, Y., Wang, P., Zhang, J., 2015. Estimation of maize yield by using a process-based model and remote sensing data in the Northeast China Plain. Phys. Chem. Earth 87–88, 142–152. https://doi.org/10.1016/j.pce.2015.08.010

Ye, X., Sakai, K., Asada, S. ichi, Sasao, A., 2008a. Application of narrow-band TBVI in estimating fruit yield in citrus. Biosyst. Eng. 99, 179–189. https://doi.org/10.1016/j.biosystemseng.2007.09.016

Ye, X., Sakai, K., Garciano, L.O., Asada, S.I., Sasao, A., 2006. Estimation of citrus yield from airborne hyperspectral images using a neural network model. Ecol. Modell. 198, 426–432. https://doi.org/10.1016/j.ecolmodel.2006.06.001

Ye, X., Sakai, K., Sasao, A., Asada, S. ichi, 2008b. Potential of airborne hyperspectral imagery to estimate fruit yield in citrus. Chemom. Intell. Lab. Syst. 90, 132–144. https://doi.org/10.1016/j.chemolab.2007.09.002

Yu, B., Shang, S., 2018. Multi-year mapping of major crop yields in an irrigation district from high spatial and temporal resolution vegetation index. Sensors (Switzerland) 18. https://doi.org/10.3390/s18113787

Zhang, L., Wang, Y., Han, L., Liu, S., Li, X., 2013. Water consumption of pear jujube trees (Ziziphus jujuba Mill.) and its correlation with trunk diameter during flowering and fruit development periods. Shengtai Xuebao/ Acta Ecol. Sin. 33, 907–915. https://doi.org/10.5846/stxb201206280908

Zhao, Y., Chen, S., Shen, S., 2013. Assimilating remote sensing information with crop model using Ensemble Kalman Filter for improving LAI monitoring and yield estimation. Ecol. Modell. 270, 30–42. https://doi.org/10.1016/j.ecolmodel.2013.08.016

Zhiyan Consulting Group., 2018. Analysis and forecast report on the development status and investment potential risks of Chinese jujube industry from 2018 to 2024. https://www.chyxx.com/research/201808/665040.html.

Zhou, G., Liu, X., Liu, M., 2019. Assimilating Remote Sensing Phenological Information into the WOFOST Model for Rice Growth Simulation. Remote Sens. 11, 268. https://doi.org/10.3390/rs11030268

Zhou, J., Cheng, G., Li, X., Hu, B.X., Wang, G., 2012a. Numerical Modelling of Wheat Irrigation using Coupled HYDRUS and WOFOST Models. Soil Sci. Soc. Am. J. 76, 648. https://doi.org/10.2136/sssaj2010.0467

Zhou, R., Damerow, L., Sun, Y., Blanke, M.M., 2012b. Using colour features of cv. "Gala" apple fruits in an orchard in image processing to predict yield. Precis. Agric. 13, 568–580. https://doi.org/10.1007/s11119-012-9269-2

Zhu, X.; Zhao, Y.; Feng, X., 2013. A methodology for estimating Leaf Area Index by assimilating remote sensing data into crop model based on temporal and spatial knowledge. Chinese Geogr. Sci. 2013, 23, 550–561.

Chapter 2

Research materials and strategy

This chapter focuses on the research materials, data, data usage, and methods, including research area and climate information, jujube tree phenology and management, field experiments, observed data at field and regional scale, data use, and the research strategy. The description of the jujube tree gives the reader a preliminary understanding of the crop.

The experimental design and research data for the entire doctoral thesis are also presented in this chapter. The same field experimental data and observational yields of 181 orchards were used across the research. The TDWI parameter is the key parameter of our study for the jujube growth simulation, and LAI is an important remotely sensed state variable. Therefore, the TDWI and LAI data of 55 observed orchards are also introduced in this chapter. Figure 2–8 may be helpful for the reader to understand the data usage of the thesis.

1. Research area and climate conditions

1.1. Study area

The study was conducted in Alaer City (80°30′E–81°58′E, 40°22′N–40°57′N) in Western China because of the relatively large and concentrated jujube planting areas there. This region represents ten small agro-ecological zones, with around 45,515 ha of jujube orchards in 2017. These farms currently produce up to 15.8% of the annual national production of jujube fruit (2017 Alaer Statistical Yearbook).

Figure 2−1 shows the study area and the location of the experimental field which was monitored for the crop model calibration. This figure also presents the 181 jujube orchards that were observed in terms of annual fruit yield in order to validate the proposed yield estimation methods. Among these fields, the leaf area index was measured at key growing stages for 55 orchards to establish an inversion model from remote sensing data. The total dry weight of jujube at emergence was also measured for these orchards for model calibration at the regional scale. These measurements and observations were performed during the growing seasons of 2016 and 2017. Meteorological data was also observed based on field weather stations because weather is one of the main driving conditions of the WOFOST model.

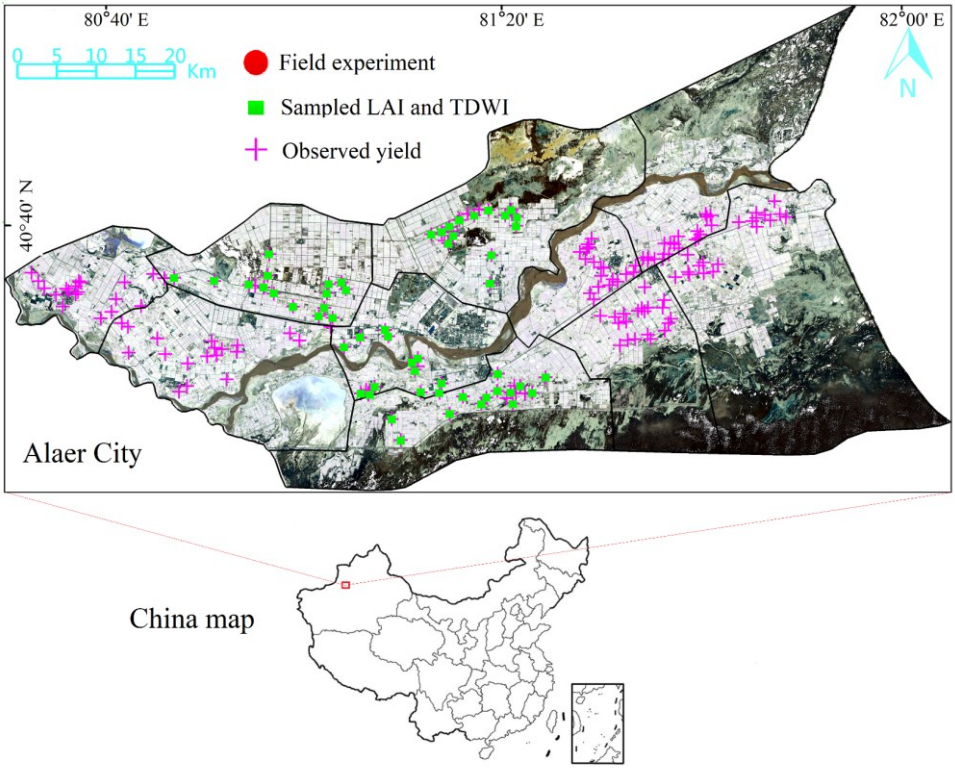

Figure 2–1: Study region and observed data for this study

1.2. Climate conditions

In the studied region, the climate is arid warm-temperate. The annual average temperature, radiation, humidity, and rainfall for 1988 to 2018 are shown in Figure 2–2 (climate data taken from NASA Prediction of Worldwide Energy Resources, https://power.larc.nasa.gov). The average temperature fluctuation between years is quite large. The maximum temperature difference is 1.59°C. All sky insolation on a horizontal surface ranges from 28.04 to 28.32 MJ m^{-2} d^{-1}, with a standard deviation (SD) value of 0.07 MJ m^{-2} d^{-1}. The inter-annual total rainfall varies greatly, showing a relatively large SD value (SD = 20.62 mm). The rainfall is less than 100 mm except for 2016. Relative humidity changes also show some volatility, which indicates that the study area has had an arid climate for a long time.

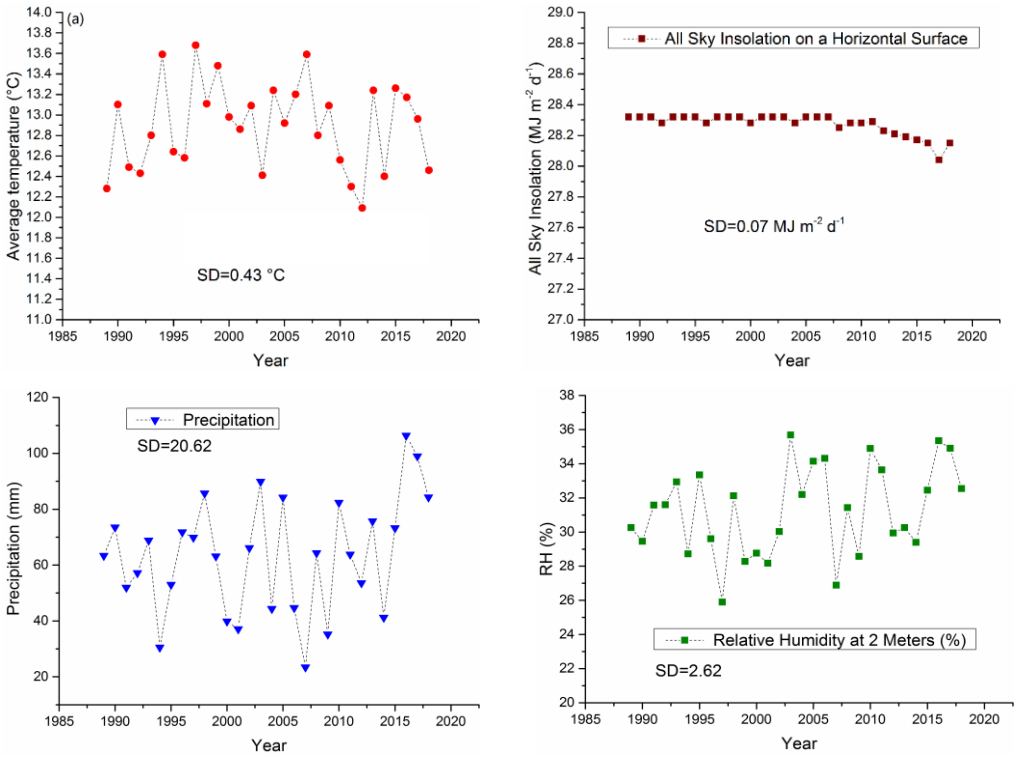

Figure 2–2: Interannual variations in major meteorological parameters from 1988 to 2018. (a) Annual mean temperature, (b) annual mean all sky insolation on a horizontal surface, (c) annual total precipitation, (d) annual mean relative humidity

Figures 2–3, 2–4, and 2–5 show the daily minimum and maximum temperatures, the daily irradiation, and the daily precipitation, respectively, from April to October of 2016 and 2017 for the field experimental area. These climate data were collected by a local weather station located in Tarim University Jujube Research and Experiment Base situated 500 m from the field experiments.

The daily minimum and maximum temperatures during the growing season (from April–October) in 2016 and 2017 ranged from 13.6°C to 2.3°C and 12.1°C to 28.2°C, respectively. The daily minimum and maximum temperatures showed a trend of first increasing and then decreasing, with a relatively large daily difference between maximum and minimum temperatures which facilitates the accumulation of reducing sugar (Kerimu et al., 2018). The average of the maximum temperatures was basically the same in 2016 and 2017. The average of the minimum temperatures in 2016 was 1.5°C higher than that of 2017. The average maximum temperatures for June, July, and August in 2016 and 2017 reached almost 31°C.

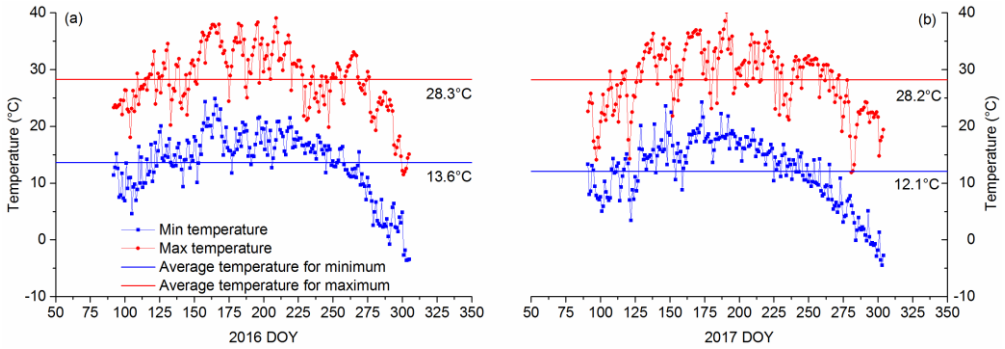

Figure 2–3: Daily minimum and maximum temperature from April to October, (a) 2016, (b) 2017. DOY: day of year. Data is from a local weather station.

The daily total radiation in the study area is strong and shows large fluctuations. The average daily radiation from April to October in 2017 was also significantly higher than in 2016, which is usually helpful for photosynthesis.

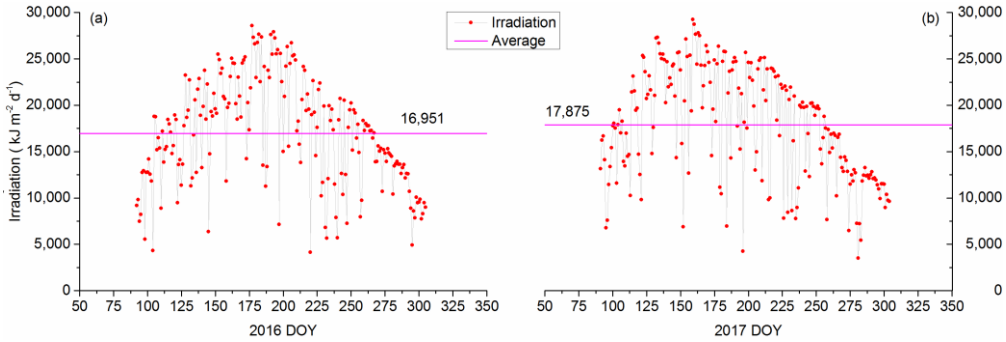

Figure 2–4: Daily total irradiation from April to October, (a) 2016, (b) 2017. DOY: day of year. Data is from a local weather station.

The study area is located on the edge of the desert, with very little rainfall of about 100 mm per year. The water demand for jujube trees depends mainly on irrigation, which is managed by the government department. Generally, a reasonable irrigation

strategy is carried out based on the temperature and rainfall conditions, combined with the water requirements of different development stages of jujube trees.

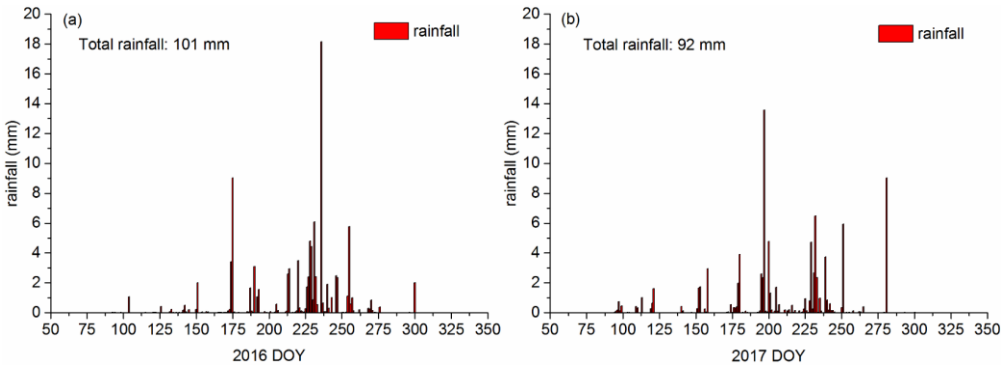

Figure 2–5: Daily total rainfall from April to October, (a) 2016, (b) 2017. DOY: day of year. Data is from a local weather station.

2. Description of jujube fruit tree

2.1. Jujube tree phenology

The cultivation and management of jujube trees is closely related to their phenological characteristics. It is important to clarify the different growth stages of jujube trees to help farmers to effectively cultivate their orchards by pruning, irrigating, fertilizing, and managing pests. Studies of periodic biological events (such as bud breaks, flushing, flowering, and fruit development) are known as phenology, which is primarily affected by the climatic conditions (Hernández et al., 2015). The phenological development of jujube trees can be divided into eight stages according to the BBCH-scale (*Biologische Bundesanstalt, Bundessortenamt, Chemische Industrie*) (Hernández et al., 2015), including bud, leaf development, shoot development, inflorescence emergence, flowering, fruit development, fruit maturity and senescence. Figure 2–6(D1–D8) shows a typical feature at each developmental stage. When the temperature is higher than the threshold temperature for emergence, the buds of the jujube tree begin to wake up from the winter dormancy and enter the developmental stage of the bud which lasts until the green tip is about 3 mm higher than the bud scale (Figure 2–6D1). Next, it enters the leaf development stage, which is the period from the first leaf separation (D2) to the complete unfolding and expansion of all leaves. Next, it enters the shoot development stage to form different branches (D3). Next, it enters the period of inflorescence emergence, from the swelling of the inflorescence bud (D4) to the first petal visible. Next, the jujube enters the flowering period, from the first flower unfolding, full flowering (50% of flowers open, D5), to the end of flowering (all the petals fall or dry, and the fruit begins to form). Next, it enters the fruit development period, from the fruit set to the standard cultivar size (D6, skin green in colour). Next, it enters the physiological maturity period. The fruit begins to fully develop, and the skin colour of the fruit gradually

changes from green to yellowish green and finally becomes reddish brown, and the fruit begins to soften and wrinkle (D7). Finally, it enters senescence and the next dormant period, the leaves begin to age and fall (D8), starting the next dormancy.

Figure 2–6: Phenological development stages of the jujube fruit tree. D1: beginning of emergence, D2: beginning of leaf development stage, D3: shoot development stage, D4: inflorescence emergence, D5: flowering period, D6: fruit development period, D7: maturity period, D8: senescence and the next dormant period (The D1and D2 images are from http://www.zao.com.cn/, and the D3-D8 images are from the field trials).

In this research, only three growing stages of jujube tree, namely emergence, flowering, and maturity, were considered for the WOFOST model calibration. The emergence date is defined as the time when the fifth leaf on the bud is unfolded because the excess buds will be cut off at this time according to the needs of production, and the initial bud weight finally retained on the jujube tree and roots can be considered as the initial input parameter TDWI (Initial Total Dry Weight) of the

WOFOST model. The fruit set time is defined as the flowering date. The time when the dry weight of the fruit is no longer increasing is defined as the date of maturity.

2.2. Jujube orchard management

Jujube cultivation management mainly includes planting density selection, irrigation, fertilization, and pruning. Tree age must also be considered in orchard management.

2.2.1. Planting density

In recent years, high-density planting patterns have been widely adopted in Xinjiang, with two to ten thousand plants per hectare. However, the cultivation density cannot increase indefinitely; excessive density could lead to an increase in canopy closure, which in turn could affect photosynthesis efficiency and yield (Zhang *et al*., 2013).

2.2.2. Pruning strategy

Pruning management can produce different tree shapes, which may affect canopy light interception and photosynthesis, thereby affecting final yield. Different tree shapes, such as cylindrical, small canopy permanent line, small canopy permanent tree, and middle trunk shape with three main branches, have an impact on the structure development, fruit yield composition, and quality of jujube fruits (Zhang *et al*., 2013), see Table 2–1. The number and the average weight of the fruits in several tree shapes are also different, which is the main factor that constitutes the yield. The tree shape with the highest yield per plant is the small canopy permanent line, followed by the small canopy permanent tree, and finally the middle trunk shape with three main branches and the cylindrical shape. The nutritional quality of different tree shapes is also different, which affects total sugar, soluble solid, organic acid, and vitamin C contents. The small canopy permanent line shape is shown in Figure 2–7, this shape gives a short tree with a simple structure, is good at intercepting light energy (Zhang *et al*., 2013), and has 3–4 main (mother) branches on the trunk extending outward at 35–45°.

Table 2–1: Yield per plant of *CV. JUN* jujube in different tree shapes

Tree shape	Average number of jujubes per plant	Average weight of fruits (g)	Average yield per plant (kg)
Cylindrical	142	18.11	2.57
Middle trunk shape with three main branches	130	17.93	2.34
Small canopy permanent tree	198	24.79	4.92
Small canopy permanent line	363	18.95	6.88

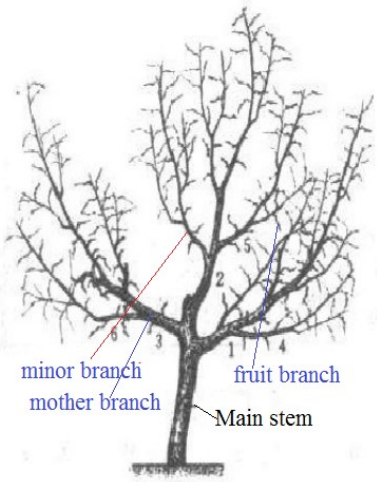

Figure 2−7: Small canopy permanent line jujube tree shape.

2.2.3. Irrigation and fertilization

Irrigation factors have significant effects on the photosynthetic characteristics of jujube leaves, such as net photosynthetic rate, transpiration rate, stomatal conductance, intercellular carbon dioxide concentration, and water use efficiency ($p<0.05$) (Bian et al., 2018). Too high or too low irrigation is not conducive to photosynthesis, growth, and the yield of jujube fruit trees. Generally, the total amount of irrigation can be calculated with reference to the soil moisture content at field capacity (Zheng et al., 2014). The amount of irrigation required during the emergence period and red ripening period is relatively small, accounting for about 27% of the irrigation amount in the growth period; the irrigation amount required during the flowering period, fruit filling period, and white ripening period is about 73% (Bian et al., 2018). Fertilization fractioning is usually adopted for jujube. It is recommended that jujube trees are fertilized once in the emergence and new shoots periods (3/15 of the total fertilization), fertilized twice in the flowering period (4/15), fertilized twice during the fruit filling period (4/15), and fertilized twice in the white ripening period (4/15), and no fertilization is recommended during the red ripening period (Bian et al. 2018). The total amount and number of irrigation and fertilization shows greater variability based on meteorological and soil structural properties.

3. Research data

The structure of the research data set is depicted in Figure 2–8, including data from detailed field experiments, observations of local orchards, and remote sensing data.

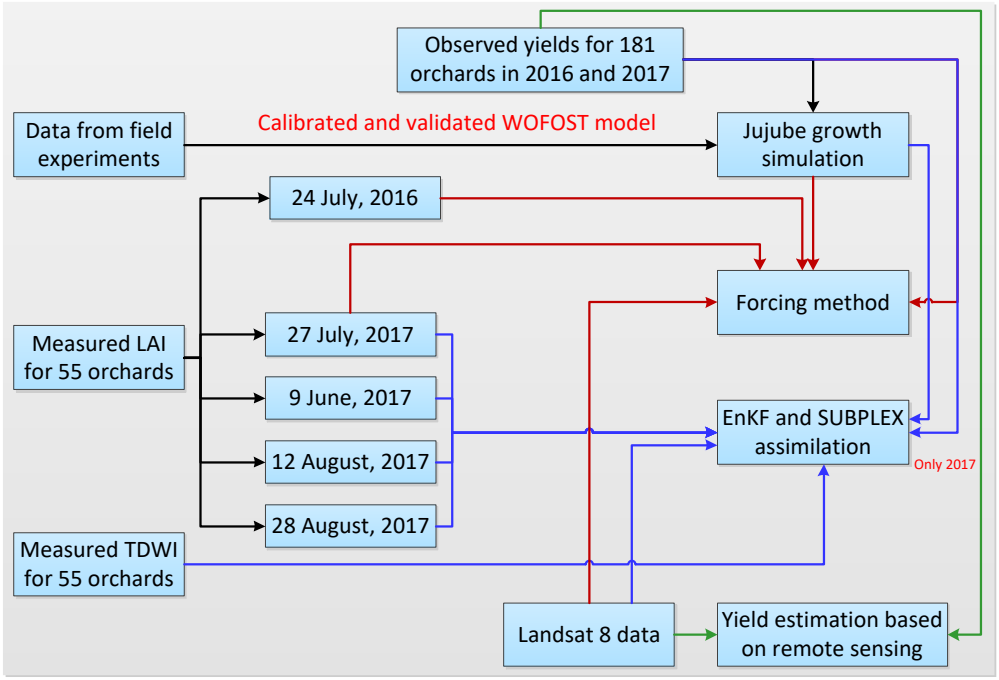

Figure 2–8: Data structure of this thesis.

3.1. Field experiments and data collection

3.1.1. Field experiment design

The WOFOST model is mainly run in two modes: potential and water-limited production. We calibrated the WOFOST model for potential mode, considering two reasons. The first reason is that the water-limited production of the WOFOST model expresses the maximum yield under rain-fed conditions, with no yield losses caused by other factors (de Wit et al., 2019). In our research area, there is very little rainfall, and the water requirement for jujube growth depends mainly on irrigation, which is managed by the local agricultural department. Therefore, the local jujube trees shall be not a complete rain-fed crops. The second reason is that irrigation time and irrigation data for each local orchard are also difficult to obtain. The unknown irrigation information may cause the uncertainty of the water-limited simulation mode.

In practice, potential yield levels can only be realized with a suitable input of fertilizers, an appropriate level of irrigation and a thorough pest and weed control (de Wit et al., 2019). In addition, there should be no damage to the crop or loss by other factors, such wind, hail, frosts. Of course, it is difficult to fully realize the potential production, but near to the potential production line can be found in well-kept trials, for example, some cultivated land and grass farms in Western Europe have achieved close to potential yield levels (de Wit 2019b).

In order to calibrate the WOFOST model for potential simulation, field experiments were conducted in two jujube orchards located in the district of Alaer in Xinjiang, China (Tarim University Jujube Research and Experiment Base), during the growing seasons of 2016–2018 (81°13'2"E, 40°34'45"N) (Figure 2–1, red circle). We chose two orchards to perform three years of experiments to avoid natural disasters or other factors that could cause the destruction of orchard trees. The soil properties of the two orchards are not much different due to their close proximity. The jujube trees were all planted in 2009, with a planting density of about 6165 trees per hectare, and a small canopy permanent line shape was used for the pruning. We chose field sites where the jujube grew evenly to carry out experiments. The amount of chemical fertilizer used referred to empirical values, which usually produces the highest yields in our experimental and local area. The difference between potential and water-limited production shows that irrigation can improve yield (de Wit 2019). Therefore, well-managed irrigation is helpful to bring the simulation closer to potential production. In our experiments, the amount and frequency of irrigation was determined based on the measured soil moisture content and the soil moisture content at field capacity. Pests and diseases were effectively controlled through standard management. The detailed fertilization and irrigation scheme was as follows:

- The amount of fertilizer applied was empirically based on historical research (BAI et al., 2019). During each jujube growing season (2016 to 2018), the fertilization amounts of converted pure nitrogen (N), phosphorus pentoxide (P_2O_5), and potassium oxide (K_2O) were 375, 240, and 300 kg ha^{-1}, respectively. A first pour of the fertilizer was spread by drip irrigation during the emergence and flowering periods (N: 50%, P_2O_5: 80%, and K_2O: 70%), and the rest of the fertilizer was applied in the fruit filling and early ripening period (N: 50%, P_2O_5: 20%, and K_2O: 30%). The chemical fertilizer was divided into seven separate fertilizations, these were applied on 8 May (emergence period), 6 June (new shoot growth period), 23 June (flowering period), 3 July (flowering period), 14 July (fruit setting period), 29 July (fruit filling period), and 11 August (fruit ripening period),.
- Irrigation experiments, with three replicates; the jujube tree was irrigated about 10 times during the main development stages (from early May to mid-August). The measured soil moisture content at field capacity (FC) was set as the lower irrigation limit control index. Soil moisture content was measured weekly. When the measured average water content was lower than the lowest limit with 65% of FC (that is, the minimum irrigation amount to ensure the yield and quality of jujube fruits) (Zheng et al., 2014), irrigation was performed with a 45 mm quota per irrigation.

3.1.2. Field data measurement and observation

Emergence, flowering (fruit set), and maturity dates were recorded. Total above-ground biomass (TAGP, the dry weight of living leaves, stems, and storage organs) and LAI during the growth period were measured approximately ten times at each sub-field experimental site. For both fields, ten trees were randomly selected, and one quarter of the stems, leaves, and fruits of each tree were brought back to the laboratory and weighed after drying at 85°C to a constant weight. The yield of the sampled loss was added to the final yield at each site (almost 411 trees per site). LAI in the experimental area was measured ten times using a scanning method. The collected

leaves were spread on A4 white paper sheets and scanned as an image file. LAI was calculated using the LA-S Plant canopy analysis system software (WSeen, Hangzhou, China). Extinction coefficients for diffuse visible light were measured using a fruit tree canopy analyser (TOP−1300, Zhejiang Top Cloud-Agri Technology Co., Ltd., China; Figure 2−9a)

CO_2 assimilation parameters, including light-use efficiency, and single leaf and maximum leaf CO_2 assimilation rates, were obtained by fitted light response curves (Ye and Yu, 2007) based on net photosynthetic rate data measured using a LI-COR 6400XT meter.

Jujube trees differ from annual crops; if the stems of the previous year are considered this can lead to exaggerated TDWI values. In this research, TDWI at emergence was redefined as the weight of the initial new organs (initial buds and roots), which was calculated by measuring the dry weight of buds and roots. The depth and weight of the roots were sampled by digging a profile and measuring it in the lab (Figure 2−9b).

For weather data, daily maximum and minimum temperatures, solar radiation, wind speed at 2 m high, actual vapour pressure, and precipitation were observed using an automatic weather station situated 500 m from the field experiments.

Figure 2–9: (a) Leaf area index (LAI) and canopy parameter measurement, (b) root depth and weight measurement.

3.2. Observations from local orchards

3.2.1. Observed yield data

In order to verify the yield estimation performance of the proposed method, the yields of 181 orchards managed by independent farmers were manually measured after harvesting at the beginning of November, see Figure 2–10. The spatial

distribution of the 181 orchards is shown in Figure 2–1 (pink marks). We selected 181 orchards with almost identical tree shapes (small canopy permanent line) for the study to avoid the effects of pruning on assimilation parameters. The 2016 jujube fruit yield ranged from 3.51 to 9.43 t ha^{-1}, with an average of 6.57 t ha^{-1} and SD (standard deviation) of 1.21 t ha^{-1}. The 2017 yield ranged from 4.79 to 10.75 t ha^{-1}, with an average of 7.74 t ha^{-1} and SD of 1.36 t ha^{-1}. The average yield in 2017 was higher than 2016. The first reason may be that the temperature in 2016 was higher than that in 2017, which caused a short dry matter accumulation time. The second reason may be that the average age of jujube trees in 2016 was less than 2017.

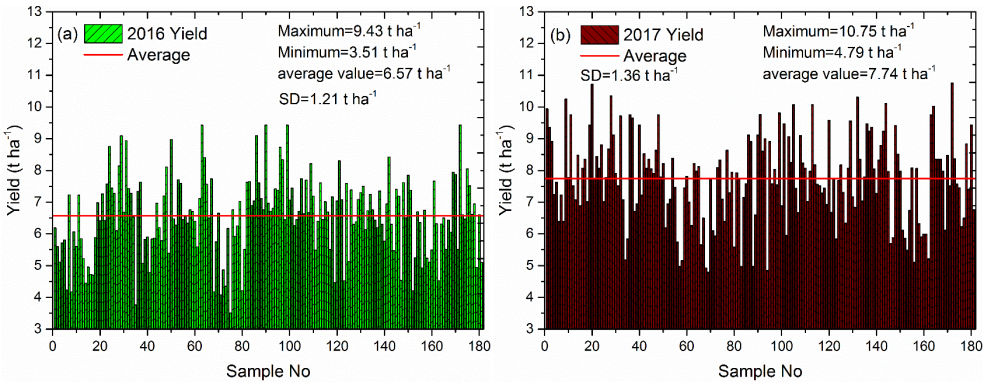

Figure 2–10: Yields (dry weight) of 181 in situ sampled orchards in 2016 (a) and 2017 (b).

3.2.2. Observed TDWI and LAI data

The observed TDWI and LAI are shown in green in Figure 2–1. It was difficult to measure LAIs for all 181 orchards on the day of the satellite coverage. In order to meet the requirements of timeliness, 55 orchards among the 181 orchards observed in 2016 and 2017 were chosen to measure two key parameters, including TDWI at the true emergence and LAI when the Landsat 8 satellite covered the study area. The centre and edge positions of each orchard were recorded using the Global Positioning System so that they could be georeferenced to the Landsat 8 remote sensing images. The time when the fifth leaf on the bud was unfolded was defined as the time of emergence. The total bud weight for an orchard was calculated by taking the measured average bud weight of nine relatively homogeneous trees multiplied by the planting density. Then, TDWI values for different orchards were calculated by measuring the dry weight of buds at each orchard and distribution coefficient from the field experiment (fixed value: 70% for buds).

LAI values on 24 July 2016 were used in this study because on this day the Landsat 8 satellite covered the study area and it was near to the maximum LAI development stages. In 2017, LAI was monitored four times during the main growth season, which was employed to establish and validate the LAI inversion model based on the remotely sensed vegetation index. In order to coincide with the time frequency of the Landsat satellite, LAI was measured on the same day when the satellite covered the study area

during four major developmental stages, including emergence, flowering, white maturity, and red maturity. For LAI measurement of 55 orchards, a fruit tree canopy analyser (TOP-1300, Zhejiang Top Cloud-Agri Technology Co., Ltd., China) calibrated by scanning method was used to quickly measure LAI to ensure real-time measurements. Each sampled plot (orchard) consisted of four relatively homogeneous subplots (30 m × 30 m) (Huang et al., 2015). LAI was measured for six 5 m × 5 m areas uniformly distributed within each subplot. Average LAI values from the four subplots were calculated to represent the unique LAI value in each orchard. Observed LAI values for 55 orchards are shown in Table 2–2.

Table 2–2: Observed Leaf Area Indices for 55 orchards.

Year	Sample Date	MAX	MIN	Average	STDEV
2016	24 July	2.36	0.96	1.61	0.36
2017	9 June	0.78	0.27	0.46	0.12
	27 July	2.51	1.03	1.76	0.37
	12 August	2.43	0.89	1.70	0.40
	28 August	2.35	0.81	1.62	0.41

3.3. Remote sensing data

For field and local scale yield estimation, both Landsat and Sentinel satellites with medium and high spatial resolution are commonly used data sources. In our research, one Landsat image can cover the entire study area but the same area is covered by four Sentinel 2 satellite images, so synthesis is required. In addition, Sentinel 2B satellite data was not available for the main growing seasons of jujube trees in 2016 and 2017. The available Landsat 8 and Sentinel 2 satellite data during the main growth period of jujube trees are shown in Table 2–3. Although the Sentinel 2A with 10 m spatial resolution is higher than the 30 m spatial resolution of Landsat 8, considering the amount of valid data and image synthesis error, Landsat 8 was selected.

Table 2–3: Available remote sensing data for this research

Year	Landsat 8		Sentinel-2A	
	Date	Amount of images needed	Date	Amount of images needed
2016	21 May	1	3 August	4
	8 July	1		
	24 July	1	23 August	4
	9 August	1		
2017	24 May	1	20 May	4
	9 June	1	/	/
	27 July	1	19 July	4
	12 August	1	8 August	4
	28 August	1	28 August	4
	13 September	1	/	/

Band 4 (red, 0.630–0.680 μm) and 5 (near-infrared, 0.845–0.885μm) from the Operational Land Imager (OLI) of the available Landsat 8 remote sensing images were used in this study for vegetation index extraction, including Normalized Difference Vegetation Index (NDVI), Soil-adjusted Vegetation Index (SAVI), Enhanced Vegetation Index (EVI), and Normalized Difference Water Index (NDWI).

4. Research methodology

The main research strategy of this thesis is shown Figure 2–11.

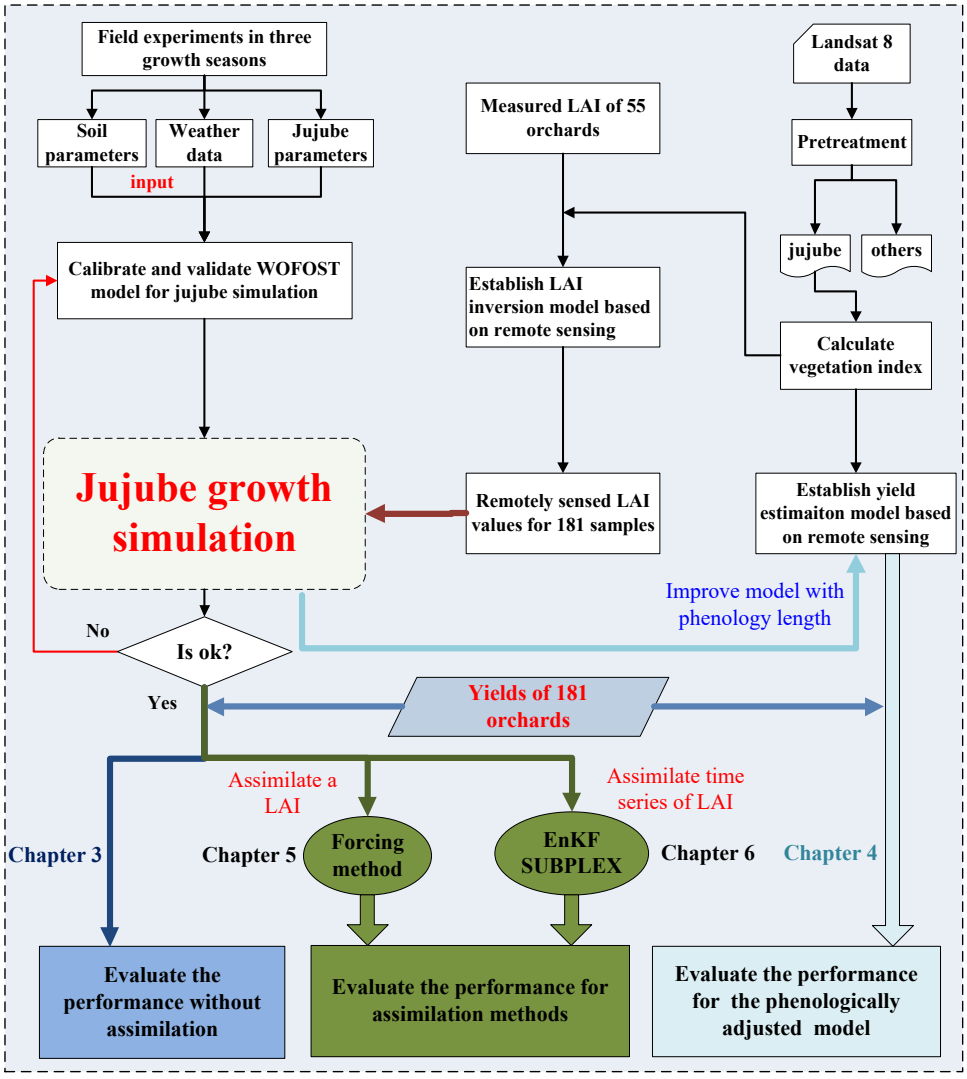

Figure 2–11: Main research strategy for this thesis.

First, the crop data files used to run the WOFOST model were recalibrated based on the field-scale experimental data set. The input crop parameters, including phenology, initial, green area, CO_2 assimilation, conversion of assimilates into biomass, maintenance respiration and biomass partitioning, were adjusted until a satisfactory biomass and LAI output were obtained to simulate jujube growth. Second, regression equations between LAI and remote sensing vegetation indices were established based on field-observed orchards to estimate the LAI values of 181 orchards. Third, the vegetation index obtained from Landsat 8 remote sensing data was used directly to estimate yield and attempts were made to improve the regression model using calculated phenological length based on the WOFOST model. Fourth, a forced method was attempted to assimilate a single remotely sensed LAI into the WOFOST model to improve yield estimation. Fifth, a SUBPLEX assimilation framework was established, and the EnKF and SUBPLEX methods were performed to assimilate the four periods of remotely sensed LAI into the calibrated WOFOST model. Finally, yield data from 181 jujube orchards were employed to evaluate the field-scale yield estimation performance of different methods, and the application limitations and advantages of the different methods were compared and discussed.

According to the research objectives of this thesis, the following special research methods are also addressed.

In Chapter 3, the crop data files used to run the WOFOST model were recalibrated based on a field-scale experimental data set. The daily average temperature measured from the local weather station and the observed emergence, flowering, and maturity dates were used to adapt the phenological parameters of the model. This includes the temperature sum from beginning to emergence (TSUMEM), the temperature sum from emergence to anthesis (flowering) (TSUM1), and the temperature sum from anthesis to maturity (TSUM2). The dry weights of leaves, stems, fruits, and above-ground biomass measured in the field experiments were mainly used to adapt the partitioning parameters such as the fraction of above-ground dry matter to leaves (FLTB), the fraction of above-ground dry matter to stems (FSTB), and the fraction of above-ground dry matter to storage organs (FOTB). The measured photosynthesis parameters were primarily used to calculate the assimilation parameters such as the light-use efficiency of a single leaf at average temperature (EFFTB) and the maximum leaf CO_2 assimilation rate (AMAXTB). The measured leaf area and leaf dry weight were used to calculate the initialization and green area parameters such as the leaf area index at emergence (LAIEM), the maximum relative increase in LAI (RGRLAI), and the specific leaf area (SLATB). Finally, the dry weight of living leaves (WLV), the dry weight of living stems (WST), the dry weight of living storage organs (WSO), TAGP (dry weight of total aboveground biomass), and LAI (leaf area index) were used to validate the performance of the parameter adaptation. The RMSE values of the simulation results for WLV, WST, WSO, TAGP, and LAI versus measured values were minimized by fine-tuning the crop parameters. The measured and observed soil and meteorological data files were imported directly into the WOFOST model. A method considering tree ages and planting densities was explored by redefining and calculating TDWI. Then, yields of 181 orchards were used to validate the performance

of field-scale yield estimation based on the calibrated WOFOST model without assimilation.

In Chapter 4, the potential of using spectral information from Landsat 8 for estimating jujube fruit yield at the field scale is evaluated. The optimal phenology time for determining a reliable jujube fruit yield estimation was determined, and the performance of different vegetation indices (VIs) for yield estimation were also compared. The key content is the exploration of an approach that uses the phenology length of growth period to improve a remote sensing-based yield estimation model. The correlations between VIs, including NDVI, SAVI, NDWI, and EVI, obtained from Landsat 8 data during the main growing period and jujube fruit yields were analysed to determine the best modelling time and VI. The phenological development time (flowering to maturity) calculated using the WOFOST model was used to correct the remote sensing-based VI yield model. The estimation accuracy was cross-validated using the observed yield data of 181 orchards.

In Chapter 5, we explored whether a single LAI (near to the maximum vegetative development stages) obtained from Landsat 8 can improve the yield simulation accuracy. The assimilation performance was evaluated by comparing the yield estimation results before and after forcing LAI. First, the regression equations between vegetation index and LAI were established based on 55 observed orchards. Second, the state variable of each orchard, here the LAI which was re-estimated by forcing the remotely sensed LAI, was input into the calibrated WOFOST model to simulate jujube fruit yield. Finally, in situ yield data for 181 orchards were employed to evaluate the performance of the forcing assimilation method.

In Chapter 6, in order to complete the SUBPLEX assimilation, the four periods of LAIs for 55 orchards during the main growing season were first inverted from remote sensing data. SUBPLEX obtained an optimal set of TDWI and SPAN values by iteratively calculating the minimum objective function values of the four remotely sensed and the simulated LAIs during the main growth stages, thereby achieving yield estimation based on the SUBPLEX assimilation method. EnKF assimilation was also performed; EnKF updates a new set of TDWI and SPAN values when acquiring a new remote sensing observation to implement a segmentation simulation. Finally, the yield estimation accuracy of the proposed SUBPLEX assimilation method was compared with the EnKF method.

5. References

Bai, T., Zhang, N., Chen, Y., Mercatoris, B. 2019. Assessing the performance of the WOFOST model in simulating jujube fruit tree growth under different irrigation regimes. Sustainability, 11, 1466. doi.org/10.3390/su11051466

Bian, Q., Wang, Z., Hu, J., He, X., Li, C., 2018. Effects of water and fertilizer supply on physiology, growth and yield of drip-irrigation jujube in the southern Xinjiang sandy area. Agricultural Research in the Arid Areas. 36(4):165-170. (In Chinese with English abstract)

de Wit, A., Boogaard, H., Fumagalli, D., Janssen, S., Knapen, R., van Kraalingen, D., Supit, I., van der Wijngaart, R., van Diepen, K. 2019. 25 Years of the WOFOST cropping systems model. *Agricultural Systems*, 168, 154–167. doi:10.1016/j.agsy.2018.06.018.

Huang, J., Tian, L., Liang, S., Ma, H., Becker-Reshef, I., Huang, Y., Su, W., Zhang, X., Zhu, D., Wu, W., 2015. Improving winter wheat yield estimation by assimilation of the leaf area index from Landsat TM and MODIS data into the WOFOST model. Agric. For. Meteorol. 204, 106–121. https://doi.org/10.1016/j.agrformet.2015.02.001

Hernández, F.C.A., Legua, P., Melgarejo, P., Martínez, R., Martínez, J.J., 2015. Phenological growth stages of jujube tree (Ziziphus jujube): Codification and description according to the BBCH scale. Ann. Appl. Biol. 166, 136–142. https://doi.org/10.1111/aab.12169

Kerimu, A., Meng, F., Nu' erpatiman, M., Patima, A., 2018. Jujube in Kashgar: Planting Meteorological Condition Analysis and Climate Quality Certification. Chinese Agricultural Science Bulletin. 34(31): 119-124. (In Chinese with English abstract)

Ye, Z., Yu, Q. 2007. Comparison of a new model of light response of photosynthesis with traditional models. Journal of Shenyang Agricultural University. 38, 771–775. (In Chinese with English abstract)

Zhang, Q., Bai, T., Wu, C., Wang, H., Liu, J., and Dang, X., 2013. Investigation on Yield and Quality of Different Tree Shapes in Direct Seeding and Orchard Construction. Northern Horticulture. 4, 18–23. (In Chinese with English abstract)

Zheng, Q., Chen, Q., Li, M., and Wang, J., 2014. Effect of Irrigation Volume on Fruit Yield and Quality of Jun-jujube under Drip Irrigation in Arid Desert Area. Xinjiang Agricultural Sciences. 51(2): 250–256. (In Chinese with English abstract)

Chapter 3

Growth simulation and yield estimation for perennial jujube fruit tree based on the WOFOST model

Crop growth modelling can be considered as one of the main methods for crop yield estimation. This chapter, which lays the foundation of this doctoral thesis, describes the implementation of a potential growth simulation of jujube trees by means of WOFOST model, including detailed parameters calibration and validation procedures. More particularly, it is explained how the perennial nature of the studied crop is accounted for in the model initially designed for annual crops. The performances of the new calibrated crop model to estimate field-scale jujube fruit yield are assessed against local 181 orchards.

*This chapter is based on: Tiecheng Bai, Tao Wang, Nannan Zhang, Youqi Chen * and Benoit Mercatoris *, 2020. Growth simulation and yield prediction for perennial jujube fruit tree by integrating age into the WOFOST model. Journal of Integrative Agriculture. 19(3): 721-734.*
** Corresponding Author.*

1. Abstract

Mathematical models have been widely employed for the simulation of growth dynamics of annual crops, thereby performing yield estimation. Their use remains limited however for fruit tree species such as the jujube tree. The objectives of this study were to investigate the potential use of a calibrated WOFOST (World Food Studies) model for estimating jujube yield. The model was established using data collected from dedicated field experiments performed in 2016–2018. Simulated growth dynamics of leaves, stems, fruits, total biomass, and leaf area index (LAI) agreed well with measured values, showing RMSE values of 0.14, 0.33, 0.37, 0.62 t ha^{-1} and 0.19 m^2 m^{-2}, and R^2 values of 0.95, 0.98, 0.99, 0.99, and 0.95, respectively. The validated errors of –2, –3, and –3 days were detected in different phenological development stages corresponding to emergence, anthesis, and maturity. In addition, in order to estimate the yields of trees of different ages, the weight of new organs (initial buds and roots) in each growing season was introduced as the initial total dry weight (TDWI), which was calculated as averaged values of trees of the same age. The results showed that R^2 and RMSE for field-scale yield estimation were 0.22 and 1.07 t ha^{-1} for 2016, and 0.04 and 1.33 t ha^{-1} for 2017, respectively. This method still suffers from uncertainty. Enhancement could be achieved by considering the influence of crop management on CO_2 assimilation or by assimilating remote sensing data during the growing season.

2. Introduction

Field-scale yield monitoring is important for precision agricultural management. Most prediction methods for fruit yield still depend on conventional techniques based, for instance, on agro-meteorological models and empirical statistical regressions between spectral vegetation indices and in-field measured yields (Ye et al., 2006; Zaman et al., 2006; Aggelopoulou et al., 2011; Zhou et al., 2012; Sun et al., 2017; Rahman et al., 2018; Bai et al., 2019a). One of the main drawbacks of such empirical approaches is that they are only validated for specific cultivars, growth stages, or certain geographical regions (Huang et al., 2015b). In contrast, cropping system modelling based on mathematical descriptions of key physical and physiological processes is considered to be a mature technology (Holzworth et al., 2014b) and has been applied in precision farming to increase the understanding of crop responses in field trials (Asseng et al., 2013; Ewert et al., 2015; de Wit et al., 2019a). Such modelling allows better consideration of the complex interactions between plants, weather, soil, and agricultural practices (de Wit et al., 2019a).

In recent decades, many crop models have been developed and optimized for different species and purposes. Some notable examples include WOFOST (World Food Studies) (van Diepen et al., 1989), DSSAT (Decision Support System for Agrotechnology Transfer) (Jones et al., 2003), EPIC (Environmental Policy Integrated Climate) (Wang et al., 2012), STICS (Multidisciplinary simulator for standard crops) (Brisson et al., 2003), and APSIM (Agricultural Production Systems simulator) (Holzworth et al., 2014a). Among them, the WOFOST model was

developed for the quantitative analysis of the growth and production of annual field crops. It has been applied to the study of climate change effects (Alexandrov et al., 2005; Reidsma et al., 2009, 2015; Kroes et al., 2011; Van Walsum et al., 2012; Supit I et al., 2012; Blanco et al., 2017; Gilardelli et al., 2018), regional yield forecasting and analysis (Rötter R et al., 1997; Supit I et al., 1997; Dobermann et al., 2000; de Wit et al., 2010; Wolf J. et al., 2011; Huang et al., 2015 a, b, 2016, 2019; Cheng et al., 2016; Ceglar et al., 2019; Zhuo et al., 2019), and the comparison of different irrigation and soil conditions (Eitzinger et al., 2004; Confalonieri et al., 2009; Todorovic et al., 2009). It can explain plant growth by using light interception and CO_2 assimilation as the growth-driving processes, and includes photosynthesis, respiration, and their changes due to environmental conditions (de Wit et al., 2005). WOFOST has also been optimized and validated over 25 years by countless researchers all over the world and used for many new crops over a broad range of climatic and management conditions (de Wit et al., 2019a). The WOFOST model can be implemented in two different ways: potential production, where crop growth is determined by irradiation, temperature, and plant characteristics only; and water-limited production, where crop growth is limited by water use. Such a crop model can be enriched by remote sensing assimilation data in order to solve scale problems and reduce uncertainties for regional yield forecasting (de Wit et al., 2007, 2008, 2012; Curnel et al., 2011; Ma et al., 2013; Tripathy et al., 2013; Liu et al., 2015; Huang et al., 2019; Zhuo et al., 2019).

Crop modelling reported in the literature has mainly been developed for annual crops, including spring barley, cotton, maize, millet, potato, rice, sorghum, soybean, sugar beet, sweet potato, and winter wheat. Few studies have focused on perennial fruit trees. In Xinjiang, jujube trees are densely planted in orchards. An existing study has confirmed that the WOFOST model can be used to simulate jujube growth in field experiments (Bai et al., 2019b). However, the yield of such a perennial crop sharply increases with tree age because of the continuous evolution of branches, canopy width, tree height, and leaf area index (He et al., 2010). This evolution is mainly reflected in the difference of the initial total dry weight (TDWI), which is directly dependent on tree age. In addition, excessive TDWI values will inevitably result in overestimation of the simulation results if the weight of the jujube tree's main stems and branches are simply added up, therefore, the TDWI parameter was redefined for accurate jujube fruit growth modelling. The aim of this study was to develop and evaluate an approach for fruit tree growth dynamic simulation and yield estimation, by integrating the tree age into the WOFOST model. To reach this goal, the following specific objectives were defined:

(i) To explore the methods for growth simulation and yield estimation of perennial jujube trees by redefining TDWI.

(ii) To evaluate whether the calibrated WOFOST model can be employed to accurately simulate the jujube development from the phenological development stages and growth dynamics of different organs in specific field experiments.

(iii) To validate the accuracy of field-scale fruit yield estimation.

3. Research data and methods

3.1. Field experiment and research data

Field experiment and data collection are described in Section 3.1 of Chapter 2. Field-measured emergence, flowering, and maturity dates and observed daily temperatures were used to calibrate and validate the phenology parameters of the WOFOST model. Total above-ground biomass (TAGP), the dry weight of living leaves, stems, and fruit, and LAI during the growth period were used to calibrate and validate the crop parameters. Observed climate data were used to drive the model. Data obtained in 2016 and 2017 were employed to calibrate the model, whereas data obtained in 2018 were used for model validation.

Observed local yield data for 181 orchards were used to evaluate the yield estimation performance of the calibrated WOFOST model at the field scale, see Section 3.2 of Chapter 2.

3.2. Redefinition and calculation of TDWI parameter

TDWI was redefined as the weight of the initial new organs (initial buds and roots) during each growing season. The initial weight of buds can be calculated by multiplying the planting density by the average weight of buds retained on a sample of trees. TDWI of the field experiments is equal to the sum of the dry weight of the buds and the roots at the time of emergence, defined as the time when the fifth leaf on the bud was unfolded (DVS=0). The ratio of the average dry weight of buds and roots measured in the field experiment is approximately 7:3. Root measurement is very difficult, so it is only measured in our field experiments as a fixed value for other orchards. TDWI values for different orchards were then calculated by measuring the dry weight of buds at each orchard and the bud-root distribution coefficient from the field experiments.

Based on experimental observations, the TDWI value of each orchard was mainly affected by the tree age. The average TDWI of each tree gradually increased with the tree age, and remained basically unchanged when the tree age was greater than 10. The TDWI values were measured in 55 orchards between 2015 and 2017. The average TDWI for 3 to 10 year-old jujube orchards were 4.88, 6.24, 9.24, 13.17, 14.28, 16.31, 19.73, and 21.61 kg ha^{-1}, for each year of increasing age respectively.

3.3. Calibration of WOFOST model

Jujube crop parameters were calibrated for the potential growth simulation from the 2016 and 2017 experiments according to the principle of average correlation and error minimization. The 2018 season data were used to validate the TAGP and LAI growth dynamics.

The calibration process of the WOFOST model was suggested in de Wit and Wolf (2010). First, the length of the growth period and the phenology can be effectively simulated for a reliable biomass and yield estimation, which was determined by the effective accumulated temperature method (van Diepen et al., 1989). TBASEM expressing the lower threshold temperature at which jujube trees begin to develop,

was set to 10°C (Sun, 2019). TEFFMX, defining the maximum effective temperature at emergence, ranged from 18 to 32 °C as given by WOFOST. The observation results show that jujube trees were sprouting normally, so the correction principle of this parameter was not to affect the growth of jujube trees during the growing season. The simulation results of TAGP and LAI of different TEFFMX in 2016 and 2017 showed that when TEFFMX was greater than 21 °C, the simulation results of TAGP and LAI were almost unchanged, see Fig. 3-1. Therefore, TEFFMX can be set to any value from 21 °C to 32 °C (default maximum value from WOFOST). TEFFMX was set to 30 °C in this study referring to the default value of most crops from WOFOST model.

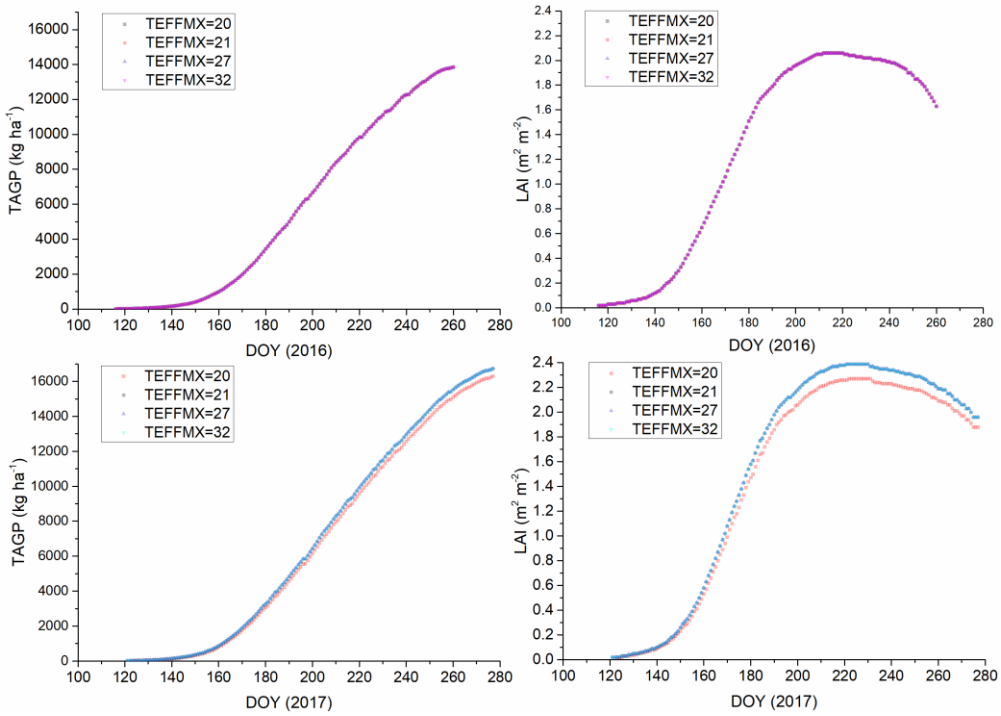

Figure 3–1: Comparison of TAGP and LAI simulation results based on different TEFFMX

TSUMEM (temperature sum from beginning to emergence), TSUM1 (temperature sum from emergence to flowering), and TSUM2 (temperature sum from flowing to maturity) were calibrated by daily average temperature and emergence, flowering, and maturity dates for the years 2016 and 2017. The DTSMTB (daily increase in temperature sum as a function of average temperature) can be calculated from the maximum suitable temperature (35.5°C; Wang et al., 2002) and minimum development temperature (10°C; Sun, 2019). TDWI was equal to the field measurement.

For LAIEM (LAI at emergence), the measured maximum value in all field experiments was less than 0.004 ha ha^{-1}, so LAIEM was set to 0.004 ha ha^{-1}. For RGRLAI (maximum relative increase in LAI), the measured maximum value was less

than 0.05, so RGRLAI was set to 0.05. SLATB (specific leaf area) was calibrated on the basis of the measured values and simulated TAGP and LAI. SPAN (life span of leaves growing at 35°C) was corrected based on LAI measured in the field during the late growing season.

Light interception and potential biomass production were mainly determined by leaf-related (SLATB, LAIEM, and RGRLAI) and CO_2 assimilation parameters. For CO_2 assimilation parameter calibration, first the daily gross CO_2-assimilation rate was calculated from the absorbed radiation and the photosynthesis-light response curve of individual leaves. Net photosynthetic rate was measured using a LI-COR 6400XT. The light response curve at 35.5°C that was fitted by a rectangular hyperbolic correction model (Ye and Yu et al., 2007) was constructed for jujube leaves (Equations (3–1) and (3–2), Figure 3–2).

$$P_n = \alpha \frac{1 - \beta \times PAR}{1 + \gamma i} PAR - R_d \qquad (3-1)$$

$$A_{max} = \alpha \left(\frac{\sqrt{\beta + \gamma} - \sqrt{\beta}}{\gamma} \right)^2 - R_d \qquad (3-2)$$

Where P_n is the net CO_2 assimilation rate, α is the efficiency of initial light use, β and γ are the fitting coefficients, PAR is the photosynthetic active radiation, and R_d is the respiration rate in the dark. In this study, $\alpha = 0.495$, $\beta = 0.000548$, $\gamma = 0.007887$, and $R_d = 2.423$.

It was confirmed that the fitted results of the rectangular hyperbolic correction model with the minimum RMSE (0.63 kg ha^{-1} h^{-1}) and almost ideal R^2 (0.998) were superior to those from either rectangular hyperbola (Baly et al., 1935; RMSE = 0.997 kg ha^{-1} h^{-1}), non-rectangular hyperbola (Thornley et al., 1976; RMSE = 0.828 kg ha^{-1} h^{-1}), or exponential equations (RMSE = 1.102 kg ha^{-1} h^{-1}). The main CO_2 assimilation parameters characterizing this curve included the initial light use efficiency, $\alpha = 0.495$; the respiration rate in the dark, R_d = 2.42; and the maximum rate of net CO_2 assimilation at high light intensity, A_{max}= 34.85. Values of α, A_{max}, and R_d at 19.5°C could also be attained in the same way. As assimilation and respiration proceed concurrently, the measured value represents the net assimilation rate, which is the difference between assimilation and respiration. Thus, to obtain the maximum CO_2 assimilation rate (AMAXTB), the measured value should be implicitly augmented by the value of the dark respiration, which assumes that it had the same rate compared to the light respiration (van Diepen et al., 1989). AMAXTB and EFFTB (light-use efficiency single leaf at average temperature) were calculated. Second, the correction factor TMPFTB was determined by the average day-time temperature and is also crop specific (de Wit et al., 2019b). Jujube trees begin to develop when the temperature is greater than 10°C. The optimal temperature for jujube development is between 19.5 to 35.5°C. Therefore, TMPFTB was set to 0, 1, and 1 when the day-time temperature was 10, 19.5, and 35.5°C, respectively. KDIFTB (extinction coefficient for diffuse visible light) was first set as a field measurement. Finally, KDIFTB,

AMAXTB, and EFFTB were calibrated on the basis of measured and simulated TAGP and LAI.

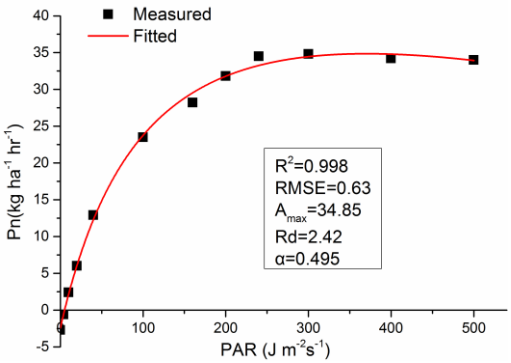

Figure 3–2: Light response curve of jujube leaf at 35.5°C

Conversion of assimilates into biomass expresses growth respiration, this includes CVL (efficiency of conversion into leaves), CVO (efficiency of conversion into storage organs), CVR (efficiency of conversion into roots), and CVS (efficiency of conversion into stems). Dry matter partitioning parameters, FRTB (fraction roots), FSTB (fraction stems), FOTB (fraction organs), and FLTB (fraction leaves), which all describe the fraction as a function of the development stage. They were calibrated using measured and simulated dry matter weights of above-ground organs. The maintenance respiration costs, Q10 (relative increase in respiration rate per 10°C temperature increase), RML (relative maintenance respiration rate of leaves), RMO (relative maintenance respiration rate of storage organs), RMR (relative maintenance respiration rate of roots), and RMS (relative maintenance respiration rate of stems), may be estimated on the basis of the quantities of proteins and minerals present in the biomass and on crop metabolic activity (de Wit et al., 2019b). RDRSTB (relative death rate of stems) was set to 0 because stems of perennial fruit trees usually do not die during development

The model evaluations were based on the comparison between simulated and observed data in 2018. The agreement between measured and simulated yield was quantified using a coefficient of determination (R^2). The root mean square error (RMSE) was used to evaluate simulation accuracy. R^2 can give the percentage of samples that can be interpreted by the model to all samples. The RMSE can show a weighted change in the error (residual) between the estimated and actual values. Due to the wide range of jujube yields, a normalized root mean square error (NRMSE, i.e., the ratio between RMSE and the average of observed values), and the ratio of performance to deviation (RPD) calculated as the ratio of the standard deviation of measured samples to the standard error of estimated values (Fleming et al., 2017), were determined as an additional evaluation of model utility. Their values were calculated by the Equations (3–3), (3–4), (3–5) and (3–6).

$$R^2 = 1 - \frac{\sum_{i=1}^{n}(y_i - \tilde{y}_i)^2}{\sum_{i=1}^{n}(y_i - \bar{y}_i)^2} \quad (3-3)$$

$$RMSE = \sqrt{\frac{\sum_{i=1}^{n}(\tilde{y}_i - y_i)^2}{n}} \quad (3-4)$$

$$NRMSE = \frac{\sqrt{\frac{\sum_{i=1}^{n}(\tilde{y}_i - y_i)^2}{n}}}{\bar{y}_i} \quad (3-5)$$

$$RPD = \frac{SD}{RMSE} \quad (3-6)$$

Where $\tilde{y}_i$ was the simulated value based on the model, y_i was the measured value, $\bar{y}_i$ was the mean of the measured values, and n was the number of samples. SD is the standard deviation of measured samples.

4. Results

4.1. Calibrated model parameters

The calibrated main parameters for the potential growth simulation are shown in Table 3−1.

Table 3–1: Calibrated model parameters.

Parameter	Description	Value	Units	Source
***Emergence**				
TBASEM	lower threshold temperature emergence	10	°C	(Sun, 2019)
TEFFMX	max. effective temperature emergence	30	°C	e
TSUMEM	temperature sum from sowing to emergence	230	°C	m-c
***Phenology parameter**				
TSUM1	temperature sum from emergence to anthesis	967	°C d^{-1}	m-c
TSUM2	temperature sum from anthesis to maturity	960	°C d^{-1}	m-c
DTSMTB0	daily increase in temperature sum as a function of average at = 0°C	0.00	°C d^{-1}	(Sun 2019)
DTSMTB100	daily increase in temperature sum as a function of average at = 10°C	0	°C d^{-1}	(Sun 2019)
DTSMTB355	daily increase in temperature sum as a function of average at = 35.5°C	25.5	°C d^{-1}	(Wang et al.,2002)
DTSMTB400	daily increase in temperature sum as a function of average at = 40°C	25.5	°C d^{-1}	(Wang et al.,2002)
***Initial parameters**				
TDWI	Redefined initial total emergence dry weight	\	kg ha^{-1}	m
LAIEM	leaf area index at emergence	0.004	ha ha^{-1}	m
RGRLAI	maximum relative increase in LAI	0.05	ha ha^{-1} d^{-1}	m
***Green area**				
SLATB000	specific leaf area when DVS = 0	0.00165	ha kg^{-1}	m-c
SLATB55	specific leaf area when DVS = 0.55	0.0013	ha kg^{-1}	m-c
SLATB100	specific leaf area when DVS = 1	0.0013	ha kg^{-1}	m-c
SLATB200	specific leaf area when DVS = 2	0.0014	ha kg^{-1}	m-c
SPAN	life span of leaves growing at 35 degrees Celsius	60	[d]	c
TBASE	lower threshold temp. for ageing of leaves	10	°C	(Sun, 2019)
***CO_2 assimilation**				
KDIFTB00	extinction coefficient for diffuse visible light at DVS = 0	0.8	\	m-c
KDIFTB200	extinction coefficient for diffuse visible light at DVS = 2	0.8	\	m-c
EFFTB19.5	light-use efficiency single leaf at average temp. = 19.5°C	0.495	kg ha^{-1} hr^{-1} J^{-1} m^2 s	m-c
EFFTB355	light-use efficiency single leaf at average temp. = 35.5°C	0.495	kg ha^{-1} hr^{-1} J^{-1} m^2 s	m-c
AMAXTB00	maximum leaf CO_2 assimilation. Rate at DVS = 0	39.0	kg ha^{-1} hr^{-1}	m-c
AMAXTB170	maximum leaf CO_2 assimilation. Rate at DVS = 1.7	39.0	kg ha^{-1} hr^{-1}	m-c

AMAXTB200	maximum leaf CO_2 assimilation. Rate at DVS = 2	20.0	kg ha^{-1} hr^{-1}	m-c
TMPFTB10	reduction factor of AMAX at 10°C	0	\	(Sun, 2019)
TMPFTB195	reduction factor of AMAX at 19.5°C	1	\	(Wang et al.,2002)
TMPFTB355	reduction factor of AMAX at 35.5°C	1	\	(Wang et al.,2002)
***Conversion of assimilates into biomass**				
CVL	efficiency of conversion into leaves	0.732	kg kg^{-1}	c
CVO	efficiency of conversion into storage organs	0.780	kg kg^{-1}	c
CVR	efficiency of conversion into roots	0.690	kg kg^{-1}	c
CVS	efficiency of conversion into stems	0.751	kg kg^{-1}	c
***Maintenance respiratio**n				
Q10	Relative increase in respiration rate per 10°C temperature increase	2	kg CH_2O kg^{-1} d^{-1}	m
RML	Relative maintenance respiration rate of leaves	0.03	kg CH_2O kg^{-1} d^{-1}	m
RMO	Relative maintenance respiration rate of storage organs	0.01	kg CH_2O kg^{-1} d^{-1}	m
RMR	Relative maintenance respiration rate of roots	0.01	kg CH_2O kg^{-1} d^{-1}	m
RMS	Relative maintenance respiration rate of stems	0.015	kg CH_2O kg^{-1} d^{-1}	m
***Partitioning parameters**				
FRTB00	fraction of total dry matter to roots at DVS = 0	0.3	kg kg^{-1}	m-c
FRTB154	fraction of total dry matter to roots at DVS = 1.54	0.0	kg kg^{-1}	m-c
FLTB00	fraction of above-ground dry matter to leaves at DVS = 0	0.67	kg kg^{-1}	m-c
FLTB012	fraction of above-ground dry matter to leaves at DVS = 0.12	0.31	kg kg^{-1}	m-c
FLTB022	fraction of above-ground dry matter to leaves at DVS = 0.22	0.41	kg kg^{-1}	m-c
FLTB032	fraction of above-ground dry matter to leaves at DVS = 0.32	0.55	kg kg^{-1}	m-c
FLTB051	fraction of above-ground dry matter to leaves at DVS = 0.51	0.4	kg kg^{-1}	m-c
FLTB097	fraction of above-ground dry matter to leaves at DVS = 0.97	0.15	kg kg^{-1}	m-c
FLTB100	fraction of above-ground dry matter to leaves at DVS = 1.00	0.1	kg kg^{-1}	m-c
FLTB145	fraction of above-ground dry matter to leaves at DVS = 1.45	0	kg kg^{-1}	m-c
FLTB200	fraction of above-ground dry matter to leaves at DVS = 2.00	0	kg kg^{-1}	m-c
FSTB00	fraction of above-ground dry matter to stems at DVS = 0	0.33	kg kg^{-1}	m-c

FSTB012	fraction of above-ground dry matter to stems at DVS = 0.12	0.69	kg kg^{-1}	m-c
FSTB022	fraction of above-ground dry matter to stems at DVS = 0.22	0.59	kg kg^{-1}	m-c
FSTB032	fraction of above-ground dry matter to stems at DVS = 0.32	0.45	kg kg^{-1}	m-c
FSTB051	fraction of above-ground dry matter to stems at DVS = 0.51	0.6	kg kg^{-1}	m-c
FSTB097	fraction of above-ground dry matter to stems at DVS = 0.97	0.85	kg kg^{-1}	m-c
FSTB100	fraction of above-ground dry matter to stems at DVS = 1.00	0.43	kg kg^{-1}	m-c
FSTB145	fraction of above-ground dry matter to stems at DVS = 1.45	0.2	kg kg^{-1}	m-c
FSTB200	fraction of above-ground dry matter to stems at DVS = 2.00	0	kg kg^{-1}	m-c
FOTB00	fraction of above-ground dry matter to storage organs at DVS = 0	0	kg kg^{-1}	m-c
FOTB012	fraction of above-ground dry matter to storage organs at DVS = 0.12	0	kg kg^{-1}	m-c
FOTB022	fraction of above-ground dry matter to storage organs at DVS = 0.22	0	kg kg^{-1}	m-c
FOTB032	fraction of above-ground dry matter to storage organs at DVS = 0.32	0	kg kg^{-1}	m-c
FOTB051	fraction of above-ground dry matter to storage organs at DVS = 0.51	0	kg kg^{-1}	m-c
FOTB097	fraction of above-ground dry matter to storage organs at DVS = 0.97	0	kg kg^{-1}	m-c
FOTB100	fraction of above-ground dry matter to storage organs at DVS = 1.00	0.47	kg kg^{-1}	m-c
FOTB145	fraction of above-ground dry matter to storage organs at DVS = 1.45	0.8	kg kg^{-1}	m-c
FOTB200	fraction of above-ground dry matter to storage organs at DVS = 2.00	1	kg kg^{-1}	m-c
***Death rates**				
RDRSTB00	Relative death rate of stems at DVS = 0	0	\	e
RDRSTB200	Relative death rate of stems at DVS = 2.0	0	\	e

Sources: e, estimated value from observed data and simulated results; m, measured; c, calibrated values based on simulated results; m–c, calibrated values on the basis of the measured values and simulated results; TDWI = 15.1 kg ha^{-1} for 2016, 17.2 kg ha^{-1} for 2017, and 19.4 kg ha^{-1} for 2018, respectively, with an increase in tree age. DVS: Development stages.

4.2. Validation of calibrated WOFOST model

4.2.1. Phenology development

The simulated time course of biomass production can be represented by three phases (Table 3–2) according to jujube growth characteristics. Field validation was employed to describe the errors of simulated emergence, anthesis (flowering), and maturity dates, which were –2, –3, and –3 days difference, respectively. In addition, the simulated length of the growth season was one day shorter than the measured value. Therefore, the model had gone through a number of phenological development stages, which serve as the controlling and steering mechanism for jujube growth.

Table 3–2: Validation of jujube development stages in 2018.

Activity	Emergence date	Anthesis date	Red maturity date
Simulation result	118th	193rd	264th
Validation result	120th	196th	267th
Difference	–2 days	–3 days	–3 days

4.2.2. Simulation of jujube growth dynamics

The indices of agreement between measured and simulated time series of WLV (dry weight of living leaves), WST (dry weight of living stems), WSO (dry weight of living storage organs), and TAGP (dry weight of total above-ground production) values are shown in Table 3–3. Calibrated and validated R^2 for WLV, WST, WSO, and TAGP ranged from 0.95 to 0.99, RMSE from 0.08 to 0.48 t ha^{-1} and 0.14 to 0.62 t ha^{-1}, respectively. Validated results showed that simulated dynamics for WLV, WST, WSO, and TAGP were accurately estimated with a RMSE of 0.14, 0.33, 0.37, 0.62 t ha^{-1} and a R^2 of 0.95, 0.98, 0.99, 0.99, respectively (Figure 3−2).

Table 3–3: Performances of the model in calibration and validation.

Year	Measured TDWI (kg ha^{-1})	R^2				RMSE (t ha^{-1})			
		WLV	WST	WSO	TAGP	WLV	WST	WSO	TAGP
Calibration									
2016	15.1	0.96	0.99	0.99	0.99	0.08	0.17	0.175	0.46
2017	17.2	0.95	0.96	0.99	0.99	0.12	0.36	0.23	0.48
Validation									
2018	19.4	0.95	0.98	0.99	0.99	0.14	0.33	0.37	0.62

Figure 3−3 also showed relative deviations of simulated and measured values, ranging from 0.03 to 0.63 for WLV, 0.05 to 0.76 for WST, 0.04 to 0.6 for WSO, and 0.02 to 0.72 for TAGP, respectively. Note that the first to fourth observations were slightly underestimated for the WLV, WST, and TAGP with high relative deviations. This bias could be attributed to a slightly lower fraction of above-ground dry matter to leaves. Therefore, the model generated a low LAI that resulted in a decrease in total photosynthesis accumulation in the early growth period. Overall, TAGP, WLV, WST, and WSO simulations are in good agreement with the measured values, see

Figure 3−2.

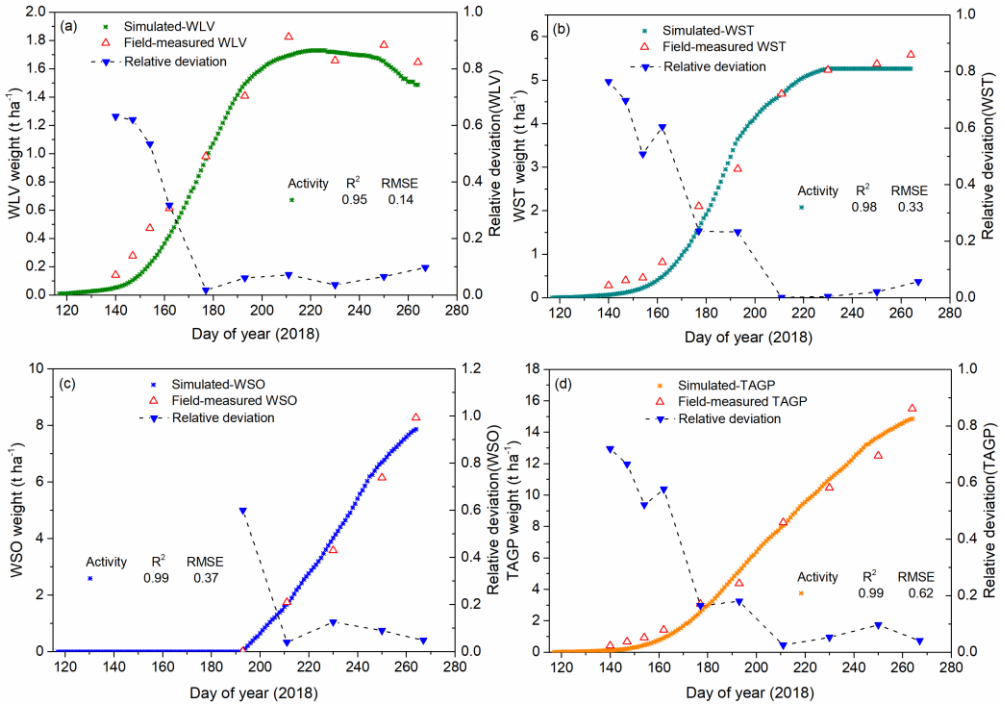

Figure 3−3: Simulated and measured the dry weight of organs in 2018. (a) Leaves, (b) stems, (c) storage organs, (d) total above-ground biomass. WLV: Living leaves, WST: Living stems, WSO: Living storage organs, TAGP: Total above-grund production.

LAI is an important output parameter which considerably affects photosynthesis and total biomass. Within the calibration datasets, the improved model showed a greater accuracy in simulating LAI values (calibrated R^2 = 0.98 for 2016, 0.96 for 2017, calibrated RMSE = 0.07 m^2 m^{-2} for 2016, 0.19 m^2 m^{-2} for 2017). Within the validation datasets, the model succeeded in reproducing timing variability for LAI in the total growth period, demonstrated by values of the agreement metrics (validated RMSE = 0.19 m^2 m^{-2} and R^2 = 0.95) (Figure 3−4). Therefore, this outcome allowed a realistic estimation of light interception and CO_2 assimilation during the main growth period. In addition, the simulated LAI change trend was in agreement with the observed time series of LAI of jujube trees. LAI conveyed an upward trend before the fruit white maturity period first, increasing slowly during emergence and rapidly from late May to early July, followed by slight decrease during the white maturity period, which peaked at the end of the fruit filling period.

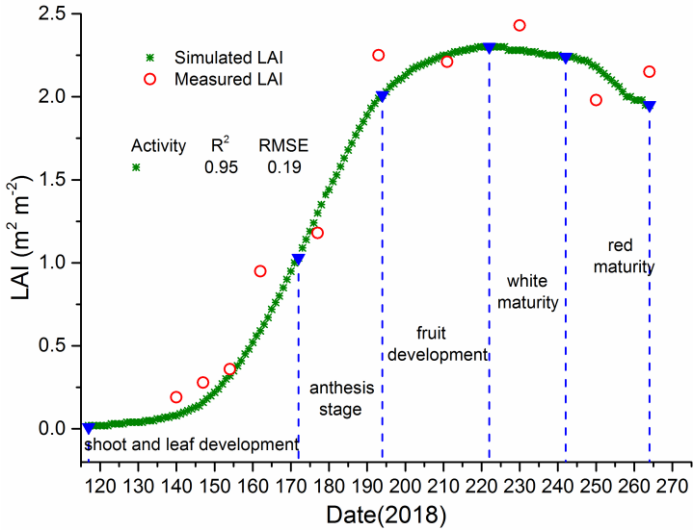

Figure 3–4: Simulated and measured LAI change trends.

4.2.3. Responses to temperature and radiation

The model allocated the produced biomass to the different organs depending on the phenological development stage. Temperature and radiation changes mainly affected the potential dry weight of different organs. Among them, temperature mainly affected the length of the growing season, including crucial growth duration between DVS = 0 and 1, and between DVS = 1 and 2 (Table 3–4), and radiation mainly affected total photosynthesis accumulation.

Table 3–4: Simulated development days, total above-ground biomass (TAGP), and yield for the nine-year-old jujube orchards

Year	Average R (kJ m^{-2} d^{-1}) DVS 0-2	Average T (°C) DVS 0-1	Days DVS 0-1	Average T (°C) DVS 1-2	Days DVS 1-2	Simulated TAGP (t ha^{-1})	Simulated yield (t ha^{-1})
2016	18875	23.8	71	23.2	73	13.61	7.34
2017	19683	23.9	71	21.2	85	16.48	9.32
2018	19516	22.9	75	23.5	71	15.14	7.95

R: represents radiation. T: represents temperature.

It should be noted that the temperatures in 2017 were slightly lower than those in 2016 and 2018, especially in the fruit filling period, so the longer growth period of 9-12 days resulted in higher potential WSO and TAGP. Although the time difference between the growth periods in 2016 and 2018 was only two days, the amount of radiation in 2018 (19516 kJ m^{-2} d^{-1}) was significantly higher than in 2016 (18875 kJ m^{-2} d^{-1}), which also resulted in a greater TAGP value and yield. Therefore, given that total biomass was determined by growth duration and daily assimilation,

the simulated yield in 2017 should be the highest, followed by 2018, and lastly 2016. Both observed and simulated results based on validation datasets agreed with our analysis, demonstrating that the calibrated model had good temperature and radiation change responses.

4.3. Yield estimation performance for different orchards

Based on the 181 samples, the scatter plots of yield estimation based on the WOFOST model are shown in Figure 3–4. The actual yield of most of the samples in 2016 was underestimated, and 2017 was overestimated. The estimated yields showed a slightly low correlation and accuracy for 2016 (R^2 = 0.22, RMSE = 1.07 t ha^{-1}) and 2017 (R^2 = 0.04, RMSE = 1.33 t ha^{-1}), see Table 3–5. The percentage RMSE was 16.3% and 17.2, respectively. The RPD values were all less than 2, indicating that the evaluation ability of the model was not high.

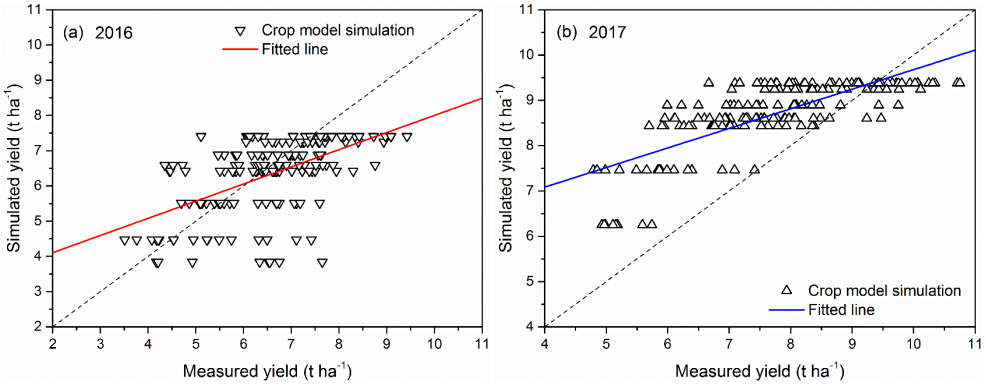

Figure 3–5: Scatter plots of yields estimation

Table 3–5: Yield estimation performance for different orchards based on the calibrated WOFOST Model

Estimation method	Year	R^2	RMSE (%) t ha^{-1}	RPD
Potential simulation	2016	0.22	1.07 (16.3)	1.13
	2017	0.04	1.33 (17.2)	1.02

5. Discussion

The proposed model expresses a potential growth simulation, which requires that the crop growth is not limited by water excess or shortage, nutrient shortage, weed competition, or pest and disease infestation (de Wit et al., 2019b). This situation is very difficult to achieve in practice. In addition, the methods of collecting regional yield data can differ in different parts of the region and might not always be accurate (Reidsma et al., 2009). Some uncertainty may be introduced into the model parameter correction and verification process. Moreover, the genetic variation of parameters can

also lead to considerable uncertainty in yield estimates (Zheng et al., 2018). Although the calibrated WOFOST model can provide an approach for simulating the growth of jujube fruit trees, there may still be some uncertainty in the method of setting the fixed TDWI for the same aged jujube orchards, resulting in a slightly low estimation accuracy. The effect appears, however, to not be optimal. This can be due to the fact that same aged trees may have different growth dynamics and yields induced by strength, height, and pruning differences.

In addition, the effect of changes in the atmospheric CO_2 concentration on the simulation results is not initially considered in the WOFOST model. Recent WOFOST implementations correct this effect by using a CO_2 dependency factor that changes the leaf level maximum assimilation rate (AMAX) and initial light utilization efficiency (EFF) (Vanuytrecht et al., 2017). Moreover, different pruning patterns and pruning quality have a great impact on the jujube yield, which is a crucial aspect for a reliable fruit yield simulation. In the process of establishing and correcting model parameters, a small canopy permanent line tree shape, which is widely employed in Xinjiang, was adopted for all orchards. However, there are other tree shapes in the actual production management, including cylindrical, a middle trunk shape with three main branches, and small canopy permanent trees. Since the tree shape affects the photosynthetic effect, the yield components such as the number of mother branches, the amount of fruiting branches, the single fruit weight, and the number of jujubes can differ greatly (Zhang et al., 2013). Of course, tree age also contributes to CO_2 flux (He 2010). Accordingly, further analysis and demonstration of the effects of different tree shapes and ages on the CO_2 assimilation rate and extinction coefficient would also improve the accuracy of jujube yield estimation.

6. Conclusions

Growth simulations of fruit trees should consider the tree age, which is one of the key factors in accurate simulation. The results show that the model accurately simulates the biomass of different organs and describes the key phenological stages in a reliable way. It is also demonstrated that the calibrated model shows some uncertainty for field-scale fruit yield estimation. Further research on the influences of canopy structure, planting density, and tree ages on CO_2 assimilation is one of most noteworthy aspects, which is expected to improve estimation accuracy and enhance adaptability. Assimilation of remote sensing information into the WOFOST model also has promise for reducing the uncertainty of input parameters. In summary, the method of incorporating tree age into the crop model can provide a scheme for modelling growth and yield estimation of other types of fruit trees.

7. References

Aggelopoulou, A.D., Bochtis, D., Fountas, S., Swain, K.C., Gemtos, T.A., Nanos, G.D. 2011. Yield prediction in apple orchards based on image processing. Precision Agriculture, 12, 448–456. doi:10.1007/s11119-010-9187-0.

Alexandrov, V.A., Eitzinger, J. 2005. The potential effect of climate change and elevated air carbon dioxide on agricultural crop production in central and southeastern Europe. Journal of Crop Improvement, 13, 291–331. doi:10.1300/J411v13n01.

Asseng, S., Ewert, F., Rosenzweig, C., Jones, J.W., Hatfield, J.L., Ruane, A.C., Boote, K.J., Thorburn, P.J., Rötter, R.P., Cammarano, D., Brisson, N., Basso, B., Martre, P., Aggarwal, P.K., Angulo, C., Bertuzzi, P., Biernath, C., Challinor, A.J., Doltra, J., Gayler, S., et al. 2013. Uncertainty in simulating wheat yields under climate change. Nature Climate Change, 3, 827–832. doi:10.1038/nclimate1916.

Bai, T., Zhang, N., Mercatoris, B., Chen, Y. 2019a. Jujube yield prediction method combining Landsat 8 Vegetation Index and the phenological length. Computers and Electronics in Agriculture, 162, 1011-1027. doi.org/10.1016/j.compag.2019.05.035.

Bai, T., Zhang, N., Chen, Y., Mercatoris, B. 2019b. Assessing the performance of the WOFOST model in simulating jujube fruit tree growth under different irrigation regimes. Sustainability, 11, 1466. doi.org/10.3390/su11051466

Baly, E.C.C. 1935. The kinetics of photosynthesis. Proceedings of the Royal Society of London. Series B, Biological Sciences, 117, 218–239. doi.org/10.1098/rspb.1935.0026

Blanco, M., Ramos, F., Van Doorslaer, B., Martínez, P., Fumagalli, D., Ceglar, A., Fernández, F.J. 2017. Climate change impacts on EU agriculture: A regionalized perspective taking into account market-driven adjustments. Agricultural Systems, 156, 52–66. doi:10.1016/j.agsy.2017.05.013.

Brisson, N., Gary, C., Justes, E., Roche, R., Mary, B., Ripoche, D., Zimmer, D., Sierra, J., Bertuzzi, P., Burger, P., Bussière, F., Cabidoche, Y.M., Cellier, P., Debaeke, P., Gaudillère, J.P., Hénault, C., Maraux, F., Seguin, B., Sinoquet, H. 2003. An overview of the crop model STICS. European Journal of Agronomy, 18, 309–332. doi:10.1016/S1161-0301(02)00110-7.

Ceglar, A., van der Wijngaart, R., de Wit, A., Lecerf, R., Boogaard, H., Seguini, L., van den Berg, M., Toreti, A., Zampieri, M., Fumagalli, D., Baruth, B. 2019. Improving WOFOST model to simulate winter wheat phenology in Europe: Evaluation and effects on yield. Agricultural Systems, 168, 168–180. doi:10.1016/j.agsy.2018.05.002.

Cheng, Z., Meng, J., Wang, Y. 2016. Improving spring maize yield estimation at field scale by assimilating time-series HJ-1 CCD data into the WOFOST model using a new method with fast algorithms. Remote Sensing, 8, 303. doi.org/10.3390/rs8040303.

Confalonieri, R., Acutis, M., Bellocchi, G., Donatelli, M. 2009. Multi-metric evaluation of the models WARM, CropSyst, and WOFOST for rice. Ecological Modelling, 220, 1395–1410. doi:10.1016/j.ecolmodel.2009.02.017.

Curnel, Y., de Wit, A.J.W., Duveiller, G., Defourny, P. 2011. Potential performances of remotely sensed LAI assimilation in WOFOST model based on an OSS experiment. Agricultural and Forest Meteorology, 151, 1843–1855. doi:10.1016/j.agrformet.2011.08.002.

de Wit, A., Boogaard, H.L., Diepen, C.A.V. 2005. Spatial resolution of precipitation and radiation: The effect on regional crop yield forecasts. Agricultural and Forest Meteorology, 135, 156–168. doi:10.1016/j.agrformet.2005.11.012.

de Wit, A., van Diepen, C.A. 2007. Crop model data assimilation with the ensemble kalman filter for improving regional crop yield forecasts. Agricultural and Forest Meteorology, 146, 38–56. doi:10.1016/j.agrformet.2007.05.004.

de Wit, A., van Diepen, C.A. 2008. Crop growth modelling and crop yield forecasting using satellite-derived meteorological inputs. International Journal of Applied Earth Observation and Geoinformation, 10, 414–425. doi:10.1016/j.jag.2007.10.004.

de Wit, A., Baruth, B., Boogaard, H., Van Diepen, K., Van Kraalingen, D., Micale, F., Te Roller, J., Supit, I., Van Den Wijngaart, R. 2010. Using ERA-INTERIM for regional crop yield forecasting in Europe. Climate Research, 44, 41–53. doi:10.3354/cr00872.

de Wit, A., Duveiller, G., Defourny, P. 2012. Estimating regional winter wheat yield with WOFOST through the assimilation of green area index retrieved from MODIS observations. Agricultural and Forest Meteorology, 164, 39–52. doi:10.1016/j.agrformet.2012.04.011.

de Wit, A., Boogaard, H., Fumagalli, D., Janssen, S., Knapen, R., van Kraalingen, D., Supit, I., van der Wijngaart, R., van Diepen, K. 2019a. 25 Years of the WOFOST cropping systems model. Agricultural Systems, 168, 154–167. doi:10.1016/j.agsy.2018.06.018.

de Wit, A., Boogaard, H., and Supit I. 2019b. System description of the WOFOST 7.2. cropping system model. Wageningen Environmental Research. September, 2019.

Dobermann, A., Dawe, D., Roetter, R.P., Cassman, K.G. 2000. Reversal of rice yield decline in a long-term continuous cropping experiment. Agronomy Journal, 92, 633–643. doi:10.2134/agronj2000.924633x.

Eitzinger, J., Trnka, M., Hösch, J., Žalud, Z., Dubrovský, M. 2004. Comparison of CERES, WOFOST and SWAP models in simulating soil water content during growing season under different soil conditions. Ecological Modelling, 171, 223–246. doi:10.1016/j.ecolmodel.2003.08.012.

Ewert, F., Rötter, R.P., Bindi, M., Webber, H., Trnka, M., Kersebaum, K.C., Olesen, J.E., van Ittersum, M.K., Janssen, S., Rivington, M., Semenov, M.A., Wallach, D., Porter, J R., Stewart, D., Verhagen, J., Gaiser, T., Palosuo, T., Tao, F., Nendel, C., Roggero, P.P., et al. 2015. Crop modelling for integrated assessment of risk to food production from climate change. Environmental Modelling and Software , 72, 287–303. doi:10.1016/j.envsoft.2014.12.003.

Fleming, A., Schenkel, F.S., Chen, J., Malchiodi, F., Bonfatti, V., Ali, R.A., Mallard, B., Corredig, M., Miglior, F., 2017. Prediction of milk fatty acid content with mid-infrared spectroscopy in Canadian dairy cattle using differently distributed model development sets. J. Dairy Sci. 100, 5073–5081. https://doi.org/10.3168/jds.2016-12102

Gilardelli, C., Confalonieri, R., Cappelli, G.A., Bellocchi, G. 2018. Sensitivity of WOFOST-based modelling solutions to crop parameters under climate change. Ecological Modelling, 368, 1–14. doi.org/10.1016/j.ecolmodel.2017.11.003.

He, T. 2010. Study on the configuration and light distribution characteristics in slope-land jujube plantation of north Shanxi, Yangling. (in Chinese with English abstract)

Holzworth, D.P., Huth, N.I., deVoil, P.G., Zurcher, E.J., Herrmann, N.I., McLean, G., Chenu, K., van Oosterom, E.J., Snow, V., Murphy, C., Moore, A.D., Brown, H., Whish, J.P.M., Verrall, S., Fainges, J., Bell, L.W., Peake, A.S., Poulton, P.L., Hochman, Z., Thorburn. P.J., et al. 2014a. APSIM - evolution towards a new generation of agricultural systems simulation. Environmental Modelling and Software, 62, 327–350. doi:10.1016/j.envsoft.2014.07.009.

Holzworth, D.P., Snow, V., Janssen, S., Athanasiadis, I.N., Donatelli, M., Hoogenboom, G., White, J.W., Thorburn, P. 2014b. Agricultural production systems modelling and

software: Current status and future prospects. Environmental Modelling and Software, 72, 276–286 . doi:10.1016/j.envsoft.2014.12.013.

Huang, J., Ma, H., Su, W., Zhang, X., Huang, Y., Fan, J., Wu, W. 2015a. Jointly assimilating MODIS LAI and ET products into the SWAP model for winter wheat yield estimation. IEEE Journal of Selected Topics in Applied Earth Observations and Remote Sensing, 8, 4060–4071. doi.org/10.1109/JSTARS.2015.2403135

Huang, J., Tian, L., Liang, S., Ma, H., Becker-Reshef, I., Huang, Y., Su, W., Zhang, X., Zhu, D., Wu, W. 2015b. Improving winter wheat yield estimation by assimilation of the leaf area index from Landsat TM and MODIS data into the WOFOST model. Agricultural and Forest Meteorology, 204, 106–121. doi:10.1016/j.agrformet.2015.02.001.

Huang, J., Sedano, F., Huang, Y., Ma, H., Li, X., Liang, S., Tian, L., Zhang, X., Fan, J., Wu, W. 2016. Assimilating a synthetic Kalman filter leaf area index series into the WOFOST model to improve regional winter wheat yield estimation. Agricultural and Forest Meteorology, 216, 188–202. doi.org/10.1016/j.agrformet.2015.10.013

Huang, J., Ma, H., Sedano, F., Lewis, P., Liang, S., Wu, Q., Su, W., Zhang, X., Zhu, D. 2019. Evaluation of regional estimates of winter wheat yield by assimilating three remotely sensed reflectance datasets into the coupled WOFOST–PROSAIL model. European Journal of Agronomy, 102, 1–13. doi.org/10.1016/j.eja.2018.10.008

Jones, J.W., Hoogenboom, G., Porter, C.H., Boote, K.J., Batchelor, W.D., Hunt, L.A., Wilkens, P.W., Singh, U., Gijsman, A.J., Ritchie, J.T. 2003. The DSSAT cropping system model. European Journal of Agronomy, 18, 235–265. doi:10.1016/S1161-0301(02)00107-7.

Kroes, J.G., Supit, I. 2011. Impact analysis of drought, water excess and salinity on grass production in the netherlands using historical and future climate data. Agriculture, Ecosystems and Environment, 144, 370–381. doi:10.1016/j.agee.2011.09.008.

Liu, F., Liu, X., Ding, C., Wu, L. 2015. The dynamic simulation of rice growth parameters under cadmium stress with the assimilation of multi-period spectral indices and crop model. Field Crops Research, 183, 225–34. https://doi.org/10.1016/j.fcr.2015.08.004.

Ma, G., Huang, J., Wu, W., Fan, J., Zou, J., Wu, S. 2013. Assimilation of MODIS-LAI into the WOFOST model for forecasting regional winter wheat yield. Mathematical and Computer Modelling, 58, 634–643. doi:10.1016/j.mcm.2011.10.038.

Rahman, M.M., Robson, A., Bristow, M. 2018. Exploring the potential of high resolution worldview-3 Imagery for estimating yield of mango. Remote Sensing, 10, 1866. doi.org/10.3390/rs10121866

Reidsma, P., Ewert, F., Boogaard, H., Diepen, K. van. 2009. Regional crop modelling in Europe: The impact of climatic conditions and farm characteristics on maize yields. Agricultural Systems, 100, 51–60. doi:10.1016/j.mehy.2010.10.015.

Reidsma, P., Wolf, J., Kanellopoulos, A., Schaap, B.F., Mandryk, M., Verhagen, J., Van Ittersum, M.K. 2015. Climate change impact and adaptation research requires integrated assessment and farming systems analysis: A case study in the netherlands. Environmental Research Letters, 10 (4). doi:10.1088/1748-9326/10/4/045004.

Rötter, R., Van Keulen, H. 1997. Variations in yield response to fertilizer application in the tropics: II. Risks and opportunities for smallholders cultivating maize on Kenya's arable land. Agricultural Systems, 53, 69–95. doi:10.1016/S0308-521X(96)00037-6.

Sun, A. 2019. Effect of Temperature Change on Winter Jujube Production in Huanghua City. Guizhou Agricultural Sciences, 47(6): 88-91. In Chinese with english abstract.

Sun, L., Gao, F., Anderson, M.C., Kustas, W.P., Alsina, M.M., Sanchez, L., Sams, B., McKee, L., Dulaney, W., White, W.A., Alfieri, J.G., Prueger, J.H., Melton, F., Post, K. 2017. Daily mapping of 30 m LAI and NDVI for grape yield prediction in California vineyards. Remote Sensing, 9, 317.

Supit, I. 1997. Predicting national wheat yields using a crop simulation and trend models. Agricultural and Forest Meteorology, 88, 199–214. doi:10.1016/S0168-1923(97)00037-3.

Supit, I., van Diepen, C.A., de Wit, A.J.W., Kabat, P., Baruth, B., Ludwig, F. 2012. Assessing climate change effects on European crop yields using the crop growth monitoring system and a weather generator. Agricultural and Forest Meteorology, 164, 96–111. doi:10.1016/j.agrformet.2012.05.005.Thornley, J.H.M. 1976. Mathematical Models in Plant Physiology. Academic Press (Inc.) London. Ltd. https://www.cabdirect.org/cabdirect/abstract/19760343677

Thornley, J H M., 1976. Mathematical models in plant physiology[M]. Academic Press (Inc.) London, Ltd., 1976.

Todorovic, M., Albrizio, R., Zivotic, L., Abi Saab, M.T., Stöckle, C., Steduto, P., 2009. Assessment of aquacrop, cropsyst, and WOFOST models in the simulation of sunfl ower growth under different water regimes. Agron. J. 101, 509–521. https://doi.org/10.2134/agronj2008.0166s

Tripathy, R., Chaudhari, K.N., Mukherjee, J., Ray, S.S., Patel, N.K., Panigrahy, S., Singh Parihar, J. 2013. Forecasting wheat yield in Punjab State of India by combining crop simulation model WOFOST and remotely sensed inputs. Remote Sensing Letters, 4, 19–28. doi:10.1080/2150704X.2012.683117.

van Diepen, C.A., Wolf, J., van Keulen, H., Rappoldt, C. 1989. WOFOST: A simulation model of crop production. Soil Use Management, 5, 16–24.

Van Walsum, P. E.V., Supit, I. 2012. Influence of ecohydrologic feedbacks from simulated crop growth on integrated regional hydrologic simulations under climate scenarios. Hydrology and Earth System Sciences, 16, 1577–1593. doi:10.5194/hess-16-1577-2012.

Vanuytrecht, E., Thorburn, P.J. 2017. Responses to atmospheric CO_2 concentrations in crop simulation models: a review of current simple and semicomplex representations and options for model development. Global Change Biology, 23, 1806–1820.

Wang, Q., Wen, Z., and Jia, Y. 2002. Study on the photosynthetic characteristics of young Jujube. Journal of Agricultural University of Hebei. 25(S1): 120-121. (in Chinese with English abstract).

Wang, X., Williams, J.R., Gassman, P.W., Baffaut, C., Izaurralde, R.C., Jeong, J., Kiniry, J. R. 2012. EPIC and APEX: Model use, calibration, and validation. Transactions of the ASABE, 55, 1447–1462. doi:10.13031/2013.42253.

Wolf, J., Hessel, R., Boogaard, H.L., De Wit, A., Akkermans, W., van Diepen, C.A. 2011. Modelling winter wheat production across Europe with WOFOST-the effect of two new zonations and two newly calibrated model parameter sets. American Society of Agronomy. Crop Science Society of America, Soil Science Society of America. https://doi.org/10.2134/advagricsystmodel2.c11 .

Ye, X., Sakai, K., Garciano, L.O., Asada, S.I., Sasao, A. 2006. Estimation of citrus yield from airborne hyperspectral images using a neural network model. Ecological Modelling, 198, 426–432. doi:10.1016/j.ecolmodel.2006.06.001.

Ye, Z., Yu, Q. 2007. Comparison of a new model of light response of photosynthesis with traditional models. Journal of Shenyang Agricultural University, 38, 771-775. (in Chinese with English abstract).

Zaman, Q.U., Schumann, A.W., Hostler, H.K. 2006. Estimation of citrus fruit yield using ultrasonically-sensed tree size. Applied Engineering in Agriculture, 22, 39–44. doi:10.13031/2013.20186.

Zhang, Q., Bai, T., Wu, C. 2013. Investigation on yield and quality of jujube in different tree shapes in direct seeding and orchard construction. Northern Horticulture, (4), 18-23. (in Chinese with English abstract).

Zheng, Y., Li, Z., Xiao, J., Yuan, W., Yan, M., Li, T., Zhang, Z. 2018. Sources of uncertainty in gross primary productivity simulated by light use efficiency models: Model structure, parameters, input data, and spatial resolution. Agricultural and Forest Meteorology, 263, 242–257. doi:10.1016/j.agrformet.2018.08.003.

Zhuo, G., Liu, X., Liu, M. 2019. Assimilating remote sensing phenological information into the WOFOST model for rice growth simulation. Remote Sensing, 11, 268. doi.org/10.3390/rs11030268.

Zhou, R., Damerow, L., Sun, Y., Blanke, M.M. 2012. Using colour features of CV. 'Gala' apple Fruits in an orchard in image processing to predict yield. Precision Agriculture, 13, 568–580. doi:10.1007/s11119-012-9269-2.

Chapter 4

Improving jujube fruit yield estimation by integrating the phenology length into a remotely sensed vegetation index regression model

Remote sensing-based regression is an important method used for yield estimation, which is easy to implement and operate. This method is different from the simulation-based method presented in Chapter 3, and does not require a large number of input parameters. In Chapter 4, a method of yield assessment based on a remotely sensed vegetation index is implemented and its performance is tested. As shown in some previous studies, the accuracy of such a method is affected by phenological information. Therefore, the phenological length of jujube growth calculated in Chapter 3 was utilized to improve the proposed remote sensing-based yield assessment method.

This chapter describes how Landsat 8 satellite data combined with phenological information was used to assess jujube fruit yield at the field scale. Further implementation details are also described, including satellite image processing, screening of vegetation indices, determination of phenological time for yield assessment, calculation of phenological length, and VI-YIELD evaluation equations.

This Chapter is based on: Tiecheng Bai, Nannan Zhang, Benoit Mercatoris, Youqi Chen*. 2019. Jujube yield prediction method combining Landsat 8 Vegetation Index and the phenological length. Computers and Electronics in Agriculture, 162, 1011-1027.* Corresponding Author.*

1. Abstract

It is challenging to have a consistent time series of vegetation indices from moderate spatial resolution Landsat Thematic Mapper images (Landsat 8) due to cloud coverage and the satellite's long revisit cycle. In addition, crop yields are correlated with phenology information, especially the fruit filling days. The objectives of this study were to identify the optimal phenology time for determining reliable jujube yield estimation, and particularly to explore an approach that used the length of the phenology growth period to improve remotely sensed estimates of inter-annual variability for jujube fruit yields. The best period for jujube yield estimation was found to be during the fruit filling period, showing higher R^2 values between vegetation indices and yields. The average NDVI from July 15 to August 15 represented a better performance for yield estimation, with the highest R^2 values of 0.74 for NDVI, 0.61 for SAVI, 0.46 for NDWI, and 0.44 for EVI, respectively. The potential of using Landsat-NDVI combined with the phenological length for field-scale jujube fruit yield estimation was proved based on 181 observed orchards, showing a validated R^2 of 0.64 and RMSE of 0.73 t ha^{-1} (11.1%) for 2016, 0.71 and 0.73 t ha^{-1} (9.5%) for 2017, respectively. The RPD values for jujube fruit yield estimation in 2016 and 2017 were 1.66 and 1.86, respectively. The proposed method was verified as having a good fit to jujube yield monitoring and mapping two months before harvest.

2. Introduction

Local and field-scale jujube growth and yield estimates before harvest allow farmers to improve yield management decision-making. Remote sensing has been widely employed to monitor crop growth conditions and estimate yields for over three decades (Bolton and Friedl, 2013). In particular, vegetation indices (VIs) such as the Normalized Difference Vegetation Index (NDVI) have been widely utilized for yield monitoring and mapping (Bolton and Friedl, 2013; Funk and Budde, 2009; Panda et al., 2010; Dempewolf et al., 2014; Mkhabela et al., 2011; de la Casa et al., 2018; Yu and Shang, 2018). In addition, other indices have also been used for crop yield estimation, like Green Leaf Area Index (GLAI) (Duchemin et al., 2008); Enhanced Vegetation Index (EVI) (Bolton and Friedl, 2013; Son et al., 2014; Kouadio et al., 2014); and the Normalized Difference Water Index (NDWI) (Bolton and Friedl, 2013).

Recently, an increasing number of remote sensing-based studies have performed yield estimation for annual crops using data collected from the National Aeronautics and Space Administration's (NASA) Moderate Resolution Imaging Spectroradiometer (MODIS) because of its high frequency observations and superior spectral resolution (Bolton and Friedl, 2013; Dempewolf et al., 2014; Kouadio et al., 2014; Ren et al., 2008; Victoria et al., 2012; Becker-Reshef et al., 2010). However, the spatial resolution of MODIS data is low, with images available at 250 m, 500 m, and 1000 m scales (Bolton and Friedl, 2013). It is therefore more suitable for large-scale crop yield estimation. Fruit trees are different from annual crops and are usually grown in specific areas which requires remote sensing data with higher spatial resolution for yield estimation, such as Landsat Thematic Mapper (TM), WorldView-

3, and ASTER. Spectral bands from these remote sensing satellites have been found to have good performance in yield estimation for grapes (Sun et al., 2017; Anastasiou et al., 2018), mangoes (Rahman et al., 2018), and olives (Sepulcre-Cantó et al., 2007), showing strong correlations. In addition, an airborne remote sensing monitoring system has also shown good yield and quality estimation ability, such as for grapes and citrus (Bonilla et al., 2015; Ye et al., 2006, 2008a, 2008b). It should be noted that NDVI is still frequently used as an index for fruit yield assessment. The Landsat 8 satellite can provide data with moderate spatial resolution (30 m) but a long repeat period (16 days), which partly limits its applications in large-scale yield estimation. However, this can generally be produced at regional scales, which has also been used for annual and fruit crop yield estimation (de la Casa et al., 2018; Sun et al., 2017; Rudorff and Batista, 1991; Hamar et al., 1996; Thenkabail, 2003; Liu et al., 2006).

The fitting equation between crop yield and vegetation index varies strongly at different developmental stages (Dempewolf et al., 2014; Brian et al., 2004; Salazar et al., 2007; Bognár et al., 2017; Wall et al., 2008). Therefore, a fixed calendar date may not be an optimal choice for yield estimation (Bolton and Friedl, 2013; Dempewolf et al., 2014; Brian et al., 2004). As a consequence, several studies have used the phenology information, time series of VIs, ground-based ancillary data, or surface parameters to adjust VIs or optimize the estimation model (Bolton and Friedl, 2013; Funk and Budde, 2009; Rojas, 2007; Reynolds et al., 2000; Prasad et al., 2006; Wang et al., 2014; Sakamoto et al., 2013). Bolton and Friedl (2013) confirmed that integrating information related to crop phenology derived from MODIS could significantly improve modelling performance within and across years. According to the conventional characterization of crop growth, a crop usually includes three main growing stages, sowing/planting or emergence, flowering, and maturity. The length of the growth period can be defined as the period between crop emergence and maturity or senescence (yellowing of leaves). The total biomass production can be calculated from the mean daily biomass production multiplied by the total growth duration (de Wit et al., 2019). A longer growth duration, especially a long fruit filling period (from flowering to maturity), usually results in higher yields. Therefore, remote sensing-based crop yield estimation models might benefit considerably from incorporating the length of the crop phenology growth period, which presents a valuable research avenue for limited Landsat 8 data or other moderate and high spatial resolution remote sensing data. Therefore, taking jujube tree yield estimation as an example in this research, an approach combining Landsat 8 VIs and phenology development length is explored to improve the yield estimation accuracy. The aims of this study are to:

(i) Evaluate the potential of using spectral information from Landsat 8 for estimating jujube fruit yield at the field scale.

(ii) Identify the optimal phenology time for determining a reliable jujube yield estimation, and compare the performance of different VIs for yield estimation.

(iii) Explore an approach that uses the phenological length to improve the remote sensing-based yield estimation model.

3. Research data and methods

3.1. Research data

The data used in this chapter included Landsat 8 images which were used to extract vegetation indices, and yield data for 181 orchards which were used to evaluate the yield estimation performance of the proposed remote sensing regression method at the local scale. For details, see Section 3.2 and 3.3 in Chapter 2, respectively.

3.2. Landsat 8 data processing

Processed available and cloud-free Landsat 8 images taken during the main growing seasons (May–September) for Alaer city from 2016 to 2017 were obtained from the United States Geological Survey (USGS, https://earthexplorer.usgs.gov/). Landsat 8 remote sensing images were obtained for four dates in 2016 (21 May, 8 July, 24 July, and 9 August), and six remote sensing images were obtained for 2017 (24 May, 9 June, 27 July, 12 August, 28 August, and 13 September). Each image covers all 181 orchards in the study area.

First, geometric correction was performed by reference to the Albers conical equal-area map projection using 50 field-measured ground control points, including road intersection, and important building and farmland intersections. The root mean square error (RMSE) of the corrected and measured locations was less than one pixel (30 m) for each Landsat image. Second, the Fast Line-of-sight Atmospheric Analysis of Spectral Hypercubes (FLAASH) model was employed to carry out an atmospheric correction. Parameters of FLAASH correction can be set as follows: sensor altitude = 705 km, ground elevation = 0.0175 km, pixel size = 30 mm, atmospheric model = sub-Arctic summer, aerosol model = urban, water column multiplier = 1.00, aerosol retrieval = 2-Band (K-T), initial visibility = 40 km, KT upper channel = SWIR 2, KT lower channel = red, maximum upper channel reflectance = 0.08, reflectance ratio = 0.50. Third, a border file for Alaer city was used to extract our research area.

A small area within the area of interest (AOI) with several orchards is shown in Figure 4–1. The RGB bands were set to SWIR, near infrared (NIR) and red bands. From the image, it is easy to distinguish between jujube trees and cotton crops.

Four vegetation indices commonly used for remote sensing yield estimation, including NDVI (Pettorelli, 2013), SAVI (Huete, 1988), NDWI (Gao, 1996) and EVI (Wardlow et al., 2007) were calculated using the Equations (4–1), (4–2), (4–3) and (4–4), respectively.

$$\mathrm{NDVI} = \frac{\rho_{nir} - \rho_{red}}{\rho_{nir} + \rho_{red}} \qquad (4-1)$$

$$\mathrm{SAVI} = \frac{\rho_{nir} - \rho_{red}}{\rho_{nir} + \rho_{red} + L} \times (1 + L) \qquad L = 0.5 \qquad (4-2)$$

$$\mathrm{NDWI} = \frac{\rho_{nir} - \rho_{swir}}{\rho_{nir} + \rho_{swir}} \qquad (4-3)$$

$$\mathrm{EVI} = 2.5 \times \frac{\rho_{nir} - \rho_{red}}{\rho_{nir} + 6.0 \times \rho_{red} - 7.5 \times \rho_{blue} + 1} \qquad (4-4)$$

Where, ρ_{nir}, ρ_{red}, ρ_{blue} and ρ_{swir} were spectral reflectances from the NIR-band, RED-band, BLUE-band, and SWIR-band of Landsat 8 images, respectively. In equation 2, L=0.5 is a widely used value in most studies, which is related to soil properties and vegetation coverage (Huete, 1988; Huang et al., 2015).

Finally, the GPS-positioned orchard boundary coordinates were used to extract the delineations of 181 orchards, respectively. The NDVI, SAVI, NDWI, and EVI values of the 181 observed orchards during the growing season were extracted based on the above processing.

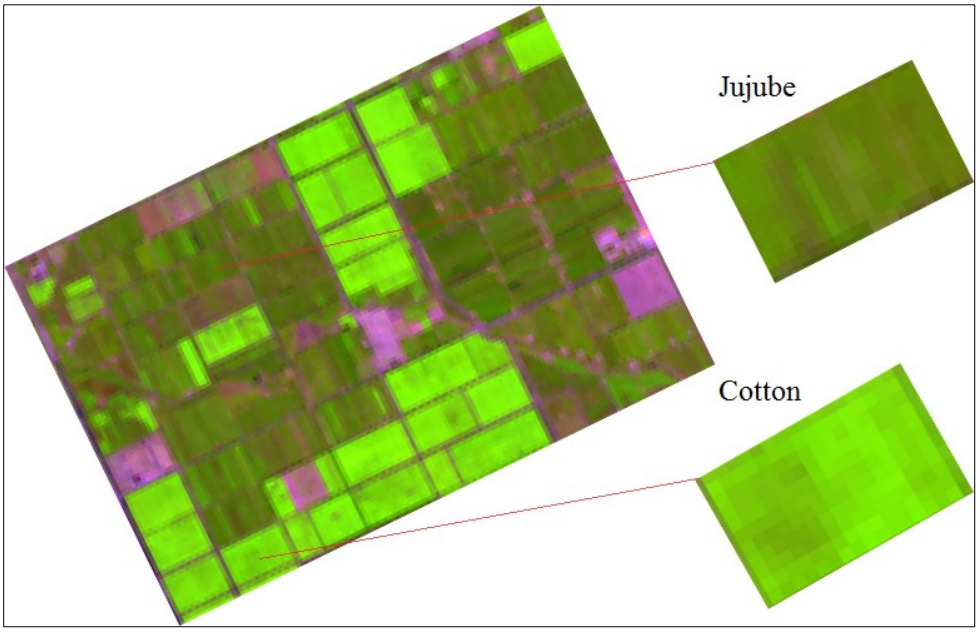

Figure 4–1: A small area of interest with several orchards. (Landsat 8, 27 July 2017)

3.3. Phenology-adjusted VI-Yield estimation approach

Previous studies have confirmed that there may be different fitting equations for crop yield and VIs, including linear (Mkhabela et al., 2005), exponential (Holzapfel et al., 2009), and power models (Dempewolf et al., 2014; Ma et al., 2001). Results have indicated that many factors, such as soil, crop type, and environment, can affect the regression model (Dempewolf et al., 2014). Therefore, different statistical regression models, based on VIs obtained during the main growing period, were separately implemented for jujube yield estimation. Results from linear, exponential, power, and logarithmic models were compared in order to select the best one. The key innovation of our approach was that the length of the growth period calculated by the

effective accumulated temperature was employed to improve the estimation model. The proposed method included two main steps:

i. Calculate the length of the jujube growth period

A crop growth season is the period between crop emergence and maturity or senescence (yellowing of leaves, expressed in degree days) (de Wit and Wolf, 2010). The phenology development stages of jujube can be defined in three important stages, which were presented as a numerical scale that ranged from 0 to 2, with 0 being emergence ($D_{s,t}$ = 0), 1 flowering ($D_{s,t}$ = 1), and 2 maturity ($D_{s,t}$ = 2). The length of growth the period, $D_{s,t}$ = 0-1 and $D_{s,t}$ = 1–2, was determined by the effective accumulated temperature sum, which was defined as a function of the daily effective temperature (FOR Community, 1994). Emergence, flowering, and maturity took place when the effective temperature sum reached the threshold temperature. The daily effective temperature (T_e) as a function of the daily average temperature (T) is depicted in Figure 4–2, which was equal to the daily average temperature minus the base temperature (T_{base}) when $T_{base} \leq T \leq T_{max,e}$. Since jujube tree would begin to sprout when the daily average temperature was greater than 10 °C, the base temperature (T_{base}) was 10 °C (Sun, 2019).. When the daily average temperature was greater than 35.5°C (maximum critical temperature, $T_{max,e}$), the daily effective temperature would not continue to increase, but was equal to a fixed value of 25.5°C.

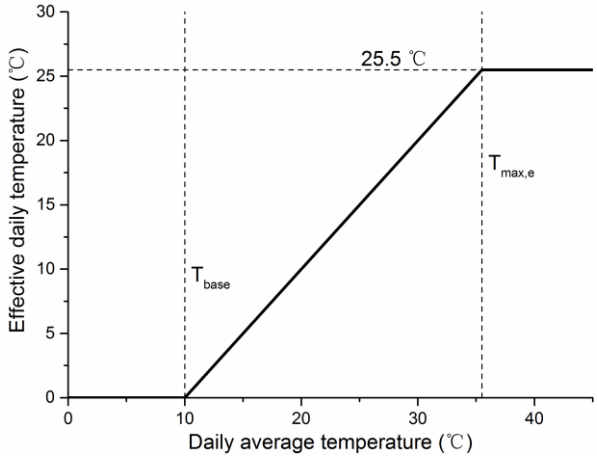

Figure 4–2: The relationship between the daily effective temperature and daily average temperature for jujube trees

The following Equations (4–5, 6, 7) were used to calculate the daily effective temperature:

$$T_e = 0 \qquad T \leq T_{\text{base}} \tag{4-5}$$

$$T_e = T - T_{base} \qquad T_{base} \leq T \leq T_{max,e} \tag{4-6}$$

$$T_e = T_{max,e} - T_{base} \qquad T \geq T_{max,e} \tag{4-7}$$

Where,

T_e: Daily effective temperature.

$T_{max,e}$: Maximum critical temperature. If the temperature goes beyond this, phenological activity does not increase.

T_{base} : Base temperature. If the temperature goes below this, phenological development will stop.

T: Daily average temperature.

Next, the development rate per day was the ratio of the daily effective temperature and accumulated temperature sum. Higher temperatures accelerate the development rate, thereby leading to shorter growing periods. In the research, a more flexible development rate relation can be obtained by Equation (4–8):

$$D_{r,t} = \frac{DT_s}{\sum T_i} \quad (4-8)$$

Where, $D_{r,t}$ is the development rate at time step t [d^{-1}], DT_s is the temperature dependent correction factor [°C], which is equal to the effective temperature sum at time step t. This can be calculated based on Equations (5), (6), and (7). $\sum T_i$ is the effective accumulated temperature sum required to complete stage i [°C d]. In our research, the effective temperature sum for emergence, emergence-flowering, and flowering-maturity were respectively 230, 967, and 960°C based on observed data from 2016 to 2017.

The development stage at time step t was equal to the integral of the development rate over the time, which can be calculated using the Equation (4–9):

$$D_{s,t} = D_{s,t-1} + D_{r,t}\Delta t \quad (4-9)$$

Where, $D_{s,t}$ is the development stage at time step t, Δt is time step [day]. Then, the length of the growth period (t) between $D_{s,t}$= 0 and $D_{s,t}$= 2, between $D_{s,t}$= 1 and $D_{s,t}$= 2 can be obtained. The development stages for jujube were calibrated and validated using observed data from 2016 to 2018 (2016 and 2017 data for calibration, 2018 data for validation), with an error of –2 days for emergence, –3 days for flowering, and –3 days for maturity (see Chapter 3). In addition, the calculated jujube phenological lengths were 144 (DVS = 0-2) and 73 days (DVS = 1-2) for 2016, and 156 (DVS = 0-2) and 85 days (DVS = 1-2) for 2017, respectively.

Finally, the adjusted fitted equation based on the length of the phenological growth period and Landsat 8 NDVI can be implemented using the Equation (4–10).

$$y = \frac{l_y}{l_b} f(NDVI) \quad (4-10)$$

Where, y is the estimated yield, $f(NDVI)$ is the fitted equation based on the yield and NDVI, l_b (days) is the phenological length of the year in which the yield and

vegetation index equations are established, which is calculated based on the model. ly is the phenological length for the year of the estimated yield. The yield estimation for other indices referred to the adjustment method for NDVI.

ii. Establish and initially validate models.

Correlations between VIs of different growth stages (independent variable) and jujube yields (dependent variable) were performed for the best modelling time and VI. The accuracy of linear, exponential, power, and logarithmic models was compared for a fit equation. The phenological development lengths between DVS = 1 and DVS = 2 were tested to improve the accuracy of the yield estimation.

The agreement between measured and estimated yields was quantified using the coefficient of determination (R^2). Due to the wide range of jujube yields, a normalized root mean square error (NRMSE, i.e., the ratio between the RMSE and the average of observed values), and RPD were used to evaluate estimation accuracy.

4. Results

4.1. Remote sensing imagery processing results

Taking NDVI as an example, NDVI changes for July in a small jujube planting area (area of interest) from 2014 to 2017 are shown in Figure 4–3. Similarly, NDVI, SAVI, NDWI, and EVI for jujube orchards during the main fruit filling period in 2016 and 2017 can be calculated. These VIs showed an increasing trend year by year due to the increasing age of the trees. Most of the pixels had a NDVI value between 0.4 and 0.8.

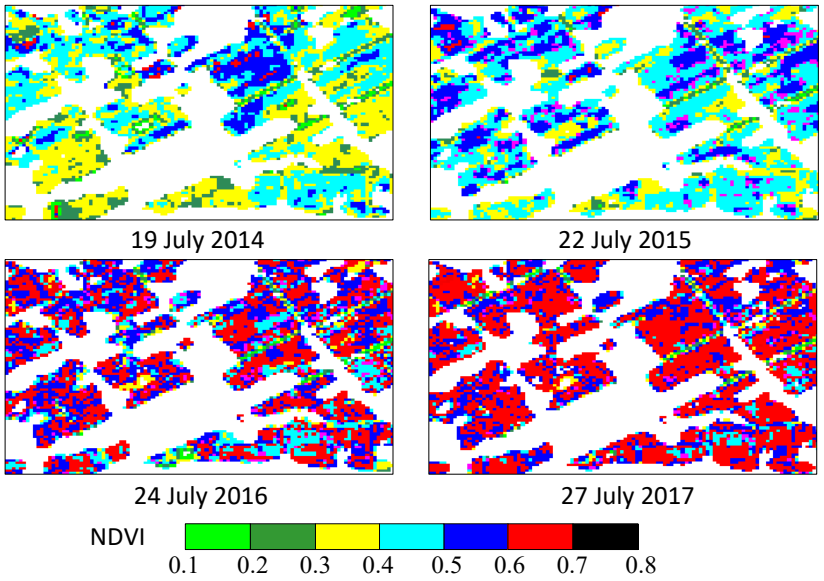

Figure 4–3: NDVI changes in a small jujube planting area in late July from 2014 to 2017.

In addition, SAVI during the main growth season ranged from 0.3 to 0.6, NDWI from 0.2 to 0.4, and EVI from 0.3 to 0.5. The average values of four VIs for August were also slightly lower than those for July, which was consistent with the result for the 181 observation orchards.

4.2. Selection of the best time for yield estimation modelling

The trends of four Landsat VIs for 181 observations during the 2016 and 2017 growing period are shown in Figure 4–4 and 4–5. The lack of available remote sensing observation data after mid-August in 2016 makes it difficult to express the dynamic changes of vegetation indices during the growing season for jujube orchards. Figure 4–5 (2017 data) can reflect the vegetation index changes of jujube trees from emergence to early maturity. The four vegetation indices value first rose to the saturation point, and then showed a downward trend with the death of leaves at the end of the growing season. Landsat data from 24 July 2016 and 27 July 2017 presented higher NDVI, SAVI, NDWI, and EVI values ranging from 0.55 to 0.80, from 0.39 to 0.57, from 0.25 to 0.43, and 0.4 to 0.63, respectively, which coincided with the early stage of fruit development.

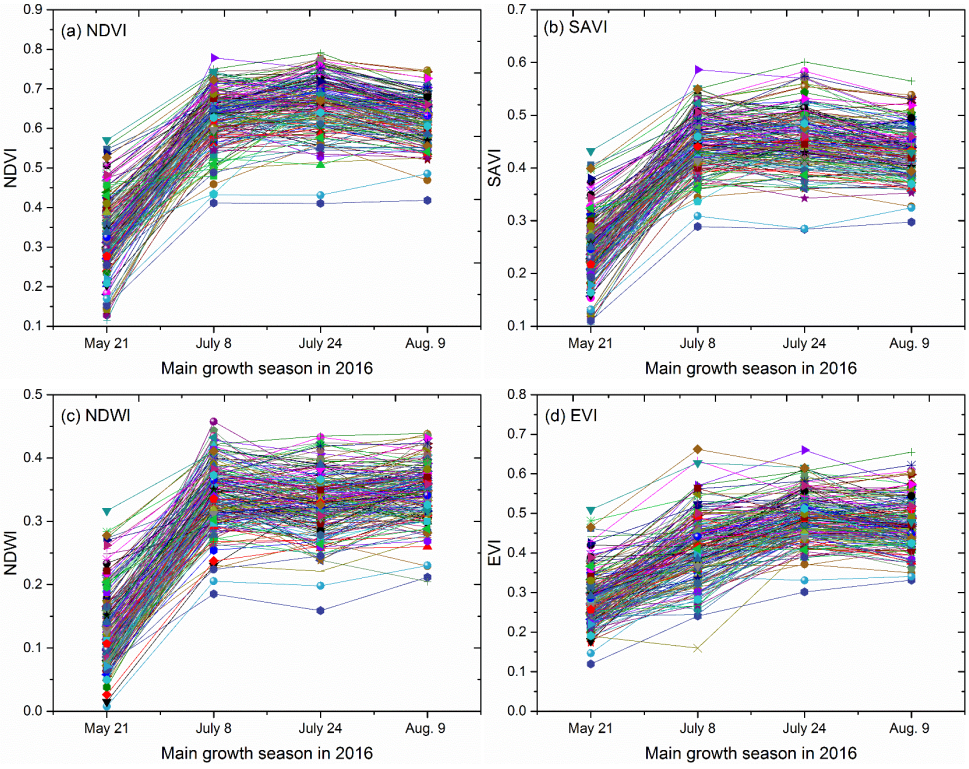

Figure 4–4: Time series of Landsat 8 vegetation indices for 181 orchards in the 2016 growth season.

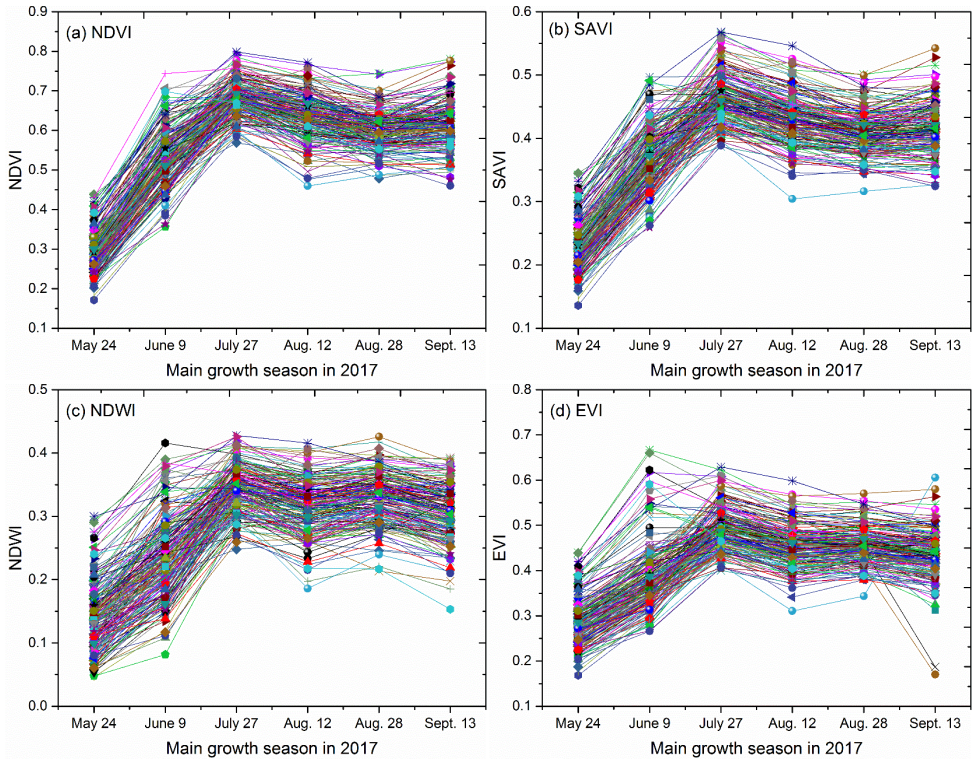

Figure 4–5: Time series of Landsat 8 vegetation indices for 181 orchards in the 2017 growth season.

The evolution of the two-year average coefficient of determination (R^2) between the VIs and final jujube fruit yields obtained from 181 orchards per year is shown in Figure 4–6(a), 4–6(b), 4–6(c), and 4–6(d). For a single VI, the correlations between the four VIs and fruit yields showed the same trend, which is low before the flowering period (10^{th} and 11^{th} half-month), and strong from flowering to fruit maturity (14^{th} to 17^{th} half-month). The R^2 values peaked during the main fruit filling period (14^{th} and 15^{th} half-months), with NDVI showing the strongest R^2 value ($R^2 = 0.71$), followed by SAVI ($R^2 = 0.59$), and finally NDWI ($R^2 = 0.41$) and EVI ($R^2 = 0.40$).

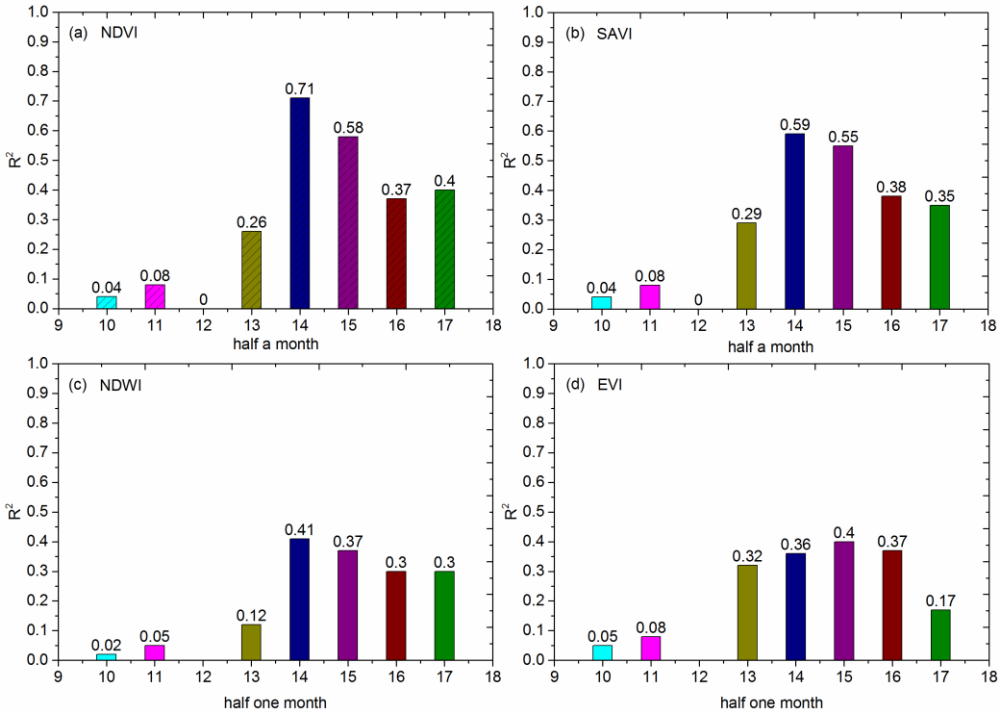

Figure 4–6: Evolution of the two year average R^2 for four vegetation indices versus jujube fruit yields based on 181 orchards from the 10th half-month (half a month) to 17th half-month. (a) NDVI (Normalized Difference Vegetation Index), (b) SAVI (Soil-adjusted Vegetation Index), (c) NDWI (Normalized Difference Water Index), (d) EVI (Enhanced Vegetation Index). Note that the 10th half-month was from 16 to 31 May, while the 17th half-month was from 1 to 15 September.

In addition, for each VI the R^2 values between maximum values, average values for June, July, and August, average values for July and August, the average values for the 14th and 15th half-months based on an exponential regression equation with best performance compared to other linear regression equations, and yields were also compared (Table 4–1). The average value for the 14th and 15th half-months represented a good performance, with an average R^2 value of 0.75 for NDVI, 0.61 for SAVI, 0.47 for NDWI, and 0.44 for EVI. NDVI was more highly correlated with yields than the other VIs. Collectively, the main fruit filling period (14th and 15th half-months) was shown to be the best time for jujube yield estimation. The average NDVI for the 14th and 15th half-months can be recommended as the best VI for yield estimation, followed by the average SAVI of the 14th and 15th half-months.

Table 4–1: R^2 values of the composite indices based on an exponential regression equation

Year	Composite indices	Average R^2			
		NDVI	SAVI	NDWI	EVI
2016	Maximum index during growth season	0.69	0.51	0.34	0.40
	Average for 6th, 7th and 8th month	/	/	/	/
	Average for 7th and 8th month	0.64	0.60	0.38	0.42
	Average for 14th and 15th half-months	0.71	0.64	0.46	0.45
2017	Maximum	0.76	0.52	0.38	0.30
	Average for 6th, 7th and 8th month	0.59	0.50	0.36	0.39
	Average for 7th and 8th month	0.72	0.54	0.44	0.42
	Average for 14th and 15th half-months	0.78	0.58	0.48	0.42

"/" represents uncalculated values because of the lack of remote sensing observations for June 2016.

4.3. Yield estimation models

Average NDVIs showed the highest R^2 values (Table 4–1), so the NDVI was used to establish the yield estimation model. Of all observations over the two years, the relationship between Landsat-NDVI and jujube yields was best described by an exponential equation, with the strongest correlation and highest accuracy. The estimation accuracy using average VIs for the 14th and 15th half-months was also significantly higher than that using other VIs, showing the strongest agreement (R^2 = 0.77) and best accuracy (RMSE = 0.66 t ha^{-1}) for 2017 (R^2 = 0.71 and RMSE = 0.65 t ha^{-1} for 2016). The modelling time was also consistent with the best time determined in fruit filling periods.

4.4. Yield estimation performance

In order to cross-validate the jujube yield estimation accuracy of the proposed method, scatterplots of validation results for 181 local orchards in 2016 and 2017, before and after phenologically adjustment, are shown in Figure 4–7.

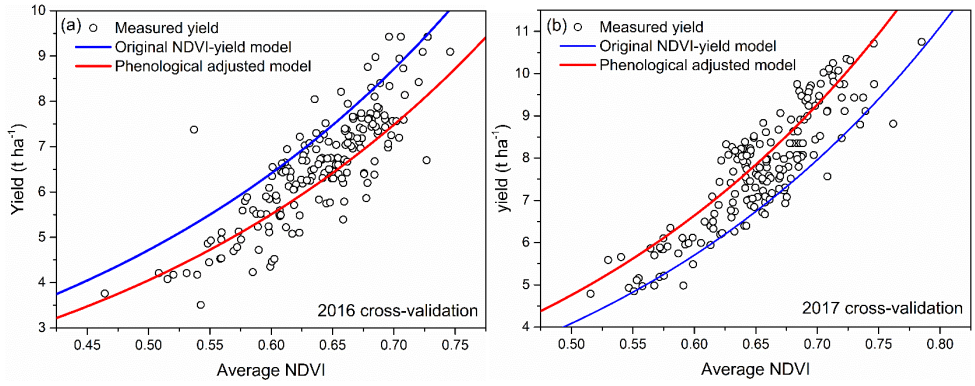

Figure 4–7: Validation results of phenology-adjusted models based on the phenological length (a) 2016 cross-validation, (b) 2017 cross-validation.

The scatterplots clearly show that the phenology-adjusted model (using the phenological length from flowering to maturity) presents better performance than without adjustment.

The details for equations and validated results are shown in Table 4–2. The verification results suggest that the estimation accuracy of the phenology-adjusted model was higher than that of the unadjusted model. The validated R^2 for the adjusted model was increased by 0.29 and 0.28 compared to the unadjusted model for 2016 and 2017, respectively. This suggests that NDVI is the most suitable index and the phenology-adjusted model presented the highest estimation precision, with the best validated R^2 = 0.71 and 0.64, and RMSE = 0.73 (11.1%) and 0.73 t ha^{-1} (9.5%) for 2016 and 2017, respectively. The RPD values for the 2016 and 2017 jujube yield estimation based on the adjusted model were 1.66 and 1.86, respectively, which were higher than the unadjusted model.

Table 4–2: Inter-annual cross-validation details for the proposed regression models.

Year	Activity	Equation	R^2	RMSE (ha^{-1})	NRMSE (%)	RPD
2016	Without adjustment	$y = 1.01914 \times e^{3.06548 \times NDVI}$	0.35	0.98	14.8	1.23
2016	Adjustment	$y = \frac{73}{85} \times 1.01914 \times e^{3.06548 \times NDVI}$	0.64	0.73	11.1	1.66
2017	Without adjustment	$y = 0.77227 \times e^{3.33227 \times NDVI}$	0.43	1.02	13.3	1.33
2017	Adjustment	$y = \frac{85}{73} \times 0.77227 \times e^{3.33227 \times NDVI}$	0.71	0.73	9.5	1.86

5. Discussion

In our research, NDVI during the main fruit filling period was found to be significantly correlated to the jujube fruit yield in all research sites. Consistent with numerous studies, the current study also demonstrated high correlations between NDVIs during the flowering and fruit filling period and crop yields (Mkhabela et al., 2011; Unganai and Kogan, 1998; Mkhabela and Mkhabela, 2000; Labus et al., 2002; Marti et al., 2007), which was considered to be the most critical period for yield estimation in most crops. The maximum development stages of the crop can also be defined by reference to their highest NDVI value to estimate crop yields (Satir and Berberoglu, 2016; Yousfi et al., 2016), which was usually during the fruit filling period. In addition, the results in this research showed that average NDVI during the main fruit filling period (14th and 15th half-months) allowed higher accuracy for jujube yield estimation than using a single NDVI, which was in agreement with previous studies that have reported higher correlations between average NDVI and crop yields. Sun et al. (2017) found that the maximum and seasonal cumulative vegetation indices and grape yields showed slightly lower correlations than the average. Mkhabela et al. (2011) found that the regression models using average NDVI for four decades rather than a single average decade NDVI showed

better estimation ability for maize yield. Hochheim and Barber (1998) also found that a 3 week average NDVI increased the coefficient of determination (R^2) and stabilized spring wheat yield estimation models. Tariqul et al. (2018) found that using the mean Landsat-NDVI can provide the maximum R^2 value for potato yield estimation. However, the estimation accuracy of the mean, maximum, and cumulative values of the vegetation indices may vary slightly due to crop varieties and growing environments.

Average temperature in the 2016 growing season was significantly higher than in 2017 (Figure 4–8). Higher average temperature usually results in a shorter growth period and lower yield (de Wit et al., 2019). Actual observations also showed that the length of jujube growing period in 2016 was significantly lower than in 2017, especially during the fruit filling period (12-day deviation). This difference also resulted in the difference between the actual average yields for 2016 and 2017. Therefore, the length of crop phenology development is likely to benefit crop yield forecasting. Hochheim and Barber (1998) also found that inter-annual differences in crop phenology across Census Agricultural Regions (CARs) normally varied by 2–3 weeks and therefore required consideration when integrating data over time. The results in this research also confirmed that the proposed phenology-adjusted model significantly improved the estimation accuracy.

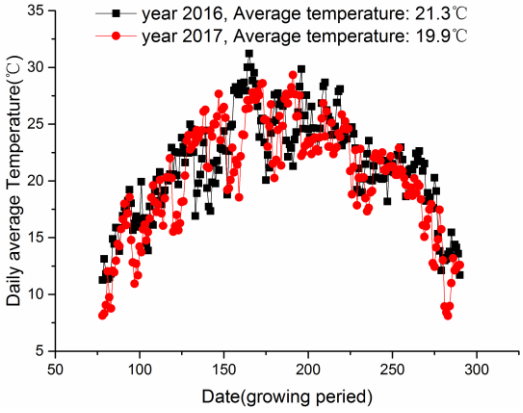

Figure 4–8: Daily average temperature of the growth season in 2016 and 2017.

MODIS data is more suitable for crop yield estimation at large regional scales. The coarser pixels of the MODIS reflectance data usually lead to higher scale errors (Huang et al., 2015). Most pixels usually represent mixtures of crops. Thus, separation of crops based on satellite-derived phenological information is likely to be challenging in many areas (Ozdogan, 2010). Conversely, Landsat or other satellites with higher spatial resolution can provide a high-precision fragmented vegetation index for yield estimation at field and regional scales (Bolton and Friedl, 2013), which has been successfully used to estimate the yield of fruit tree crops. Sun et al. (2017) used the cumulative NDVI from TM satellites to estimate grape yield, with relative errors ranging from 10 to 18% and correlations from 0.62 to 0.77. Anastasiou et al. (2018)

established regression models between TM satellite-derived GNDVI and table grape yield, showing a coefficient of determination of 0.33 and RMSE of 5382 kg ha^{-1}. In addition, Rahman et al. (2018) explored the potential of WorldView-3 imagery for estimating the yield of mangoes based on all sampled trees from three orchards in two growing seasons, showing a strong correlation ($R^2 = 0.70$). In this research, NDVI derived from Landsat 8 was also confirmed to be well correlated with jujube fruit yield. Therefore, moderate and high spatial resolution remote sensing images have potential for yield estimation of fruit tree crops at the field scale. It is worth noting that each observed orchard selected in this research is more than 45 pixels in a Landsat image. If the model is used to estimate the yield of an individual orchard with a small acreage, the estimation accuracy may be reduced because of the mixed pixels. For the yield estimation of an individual jujube orchard with a small area, a higher spatial resolution remote sensing satellite or airborne dataset may be more appropriate.

Although the single Landsat satellite has a relatively long revisit cycle of 16 days, at present both Landsat 7 and 8 data can be available, which can be collected at one location every 8 days, depending on cloud coverage. Tariqul Islam et al. (2018) successfully used Landsat 5, 7, and 8 data to build a time series of NDVI for potato yield estimation, with a highly significant coefficient of correlation ($R^2 = 0.81$). It is also possible to construct a time series of NDVI based on Landsat 7 and 8 combined with Sentinel satellite data for our study area to estimate jujube yields, which needs to be determined by further research. In addition, the combination of Landsat and MODIS data has also been successfully applied to improve the accuracy of crop yield estimation, such as maize and soybeans (Bolton and Friedl, 2013), winter wheat (Huang et al., 2015), and corn (Doraiswamy et al., 2005). Usually, classification of the study area is performed by using remote sensing images with medium or high spatial resolution. For large-scale jujube yield estimation, it is worth exploring a combined time series of MODIS and Landsat data based on the proposed phenology-adjusted model. The 30 m land-use and crop type map based on Landsat data can be employed to determine the percentage of jujube areas in each MODIS image, thereby achieving large-scale monitoring for jujube yields.

Note that our research assumes that the phenological length of crop growth is only affected by temperature. The effect of day length and other factors could be taken into account if necessary when studying specific species or cultivars (Holzapfel et al., 2009). Moreover, different types of crops frequently present distinct phenological lengths, which can be calculated from the daily average temperature and the effective accumulated temperature sum, including TSUM1 (temperature sum from emergence to flowering) and TSUM2 (temperature sum from flowering to maturity) (de Wit et al., 2019). TSUM1 and TSUM2 values for some major crops are available in the WOFOST model software. However, the accumulated temperature required for crop growth could vary a lot with species and growing areas, and the phenological length needs to be verified by experiments.

6. Conclusions

Our results showed that the main fruit filling period was the best time to estimate jujube yields. NDVI was better correlated with jujube yield than SAVI, NDWI, and EVI. The average NDVI of the 14^{th} and 15^{th} half-months was verified to fit best for yield estimation, with the highest R^2. In addition, the relationship between Landsat 8-NDVI and jujube yields was well described by an exponential function. More importantly, the Landsat-NDVI yield estimation model was effectively optimized by introducing the phenological length as a key parameter, highlighting the potential of combining medium spatial resolution Landsat 8 images and phenology.

7. References

Anastasiou E., Balafoutis A., Darra N., Fountas S., Xanthopoulos G., Psiroukis V. and Biniari A., 2018. Satellite and proximal sensing to estimate the yield and quality of table grapes, Agriculture 8, 94.

Becker-Reshef I., Vermote E., Lindeman M. and Justice C., 2010. A generalized regression-based model for forecasting winter wheat yields in Kansas and Ukraine using MODIS data, Remote Sens. Environ. 114, 1312–1323.

Bognár P., Kern A., Pásztor S., Lichtenberger J., Koronczay D. and Ferencz C., 2017. Yield estimation and forecasting for winter wheat in Hungary using time series of modis data, Int. J. Remote Sens. 38, 3394–3414.

Bolton D.K. and Friedl M.A., 2013. Forecasting crop yield using remotely sensed vegetation indices and crop phenology metrics, Agric. For. Meteorol. 173, 74–84.

Bonilla I., De Toda F.M. and Martínez-Casasnovas J.A., 2015. Vine vigor, yield and grape quality assessment by airborne remote sensing over three years: Analysis of unexpected relationships in cv. tempranillo, Spanish J. Agric. Res. 13, 1–8.

Brian McConkey P.B., Lafond G.P., Moulin A. and Pelcat Y., 2004. Optimal time for remote sensing to relate to crop grain yield on the Canadian prairies, Can. J. Plant Sci. 84, 97–103.

de la Casa A., Ovando G., Bressanini L., Martínez J., Díaz G. and Miranda C., 2018. Soybean crop coverage estimation from NDVI images with different spatial resolution to evaluate yield variability in a plot, ISPRS J. Photogramm. Remote Sens. 146, 531–547.

de Wit, A., Boogaard, H., and Supit I. 2019. System description of the WOFOST 7.2. cropping system model. Wageningen Environmental Research. September, 2019.

Dempewolf J., Adusei B., Becker-Reshef I., Hansen M., Potapov P., Khan A. and Barker B., 2014. Wheat yield forecasting for Punjab Province from vegetation index time series and historic crop statistics, Remote Sens. 6, 9653–9675.

Doraiswamy P.C., Sinclair T.R., Hollinger S., Akhmedov B., Stern A. and Prueger J., 2005. Application of MODIS derived parameters for regional crop yield assessment, Remote Sens. Environ. 97, 192–202.

Duchemin B., Maisongrande P., Boulet G. and Benhadj I., 2008. A simple algorithm for yield estimates: evaluation for semi-arid irrigated winter wheat monitored with green leaf area index, Environ. Model. Softw. 23, 876–892.

The, F.O.R., Community, E., 1994. An agricultural information system system description of the wofost 6.0 crop simulation model implemented in CGMS Volume 1 : Theory and Algorithms.

Funk C. and Budde M.E., 2009. Phenologically-tuned MODIS NDVI-based production anomaly estimates for Zimbabwe, Remote Sens. Environ. 113, 115–125.

Gao B.C., 1996. NDWI – a normalized difference water index for remote sensing of vegetation liquid water from space, Remote Sens. Environ. 58, 257–266.

Hamar D., Ferencz C., Lichtenberger J. and Ferencz-Árkos J., 1996. Yield estimation for corn and wheat in the hungarian great plain using landsatmss data, Int. J. Remote Sens. 17, 1689–1699.

Hochheim K.P. and Barber D.G., 1998. Spring wheat yield estimation for western canada using NOAA NDVI Data, Can. J. Remote Sens. 24, 17–27.

Holzapfel C.B., Lafond G.P., Brandt S.A., Bullock P.R., Irvine R.B., 2009. Morrison M.J., May W.E. and James D.C., Estimating canola (Brassica napus L.) yield potential using an active optical sensor, Can. J. Plant Sci. 89, 1149–1160.

Huang J., Tian L., Liang S., Ma H., Becker-Reshef I., Huang Y., Su W., Zhang X., Zhu D. and Wu W., 2015. Improving winter wheat yield estimation by assimilation of the leaf area index from Landsat TM and MODIS data into the WOFOST model, Agric. For. Meteorol. 204, 106–121.

Huete A., 1988. A soil-adjusted vegetation index (SAVI), Remote Sens. Environ. 25, 295–309.

Kouadio L., Newlands N.K., Davidson A., Zhang Y. and Chipanshi A., 2014. Assessing the performance of MODIS NDVI and EVI for seasonal crop yield forecasting at the ecodistrict scale, Remote Sens. 6, 10193–10214.

Labus M.P., Nielsen G.A., Lawrence R.L., Engel R. and Long D.S., 2002. Wheat yield estimates using multi-temporal NDVI satellite imagery, Int. J. Remote Sens. 23, 4169–4180.

Liu L., Wang J., Bao Y., Huang W., Ma Z. and Zhao C., 2006. Predicting winter wheat condition, grain yield and protein content using multi-temporal EnviSat-ASAR and Landsat TM satellite images, Int. J. Remote Sens. 27, 737–753.

Ma B.L., Dwyer L.M., Costa C., Cober E.R. and Morrison M.J., 2001. Early prediction of soybean yield from canopy reflectance measurements, Agron. J. 93, 1227–1234.

Marti J., Bort J., Slafer G.A. and Araus J.L., 2007. Can wheat yield be assessed by early measurements of Normalized Difference Vegetation Index?, Ann. Appl. Biol. 150, 253–257.

Mkhabela M.S. and Mkhabela M.S., 2000. Exploring the Possibilities of Using Noaa, Vhrr Data To Forecast Cotton Yield in Swaziland, UNISWA J. Agric. 9, 13–21.

Mkhabela M.S., Mkhabela M.S. and Mashinini N.N., 2005. Early maize yield forecasting in the four agro-ecological regions of Swaziland using NDVI data derived from NOAA's-AVHRR, Agric. For. Meteorol. 129, 1–9.

Mkhabela M.S., Bullock P., Raj S., Wang S. and Yang Y., 2011. Crop yield forecasting on the Canadian Prairies using MODIS NDVI data, Agric. For. Meteorol. 151, 385–393.

Ozdogan M., 2010. The spatial distribution of crop types from MODIS data: Temporal unmixing using Independent Component Analysis, Remote Sens. Environ. 114, 1190–1204.

Panda S.S., Ames D.P. and Panigrahi S., 2010. Application of vegetation indices for agricultural crop yield prediction using neural network techniques, Remote Sens. 2, 673–696.

Pettorelli, N., 2013. The Normalized Difference Vegetation Index; ISBN 9780191810145.

Prasad A.K., Chai L., Singh R.P. and Kafatos M. 2006. Crop yield estimation model for Iowa using remote sensing and surface parameters, Int. J. Appl. Earth Obs. Geoinf. 8, 26–33.

Rahman M.M., Robson A. and Bristow M., 2018. Exploring the potential of high resolution worldview-3 Imagery for estimating yield of mango, Remote Sens. 10, 12.

Ren J., Chen Z., Zhou Q. and Tang H., 2008. Regional yield estimation for winter wheat with MODIS-NDVI data in Shandong, China, Int. J. Appl. Earth Obs. Geoinf. 10, 403–413.

Reynolds C.A., Yitayew M., Slack D.C., Hutchinson C.F., 2000. Huete A. and Petersen M.S., Estimating crop yields and production by integrating the FAO Crop Specific Water Balance model with real-time satellite data and ground-based ancillary data, Int. J. Remote Sens. 21, 3487–3508.

Rojas O., 2007. Operational maize yield model development and validation based on remote sensing and agro-meteorological data in Kenya, Int. J. Remote Sens. 28, 3775–3793.

Rudorff A.F. and Batista G.T., 1991. Wheat yield estimation at the farm level using tm landsatand agrometeorological data, Int. J. Remote Sens. 12, 2477–2484.

Sakamoto T., Gitelson A.A. and Arkebauer T.J., 2013. MODIS-based corn grain yield estimation model incorporating crop phenology information, Remote Sens. Environ. 131, 215–231.

Salazar L., Kogan F. and Roytman L., 2007. Use of remote sensing data for estimation of winter wheat yield in the United States, Int. J. Remote Sens. 28, 3795–3811.

Satir O. and Berberoglu S., 2016. Crop yield prediction under soil salinity using satellite derived vegetation indices, F. Crop. Res. 192, 134–143.

Sepulcre-Cantó G., Zarco-Tejada P.J., Jiménez-Muñoz J.C., Sobrino J.A., Soriano M.A., Fereres E., Vega V. and Pastor M., 2007. Monitoring yield and fruit quality parameters in open-canopy tree crops under water stress. Implications for ASTER, Remote Sens. Environ. 107, 455–470.

Son N.T., Chen C.F., Chen C.R., Minh V.Q. and Trung N.H., 2014. A comparative analysis of multitemporal MODIS EVI and NDVI data for large-scale rice yield estimation, Agric. For. Meteorol. 197, 52–64.

Sun, A. 2019. Effect of Temperature Change on Winter Jujube Production in Huanghua City. Guizhou Agricultural Sciences, 47(6): 88-91. In Chinese with english abstract.

Sun L., Gao F., Anderson M.C., Kustas W.P., Alsina M.M., Sanchez L., Sams B., McKee L., Dulaney W., White W.A., et al., 2017. Daily mapping of 30 m LAI and NDVI for grape yield prediction in California vineyards, Remote Sens. 9, 4.

Tariqul Islam A.F.M., Tahsin A., Razzaque S., Saiful Islam A.K.M., Newton I.H. and Tarekul Islam G.M., 2018. Yield prediction model for potato using landsattime series images driven vegetation indices, Remote Sens. Earth Syst. Sci. 1, 29–38.

Thenkabail P.S., 2003. Biophysical and yield information for precision farming from near-real-time and historical LandsatTM images, Int. J. Remote Sens. 24, 2879–2904.

Unganai L.S. and Kogan F.N., 1998. Drought monitoring and corn yield estimation in southern Africa from AVHRR data, Remote Sens. Environ. 63, 219–232.

Victoria D. de C., da Paz A.R., Coutinho A.C., Kastens J. and Brown J.C., 2012. Cropland area estimates using Modis NDVI time series in the state of Mato Grosso, Brazil, Pesqui. Agropecu. Bras. 47, 1270–1278.

Wall L., Larocque D. and Léger P.M., 2008. The early explanatory power of NDVI in crop yield modelling, Int. J. Remote Sens. 29, 2211–2225.

Wang M., Tao F.L. and Shi W.J., 2014. Corn yield forecasting in northeast china using remotely sensed spectral indices and crop phenology metrics, J. Integr. Agric. 13, 1538–1545.

Wardlow B.D., Egbert S.L. and Kastens J.H., 2007. Analysis of time-series MODIS 250 m vegetation index data for crop classification in the U.S. Central Great Plains, Remote Sens. Environ. 108, 290–310.

Wofost Model. Available online: <https://www.wur.nl/en/Research-Results/Research-Institutes/Environmental-Research/Facilities-Products/Software-and-models/WOFOST/Downloads-WOFOST.htm> (accessed on Jan 19, 2019).

Ye X., Sakai K., Garciano L.O., Asada S.I. and Sasao A., 2006. Estimation of citrus yield from airborne hyperspectral images using a neural network model, Ecol. Modell. 198, 426–432.

Ye X., Sakai K., Sasao A. and Asada S., 2008a. Potential of airborne hyperspectral imagery to estimate fruit yield in citrus, Chemom. Intell. Lab. Syst. 90, 132–144.

Ye X., Sakai K., Asada S. Ichi and Sasao A., 2008b. Application of narrow-band TBVI in estimating fruit yield in citrus, Biosyst. Eng. 99, 179–189.

Yousfi S., Kellas N., Saidi L., Benlakehal Z., Chaou L., Siad D., Herda F., Karrou M., Vergara O., Gracia A., et al., 2016. Comparative performance of remote sensing methods in assessing wheat performance under Mediterranean conditions, Agric. Water Manag. 164, 137–147.

Yu B. and Shang S., 2018. Multi-year mapping of major crop yields in an irrigation district from high spatial and temporal resolution vegetation index, Sensors (Switzerland) 18, 11.

Chapter 5

Improving jujube fruit yield estimation by assimilating a single Landsat remotely sensed LAI into the WOFOST model

This chapter describes the use of a forced method to assimilate a single remotely sensed LAI in order to improve yield estimation based on the WOFOST model calibrated in Chapter 3. When crop growth models are applied at regional scales, critical input parameters or state variables may be affected by factors such as genetics, management, and pests and diseases of the crop. Remote sensing technology can provide more accurate local state variables during crop development periods, which is helpful for improving the accuracy of crop growth simulations.

Firstly, a LAI regression model based on a vegetation index obtained from Landsat 8 was established, built on cross-validation of 2016 and 2017 data to produce the LAI for local jujube orchards. Secondly, a single LAI near to the maximum vegetative development stage was assimilated into the calibrated WOFOST model to improve the estimation of jujube fruit yield. The contribution of LAI at different phenological development stages to assimilation accuracy was also compared and discussed.

This chapter is based on: Tiecheng Bai, Nannan Zhang, Benoit Mercatoris, and Youqi Chen*, 2019. Improving jujube fruit tree yield estimation at the field scale by assimilating a single Landsat remotely-sensed LAI into the WOFOST model. Remote Sensing, 11(9), 1119 (pp. 1-22).*
** Corresponding Author.*

1. Abstract

Few studies have focused on yield estimation of perennial fruit tree crops by integrating remotely sensed information into crop models. This study presents an attempt to assimilate a single leaf area index (LAI) at near to maximum vegetative development stages derived from Landsat satellite data into a calibrated WOFOST model to estimate field-scale fruit yields. Normalized Difference Vegetation Index (NDVI) showed better performance for LAI estimation than a Soil-adjusted Vegetation Index (SAVI) during the fruit filling periods, with better agreement and accuracy (R^2 = 0.79, RMSE = 0.16 m^2 m^{-2} for 2016, and R^2 = 0.88, RMSE = 0.13 m^2 m^{-2} for 2017). The assimilation after forcing LAI improved the yield estimation accuracy compared with the unassimilated simulation, showing a R^2 of 0.62 and RMSE of 0.74 t ha^{-1} for 2016, and R^2 of 0.59 and RMSE of 0.87 t ha^{-1} for 2017. The RPD value after forced assimilation was also increased from 1.13 to 1.63 for 2016, and 1.02 to 1.56 for 2017. This research provides a strategy to employ remotely sensed state variables and a crop growth model to improve field-scale yield estimates for fruit tree crops.

2. Introduction

The regional-scale jujube fruit yield estimation before harvest is essential for national planting policies, food security, and export strategies. More importantly, field-scale jujube growth and yield estimates before harvest allow farmers to improve yield management decision-making, such as irrigation, fertilization, pruning, and density selection (Schulthess et al., 2013), which is also an important research topic for precision agriculture and forestry. Yield spatial distribution data can be used to determine crop and soil investments, nutrient applications, and farm trials. The spatial variability of yield data at a particular location can often respond to factors that affect yield (Oliver, 2010).

Cropping systems modelling based on mathematical descriptions expresses and quantifies the crop development process as influenced by climate, soil, and management conditions. This is considered to be a mature method for yield estimation (de Wit et al., 2019). Over the past decades, such crop models have been developed for different crops and purposes. Prominent models are WOFOST (World Food Studies) (van Diepen et al., 1989), DSSAT (Decision Support System for Agrotechnology Transfer) (Jones et al., 2003), EPIC (Environmental Policy Integrated Climate) (Wang et al., 2013), STICS (multidisciplinary simulator for standard crops) (Brisson et al., 2003), APSIM (Agricultural Production Systems Simulator) (Holzworth et al., 2014), SWAP (Soil, Water, Atmosphere, and Plant) (Van Dam et al., 1997), AquaCrop (a crop-water productivity model) (Raes et al., 2009), and CropSyst (Cropping Systems Simulation Model) (Stöckle et al., 2003). However, the spatial variation of input parameters of such models should be accounted for when crop yields are estimated over large regions (Jin et al., 2018). The uncertainties of soil properties (soil moisture and field capacity, etc.), and initial and canopy state variables (sowing date, initial dry weight, LAI, biomass, etc.) may affect

the accuracy of crop growth simulation and yield assessments (de Wit et al., 2012, 2019).

Remote sensing (RS) data can provide information about meteorological, vegetation, and soil conditions. More specifically, crop variables, such as LAI (Fang et al., 2011; Jiang et al., 2014; Nearing et al., 2012; Yao et al., 2015), biomass (Jin et al., 2015), leaf nitrogen accumulation (Huang et al., 2013), evapotranspiration (Bastiaanssen and Ali, 2003; Huang et al., 2015a), and soil moisture (Chakrabarti et al., 2014; Dente et al., 2008; Ines et al., 2013), can be observed from remote sensing data over large areas. Such RS data are often integrated into crop models to adjust and optimize input parameters and state variables in order to improve simulation results at field and regional scales. RS data have also been employed to accurately monitor crop phenology, which controls crop biomass accumulation length and distribution during the growth period (Sakamoto et al., 2013). In the last 15 years, new satellite data has become available, such as optical remote sensing data with medium and high spatial and temporal resolution (Sentinel-2, Landsat 8, RapidEye, WorldView-2, SPOT-6, GeoEye-1, Huanjing-1, Gaofen-1, et al.) and radar satellite data (ENVISAT, Sentinel-1, ALOS, ALOS-2, RADARSAT-2, TERRASAR-X, COSMO, etc.). These provide more timely and reliable data for crop model inputs (Jin et al., 2018).

Assimilation methods are often used to integrate remote sensing data into crop growth models, mainly including calibration methods, forcing methods, and updating methods (Argent, 2014; Delécolle et al., 1992; Dorigo et al., 2007; Moulin et al., 1998). In general, the main purpose of assimilation is to integrate canopy state variables or soil properties that are closely related to the crop growth process to optimize the key input parameters for the crop model. These methods have been employed to improve the estimation accuracy of crop yields at a regional scale (Chen et al., 2018; Curnel et al., 2011; Dente et al., 2008; Guo et al., 2017; Huang et al., 2019, 2016, 2015a, 2015b; Li et al., 2017; Xie et al., 2017) and at the field scale (Cheng et al., 2016; Donohue et al., 2018; Gilardelli et al., 2018; Silvestro et al., 2017; Jin et al., 2016).

For calibration methods, an optimization algorithm is employed to minimize the difference between the remote sensing observed values and the crop model simulated values for re-calibrating and optimizing the input parameters of crop models. The main optimization algorithms include the Maximum Likelihood Solution (MLS) (Dente et al., 2008), simplex search algorithm (Ma et al., 2013), Least Squares Method (LSM) (Zhao et al., 2013), Powell's Conjugate Direction Method (PCDM) (Fang et al., 2011), Shuffled Complex Evolution (SCE-UA) (Wang et al., 2014), Three-Dimensional Variational Data Assimilation (3DVAR) (Lorenc et al., 2000), Four-Dimensional Variational Data Assimilation (4DVAR) (Trémolet, 2007), Very Fast Annealing Algorithm (VFSA) (Dong et al., 2013), and Particle Swarm Optimization Algorithm (PSO) (Liu et al., 2015). For forcing methods, the simulated value of a crop growth state variable is directly replaced by a remotely sensed value to improve the simulated result (Jin et al., 2018) This has been performed for state variables such as LAI, above-ground biomass (AGB), yield, transpiration (Hadria et al., 2006; K. R. Schneider, 2003; Yao et al., 2015; Tripathy et al., 2013), and flowering date (Jongschaap, 2007). The updating method focuses on continuously updating crop model simulation data, methods include the Kalman Filter (KF) (Aubert et al., 2003;

Pellenq and Boulet, 2004), Ensemble Kalman Filter (EnKF) (Crow and Wood, 2003), Particle Filter (PF) (Moradkhani et al., 2005), and Hierarchical Bayesian Method (HBM) (Plant and Holland, 2011; Sahu et al., 2009). The correct orthogonal decomposition technique and the aggregate square root filtering method in EnKF, 4DVAR, PF, and 4DVAR (POD4DVAR) are used to combine the state variables of the remote sensing data and the crop model with the estimated soil moisture, AGB, LAI, and yield (Bolten et al., 2010; de Wit and van Diepen, 2007; Li et al., 2014). In short, it is generally believed that the yield estimation based on crop models can be improved by combining biophysical variables from remotely sensed data during the growing period (de Wit et al., 2012).

However, almost all crop growth models and assimilation methods have been employed and improved for annual crops. Few studies have focused on production simulation and assimilation of perennial fruit trees. Although existing research has confirmed that a crop growth model (WOFOST) can be used to simulate jujube growth in field experiments by calibrating input parameters (Bai et al., 2019), the difference in actual tree age and planting density may also lead to uncertainties. This difference shows a strong influence on jujube fruit yield. The main objective of this study was to use a remote sensing assimilation method to reduce the uncertainty of state variables associated with tree age and planting density and improve field-scale yield estimation accuracy. To accomplish this goal, the following specific objectives were defined:

i. To explore whether a single LAI (near to the maximum vegetative development stages) obtained from Landsat 8 with medium spatial resolution can improve the field-scale yield simulation accuracy for a fruit tree crop;
ii. To evaluate the assimilation performance by comparing the yield estimation results before and after forcing LAI, as well as to explore and compare the accuracy of yield estimation of forcing LAI at different phenological periods.

3. Research data and methods

3.1. Research data

The available Landsat 8 data from near to the maximum vegetative development stages were used to extract vegetation indices (VI), see Section 3.3 in Chapter 2. The measured LAI in 55 local orchards were used to calibrate and validate the LAI-VI regression model, see Section 3.2.2 in Chapter 2. Yield data for 181 orchards were used to evaluate the fruit yield estimation performance of the proposed forcing method at the local scale, see Section 3.2.1 in Chapter 2.

3.2. Research framework

The core of our strategy was to force a single LAI at near to the maximum vegetative development stages from Landsat 8 remote sensing data into the WOFOST model to improve jujube fruit yield estimation accuracy, and compare the estimation performance before and after the forced LAI. The research included three key steps:

(i) Model calibration for fruit yield estimation without forcing LAI, see Chapter 3.

(ii) A single LAI derived by regression from Landsat data at a near-maximum vegetative stage and forced into the calibrated WOFOST model to improve fruit yield estimation.

(iii) An assessment of the fruit yield estimation accuracy before and after forcing LAI with a discussion about the developmental stage at which the forcing is performed.

3.3. Forcing remotely sensed LAI and yield estimation

Based on LAI data from 55 monitored orchards, the accuracy of the NDVI-LAI or SAVI-LAI regression model for 2016 and 2017 was cross-validated. The validated VI-LAI model was employed to estimate LAI values for 181 orchards. Since maximum LAI played a dominant role in improving assimilation accuracy compared with LAI during other phenological stages (Huang et al., 2015b), LAI derived from Landsat 8 data at a near-peak vegetative stages (24 July 2016 and 27 July 2017) was forced into the calibrated WOFOST model to replace the state variable. The replaced value of this state variable determines the growth rate of the state variables at the next time step. Therefore, it was assumed that the final simulated yield was close to the actual value (Tripathy et al., 2013).

3.4. Accuracy evaluation

The coefficient of determination (R^2) was used to evaluate the agreement between estimated or simulated values and measured values. The root mean square error (RMSE) and a normalized root mean square error (NRMSE) were employed to quantify the estimation accuracy. The relative bias error (RBE, %), the mean absolute error (MAE, %), and RPD were also used to evaluate estimation performance, RBE and MAE are shown in Equations (5–1) and (5–2), respectively:

$$\mathrm{RBE}(\%) = \frac{\tilde{y}_i - y_i}{y_i} \times 100 \qquad (5-1)$$

$$\mathrm{MAE}(\%) = \frac{\sum_{i=1}^{n} |\tilde{y}_i - y_i|}{n \times \bar{y}_i} \times 100 \qquad (5-2)$$

Where $\tilde{y}_i$ was the estimated or simulated values, y_i was the observed or measured values, $\bar{y}_i$ was the mean of the observed or measured values, and n was the number of samples.

4. Results

4.1. Remotely sensed LAI

In the calibration or validation sets, the LAI regression results using NDVI were higher than using SAVI. The best regression equation for LAI and NDVI is shown in Table 5–1. For the year 2016, calibrated R^2 and RMSE were 0.89 and 0.12 $m^2\ m^{-2}$ (6.8%) for NDVI, 0.79 and 0.17 $m^2\ m^{-2}$ (9.7%) for SAVI, respectively, and the validated R^2 and RMSE were 0.79 and 0.16 $m^2\ m^{-2}$ (10.1%) for NDVI, 0.51 and 0.25 $m^2\ m^{-2}$ (15%) for SAVI, respectively. For 2017, NDVI also showed better LAI

estimation performance, with a validated R^2 of 0.88 and RMSE of 0.13 m^2 m^{-2} (7.3%). Previous studies have also confirmed that NDVI may perform better for estimating LAI than SAVI when vegetation coverage is high (Huang et al., 2015b).

Table 5–1: Leaf Area Index regression model (cross-validation of 2016 versus 2017).

Year	Equation	Calibration		Validation	
Accuracy		R^2	RMSE (m^2 m^{-2})	R^2	RMSE (m^2 m^{-2})
2016	$LAI = 0.1115 \times e^{4.00316 \times NDVI}$	0.89	0.12 (6.8%)	0.79	0.16 (10.1%)
	$LAI = 0.1367 \times e^{5.33345 \times SAVI}$	0.79	0.17 (9.7%)	0.51	0.25 (15.4)
2017	$LAI = 0.1417 \times e^{3.63713 \times NDVI}$	0.80	0.16 (9.9%)	0.88	0.13 (7.3%)
	$LAI = 0.2733 \times e^{3.81461 \times SAVI}$	0.65	0.21 (13.0)	0.72	0.21 (12.0%)

Brackets expressed the percentage of RMSE to the measured average LAI.

The scatter plots of the 2016 and 2017 cross-validation results based on the NDVI regression equation are shown in Figure 5–1, with good estimations for LAI (RPD = 2.22 and 2.93 for 2016 and 2017, respectively).

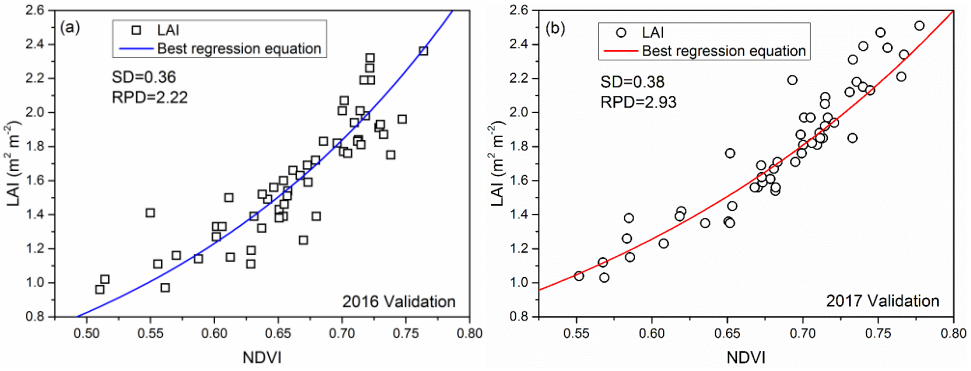

Figure 5–1: Calibrated and validated Leaf Area Index inversion models based on Normalized Difference Vegetation Index. SD = Standard deviation, RPD = SD/RMSE.

4.2. Yield estimation performance based on forcing method

4.2.1. Above-ground biomass simulation after forcing LAI

Taking the third orchard of LAI observations as an example, the simulated dry weight of leaves, stems, and total above-ground biomass before and after forcing LAI are shown in Figure 5–2. The values of all growth parameters after forcing became lower than their respective values before forcing. The fruit yield and LAI at forcing were reduced from 7,938 to 6,610 kg ha^{-1} and 2.31 to 1.81 m^2 m^{-2}, respectively. With these corrections in modelled growth parameters after assimilation, the actual fruit yield per orchard was re-estimated.

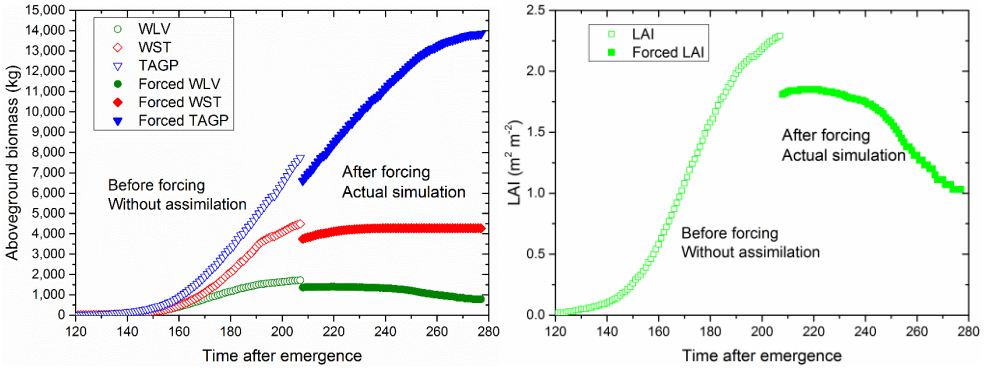

Figure 5–2: Simulated dry weight of leaves (WLV), dry weight of stems (WST), dry weight of total above-ground biomass (TAGP), and leaf area index (LAI) before and after forcing.

4.2.2. Yield estimation after forcing LAI

For the forcing method, the mean absolute error (MAE, %) of simulated yields versus measured values was 9.2% and 10.7% for 2016 and 2017, respectively (Figure 5–3). The relative percentage difference (RBE, %) of more than half of the samples was between –10% and 10% (62% for 2016 and 54% for 2017). More than 90% of the samples showed an estimated deviation between –20% and 20%

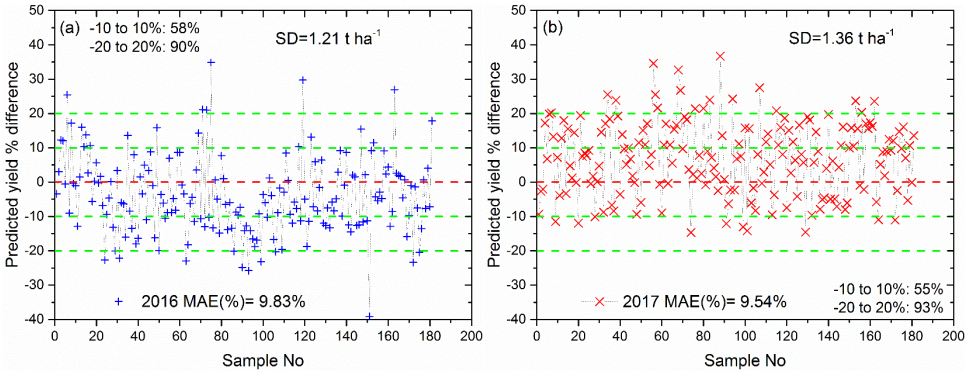

Figure 5–3: Relative percentage difference for fruit yield estimation for 2016(a) and 2017(b). MAE = Mean absolute error.

4.3. Comparison of yield estimation performance before and after forcing LAI

The scatterplots before and after forcing remotely-sensed LAI versus measured values are shown in Figure 5–4. The simulated yield without forcing LAI clearly deviated from the actual value. The results also indicated that there was still a high error in setting the default TDWI value for the same aged jujube orchards. The simulation performance of the model was significantly improved when the LAI at near

to the maximum vegetative development stages was forced into the calibrated WOFOST model. However, for the assimilation methods, actual yields were overestimated and underestimated at low yields and high yields, respectively. The reason for this may be that the CO_2 assimilation rate without forcing LAI was affected by tree age, a factor that was not considered in this study, which led to the overestimation of the yield at low tree age and underestimation at high tree age.

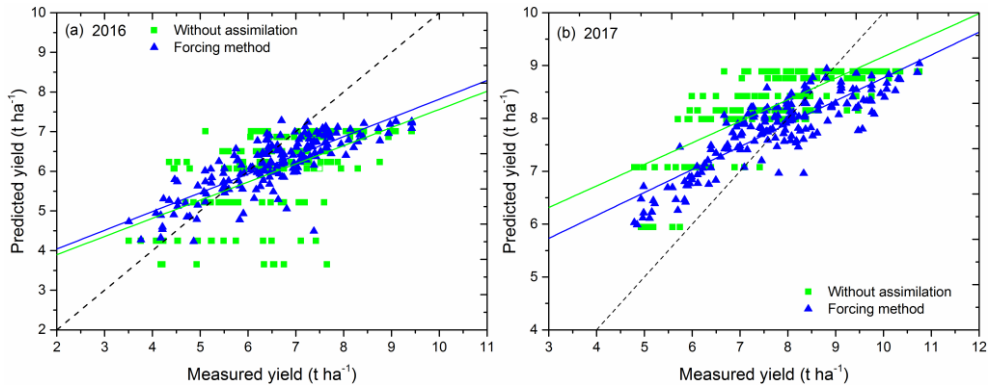

Figure 5–4: (a) Estimated versus measured yields of assimilation versus without assimilation. (a) 2016, (b) 2017.

Figure 5–5 shows the distributions of RBE (%) values before and after forcing the remotely sensed LAI. The forcing method resulted in RBE that were distributed more centrally around zero compared to the simulation without assimilation. Only two samples were overestimated and underestimated more than 30% in 2016 and 2017, respectively. The results also indicate the better performance of the assimilation-based estimation in reproducing spatial distribution for jujube yields.

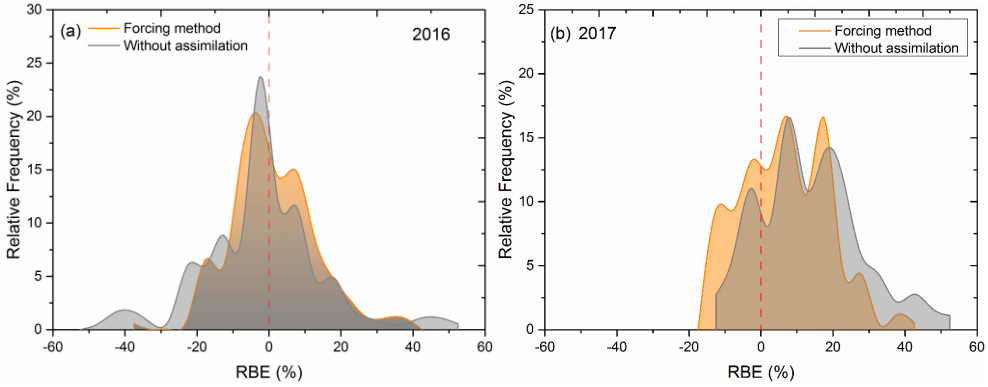

Figure 5–5: Frequency distributions (%) of relative bias error (RBE; %) resulting from the comparison between observed and simulated yields. RBE% = 0% (red line) represents the perfect estimation. Bin size is equal to 5.

The positive results achieved by the assimilation method were also confirmed by the indices of agreement and error between simulated and observed yields (Table 5–2). The assimilation method showed the better performance, with a R^2 of 0.62 and RMSE of 0.74 t ha^{-1} (11.3%) for 2016, and a R^2 of 0.59 and RMSE of 0.87 t ha^{-1} (11.3%) for 2017 compared to without assimilation (R^2 = 0.22, RMSE = 1.07 t ha^{-1} (16.3%) for 2016 and R^2 = 0.04, RMSE = 1.33 t ha^{-1} (17.2%) for 2017). The RPD values after forcing assimilation were also increased by 44% and 53% for 2016 and 2017, respectively.

Table 5–2: Accuracy comparison before and after assimilation

Estimation method	Year	R^2	RMSE (%) t ha^{-1}	RPD
Without assimilation	2016	0.22	1.07 (16.3)	1.13
	2017	0.04	1.33 (17.2)	1.02
Forcing LAI (assimilation)	2016	0.62	0.74 (11.3)	1.63
	2017	0.59	0.87 (11.3)	1.56

a. Numbers in brackets are percentages of root mean square error (RMSE) to average actual yields. LAI = leaf area index, RPD = standard deviation/RMSE.

4.4. Selection of the phenological periods of forced LAI

The accuracy of estimated jujube fruit yields using LAI from different phenological periods in 2017 is shown in Table 5–3. The LAI in the fruit filling period has the highest contribution to the estimation accuracy of forced assimilation, followed by the white ripening period, then the red ripening period, and finally the new leaf and stem development period. The LAI at the fruit filling and white ripening stages could be closer to the maximum LAI. Therefore, forcing at this period obtains a relatively high yield evaluation accuracy. Previous studies have proved that the heading LAI plays a key role in improving assimilation accuracy compared with LAI during other phenological stages (Huang et al., 2015b; Tripathy et al., 2013). In addition, jujube yield is highly correlated with the maximum LAI (Yang et al., 2012).

Table 5–3: Accuracy of the yield estimation using LAI from different phenological periods in 2017.

Phenological stage	R^2	RMSE (%) t ha^{-1}	RPD
Leaf and stem development (9 June)	/	1.67 (21.6)	0.81
Fruit filling (27 July)	0.59	0.87 (11.3)	1.56
White maturity (12 August)	0.54	0.92 (11.9)	1.48
Red ripening maturity (28 August)	0.35	1.09 (14.1)	1.25

5. Discussion

Previous studies have reported the use of remote sensing (Landsat 7 and 8) vegetation indices to estimate fruit crop yields at field scale, showing low relative errors from 6.9% to 11.5% for grape yield estimation (Sun et al., 2017). Rahman et al. (2018) also explored the potential of WorldView-3 imagery for predicting the yield of mangoes, showing a R^2 value ranging from 0.79–0.93 and RMSE from 7.9–9.1 kg tree^{-1} for three orchards. However, phenology information should be considered when performing crop yield estimations, and a time series of VI could be useful for crop yield forecasting (Yang et al., 2012). Although remote sensing satellites with medium and high spatial resolution have the potential to be used for field-scale yield estimation, it is a challenge to construct a time series of vegetation indices for the consideration of phenological information due to low temporal resolution. In contrast, crop growth models can take into account the growth process of the phenology. However, for the estimation method using the WOFOST model, the fruit yields of most jujube orchards were overestimated in 2017. The main reason may be that uncertainty in strongly varying tree age and planting densities may be introduced into the model structure, which may lead to a simulated yield bias for different orchards.

An approach forcing the LAI at near the peak vegetative stage into a calibrated WOFOST model was attempted to reduce the uncertainty and simulate the yield for a perennial jujube fruit tree crop at the field scale, showing better performance. Actual yields were slightly overestimated and underestimated at low and high values in 2016 and 2017, respectively. Two reasons may cause this deviation. The first may be that the CO_2 assimilation rate increased with the increase of tree age. The CO_2 assimilation parameters are set to fixed values in this research, which can lead to overestimation of yield at low tree age and underestimation at high tree age. The second reason may be the genetic varieties of phenological stages and crop characteristics, such as special leaf area (SLATB) and CO_2 assimilation parameters, thereby influencing potential yield. These parameters are expected to be further optimized by the assimilation of remote sensing information.

Assimilation accuracy based on the forcing method mainly relied on the accuracy of the state variables obtained by remote sensing. For Landsat satellite data with a resolution of 30 m, mixed pixels are inevitably present in the process of inverting LAI and estimating yields. In particular, the pixels may be mixed with shelter forest foliage and roads at the edge of the orchard, resulting in a decrease in the accuracy of the observed LAI. These errors from remote sensing observation data may be introduced into crop models when the assimilation is completed. Remote sensing data with higher spatial resolution can provide high-precision state variable estimation and can be recommended for inverting state variables to improve the accuracy of the observed variables. In addition, the combination of higher spatial resolution satellite data and Landsat satellite data is also expected to improve LAI inversion accuracy and yield estimation capabilities. Although calibration and updating methods with greater flexibility can minimize the simulation error and the remote sensing inversion error, they require sufficient observation points (Jin et al., 2018). High spatial resolution

satellites typically have low temporal resolution and it is often challenging to obtain more efficient observations. Therefore, fully exploiting the potential of single observational data is valuable for the remote sensing assimilation of fruit tree crops planted in a specific region.

In this study, LAI was assimilated into the crop model as the only state variable. Although LAI is an important indicator for canopy light interception and CO_2 assimilation, a single LAI does not accurately express the effect of effective radiation, temperature, nitrogen, and soil moisture content on jujube yield (Huang et al., 2015b). LAI, biomass, leaf nitrogen accumulation, evapotranspiration, and soil moisture obtained from remote sensing data can be expected to assimilate into the calibrated WOFOST model to optimize state variables and improve the accuracy of simulated jujube yields. In addition, the WOFOST model is carried out using a potential production simulation; the effects of other factors such as water stress are not considered. Temporal evolution of LAI and final yields can change with irrigation management and soil properties in different regions. The state variable SM (soil moisture content) can be recommended to respond to water transport conditions in rain-fed or irrigated jujube orchards when the model is applied in a water-limited production simulation (de Wit et al., 2019). Moreover, differences in plant diseases and pests, nitrogen stress, and jujube genetic parameters are not considered in the study. These several limiting factors can occur in the field, so that the external conditions are beyond the boundary conditions of the effective model range and influence the yield estimation accuracy when carrying out data assimilation (Jin et al., 2018). How to respond to these factors in the model will be a valuable avenue of research.

6. Conclusions

In this study, the WOFOST process-based growth model was tested to estimate the jujube fruit yield at a field scale. The modelling accuracy was enhanced by incorporating a single remotely sensed LAI at near to the maximum vegetative development period from Landsat 8 data into the growth model. Results indicated that the proposed method may be promising when using long-revisit cycle and medium spatial resolution remote sensing satellites for assimilation research. Note that the proposed method shows a slight deviation in high-yield and low-yield orchards, which may occur because the effect of tree age on CO_2 assimilation parameters and specific leaf parameters is not considered. In addition, when the model is applied to orchards with different pruning schemes, the CO_2 assimilation parameters may also need to be re-corrected. In future research work, the following points could be investigated:

(i) Assimilation of remotely sensed soil moisture content into the WOFOST model to determine the effects of irrigation and rainfall on the simulation results.

(ii) The influence of tree age and shape on CO2 assimilation parameters and the use of remote sensing data to optimize these parameters are worth exploring in order to improve simulation accuracy in high-yield and low-yield jujube orchards.

(iii) Whether assimilating a time series remotely sensed state variables can obtain better fruit yield prediction performance.

7. References

Argent, R., 2014. Land Surface Observation, Modelling and Data Assimilation. Environ. Model. Softw. 57, 248–249. https://doi.org/10.1016/j.envsoft.2014.02.009

Aubert, D., Loumagne, C., Oudin, L., 2003. Sequential assimilation of soil moisture and streamflow data in a conceptual rainfall - Runoff model. J. Hydrol. 280, 145–161. https://doi.org/10.1016/S0022-1694(03)00229-4

Bai, T., Zhang, N., Chen, Y., Mercatoris, B., 2019. Assessing the performance of the WOFOST model in simulating jujube fruit tree growth under different irrigation regimes. Sustain. 11. https://doi.org/10.3390/su11051466

Bastiaanssen, W.G.M., Ali, S., 2003. A new crop yield forecasting model based on satellite measurements applied across the Indus Basin, Pakistan. Agric. Ecosyst. Environ. 94, 321–340. https://doi.org/10.1016/S0167-8809(02)00034-8

Bolten, J.D., Crow, W.T., Jackson, T.J., Zhan, X., Reynolds, C.A., 2010. Evaluating the Utility of Remotely Sensed Soil Moisture Retrievals for Operational Agricultural Drought Monitoring. IEEE J. Sel. Top. Appl. Earth Obs. Remote Sens. 3, 57–66. https://doi.org/10.1109/JSTARS.2009.2037163

Brisson, N., Gary, C., Justes, E., Roche, R., Mary, B., Ripoche, D., Zimmer, D., Sierra, J., Bertuzzi, P., Burger, P., Bussière, F., Cabidoche, Y.M., Cellier, P., Debaeke, P., Gaudillère, J.P., Hénault, C., Maraux, F., Seguin, B., Sinoquet, H., 2003. An overview of the crop model STICS, in: European Journal of Agronomy. pp. 309–332. https://doi.org/10.1016/S1161-0301(02)00110-7

Chakrabarti, S., Bongiovanni, T., Judge, J., Zotarelli, L., Bayer, C., 2014. Assimilation of SMOS soil moisture for quantifying drought impacts on crop yield in agricultural regions. IEEE J. Sel. Top. Appl. Earth Obs. Remote Sens. 7, 3867–3879. https://doi.org/10.1109/JSTARS.2014.2315999

Chen, Y., Zhang, Z., Tao, F., 2018. Improving regional winter wheat yield estimation through assimilation of phenology and leaf area index from remote sensing data. Eur. J. Agron. 101, 163–173. https://doi.org/10.1016/j.eja.2018.09.006

Cheng, Z., Meng, J., Wang, Y., 2016. Improving spring maize yield estimation at field scale by assimilating time-series HJ-1 CCD data into the WOFOST model using a new method with fast algorithms. Remote Sens. 8. https://doi.org/10.3390/rs8040303

Crow, W.T., Wood, E.F., 2003. The assimilation of remotely sensed soil brightness temperature imagery into a land surface model using Ensemble Kalman filtering: A case study based on ESTAR measurements during SGP97. Adv. Water Resour. 26, 137–149. https://doi.org/10.1016/S0309-1708(02)00088-X

Curnel, Y., de Wit, A.J.W., Duveiller, G., Defourny, P., 2011. Potential performances of remotely sensed LAI assimilation in WOFOST model based on an OSS Experiment. Agric. For. Meteorol. 151, 1843–1855. https://doi.org/10.1016/j.agrformet.2011.08.002

de Wit, A., Boogaard, H., Fumagalli, D., Janssen, S., Knapen, R., van Kraalingen, D., Supit, I., van der Wijngaart, R., van Diepen, K., 2019. 25 years of the WOFOST cropping systems model. Agric. Syst. 168, 154–167. https://doi.org/10.1016/j.agsy.2018.06.018

de Wit, A., Duveiller, G., Defourny, P., 2012. Estimating regional winter wheat yield with WOFOST through the assimilation of green area index retrieved from MODIS observations. Agric. For. Meteorol. 164, 39–52. https://doi.org/10.1016/j.agrformet.2012.04.011

de Wit, A.J.W., van Diepen, C.A., 2007. Crop model data assimilation with the Ensemble Kalman filter for improving regional crop yield forecasts. Agric. For. Meteorol. 146, 38–56. https://doi.org/10.1016/j.agrformet.2007.05.004

Delécolle, R., Maas, S.J., Guérif, M., Baret, F., 1992. Remote sensing and crop production models: present trends. ISPRS J. Photogramm. Remote Sens. 47, 145–161. https://doi.org/10.1016/0924-2716(92)90030-D

Dente, L., Satalino, G., Mattia, F., Rinaldi, M., 2008. Assimilation of leaf area index derived from ASAR and MERIS data into CERES-Wheat model to map wheat yield. Remote Sens. Environ. 112, 1395–1407. https://doi.org/10.1016/j.rse.2007.05.023

Dong, Y., Zhao, C., Yang, G., Chen, L., Wang, J., Feng, H., 2013. Integrating a very fast simulated annealing optimization algorithm for crop leaf area index variational assimilation. Math. Comput. Model. 58, 877–885. https://doi.org/10.1016/j.mcm.2012.12.013

Donohue, R.J., Lawes, R.A., Mata, G., Gobbett, D., Ouzman, J., 2018. Towards a national, remote-sensing-based model for predicting field-scale crop yield. F. Crop. Res. 227, 79–90. https://doi.org/10.1016/j.fcr.2018.08.005

Dorigo, W.A., Zurita-Milla, R., de Wit, A.J.W., Brazile, J., Singh, R., Schaepman, M.E., 2007. A review on reflective remote sensing and data assimilation techniques for enhanced agroecosystem modelling. Int. J. Appl. Earth Obs. Geoinf. 9, 165–193. https://doi.org/10.1016/j.jag.2006.05.003

Fang, H., Liang, S., Hoogenboom, G., 2011. Integration of MODIS LAI and vegetation index products with the CSM-CERES-Maize model for corn yield estimation. Int. J. Remote Sens. 32, 1039–1065. https://doi.org/10.1080/01431160903505310

Gilardelli, C., Confalonieri, R., Cappelli, G.A., Bellocchi, G., 2018. Sensitivity of WOFOST-based modelling solutions to crop parameters under climate change. Ecol. Modell. 368, 1–14. https://doi.org/10.1016/j.ecolmodel.2017.11.003

Guo, C., Zhang, L., Zhou, X., Zhu, Y., Cao, W., Qiu, X., Cheng, T., Tian, Y., 2017. Integrating remote sensing information with crop model to monitor wheat growth and yield based on simulation zone partitioning. Precis. Agric. 1–24. https://doi.org/10.1007/s11119-017-9498-5

Hadria, R., Duchemin, B., Lahrouni, A., Khabba, S., Er-Raki, S., Dedieu, G., Chehbouni, A.G., Olioso, A., 2006. Monitoring of irrigated wheat in a semi-arid climate using crop modelling and remote sensing data: Impact of satellite revisit time frequency. Int. J. Remote Sens. 27, 1093–1117. https://doi.org/10.1080/01431160500382980

Holzworth, D.P., Huth, N.I., deVoil, P.G., Zurcher, E.J., Herrmann, N.I., McLean, G., Chenu, K., van Oosterom, E.J., Snow, V., Murphy, C., Moore, A.D., Brown, H., Whish, J.P.M., Verrall, S., Fainges, J., Bell, L.W., Peake, A.S., Poulton, P.L., Hochman, Z., Thorburn, P.J., Gaydon, D.S., Dalgliesh, N.P., Rodriguez, D., Cox, H., Chapman, S., Doherty, A., Teixeira, E., Sharp, J., Cichota, R., Vogeler, I., Li, F.Y., Wang, E., Hammer, G.L., Robertson, M.J., Dimes, J.P., Whitbread, A.M., Hunt, J., van Rees, H., McClelland, T., Carberry, P.S., Hargreaves, J.N.G., MacLeod, N.,

McDonald, C., Harsdorf, J., Wedgwood, S., Keating, B.A., 2014. APSIM - Evolution towards a new generation of agricultural systems simulation. Environ. Model. Softw. 62, 327–350. https://doi.org/10.1016/j.envsoft.2014.07.009

Huang, J., Ma, H., Sedano, F., Lewis, P., Liang, S., Wu, Q., Su, W., Zhang, X., Zhu, D., 2019. Evaluation of regional estimates of winter wheat yield by assimilating three remotely sensed reflectance datasets into the coupled WOFOST–PROSAIL model. Eur. J. Agron. 102, 1–13. https://doi.org/10.1016/j.eja.2018.10.008

Huang, J., Ma, H., Su, W., Zhang, X., Huang, Y., Fan, J., Wu, W., 2015a. Jointly Assimilating MODIS LAI and et Products into the SWAP Model for Winter Wheat Yield Estimation. IEEE J. Sel. Top. Appl. Earth Obs. Remote Sens. 8, 4060–4071. https://doi.org/10.1109/JSTARS.2015.2403135

Huang, J., Sedano, F., Huang, Y., Ma, H., Li, X., Liang, S., Tian, L., Zhang, X., Fan, J., Wu, W., 2016. Assimilating a synthetic Kalman filter leaf area index series into the WOFOST model to improve regional winter wheat yield estimation. Agric. For. Meteorol. 216, 188–202. https://doi.org/10.1016/j.agrformet.2015.10.013

Huang, J., Tian, L., Liang, S., Ma, H., Becker-Reshef, I., Huang, Y., Su, W., Zhang, X., Zhu, D., Wu, W., 2015b. Improving winter wheat yield estimation by assimilation of the leaf area index from Landsat TM and MODIS data into the WOFOST model. Agric. For. Meteorol. 204, 106–121. https://doi.org/10.1016/j.agrformet.2015.02.001

Huang, Y., Zhu, Y., Li, W., Cao, W., Tian, Y., 2013. Assimilating Remotely Sensed Information with the WheatGrow Model Based on the Ensemble Square Root Filter forImproving Regional Wheat Yield Forecasts. Plant Prod. Sci. 16, 352–364. https://doi.org/10.1626/pps.16.352

Ines, A.V.M., Das, N.N., Hansen, J.W., Njoku, E.G., 2013. Assimilation of remotely sensed soil moisture and vegetation with a crop simulation model for maize yield prediction. Remote Sens. Environ. 138, 149–164. https://doi.org/10.1016/j.rse.2013.07.018

Jiang, Z., Chen, Z., Chen, J., Liu, J., Ren, J., Li, Z., Sun, L., Li, H., 2014. Application of crop model data assimilation with a particle filter for estimating regional winter wheat yields. IEEE J. Sel. Top. Appl. Earth Obs. Remote Sens. 7, 4422–4431. https://doi.org/10.1109/JSTARS.2014.2316012

Jin, X., Kumar, L., Li, Z., Feng, H., Xu, X., Yang, G., Wang, J., 2018. A review of data assimilation of remote sensing and crop models. Eur. J. Agron. https://doi.org/10.1016/j.eja.2017.11.002

Jin, X., Kumar, L., Li, Z., Xu, X., Yang, G., Wang, J., 2016. Estimation of winter wheat biomass and yield by combining the aquacrop model and field hyperspectral data. Remote Sens. 8. https://doi.org/10.3390/rs8120972

Jin, X., Yang, G., Xu, X., Yang, H., Feng, H., Li, Z., Shen, J., Zhao, C., Lan, Y., 2015. Combined multi-temporal optical and radar parameters for estimating LAI and biomass in winter wheat using HJ and RADARSAR-2 data. Remote Sens. 7, 13251–13272. https://doi.org/10.3390/rs71013251

Jones, J.W., Hoogenboom, G., Porter, C.H., Boote, K.J., Batchelor, W.D., Hunt, L.A., Wilkens, P.W., Singh, U., Gijsman, A.J., Ritchie, J.T., 2003. The DSSAT cropping system model, in: European Journal of Agronomy. pp. 235–265. https://doi.org/10.1016/S1161-0301(02)00107-7

Jongschaap, R.E.E., 2007. Sensitivity of a crop growth simulation model to variation in LAI and canopy nitrogen used for run-time calibration. Ecol. Modell. 200, 89–98. https://doi.org/10.1016/j.ecolmodel.2006.07.015

Li, H., Chen, Z., Liu, G., Jiang, Z., Huang, C., 2017. Improving winter wheat yield estimation from the CERES-Wheat model to assimilate leaf area index with different assimilation methods and spatio-temporal scales. Remote Sens. 9. https://doi.org/10.3390/rs9030190

Li, Y., Zhou, Q., Zhou, J., Zhang, G., Chen, C., Wang, J., 2014. Assimilating remote sensing information into a coupled hydrology-crop growth model to estimate regional maize yield in arid regions. Ecol. Modell. 291, 15–27. https://doi.org/10.1016/j.ecolmodel.2014.07.013

Liu, F., Liu, X., Zhao, L., Ding, C., Jiang, J., Wu, L., 2015. The Dynamic Assessment Model for Monitoring Cadmium Stress Levels in Rice Based on the Assimilation of Remote Sensing and the WOFOST Model. IEEE J. Sel. Top. Appl. Earth Obs. Remote Sens. 8, 1330–1338. https://doi.org/10.1109/JSTARS.2014.2371058

Lorenc, A.C., Ballard, S.P., Bell, R.S., Ingleby, N.B., Andrews, P.L.F., Barker, D.M., Bray, J.R., Clayton, A.M., Dalby, T., Li, D., Payne, T.J., Saunders, F.W., 2000. The Met. Office global three-dimensional variational data assimilation scheme. Q. J. R. Meteorol. Soc. 126, 2991–3012. https://doi.org/10.1256/smsqj.57001

Ma, G., Huang, J., Wu, W., Fan, J., Zou, J., Wu, S., 2013. Assimilation of MODIS-LAI into the WOFOST model for forecasting regional winter wheat yield. Math. Comput. Model. 58, 634–643. https://doi.org/10.1016/j.mcm.2011.10.038

Moradkhani, H., Hsu, K.L., Gupta, H., Sorooshian, S., 2005. Uncertainty assessment of hydrologic model states and parameters: Sequential data assimilation using the particle filter. Water Resour. Res. 41, 1–17. https://doi.org/10.1029/2004WR003604

Moulin, S., Bondeau, A., Delecolle, R., 1998. Combining agricultural crop models and satellite observations: From field to regional scales. Int. J. Remote Sens. https://doi.org/10.1080/014311698215586

Nearing, G.S., Crow, W.T., Thorp, K.R., Moran, M.S., Reichle, R.H., Gupta, H. V., 2012. Assimilating remote sensing observations of leaf area index and soil moisture for wheat yield estimates: An observing system simulation experiment. Water Resour. Res. 48. https://doi.org/10.1029/2011WR011420

Oliver. M. A. Geostatistical Applications for Precision Agriculture, 2010. , Geostatistical Applications for Precision Agriculture. https://doi.org/10.1007/978-90-481-9133-8

Pellenq, J., Boulet, G., 2004. A methodology to test the pertinence of remote-sensing data assimilation into vegetation models for water and energy exchange at the land surface. Agronomie 24, 197–204. https://doi.org/10.1051/agro:2004017

Plant, N.G., Holland, K.T., 2011. Prediction and assimilation of surf-zone processes using a Bayesian network. Part II: Inverse models. Coast. Eng. 58, 256–266. https://doi.org/10.1016/j.coastaleng.2010.11.002

Raes, D., Steduto, P., Hsiao, T.C., Fereres, E., 2009. Aquacrop-The FAO crop model to simulate yield response to water: II. main algorithms and software description. Agron. J. 101, 438–447. https://doi.org/10.2134/agronj2008.0140s

Rahman, M.M., Robson, A., Bristow, M., 2018. Exploring the potential of high resolution worldview-3 Imagery for estimating yield of mango. Remote Sens. 10. https://doi.org/10.3390/rs10121866

Sahu, S.K., Yip, S., Holland, D.M., 2009. Improved space-time forecasting of next day ozone concentrations in the eastern US. Atmos. Environ. 43, 494–501. https://doi.org/10.1016/j.atmosenv.2008.10.028

Sakamoto, T., Gitelson, A.A., Arkebauer, T.J., 2013. MODIS-based corn grain yield estimation model incorporating crop phenology information. Remote Sens. Environ. 131, 215–231. https://doi.org/10.1016/j.rse.2012.12.017

Schneider, K., 2003. Assimilating remote sensing data into a land-surface process model. Int. J. Remote Sens. 24, 2959–2980. https://doi.org/10.1080/01431160210154803

Schulthess, U., Timsina, J., Herrera, J.M., McDonald, A., 2013. Mapping field-scale yield gaps for maize: An example from Bangladesh. F. Crop. Res. 143, 151–156. https://doi.org/10.1016/j.fcr.2012.11.004

Silvestro, P.C., Pignatti, S., Pascucci, S., Yang, H., Li, Z., Yang, G., Huang, W., Casa, R., 2017. Estimating wheat yield in China at the field and district scale from the assimilation of satellite data into the Aquacrop and simple algorithm for yield (SAFY) models. Remote Sens. 9. https://doi.org/10.3390/rs9050509

Stöckle, C.O., Donatelli, M., Nelson, R., 2003. CropSyst, a cropping systems simulation model, in: European Journal of Agronomy. pp. 289–307. https://doi.org/10.1016/S1161-0301(02)00109-0

Sun, L., Gao, F., Anderson, M.C., Kustas, W.P., Alsina, M.M., Sanchez, L., Sams, B., McKee, L., Dulaney, W., White, W.A., Alfieri, J.G., Prueger, J.H., Melton, F., Post, K., 2017. Daily mapping of 30 m LAI and NDVI for grape yield prediction in California vineyards. Remote Sens. 9. https://doi.org/10.3390/rs9040317

Trémolet, Y., 2007. Model-error estimation in 4D-Var. Q. J. R. Meteorol. Soc. 133, 1267–1280. https://doi.org/10.1002/qj.94

Tripathy, R., Chaudhari, K.N., Mukherjee, J., Ray, S.S., Patel, N.K., Panigrahy, S., Singh Parihar, J., 2013. Forecasting wheat yield in Punjab state of India by combining crop simulation model WOFOST and remotely sensed inputs. Remote Sens. Lett. 4, 19–28. https://doi.org/10.1080/2150704X.2012.683117

Van Dam, J.C., Wesseling, J.G., Feddes, R. a., Kabat, P., Walsum, P.E.V. Van, Diepen, C. a. Van, 1997. Theory of SWAP version 2.0: Softw. Man. 153.

van Diepen, C.A., Wolf, J., van Keulen, H., Rappoldt, C., 1989. WOFOST: a simulation model of crop production. Soil Use Manag. 5, 16–24. https://doi.org/10.1111/j.1475-2743.1989.tb00755.x

Wang, H., Zhu, Y., Li, W., Cao, W., Tian, Y., 2014. Integrating remotely sensed leaf area index and leaf nitrogen accumulation with RiceGrow model based on particle swarm optimization algorithm for rice grain yield assessment. J. Appl. Remote Sens. 8, 083674. https://doi.org/10.1117/1.JRS.8.083674

Wang, X., Williams, J. R., Gassman, P. W., Baffaut, C., Izaurralde, R. C., Jeong, J., and Kiniry, J. R., 2013. EPIC and APEX: Model Use, Calibration, and Validation. Trans. ASABE 55, 1447–1462. https://doi.org/10.13031/2013.42253

Xie, Y., Wang, P., Bai, X., Khan, J., Zhang, S., Li, L., Wang, L., 2017. Assimilation of the leaf area index and vegetation temperature condition index for winter wheat yield estimation using Landsat imagery and the CERES-Wheat model. Agric. For. Meteorol. 246, 194–206. https://doi.org/10.1016/j.agrformet.2017.06.015

Yang, W., Gao, J., Xu, C., 2012. The correlation analysis of leaf area index and yield of red jujube. Xinjiang Agricultural Sciences, 49, 1397-1400. (In Chinese with English abstract)

Yao, F., Tang, Y., Wang, P., Zhang, J., 2015. Estimation of maize yield by using a process-based model and remote sensing data in the Northeast China Plain. Phys. Chem. Earth 87–88, 142–152. https://doi.org/10.1016/j.pce.2015.08.010

Zhao, Y., Chen, S., Shen, S., 2013. Assimilating remote sensing information with crop model using Ensemble Kalman Filter for improving LAI monitoring and yield estimation. Ecol. Modell. 270, 30–42. https://doi.org/10.1016/j.ecolmodel.2013.08.016

Chapter 6

Assimilation of a time series of remotely sensed LAI into the WOFOST model to improve the field-scale jujube fruit yield estimation

In the previous chapter, a remotely sensed LAI was assimilated into the WOFOST growth model to improve the fruit yield estimation accuracy for jujube fruits. This approach gave promising results but remains limited by the correction of a state variable at a single specific time during the growing season. In this spirit, this chapter presents attempts to assimilate a time series of remotely sensed LAI to improve jujube yield estimation by using the EnKF and SUBPLEX methods, respectively. The main innovation of this chapter is to develop a new calibration assimilation method – SUBPLEX. The assimilation accuracy for jujube fruit yield estimation of the proposed SUBPLEX with a widely used sequential method (EnKF) is compared.

Firstly, the assimilation mechanism and implementation process of the EnKF and SUBPLEX algorithms are described, and the effect of parameter settings on assimilation accuracy is also analysed. Secondly, the accuracy of jujube fruit yield estimation of the two assimilation methods is evaluated by assimilating field-measured and remotely sensed LAI, respectively. Finally, for the proposed SUBPLEX method, the contribution of LAI at different phenological development stages to the assimilation accuracy is discussed.

This chapter is based on：Tiecheng Bai, Shanggui Wang, Wenbo Meng, Nannan Zhang, Tao Wang, Youqi Chen and Benoit Mercatoris, 2019. Assimilation of remotely sensed LAI into WOFOST model with the SUBPLEX algorithm for improving the field-scale jujube yield forecasts. Remote Sensing. 11(16), 1945(pp.1-20). * Corresponding Author.*

1. Abstract

In order to enhance the simulated accuracy of jujube fruit yields at the field scale, this study employs the SUBPLEX algorithm to assimilate remotely sensed LAI of four key growth stages into a calibrated WOFOST model, and compares the accuracy of such an assimilation with the widely used Ensemble Kalman Filter (EnKF) assimilation. LAIs obtained from remote sensing were assimilated into the WOFOST model to re-calibrate input TDWI (initial total crop dry weight) and SPAN (life span of leaves growing at 35°C) parameters. Results showed that both SUBPLEX and EnKF assimilations significantly improved yield estimation performance compared with the un-assimilated simulation. The SUBPLEX (R^2 = 0.78 and RMSE = 0.64 t ha^{-1}) also showed slightly better yield estimation accuracy compared with EnKF assimilation (R^2 = 0.66 and RMSE = 0.79 t ha^{-1}), especially for high-yield and low-yield jujube orchards. SUBPLEX assimilation produced a relative bias error (RBE, %) that was more concentrated near zero, being lower than 10% in 80.1%, and lower than 20% in 96.1% for SUBPLEX, 80.1% and 93.9% for EnKF, respectively. The study provided a new assimilation scheme based on the SUBPLEX algorithm to combine remotely sensed information and a crop growth model to improve field-scale fruit crop yield estimates.

2. Introduction

Jujube (*Zizyphus jujuba*) is a significant economically valuable tree species in China with approximately 3,250,000 farmed hectares in 2017, and the fruit has important nutritional and medicinal value (Chen et al., 2016; Li et al., 2007). Field-scale jujube growth monitoring and yield estimation allow farmers to make management decisions, such as precision planting, irrigation optimization, fertilization, and pest management, which are also important components of precision agriculture and horticulture.

Assimilation of remote sensing information into crop models is considered to be a key technical tool for yield prediction. The goal of assimilation is to reduce the uncertainty in the spatial distribution of crop parameters, soil properties, and meteorological data of crop model applications in large areas (Jin et al., 2018). The key input parameters or state variables, such as phenology information (Zhuo et al., 2019), leaf area index (LAI) (Fang et al., 2008; Huang et al., 2015a, 2015b, 2016; Nearing et al., 2012; Yao et al., 2015), biomass (Jin et al., 2015), crop transpiration (ET) (Huang et al., 2015a), and soil moisture (SM) (Chakrabarti et al., 2014; Ines et al., 2013; Mishra et al., 2015; Nearing et al., 2012; Wang et al., 2013; Zhuo et al., 2019), can be observed from remote sensing data. In recent years, data assimilation methods, including variational (calibration) and sequential (update) methods, have been used to integrate remote sensing data into crop models to improve the estimation accuracy of canopy state variables and yields at the field, regional, and national scale (Huang et al., 2019b).

The variational method takes all available observations during the main growth season and attempts to fit the model to the observations by minimizing the cost function, thereby optimizing the initial parameters of crop models. Several variational

methods for remote sensing and crop model assimilation have been reported, including, Shuffled Complex Evolution simplex algorithm (SCE-UA) (Dong et al., 2016; Huang et al., 2019b, 2015a; Ma et al., 2013; Ren et al., 2010), Four-dimensional Variational Data Assimilation (4DVAR) (Dong et al., 2013a, 2013b; He et al., 2015; Huang et al., 2015b; Jin et al., 2016), Particle Swarm Optimization (PSO) (Guo et al., 2017; Jin et al., 2015; Jin et al., 2017; Li et al., 2015; Liu et al., 2015; Silvestro et al., 2017), Powell's Conjugate Direction Method (PCMD) (Fang et al., 2011, 2008; He et al., 2015; Tian et al., 2013), Simplex Search Algorithm (SSA) (Claverie et al., 2009; Jégo et al., 2012), Maximum Likelihood Solution (MLS) (Dente et al., 2008), Golden Section Searching (GSS) (Hu et al., 2014), and Annealing Algorithm (AA) (Dong et al., 2013a; Jin et al., 2016; Morel et al., 2014). Canopy LAI is a state variable used by most studies because it directly reflects the growth of the crop. In addition, FAPAR (Hu et al., 2014; Morel et al., 2014), ET (Huang et al., 2015a; Ines et al., 2006), leaf nitrogen accumulation (Wang et al., 2014), vegetation indices (Dong et al., 2013a; Fang et al., 2011; Guo et al., 2017), and band reflectance (Huang et al., 2019b) have also demonstrated potential as state variables for remote sensing assimilation to optimize initial parameters for crop models. The variational method attributes the model input, output, and the model's own error to the uncertainty of the initial conditions or the parameters of the model, and does not consider the state variable estimation error during the time evolution of the model parameters. Therefore, in practical applications, the assimilation accuracy of the variational method often depends on the quality and accuracy of external observation data.

Sequential methods directly update the state variables of a modelling system when observations become available. The magnitude of the state update then depends on the uncertainty in both the model state and the observation. Examples of sequential approaches are the Ensemble Kalman Filter (EnKF) (Bolten et al., 2010; Chakrabarti et al., 2014; Cheng et al., 2018; Curnel et al., 2011; de Wit and van Diepen, 2007; Huang et al., 2016; Ines et al., 2013; Li et al., 2014; Ma et al., 2013; Nearing et al., 2012; Pauwels et al., 2007; Silvestro et al., 2017; Wang et al., 2013; Wu et al., 2012; Xie et al., 2017; Zhao et al., 2013; Zhu et al., 2013), Particle Filter (PF) (Jiang et al., 2014), Constant Gain Kalman Filter (CGKF) (Chen et al., 2018; Vazifedoust et al., 2009), and Ensemble Square Root Filter (EnSRF) (Huang et al., 2013; Mishra et al., 2015). For the state variables of sequential methods, LAI is the most focused, followed by soil moisture content (SM). The reported studies also show that the EnKF algorithm has been adopted by more researchers to improve assimilation accuracy.

EnKF continuously updates a new set of input parameters at each observation point. If the state variable statistic error of remote sensing is a Gaussian distribution, the EnKF method is considered to be the preferred assimilation method because most crop growth models are nonlinear (Huang et al., 2019a). However, the assimilation accuracy of the EnKF method is also easily affected by phenological shifts (Curnel et al., 2011). If the phenology information is uncertain, the variational method is usually superior to the sequential method, which can reduce the accumulation and diffusion of remote sensing data errors in the assimilation process (Jin et al., 2018). Of course, it also requires more computing time. The SUBPLEX method is based on the Nelder–Mead Simplex algorithm (NMS), which determines an improved set of subspaces and

then uses NMS to search each subspace (Rowan, 1990). For most applications, SUBPLEX shows higher computational efficiency for the unconstrained optimization of general multivariate functions than the simplex searching method (Jonsén et al., 2009). In principle, SUBPLEX is one of the variational assimilation methods, which is different from the EnKF assimilation process. It calculates a set of optimal input parameters based on the error of all remote sensing observations and simulated values. In addition, when the number of remote sensing observations is large, the SUBPLEX method can divide the observation points into several lower-dimensional vectors, thereby improving computational efficiency. More importantly, for objective functions affected by remote sensing observation error, the measurement replication option of SUBPLEX can be used to avoid convergence to a false minimum (Rowan, 1990). Whether the SUBPLEX algorithm has the potential to be applied to the assimilation of remote sensing and crop growth models is a valuable avenue of research.

In addition, almost all remote sensing and crop growth model assimilation studies focus on annual crops, and few studies have discussed growth simulation and assimilation of perennial fruit tree crops. Therefore, the objective of this study is to develop a data assimilation framework based on an unconstrained optimization algorithm (SUBPLEX) that integrates remotely sensed LAI into a calibrated WOFOST model to improve the jujube fruit yield estimation at the field scale. To accomplish this goal, the following two specific objectives are defined:

i. To develop the SUBPLEX algorithm to optimize the key input parameters of the WOFOST model for reducing uncertainty, thereby improving field-scale fruit yield estimation for local jujube orchards.
ii. To compare the yield estimation performance of the proposed SUBPLEX assimilation with the EnKF method.

3. Research data and methods

3.1. Research data

The available time series of Landsat 8 data were used to extract vegetation indices (VI) and calculate LAIs for four development periods, see Section 3.3 in Chapter 2. LAIs measured in 55 local orchards were used to calibrate and validate the LAI-VI regression model, see Section 3.2.2 in Chapter 2. Yield data for 181 orchards were used to evaluate the yield estimation performance of the proposed EnKF and SUBPLEX assimilation methods at the local scale, see Section 3.2.1 in Chapter 2.

3.2. Remotely-sensed LAI

Four Landsat 8 satellite data images with a spatial resolution of 30 m, taken during the main growth season in 2017, were acquired from the United States Geological Survey (USGS, https://earthexplorer.usgs.gov/). The dates of the available remote sensing images are 9 June, 27 July, 12 August, and 28 August, and correspond to emergence, fruit filling, and maturity periods. Band 4 (red, 0.630–0.680 μm) and 5 (near-infrared, 0.845–0.885μm) from the Operational Land Imager (OLI) were used

in this study for vegetation index extraction and establishing the LAI regression model. Geometric and atmospheric corrections were carried out for the Landsat 8 data by reference to the Albers conical equal-area map projection using 50 field-measured ground control points and the Fast Line-of-sight Atmospheric Analysis of Spectral Hypercubes (FLAASH) model, respectively. The parameter settings refer to a previous study (Bai et al., 2019b).

Since the spectral information of the crop is strongly influenced by the soil background, a soil-adjusted vegetation index (SAVI) may be a suitable choice to establish a statistical relationship during the period before the soil is covered by vegetation (Huete, 1988). Referring to the research method of Huang et al. (2015b), the LAI inversion models at four different developmental stages were established separately. Furthermore, the accuracy of the LAI statistical regression model based on remotely sensed NDVI and SAVI was compared to determine a suitable index. 37 of the 55 samples were used to calibrate the LAI model and the remaining 18 samples were employed to validate the model. SAVI (Huete, 1988) and NDVI (Pettorelli, 2013), can be calculated using Equations (1) and (2) of Chapter 4, respectively.

3.3. Assimilation strategy

3.3.1. Selection of reinitialized parameters for WOFOST

Previous studies have indicated that TDWI and SPAN parameters show significant uncertainty in regional applications of crop models. After optimizing these two parameters by the assimilation method, the estimation accuracy of crop yield can be significantly improved (de Wit et al., 2012; Huang et al., 2015b). The TDWI of perennial jujube trees is strongly influenced by tree age and planting density, showing uncertainty in the same area (Bai et al., 2019a). The trends in the impact of TDWI and SPAN on the jujube LAI produced by the WOFOST model are shown in Figure 6–1a, b.

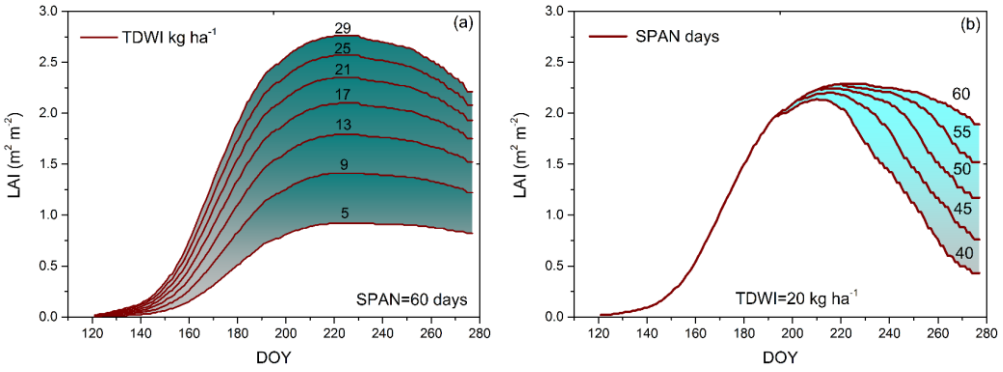

Figure 6–1: Evolution of the simulated leaf area index (LAI) profiles produced by the WOFOST model (a) LAI versus initial total crop dry weight (TDWI), (b) LAI versus the life span of leaves growing at 35°C (SPAN).

The initial growth rate and maximum leaf area index increased with the increase of TDWI, but the growth rate gradually decreased. SPAN determines the rate at which

green leaves will turn brown and, therefore, affected the leaf senescence rate and effective green leaf index in the late growing season (de Wit et al., 2012). In addition, SPAN explains to some extent the effects of water, nutritional stress, insect and disease factors on crop growth and yield (Curnel et al., 2011; Huang et al., 2015b). Thus, TDWI and SPAN input parameters were selected and recalibrated by assimilating a remotely sensed LAI. The simulated jujube fruit yield was affected by the TDWI–SPAN joint distributions (Figure 6–2).

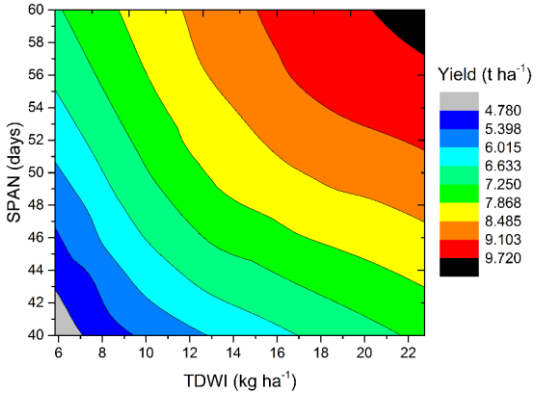

Figure 6–2: The effect of TDWI–SPAN joint distributions on jujube fruit yield. TDWI = initial total dry weight, SPAN = life span of leaves growing at 35°C).

3.3.2. Assimilation methods

Figure 6–3 shows the assimilation flowchart for the SUBPLEX and EnKF methods. For the simulation without assimilation, orchards of the same age were set to the same TDWI values based on measurements from different orchards, see Chapter 3. SPAN is equal to 60, which was the calibrated value in field experiments.

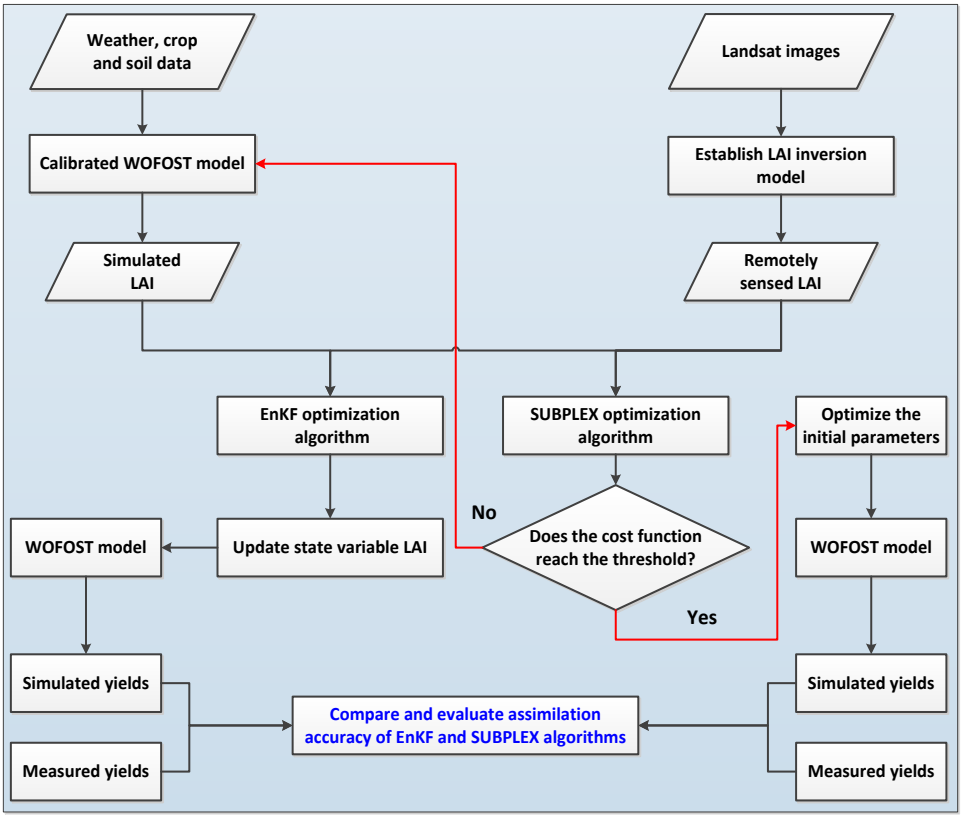

Figure 6–3: Assimilation flowchart

3.2.2.1. Ensemble Kalman Filter (EnKF)

Based on the work of Evensen (2003), the theoretical framework and actual implementation of EnKF are performed by the following steps.

First the Kalman gain (K) is calculated by Equation (6–1).

$$K = \frac{P_e \ H^T}{(HP_e \ H^T + R_e \ )} \qquad (6-1)$$

The Kalman gain weights the uncertainty of the simulated values, given by its variance P_e, against the uncertainty of the observations, given by its variance R_e. H is the measurement operator.

The Kalman state updates are then computed by Equation (6–2).

$$A^a = A + K(D - HA) \qquad (6-2)$$

The matrix with updated values of the states A^a, also called the analysed states, is computed by augmenting the old states A with the difference between the observed values D and simulated values A multiplied by the Kalman gain K. The additional part is called the innovation.

Because only one state variable of LAI is assimilated into the WOFOST model and the model state is observed directly (de Wit., 2007; Curnel et al., 2011), the measurement operator H is an identity matrix. Equation (2) then reduces to Equation (6-3).

$$A_i^a = A_i + \frac{P_e}{(P_e + R_e)}(D_i - A_i) \quad (6-3)$$

where A_i^a and A_i are the analysed and forecasted LAI state for ensemble member i, P_e and R_e are the variances matrices on the modelled LAI and the assimilated LAI, respectively, and D_i is the perturbed LAI observation which is used to update ensemble member i (de Wit., 2007).

Assimilated LAI was generated by using Equation (6–4) (Curnel et al., 2011).

$$LAI_{AS,i} = LAI_{OB,i} + \varepsilon_i \quad with \ \ \varepsilon_i \sim N(0, \sigma_i) \quad (6-4)$$

where, $LAI_{AS,i}$ was the assimilated LAI at time i, $LAI_{OB,i}$ was the remotely-sensed LAI at time i, and ε_i was the perturbed the uncertainty on remotely-sensed LAI.

The standard deviation σ_i was set as the ratio of the remotely-sensed LAI values, see Equation (6–5).

$$\sigma_i = CV \times LAI_{OB,i} \quad (6-5)$$

where, the calibrated and validated average % error for the remotely-sensed LAI was almost 10% (Table 6–2). Therefore, CV was equal to 10%.

It is assumed that there is uncertainty in the model parameters for initial conditions like the initial total crop dry weight (TDWI) and life span of leaves (SPAN). These two parameters were treated as Gaussian random variables with a default value (TDWI = 15 kg ha^{-1}, SPAN = 50 days) and a standard deviation (5 kg ha^{-1} for TDWI, 4 days for SPAN) which were defined by the observed value and its uncertainty from experience. The default value for TDWI was taken from the average of 55 observed orchards. A field-corrected SPAN value of 60 days under potential simulation was considered as the upper limit. SPAN may be influenced by water, nutrients, pests and diseases; the SPAN value of different orchards may be lower than the potential value, so a possible lower limit of 40 days was set. Therefore, the default value for SPAN was set to 50 days. The ensemble size was set to 50 because previous research has shown that this scale can achieve good assimilation performance (de Wit and van Diepen, 2007). Each ensemble member receives a value for the respective parameter which is drawn from the distribution of each parameter (Figure 6–4) and this value will override the default value (de Wit et al., 2017).

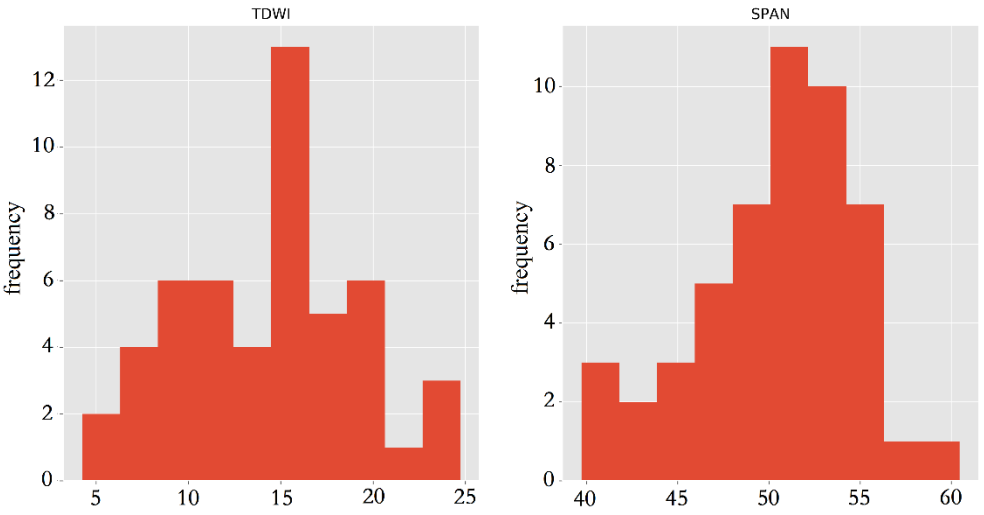

Figure 6–4: The distribution of setting TDWI and SPAN. TDWI = initial total dry weight (kg ha^{-1}), SPAN = life span of leaves growing at 35°C (days). (Only one assimilated observation variable, here LAI)

The assimilation details of the EnKF method can be found in an existing study (de Wit and van Diepen, 2007). EnKF updates a new set of TDWI and SPAN values when acquiring a new remote sensing observation point to implement the segmentation simulation.

3.2.2.2. SUBPLEX assimilation method

The key innovation of this research was to use the SUBPLEX method (Rowan, 1990) to achieve the assimilation of the remotely sensed LAI into the WOFOST model. The objective function calculator ran the WOFOST model with the given set of input parameters, collected the simulation results, and computed the differences between the observations. Different objective functions can be selected. In this study, the objective function $f(x)$ for SUBPLEX was constructed as the root mean squared error (RMSE), see Equation (6–6).

$$f(x) = \sqrt{\frac{1}{n}\sum_{i=1}^{n}\left(x_{s,i} - x_{o,i}\right)^2} \qquad (6-6)$$

where $x_{s,i}$ and $x_{o,i}$ represent the simulated and observed LAI values of the ith sample, respectively, and where n is the number of observation points.

Relative tolerance for convergence (ε) determines the threshold at which the objective function converges. In theory, a smaller ε value will result in better assimilation accuracy. However, a lower tolerance value will require more function evaluations. In this research, based on the LAIs of 55 field measurements, the minimum objective function of LAIs for the four periods ranged from 0.01 to 0.27,

with an average of 0.1. The test results also showed that when the ε value was reduced from 0.05 to 0.01, the coefficient of determination and accuracy of the yield estimation were only slightly improved, so in order to maintain calculation efficiency, the ε value was set to 0.05. Therefore, when the objective function $f(x)$ was less than this value, the assimilation process ended.

The key to implement the SUBPLEX method is to set the step sizes and subspaces, and then use a simplex searching algorithm NMS to search each subspace to perform an inner minimization. The step sizes, stored in the vector step, determine both the scale and orientation of the initial simplex used in the inner minimizations. For the first cycle, the step is equal to the initial step. Then, the step is rescaled according to how much progress is made during the previous cycle. The rescaled step is shown in Equation (6–7):

$$step = \begin{cases} min(max(\|\Delta x\|_1/(\|step\|_1, \omega), 1/\omega) \cdot step & if \ \ nsubs \ > 1 \\ \varphi \cdot step & if \ \ nsubs \ = 1 \end{cases} \quad (6-7)$$

where Δx represents the difference of observed and simulated LAI after successive iterations, $nsubs$ represents the number of subspaces. When there is only one subspace, the factor φ that represents the simplex reduction coefficient is used to reduce the size of the simplex for the same step amount. If the φ value is reduced, the subspace search becomes more accurate. ω represents the step reduction coefficient, which is employed to control the degree to which step can be modified. A smaller ω value can usually converge quickly to a local minimum. Conversely, a larger ω value will reduce the rate of convergence, but a more comprehensive search can be achieved to obtain a smaller objective function value. Next, the *i*th component of the step is reset by Equation (6–8):

$$\text{step}_\text{i} \ = \ \begin{cases} \text{sign}(\Delta x_i) \cdot |-\text{step}_\text{i}| & \text{if } \Delta x_i \neq 0 \\ -\text{step}_\text{i} & \text{if } \Delta x_i \ = \ 0 \end{cases} \quad (6-8)$$

To set subspaces, the relationship between $nsubs$ and the subspace dimensions ns_i is shown in Equation (6–9):

$$\sum_{i \ = \ 1}^{nsubs} ns_i \ = \ n \quad (6-9)$$

And $nsmin \leq nsi \leq nsmax,$ for $i = 1, \ldots, nsubs.$ Here $nsmin$ and nsmax represent the minimum and maximum subspace dimensions, respectively.

And $1 \leq nsmin \leq nsmax \leq n, nsmin\lceil n/nsmax \rceil \leq n.$

The first step in determining the subspaces is to sort the components of the vector of progress by decreasing magnitude. The vector of progress is denoted by Equation (6–10):

$$\Delta x \ = \ (\Delta x_1, \ldots, \Delta x_n)^T \quad (6-10)$$

Next, sorting of Δx occurs, see Equation (6–11):

$$\widetilde{\Delta x} = \left(\Delta x_{p1}, \ldots, \Delta x_{pn}\right)^T \quad (6-11)$$

where $\left|\Delta x_{pi}\right| \geq \left|\Delta x_{pi+1}\right|$.

Specifically, the first subspace dimension ns_1 is defined by Equation (6–12):

$$ns_1 = \begin{cases} \dfrac{\left\|\left(\Delta x_{p1}, \ldots, \Delta x_{pk}\right)^T\right\|_1}{k} - \dfrac{\left\|\left(\Delta x_{p1}, \ldots, \Delta x_{pn}\right)^T\right\|_1}{n-k} & \text{if } k < n \\ \dfrac{\left\|\left(\Delta x_{p1}, \ldots, \Delta x_{pn}\right)^T\right\|_1}{n-k} & \text{if } k = n \end{cases} \quad (6-12)$$

where $nsmin \leq k \leq nsmax$ and $nsmin\lceil (n-k)/nsmax \rceil \leq n-k$.

The first constraint forces ns_1 into the proper range, and the second constraint guarantees that the remaining $(n - ns_1)$ vector can be partitioned. The process is repeated to determine ns_2, ns_3, etc.

After the step sizes and subspaces are set, the NSM algorithm is used to search each subspace to minimize the cost function. The setting and selecting parameters for data assimilation are shown in Table 6–1. TDWI_range values were set based on the range of TDWI for field measurements. The range of SPAN values considered the same limitations as the EnKF method. An upper limit value for the SPAN parameter (60 days) was set, which is a calibration value from the potential growth simulation based on field experiments. Considering that this parameter may be affected by various stresses, such as water, nutrients, pests and diseases, the SPAN value of different orchards may be lower than the potential value, so a possible lower limit of 40 days for 181 orchards was set. The ε value was set with reference to the minimum value that the objective function $f(x)$ of all observation points can reach. The initial step was set to the expected value of an artificial setting according to the actual meaning of the parameter to be optimized, which can be further optimized by using the SUBPLEX algorithm at the iteration process. In theory, smaller φ and larger ω values can produce smaller objective function values, but the computational efficiency will decrease accordingly. The actual test also showed that when φ was less than the usual value of 0.25 and ω was greater than the usual value of 0.1 (Rowan, 1990), the minimized objective function value was not significantly improved, so φ and ω were set to 0.25 and 0.1, respectively.

SUBPLEX obtained an optimal set of TDWI and SPAN values by iteratively calculating the minimum objective function values of the four remotely sensed and simulated LAIs during the main growth stages, thereby achieving yield estimation based on the SUBPLEX assimilation method.

Table 6–1: SUBPLEX assimilation settings

Name	Description	Set value
n	the number of assimilated LAI	4
f	function to be minimized	Equation (1)
m	the number of optimized parameters for WOFOST	2
φ	simplex reduction coefficient (0<φ<1)	0.25
ω	step reduction coefficient (0<ω<1)	0.1
ε	relative tolerance of convergence	0.05
TDWI_range	the range of TDWI	5–30
SPAN_range	the range of SPAN	40–60
max-evaluation	maximum number of evaluations allowed	200
Initial step	the initial step size to compute numerical gradients	0.5 for TDWI 1 for SPAN

4. Results

4.1. Remotely sensed LAI

The statistical regression models between vegetation index (NDVI or SAVI) and LAI for the four jujube key growth periods are shown in Equations (6–13, 14, 15 and 16), respectively, which are obtained from regressions of 37 field-measured LAI and SAVI or NDVI (Figure 6–5). The difference between the 37 samples for each period was extremely significant ($p < 0.001$). On 9 June, between emergence and flowering, SAVI was used to establish the LAI linear regression model, while in other development stages NDVI was employed to invert LAI (exponential model) to obtain a more accurate model. Previous studies have also shown that SAVI exhibits better LAI statistical regression performance before the soil is covered by vegetation. NDVI performs better when vegetation coverage is higher (Huang et al., 2015b).

$$\text{9 June 2017: } \mathrm{LAI} = 2.08112 \times \mathrm{SAVI} - 0.2889 \quad p<0.001 \qquad (6-13)$$

$$\text{27 July 2017: } \mathrm{LAI} = 0.11071 \times e^{4.01646 \times \mathrm{NDVI}} \quad p<0.001 \qquad (6-14)$$

$$\text{12 August 2017: } \mathrm{LAI} = 0.18101 \times e^{3.48957 \times \mathrm{NDVI}} \quad p<0.001 \qquad (6-15)$$

$$\text{28 August 2017: } \mathrm{LAI} = 0.16731 \times e^{3.69701 \times \mathrm{NDVI}} \quad p<0.001 \qquad (6-16)$$

Table 6–2 shows the detailed results of calibration and validation LAI inversion models at four growth periods in 2017. The average R^2 for calibration and validation was 0.82 and 0.80, respectively, with a range from 0.71 to 0.92. The calibrated and validated average % error was 9.9% and 10.4%, respectively. Except for 12 August 2017, the consistency and accuracy of correction sets for other days was slightly higher than the validation sets. The verification results show that the established model accurately expressed the LAI values of different phenological development stages.

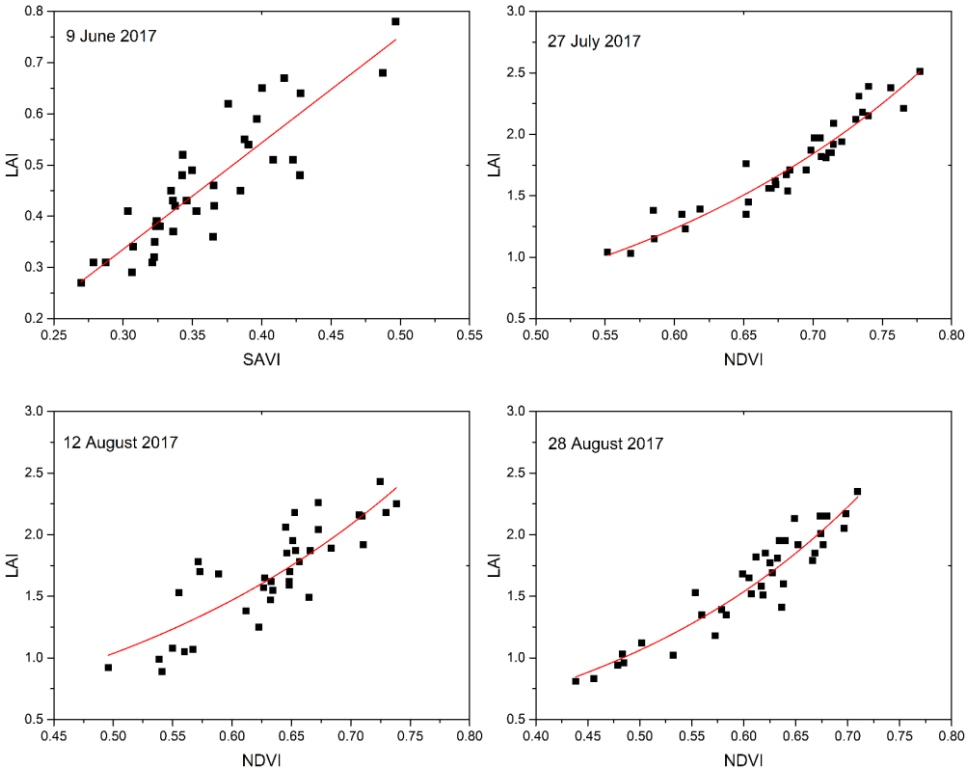

Figure 6–5: Leaf area index (LAI) inversion models for four phenological development dates.

Table 6–2: The comparison of LAI inversion models for four key periods

Date	Calibrated R^2	Calibrated RMSE (%) m^2 m^{-2}	Validated R^2	Validated RMSE (%) m^2 m^{-2}
9 June	0.77	0.06 (12.7)	0.77	0.06 (12.5)
27 July	0.92	0.11 (6.2)	0.84	0.14 (8.1)
12 August	0.71	0.23 (13.6)	0.78	0.18 (10.5)
28 August	0.88	0.12 (7.1)	0.81	0.17 (10.4)

4.2. Assimilation process

4.2.1. EnKF assimilation process

Taking a sample as an example, the LAI observed in the four key growth stages was 0.54, 2.12, 1.87, and 1.95 m^2 m^{-2}, respectively. The simulated outputs for the variable LAI for each ensemble member were plotted on a graph, see Figure 6–6, which clearly shows the impact of the observations on the simulated value. At each time step where an observation of LAI was available, the uncertainty in the ensemble was strongly

reduced, which was demonstrated by the reduction of the variability in the simulated ensemble. The red line represents the final simulated state variable, here LAI, which was brought forward in time until an observation was available (red dot). At this point, an analysis step was performed to adjust the state of the model based on the observed LAIs, which resulted in a "jump" in the simulated state. The model was then advanced in time until the next observation was reached, and the process was repeated.

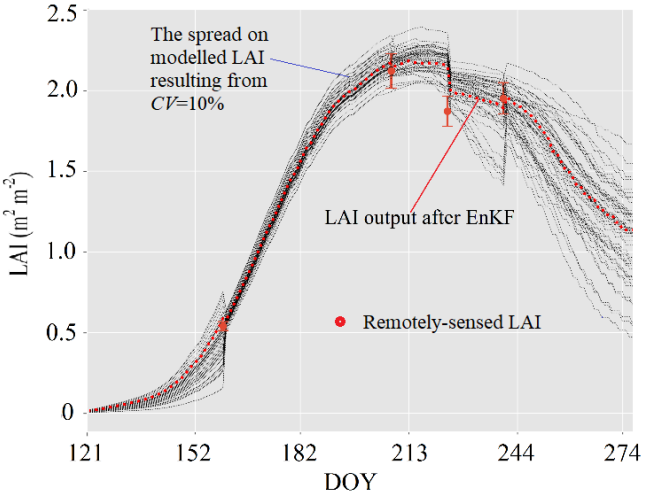

Figure 6–6: The spread on modelled LAI resulting from $CV = 10\%$ for EnKF assimilation process.

4.2.2. SUBPLEX assimilation process

Taking the same sample that was used in the above section as an example, the blue line in Figure 6–7 demonstrates the principle of a variational method of SUBPLEX. The model was first run without data assimilation (first guess). Next, all observations with an assimilation window were collected to adjust the model until it better matched the observations (analysis). In this process, model parameters or other properties were adjusted to minimize the cost function. After 28 iterations, a combination of TDWI and SPAN was screened (TDWI = 17.4 kg ha^{-1}, SPAN = 49 days), with 8.9% difference against measured TDWI = 19.1 kg ha^{-1}. Note that Figure 6–7 only shows a sample to illustrate the difference in the assimilation process of the two methods for all 181 samples, of which in 100 samples the yield estimation accuracy of the SUBPLEX method was superior to the EnKF method.

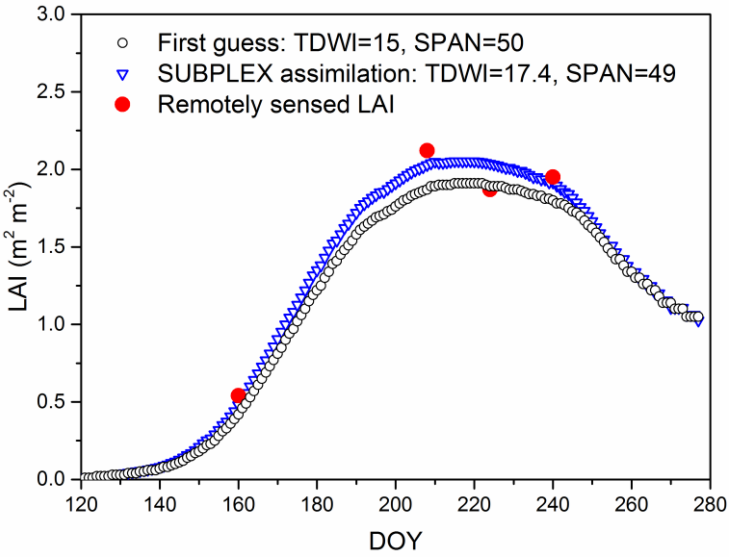

Figure 6–7: SUBPLEX assimilation process.

4.3. Yield estimation performance based on field-measured LAI

The 55 field-measured LAIs were assimilated into the WOFOST model to verify the performance of the reinitialized input parameters. For the TDWI parameter, when the remotely sensed LAI was not assimilated, the average TDWI value of the same aged orchards was input to the WOFOST model. The average TDWI for 3 to 10 year-old jujube orchards were 4.88, 6.24, 9.24, 13.17, 14.28, 16.31, 19.73, and 21.61 kg ha^{-1}, which came from the average values from 2015 to 2017. Figure 6–8a showed that TDWI values without assimilation was significantly higher than the measured value of 55 orchards in 2017. The reason was that the planting density of jujube trees in young orchards was usually higher, and the quality of jujube fruits was poor. Therefore, most fruit farmers cut down some fruit trees at the end of 2016 to provide the quality of jujube fruits, thereby resulting in the unassimilated TDWI value being significantly higher than the measured value in 2017. Scatter plots for re-calibrated TDWIs based on SUBPLEX assimilation versus 55 measured TDWIs are shown in Figure 6–8a, with a R^2 of 0.86. After SUBPLEX assimilation, the accuracy of the corrected TDWI with a RMSE of 1.88 kg ha^{-1} was significantly higher than that of the unassimilated LAI (RMSE = 5.09 kg ha^{-1}), and the calibrated average TDWI value of 13.91 kg ha^{-1} showed an error of 3.3% compared with field-measured average value of 13.46 kg ha^{-1}. The samples with an estimation error between −10% and 10%, −20% and 20% accounted for 41.6% and 83.6%, respectively (Figure 6–8b). These values showed better performance for TDWI calibration than the simulation without assimilation which had 21.8%, 36.4%, and 49% of −10–10%, −20–20%, and −40–40%, respectively. RBE values after SUBPLEX assimilation were distributed more centrally around zero compared with the values obtained by the simulation without assimilation. For the SPAN parameter, validating its spatial distribution was

difficult due to a lack of corresponding measured data. The results also suggest that SUBPLEX assimilation reduced the uncertainty of TDWI and SPAN input parameters to some extent.

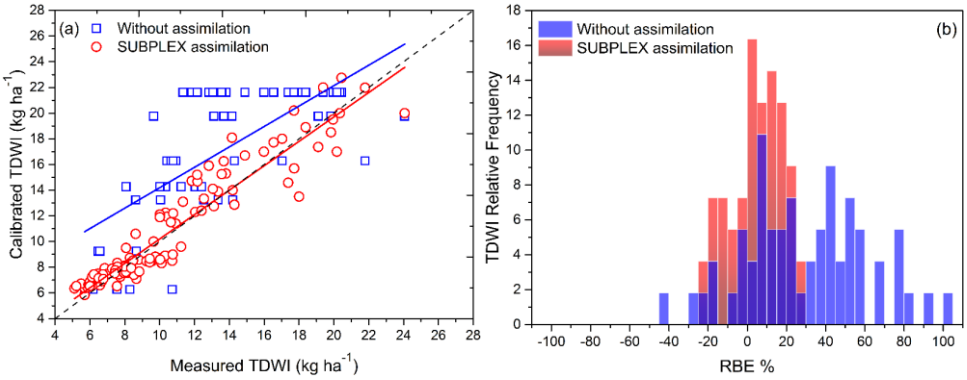

Figure 6–8: (a) Scatter plots for re-calibrated versus measured TDWI, (b) Frequency distribution for RBE based on recalibrated and measured TDWI. Bin size = 5.

Based on field-measured LAI, the yield estimation performance of two assimilation methods is presented in Table 6–3.

Table 6–3: Comparison of the estimated yield based on field-measured LAI.

	Mean t ha^{-1}	**Maximum t ha^{-1}**	**Minimum t ha^{-1}**	**R^2**	**RMSE (%) t ha^{-1}**
Field-measured yield of the 55 samples	7.931	10.71	4.848	–	–
Simulation without assimilation	8.271	8.89	5.946	0.58	0.95 (12.1)
EnKF assimilation	7.717	9.887	5.303	0.81	0.65 (8.2)
SUBPLEX assimilation	7.707	9.713	4.791	0.86	0.55 (7.0)

Both SUBPLEX and EnKF significantly improved yield estimation accuracy compared with the unassimilated results, with higher R^2 and lower RMSE values. The results also show that the SUBPLEX assimilate on accuracy (R^2 = 0.86, RMSE = 0.55 t ha^{-1} (7%)) was slightly higher than EnKF (R^2 = 0.81, RMSE = 0.65 t ha^{-1} (8.2%)), and significantly higher than simulation without assimilation. The simulated yields without assimilation overestimated the actual average yield, with an error of 12.1%. SUBPLEX and ENKF assimilations produced only 2.7% and 2.8% estimation errors for average yield, respectively, indicating better performance. For maximum yield estimation, EnKF was slightly more accurate, while for minimum yield estimation, SUBPLEX was slightly better. However, both methods showed slightly higher errors in the maximum yield estimation with a value around 7.6%. The jujube yield estimation using the field-measured LAI assimilation in the WOFOST model

indicated that SUBPLEX had the potential to be an effective assimilation method and demonstrated better accuracy than the EnKF method.

4.4. Yield estimation performance based on remotely sensed LAI

After carrying out SUBPLEX assimilation, the joint distribution of TDWI and SPAN for 181 samples was generated to provide variability in parameter distribution between different samples (Figure 6–9a). Explaining the shapes of the distribution was difficult because they were the result of many interaction factors (de Wit et al., 2012), such as meteorological conditions, pests and diseases, and nutritional stress. However, TDWI values recalibrated by SUBPLEX assimilation ranged from 5.84 to 22.75 kg ha^{-1}, showing high variability between orchards. SPAN values ranged from 40 to 60 days with an average of 49.73 days. Figure 6–9b shows that the SUBPLEX algorithm used fewer function calls (iteration times) to complete data assimilation, ranging from 9 to 77 with an average of 40, at relative tolerance $\varepsilon = 0.05$. The low number of iterations also indicates that the SUBPLEX algorithm showed a relatively high computational efficiency to some extent.

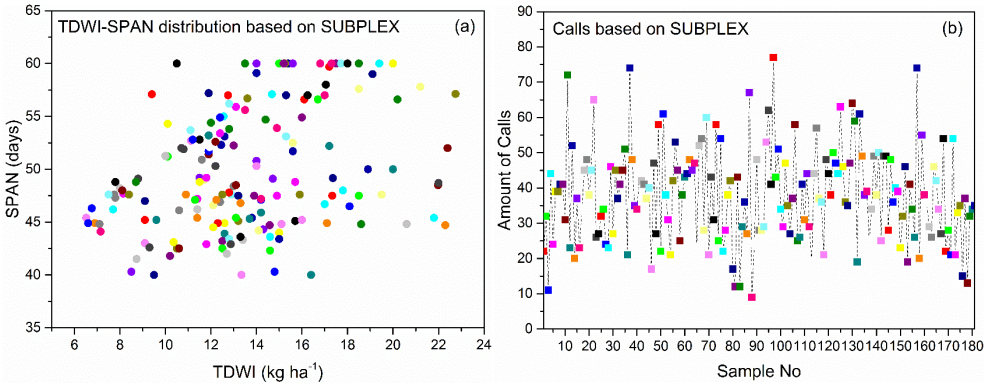

Figure 6–9: (a) TDWI-SPAN distribution for 181 samples, (b) Number of iterations for each sample. TDWI = initial total dry weight, SPAN = life span of leaves growing at 35°C.

The scatter plots of the simulated yields achieved from the unassimilated, EnKF, and SUBPLEX versus actual yields are shown in Figure 6–10a. The WOFOST-estimated yield without assimilation simulation exhibited poor spatial distribution and estimation performance, clearly deviating from the line y = x and 71.8% of the samples were severely overestimated. Both EnKF and SUBPLEX assimilations significantly improved yield simulation performance with a scatter distribution closer to the line y = x. Although the dispersion of yield estimation achieved by the SUBPLEX method was higher than that of EnKF, SUBPLEX showed better performance in high-yield and low-yield areas. Compared with the simulation without assimilation and the EnKF method, the SUBPLEX assimilation produced a relative bias error (RBE, %) that was more concentrated near zero (Figure 6–10b). The absolute RBE for yield simulation was lower than 10% in 80.1% and lower than 20% in 96.1% for SUBPLEX, 80.1% and 93.9% for EnKF.

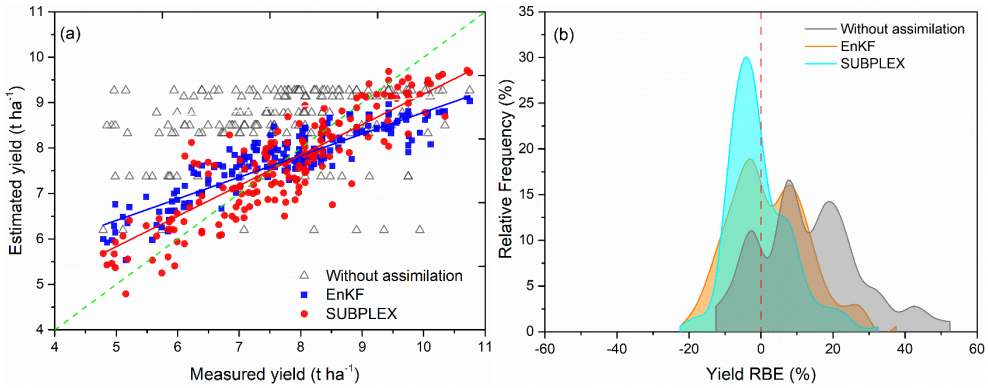

Figure 6–10: (a) Yield estimation scatter plots for Ensemble Kalman Filter (EnKF), SUBPLEX, and simulation without assimilation, (b) Frequency distribution for relative bias error (RBE) achieved from the contrast between simulated and observed yields. Bin size = 5.

The positive results achieved by SUBPLEX or EnKF assimilations were also confirmed by the indices of agreement and detailed estimation error (Table 6–4). The WOFOST without assimilation showed lower yield estimation accuracy, with a R^2 of 0.14, RMSE of 1.26 t ha^{-1} (16.3%), MAE (mean absolute error, %) value of 15.4%, and average RBE of 13.28%. Both SUBPLEX and EnKF methods improved the simulated accuracy, with a much higher coefficient of determination ($R^2 \geq 0.66$) and lower error (RMSE $\leq$ 0.79 t ha^{-1}). In addition, average RBE values from the two assimilation methods agreed with the results shown in Figure 6–10b, giving lower values which showed that the error distributions were uniform to some extent. SUBPLEX also indicated slightly better assimilation performance with an improvement of R^2 (increased by 18.2%), RMSE (reduced by 19.0), and MAE (reduced by 22.3%) compared to EnKF. SUBPLEX assimilation showed the highest RPD value greater than 2, with a better evaluation capability.

Table 6–4: Validation results of the yield estimation using remotely sensed leaf area index

Methods	R^2	RMSE (%) t ha^{-1}	MAE, %	Average RBE, %	RPD
Without assimilated simulation	0.14	1.26 (16.3)	15.4	13.28	1.28
EnKF with remotely sensed LAI	0.66	0.79 (10.2)	8.81	2.16	1.73
SUBPLEX with remotely sensed LAI	0.78	0.64 (8.3)	6.85	−0.39	2.13

4.5. The choice of phenology periods of assimilation LAI

In theory, more state variables of remote sensing observations can produce better assimilation accuracy. In practice, satellite data for key crop growth seasons may not be available due to revisit cycles and cloud coverage limitations. Loss of remote sensing observations at critical developmental stages may have a key impact on model performance. To further discuss the sensitivity of LAI during different phenological

stages and the two assimilation methods to yield estimation, only three field-measured LAIs from 55 observations were employed to establish assimilation strategies to compare the yield estimation performance of the EnKF and SUBPLEX methods (Table 6–5). In this part of the study, the LAI measured by the instrument was used, so the CV value was set to 5% recommended by OSSE.

Table 6–5: Model performance of SUBPLEX versus EnKF when missing an observation.

	Available observations	R^2	RMSE (%)	MAE, %	Average RBE, %
SUBPLEX	Four observations	0.86	0.55	5.77	−2.3
	Without 9 June	0.84	0.59	6.04	−1.75
	Without 27 July	0.85	0.58	6.01	−1.48
	Without 12 August	0.81	0.65	6.35	−3.31
	Without 28 August [(a)]	0.36	1.18	12.3	0.23
	Without 28 August [(b)]	0.73	0.77	9.02	4.49
EnKF	Four observations	0.81	0.65	6.78	−1.42
	Without 9 June	0.65	0.88	8.78	−7.69
	Without 27 July	0.75	0.75	7.93	−1.87
	Without 12 August	0.74	0.76	7.98	−1.59
	Without 28 August	0.71	0.81	8.73	−1.02

(a) represents that total initial dry weight (TDWI) and SPAN (life span of leaves growing at 35°C) parameters are calibrated. (b) represents that only TDWI is calibrated, SPAN is equal to a fixed value that is calibrated by SUBPLEX. RMSE = root mean square error, MAE = mean absolute error, RBE = relative bias error, EnKF = Ensemble Kalman Filter.

The results show that when the observation data on 9 June, 27 July, or 12 August are missing, respectively, the performance of the SUBPLEX assimilation is still higher than that of the EnKF method. When the observation data of 28 August is missing, the performance of the SUBPLEX method drops sharply, and its accuracy is also significantly lower than that of the EnKF method. The main reason should be that the SPAN parameter mainly affects the LAI change in the late growing season, while the lack of LAI (28 August) in the maturity period leads to a larger error in the corrected SPAN parameters, with a mean deviation of 2.7 days compared to the use of four LAIs. Further tests showed that when the SPAN parameter was set to a fixed value (calibrated by SUBPLEX, 50), the R^2 and RMSE of the yield estimation were improved to 0.73 and 0.77 t ha^{-1}, respectively, which was also slightly higher than the EnKF assimilation accuracy under the same conditions. This finding indicates that when using the SUBPLEX method to optimize SPAN parameters, the assimilated LAI should include at least one observation point in the middle and late stages of maturity. If this observation point is not available, design of an average SPAN for SUBPLEX assimilation is recommended. In addition, the combination of high or medium spatial resolution remote sensing satellite data, such as Landsat and Sentinel satellites, can be recommended to obtain more remotely sensed state variables.

5. Discussion

In this study, SUBPLEX demonstrates slightly better global yield estimation performance than EnKF. The detailed results also indicate that the accuracy of ENKF in 100 of the 181 samples is lower than that of SUBPLEX. The reason may be that the tree age and physiological genetic factors may affect the actual emergence date and phenology time of jujube trees. The premise of ensuring the accuracy of the EnKF method is that the growth cycle between the model and the satellite observations (planting date plus phenology) is correct. If the phenological development time has a large error, the sequential approach of EnKF may result in lower simulation accuracy (de Wit and van Diepen, 2007).

The uncertainty of crop model parameters and remote sensing observations is an important factor affecting the performance of the EnKF assimilation system. Determining and analysing this uncertainty is also an important step to improve the accuracy of EnKF assimilation (Huang et al., 2016). EnKF is essentially a Monte Carlo approximation of the Kalman filter and assumes that the probability distributions of the observed and simulated errors are Gaussian (Huang et al., 2019a). In the research, we assume that the simulation error is caused by the key input parameters TDWI and SPAN, which are treated as Gaussian random variables with a mean equal to the default value. However, the actual observed LAI does not fully satisfy the Gaussian distribution, which is the main issue that affects the accuracy of jujube fruit yield estimation. In addition, since the time and space of the variances on the modelled LAI and the observed LAI (both P_e and R_e) are variable, it is not easy to infer the correct variance. Artificially inflating the observation variance (R_e) can demonstrate the effect of increased variance on the distribution of normalized innovations (de Wit et al., 2007) and enlarge Kalman gain to reduce the effect of filter divergence (Huang et al., 2016). If the error of the remote sensing data product is Gaussian, EnKF is a good data assimilation option (Huang et al., 2019a).

The SUBPLEX as a kind of variational method may reduce the accumulation and diffusion of remote sensing data errors in the assimilation process (Jin et al., 2018). SUBPLEX's process is to optimize TDWI and SPAN parameters in the WOFOST model in order to ensure that the remotely sensed LAI and the simulated LAI match as well as possible. Then, the corrected TDWI and SPAN parameters will be used to re-drive the WOFOST model. If the WOFOST model is run from a shifted phenology time, the emergence, flowering, and maturity dates will be offset. However, the entire simulation curve is shifted overall, so it has little effect on the final simulated yield. For example, when TDWI and SPAN are set to a fixed value (TDWI = 21.6 kg ha^{-1}, SPAN = 53 days) and the corrected WOFOST model is run for 115 days, 118 days, and 121 days, respectively, then the simulated yields are 9.039, 9.203, and 9.271. Obviously, when the phenological time deviation is six days, there is only a relatively small 2.5% yield estimation error. It is speculated that when the phenological development time is uncertain, the use of SUBPLEX would usually result in better assimilation accuracy for yield estimation than using the EnKF method.

The present research also compares the computational efficiency of SUBPLEX and the brute force optimization method, finding higher computational efficiency for

SUBPLEX. Still taking the sample of Section 3.2 as an example, there were 1000 function calls for the forced method, while the SUBPLEX method used only 25 function calls. The SUBPLEX algorithm can find a solution with a similar accuracy with in a much shorter iteration time. Of course, the computation time is closely related to the initial steps of TDWI and SPAN. When the initial step size of TDWI and SPAN is adjusted to 0.1 and 0.5, respectively, the iteration number of the cost function is increased to 43, and when they are adjusted to 0.05 and 0.1, the number of iterations is increased to 76. The running time test also shows that the SUBPLEX method runs slightly longer than the EnKF method. However, the time difference is usually less than ten seconds for different samples, which is a speed that can be fully accepted. However, the yield estimation accuracy of SUBPLEX assimilation is higher than EnKF.

The setting of the key parameters of SUBPLEX will directly affect the minimization of the objective function of remote sensing inversion and model simulation, which will affect the optimization accuracy of the parameters and the final simulation yield, such as relative tolerance for convergence ε, simplex reduction coefficient φ, and step reduction coefficient ω. Smaller ε, φ, and larger ω values usually result in a minimized objective function and, of course, the computation time increases. In our study, the minimization of the objective function of all samples ranges from 0.001 to 0.26, with most samples between 0.05 and 0.1. Furthermore, when trying to decrease ε from 0.05 to 0.01, the R^2 value only increases by 0.0015, and the RMSE decreases by 0.003 t ha^{-1}. Similarly, when φ decreases from 0.25 and ω increases from 0.1, the final yield assimilation accuracy is not significantly improved. Therefore, $\varepsilon = 0.05$, $\varphi = 0.25$, and $\omega = 0.1$ are set in the study. It is recommended that when the SUBPLEX algorithm is used for remote sensing assimilation, the parameter setting could refer to the range of the minimum value of the objective function. When the parameter adjustment cannot significantly improve the objective function value, the parameter value at this time can be used as a suitable choice. In the future, further research on parameter optimization settings and automatic search methods has significant interest for exploring SUBPLEX assimilation. Comparison of the accuracy and computational efficiency of the SUBPLEX and the 4DVAR variational algorithm is also worth exploring.

6. Conclusions

In this study, the SUBPLEX algorithm was tested to assimilate remotely sensed data into the WOFOST model to improve the modelling accuracy for jujube yield at the field scale. The state variables, here LAIs, from the four key development stages, were assimilated into a validated WOFOST model to optimize the initial input parameters, TDWI and SPAN, thereby improving yield estimation for jujube fruit trees. The results indicated that the assimilation method has the potential to enhance the yield estimation accuracy compared with the unassimilated simulation, and the SUBPLEX method showed slightly better yield estimation performance versus EnKF assimilation. EnKF assimilation overestimated the actual yields in high-yield orchards and underestimated yields in low-yield orchards. The SUBPLEX method can reduce the

effect of phenological shift on assimilation accuracy to some extent, thereby producing a more accurate yield simulation. The results indicate that the SUBPLEX algorithm can be considered to be a promising assimilation method for remotely sensed information and crop growth models. In the future, the assimilation performance of the SUBPLEX method applied to other crops at the field and regional scales needs to be further tested and compared. In addition, the determination and automatic optimization of the initial input parameters of SUBPLEX assimilation, such as initial step size, relative tolerance and initial values of the parameters to be re-calibrated, are worthy of further research and exploration to enhance its computational efficiency and assimilation accuracy.

7. References

Bai, T., Zhang, N., Mercatoris, B., Chen, Y., 2019a. Improving Jujube Fruit Tree Yield Estimation at the Field Scale by Assimilating a Single Landsat Remotely-Sensed LAI into the WOFOST Model. Remote Sens. 11, 1119. https://doi.org/10.3390/rs11091119

Bai, T., Zhang, N., Mercatoris, B., Chen, Y., 2019b. Jujube yield prediction method combining Landsat 8 Vegetation Index and the phenological length. Comput. Electron. Agric. 162, 1011–1027. https://doi.org/10.1016/j.compag.2019.05.035

Bolten, J.D., Crow, W.T., Jackson, T.J., Zhan, X., Reynolds, C.A., 2010. Evaluating the Utility of Remotely Sensed Soil Moisture Retrievals for Operational Agricultural Drought Monitoring. IEEE J. Sel. Top. Appl. Earth Obs. Remote Sens. 3, 57–66. https://doi.org/10.1109/JSTARS.2009.2037163

Chakrabarti, S., Bongiovanni, T., Judge, J., Zotarelli, L., Bayer, C., 2014. Assimilation of SMOS soil moisture for quantifying drought impacts on crop yield in agricultural regions. IEEE J. Sel. Top. Appl. Earth Obs. Remote Sens. 7, 3867–3879. https://doi.org/10.1109/JSTARS.2014.2315999

Chen, J., Lam, C., Li, Z., Yao, P., Lin, H., Dong, T., Tsim, K., 2016. Chemical and Biological Assessment of Ziziphus jujuba (Jujubes) Fruit from China of Different Geographical Sources and Developmental Stages: Chemical Composition and Possible Targets in Developing Health Food Products, in: Chinese Dates: A Traditional Functional Food. pp. 83–97. https://doi.org/10.1201/b20025-8

Chen, Y., Zhang, Z., Tao, F., 2018. Improving regional winter wheat yield estimation through assimilation of phenology and leaf area index from remote sensing data. Eur. J. Agron. 101, 163–173. https://doi.org/10.1016/j.eja.2018.09.006

Cheng, Z., Meng, J., Qiao, Y., Wang, Y., Dong, W., Han, Y., 2018. Preliminary study of soil available nutrient simulation using a modified WOFOST model and time-series remote sensing observations. Remote Sens. 10. https://doi.org/10.3390/rs10010064

Claverie, M., Demarez, V., Duchemin, B., Hagolle, O., Keravec, P., Marciel, B., Ceschia, E., Dejoux, J.F., Dedieu, G., 2009. Spatialization of crop leaf area index and biomass by combining a simple crop model safy and high spatial and temporal resolutions remote sensing data, in: International Geoscience and Remote Sensing Symposium (IGARSS). https://doi.org/10.1109/IGARSS.2009.5418296

Curnel, Y., de Wit, A.J.W., Duveiller, G., Defourny, P., 2011. Potential performances of remotely sensed LAI assimilation in WOFOST model based on an OSS Experiment. Agric. For. Meteorol. 151, 1843–1855. https://doi.org/10.1016/j.agrformet.2011.08.002

de Wit, A.J.W., 2017. 08_data_assimilation_with_the_EnKF.ipynb. https://github.com/ajwde Wit/pcse_notebooks.

de Wit, A., Duveiller, G., Defourny, P., 2012. Estimating regional winter wheat yield with WOFOST through the assimilation of green area index retrieved from MODIS observations. Agric. For. Meteorol. 164, 39–52. https://doi.org/10.1016/j.agrformet.2012.04.011

de Wit, A.J.W., van Diepen, C.A., 2007. Crop model data assimilation with the Ensemble Kalman filter for improving regional crop yield forecasts. Agric. For. Meteorol. 146, 38–56. https://doi.org/10.1016/j.agrformet.2007.05.004

Dente, L., Satalino, G., Mattia, F., Rinaldi, M., 2008. Assimilation of leaf area index derived from ASAR and MERIS data into CERES-Wheat model to map wheat yield. Remote Sens. Environ. 112, 1395–1407. https://doi.org/10.1016/j.rse.2007.05.023

Dong, T., Liu, J., Qian, B., Zhao, T., Jing, Q., Geng, X., Wang, J., Huffman, T., Shang, J., 2016. Estimating winter wheat biomass by assimilating leaf area index derived from fusion of Landsat-8 and MODIS data. Int. J. Appl. Earth Obs. Geoinf. 49, 63–74. https://doi.org/10.1016/j.jag.2016.02.001

Dong, Y., Wang, J., Li, C., Yang, G., Wang, Q., Liu, F., Zhao, J., Wang, H., Huang, W., 2013a. Comparison and analysis of data assimilation algorithms for predicting the leaf area index of crop canopies. IEEE J. Sel. Top. Appl. Earth Obs. Remote Sens. 6, 188–201. https://doi.org/10.1109/JSTARS.2012.2208943

Dong, Y., Zhao, C., Yang, G., Chen, L., Wang, J., Feng, H., 2013b. Integrating a very fast simulated annealing optimization algorithm for crop leaf area index variational assimilation. Math. Comput. Model. 58, 877–885. https://doi.org/10.1016/j.mcm.2012.12.013

Evensen, G., 2003. The Ensemble Kalman Filter: theoretical formulation and practical implementation. Ocean Dyn. 53, 343–367

Fang, H., Liang, S., Hoogenboom, G., 2011. Integration of MODIS LAI and vegetation index products with the CSM-CERES-Maize model for corn yield estimation. Int. J. Remote Sens. 32, 1039–1065. https://doi.org/10.1080/01431160903505310

Fang, H., Liang, S., Hoogenboom, G., Teasdale, J., Cavigelli, M., 2008. Corn-yield estimation through assimilation of remotely sensed data into the CSM-CERES-Maize model. Int. J. Remote Sens. 29, 3011–3032. https://doi.org/10.1080/01431160701408386

Guo, C., Zhang, L., Zhou, X., Zhu, Y., Cao, W., Qiu, X., Cheng, T., Tian, Y., 2017. Integrating remote sensing information with crop model to monitor wheat growth and yield based on simulation zone partitioning. Precis. Agric. 1–24. https://doi.org/10.1007/s11119-017-9498-5

He, B., Li, X., Quan, X., Qiu, S., 2015. Estimating the aboveground dry biomass of grass by assimilation of retrieved LAI into a crop growth model. IEEE J. Sel. Top. Appl. Earth Obs. Remote Sens. 8, 550–561. https://doi.org/10.1109/JSTARS.2014.2360676

Hu, S., Mo, X., Lin, Z., 2014. Optimizing the photosynthetic parameter Vcmax by assimilating MODIS-fPAR and MODIS-NDVI with a process-based ecosystem model. Agric. For. Meteorol. 198, 320–334. https://doi.org/10.1016/j.agrformet.2014.09.002

Huang, J, Gómez-Dans J, Huang H, Ma H, Wu Q, Lewis P, Liang S, Chen Z, Xue J, Wu Y, Zhao F, Wang J, Xie X., 2019a. Assimilation of remote sensing into crop growth models: current status and perspectives. Agric. For. Meteorol. 276-277, 107609. doi:10.1016/j.agrformet.2019.06.008.

Huang, J., Ma, H., Sedano, F., Lewis, P., Liang, S., Wu, Q., Su, W., Zhang, X., Zhu, D., 2019b. Evaluation of regional estimates of winter wheat yield by assimilating three remotely sensed reflectance datasets into the coupled WOFOST–PROSAIL model. Eur. J. Agron. 102, 1–13. https://doi.org/10.1016/j.eja.2018.10.008

Huang, J., Ma, H., Su, W., Zhang, X., Huang, Y., Fan, J., Wu, W., 2015a. Jointly Assimilating MODIS LAI and et Products into the SWAP Model for Winter Wheat Yield Estimation. IEEE J. Sel. Top. Appl. Earth Obs. Remote Sens. 8, 4060–4071. https://doi.org/10.1109/JSTARS.2015.2403135

Huang, J., Sedano, F., Huang, Y., Ma, H., Li, X., Liang, S., Tian, L., Zhang, X., Fan, J., Wu, W., 2016. Assimilating a synthetic Kalman filter leaf area index series into the WOFOST model to improve regional winter wheat yield estimation. Agric. For. Meteorol. 216, 188–202. https://doi.org/10.1016/j.agrformet.2015.10.013

Huang, J., Tian, L., Liang, S., Ma, H., Becker-Reshef, I., Huang, Y., Su, W., Zhang, X., Zhu, D., Wu, W., 2015b. Improving winter wheat yield estimation by assimilation of the leaf area index from Landsat TM and MODIS data into the WOFOST model. Agric. For. Meteorol. 204, 106–121. https://doi.org/10.1016/j.agrformet.2015.02.001

Huang, Y., Zhu, Y., Li, W., Cao, W., Tian, Y., 2013. Assimilating Remotely Sensed Information with the WheatGrow Model Based on the Ensemble Square Root Filter forImproving Regional Wheat Yield Forecasts. Plant Prod. Sci. 16, 352–364. https://doi.org/10.1626/pps.16.352

Huete, A.R., 1988. A soil-adjusted vegetation index (SAVI). Remote Sens. Environ. 25, 295–309. https://doi.org/10.1016/0034-4257(88)90106-X

Ines, A.V.M., Das, N.N., Hansen, J.W., Njoku, E.G., 2013. Assimilation of remotely sensed soil moisture and vegetation with a crop simulation model for maize yield prediction. Remote Sens. Environ. 138, 149–164. https://doi.org/10.1016/j.rse.2013.07.018

Ines, A.V.M., Honda, K., Das Gupta, A., Droogers, P., Clemente, R.S., 2006. Combining remote sensing-simulation modelling and genetic algorithm optimization to explore water management options in irrigated agriculture. Agric. Water Manag. https://doi.org/10.1016/j.agwat.2005.12.006

Jégo, G., Pattey, E., Liu, J., 2012. Using Leaf Area Index, retrieved from optical imagery, in the STICS crop model for predicting yield and biomass of field crops. F. Crop. Res. 131, 63–74. https://doi.org/10.1016/j.fcr.2012.02.012

Jiang, Z., Chen, Z., Chen, J., Liu, J., Ren, J., Li, Z., Sun, L., Li, H., 2014. Application of crop model data assimilation with a particle filter for estimating regional winter wheat yields. IEEE J. Sel. Top. Appl. Earth Obs. Remote Sens. 7, 4422–4431. https://doi.org/10.1109/JSTARS.2014.2316012

Jin, H., Li, A., Wang, J., Bo, Y., 2016. Improvement of spatially and temporally continuous crop leaf area index by integration of CERES-Maize model and MODIS data. Eur. J. Agron. 78, 1–12. https://doi.org/10.1016/j.eja.2016.04.007

Jin, M., Liu, X., Wu, L., Liu, M., 2015. An improved assimilation method with stress factors incorporated in the WOFOST model for the efficient assessment of heavy metal stress

levels in rice. Int. J. Appl. Earth Obs. Geoinf. 41, 118–129. https://doi.org/10.1016/j.jag.2015.04.023

Jin, X., Kumar, L., Li, Z., Feng, H., Xu, X., Yang, G., Wang, J., 2018. A review of data assimilation of remote sensing and crop models. Eur. J. Agron. https://doi.org/10.1016/j.eja.2017.11.002

Jin, X., Li, Z., Yang, G., Yang, H., Feng, H., Xu, X., Wang, J., Li, X., Luo, J., 2017. Winter wheat yield estimation based on multi-source medium resolution optical and radar imaging data and the AquaCrop model using the particle swarm optimization algorithm. ISPRS J. Photogramm. Remote Sens. 126, 24–37. https://doi.org/10.1016/j.isprsjprs.2017.02.001

Jin, X., Yang, G., Xu, X., Yang, H., Feng, H., Li, Z., Shen, J., Zhao, C., Lan, Y., 2015. Combined multi-temporal optical and radar parameters for estimating LAI and biomass in winter wheat using HJ and RADARSAR-2 data. Remote Sens. 7, 13251–13272. https://doi.org/10.3390/rs71013251

Jonsén, P., Isaksson, E., Sundin, K.G., Oldenburg, M., 2009. Identification of lumped parameter automotive crash models for bumper system development. Int. J. Crashworthiness 14, 533–541. https://doi.org/10.1080/13588260902837262

Li, J.W., Fan, L.P., Ding, S.D., Ding, X.L., 2007. Nutritional composition of five cultivars of chinese jujube. Food Chem. 103, 454–460. https://doi.org/10.1016/j.foodchem.2006.08.016

Li, Y., Zhou, Q., Zhou, J., Zhang, G., Chen, C., Wang, J., 2014. Assimilating remote sensing information into a coupled hydrology-crop growth model to estimate regional maize yield in arid regions. Ecol. Modell. 291, 15–27. https://doi.org/10.1016/j.ecolmodel.2014.07.013

Li, Z., Wang, J., Xu, X., Zhao, C., Jin, X., Yang, G., Feng, H., 2015. Assimilation of two variables derived from hyperspectral data into the DSSAT-CERES model for grain yield and quality estimation. Remote Sens. 7, 12400–12418. https://doi.org/10.3390/rs70912400

Liu, F., Liu, X., Ding, C., Wu, L., 2015. The dynamic simulation of rice growth parameters under cadmium stress with the assimilation of multi-period spectral indices and crop model. F. Crop. Res. 183, 225–234. https://doi.org/10.1016/j.fcr.2015.08.004

Ma, G., Huang, J., Wu, W., Fan, J., Zou, J., Wu, S., 2013. Assimilation of MODIS-LAI into the WOFOST model for forecasting regional winter wheat yield. Math. Comput. Model. 58, 634–643. https://doi.org/10.1016/j.mcm.2011.10.038

Ma, H., Huang, J., Zhu, D., Liu, J., Su, W., Zhang, C., Fan, J., 2013. Estimating regional winter wheat yield by assimilation of time series of HJ-1 CCD NDVI into WOFOST-ACRM model with Ensemble Kalman Filter. Math. Comput. Model. 58, 759–770. https://doi.org/10.1016/j.mcm.2012.12.028

Mishra, A.K., Ines, A.V.M., Das, N.N., Prakash Khedun, C., Singh, V.P., Sivakumar, B., Hansen, J.W., 2015. Anatomy of a local-scale drought: Application of assimilated remote sensing products, crop model, and statistical methods to an agricultural drought study. J. Hydrol. 526, 15–29. https://doi.org/10.1016/j.jhydrol.2014.10.038

Morel, J., Todoroff, P., Bégué, A., Bury, A., Martiné, J.F., Petit, M., 2014. Toward a satellite-based system of sugarcane yield estimation and forecasting in smallholder farming

conditions: A case study on reunion island. Remote Sens. 6, 6620–6635. https://doi.org/10.3390/rs6076620

Nearing, G.S., Crow, W.T., Thorp, K.R., Moran, M.S., Reichle, R.H., Gupta, H. V., 2012. Assimilating remote sensing observations of leaf area index and soil moisture for wheat yield estimates: An observing system simulation experiment. Water Resour. Res. 48. https://doi.org/10.1029/2011WR011420

Pauwels, V.R.N., Verhoest, N.E.C., De Lannoy, G.J.M., Guissard, V., Lucau, C., Defourny, P., 2007. Optimization of a coupled hydrology-crop growth model through the assimilation of observed soil moisture and leaf area index values using an ensemble Kalman filter. Water Resour. Res. 43. https://doi.org/10.1029/2006WR004942

Pettorelli, N., 2013. The Normalized Difference Vegetation Index, The Normalized Difference Vegetation Index. https://doi.org/10.1093/acprof:osobl/9780199693160.001.0001.

Ren, J., Liu, X., Chen, Z., Tang, H., 2010. Extracting spatial information of harvest index for winter wheat based on modis NDVI in North China, in: International Geoscience and Remote Sensing Symposium (IGARSS). pp. 2143–2146. https://doi.org/10.1109/IGARSS.2010.5651877

Rowan, T.H., 1990. Functional stability analysis of numerical algorithms. Ph.D. thesis.

Silvestro, P.C., Pignatti, S., Pascucci, S., Yang, H., Li, Z., Yang, G., Huang, W., Casa, R., 2017. Estimating wheat yield in China at the field and district scale from the assimilation of satellite data into the Aquacrop and simple algorithm for yield (SAFY) models. Remote Sens. 9. https://doi.org/10.3390/rs9050509

Tian, L., Li, Z., Huang, J., Wang, L., Su, W., Zhang, C., Liu, J., 2013. Comparison of Two Optimization Algorithms for Estimating Regional Winter Wheat Yield by Integrating MODIS Leaf Area Index and World Food Studies Model. Sens. Lett. 11, 1261–1268. https://doi.org/10.1166/sl.2013.2871

Vazifedoust, M., van Dam, J.C., Bastiaanssen, W.G.M., Feddes, R.A., 2009. Assimilation of satellite data into agrohydrological models to improve crop yield forecasts. Int. J. Remote Sens. 30, 2523–2545. https://doi.org/10.1080/01431160802552769

Wang, H., Zhu, Y., Li, W., Cao, W., Tian, Y., 2014. Integrating remotely sensed leaf area index and leaf nitrogen accumulation with RiceGrow model based on particle swarm optimization algorithm for rice grain yield assessment. J. Appl. Remote Sens. 8, 083674. https://doi.org/10.1117/1.JRS.8.083674

Wang, J., Li, X., Lu, L., Fang, F., 2013. Estimating near future regional corn yields by integrating multi-source observations into a crop growth model. Eur. J. Agron. 49, 126–140. https://doi.org/10.1016/j.eja.2013.03.005

Wu, S., Huang, J., Liu, X., Fan, J., Ma, G., Zou, J., 2012. Assimilating MODIS-LAI into crop growth model with EnKF to predict regional crop yield, in: IFIP Advances in Information and Communication Technology. pp. 410–418. https://doi.org/10.1007/978-3-642-27275-2_46

Xie, Y., Wang, P., Bai, X., Khan, J., Zhang, S., Li, L., Wang, L., 2017. Assimilation of the leaf area index and vegetation temperature condition index for winter wheat yield estimation using Landsat imagery and the CERES-Wheat model. Agric. For. Meteorol. 246, 194–206. https://doi.org/10.1016/j.agrformet.2017.06.015

Yao, F., Tang, Y., Wang, P., Zhang, J., 2015. Estimation of maize yield by using a process-based model and remote sensing data in the Northeast China Plain. Phys. Chem. Earth 87–88, 142–152. https://doi.org/10.1016/j.pce.2015.08.010

Zhao, Y., Chen, S., Shen, S., 2013. Assimilating remote sensing information with crop model using Ensemble Kalman Filter for improving LAI monitoring and yield estimation. Ecol. Modell. 270, 30–42. https://doi.org/10.1016/j.ecolmodel.2013.08.016

Zhuo, W.; Huang, J.; Li, L.; Zhang, X.; Ma, H.; Gao, X.; Huang, H.; Xu, B.; Xiao, X., 2019. Assimilating Soil Moisture Retrieved from Sentinel-1 and Sentinel-2 Data into WOFOST Model to Improve Winter Wheat Yield Estimation. Remote Sens. 11, 1618.

Zhu, X., Zhao, Y., Feng, X., 2013. A methodology for estimating Leaf Area Index by assimilating remote sensing data into crop model based on temporal and spatial knowledge. Chinese Geogr. Sci. 23, 550–561.

Chapter 7

General discussion, conclusions, and perspectives

1. General discussion

1.1. Performance comparison of the proposed yield estimation methods

At present, remote sensing regression, crop growth models, and assimilation methods are widely used for crop yield estimation at different scales, including field, farm, local, regional, country, and global scales (Huang et al., 2019a; Weiss et al., 2020). Establishing an empirical relationship between in situ yield statistics and remotely sensed indicators is a straightforward method of yield estimation (Weiss et al., 2020). Sun et al. (2017) used the cumulative NDVI from TM satellites to estimate grape yields, with relative errors ranging from 10 to 18% and correlations from 0.62 to 0.77. Anastasiou et al. (2018) established regression models between TM satellite-derived GNDVI and table grape yields, showing a coefficient of determination of 0.33. In addition, Rahman et al. (2018) explored the potential of WorldView-3 imagery for estimating the yield of mangoes based on all sampled trees from three orchards in two growing seasons, showing a strong correlation ($R^2 = 0.70$). A mechanistic crop growth model simulates the growth of crops and estimates yield by studying the relationship between crop growth and the environment (Jin et al., 2018). The assimilation approach aims to provide a formal and well-understood yield assessment method by combining the advantages of crop growth models and remote sensing observations (Huang et al., 2019a). In theory, any empirical relationship model involving yield and satellite observation indices can be replaced by assimilating remotely sensed data or major state variables into a mechanistic crop growth model (Weiss et al., 2020). In this thesis, we attempted to test and compare the three kinds of fruit yield estimation methods (six modes) at the field scale for local jujube orchards, including WOFOST simulation without assimilation, remote sensing-based VI regression, phenology-adjusted remote sensing-based VI regression, forcing method, EnKF assimilation, and SUBPLEX assimilation. The comparison of yield estimation performance for the methods is shown in Table 7–1. Although the corrected WOFOST adequately expressed the developmental dynamics of TAGP and LAI in jujube trees in field experiments, the unassimilated WOFOST model exhibits a poor estimation performance for field-scale jujube fruit yield, with a low coefficient of determination (R^2) and a high root mean square error (RMSE). The main reason for this is probably that the calibrated model is based on the field experiments. However, when the calibrated model is used for the yield estimation of different orchards in the local agro-ecological zones, the key input parameters may be uncertain, such as TDWI and SPAN which may be affected by tree age, planting density, and management. This may lead to a large yield simulation error. Research results show that all the assimilation approaches significantly improved the jujube fruit yield estimation compared with the WOFOST model without assimilation. The phenology length from flowering to maturity corrected by the WOFOST model also significantly improved the remote sensing-based yield assessment. Generally, for jujube fruit yield estimation at the field scale in 2017, the best results achieved by the SUBPLEX assimilation method are also confirmed by the indices of agreement and error ($R^2 = 0.78$, RPD = 2.13, NRMSE = 8.3%), followed by the phenology-adjusted remotely sensed NDVI regression method ($R^2 = 0.71$, RPD = 1.86, NRMSE = 9.5%),

and EnKF assimilation (R^2 = 0.66, RPD = 1.73, NRMSE = 10.2%), and finally the forcing method and NDVI regression method without phenological adjustment. If the RPD value is more than 2, then the model has good evaluation ability (Fleming et al., 2017). For all methods, only the SUBPLEX method had a RPD value greater than 2. Therefore, SUBPLEX method may obtain better jujube fruit yield estimation accuracy at the field scale.

Table 7–1: Comparison of yield estimation performance of the methods proposed in the thesis.

Estimation method	Year	R^2	RMSE t ha^{-1}	NRMSE (%)	RPD
Simulation without assimilation	2016	0.22	1.07	16.3	1.13
	2017	0.04	1.33	17.2	1.02
NDVI regression without phenological adjustment	2016	0.35	0.98	14.8	1.23
	2017	0.43	1.02	13.3	1.33
NDVI regression with phenological adjustment	2016	0.64	0.73	11.1	1.66
	2017	0.71	0.73	9.5	1.86
Forcing method	2016	0.62	0.74	11.3	1.63
	2017	0.59	0.87	11.3	1.56
EnKF assimilation	2017	0.66	0.79	10.2	1.73
SUBPLEX assimilation	2017	0.78	0.64	8.3	2.13

Figure 7–1 shows the detailed yield assessment results based on different methods for 181 jujube orchards in 2017, with frequency distributions of relative bias error (RBE, %). The SUBPLEX assimilation method result in relative bias errors that are distributed more centrally around zero compared with other methods. The results also indicate that the yield estimation error based on SUBPLEX and EnKF methods are closer to the uniform distribution. For the other four estimation methods, WOFOST simulation without assimilation, phenology-adjusted remote sensing-based VI regression, and forcing methods overestimate the yields of most jujube orchards; which are not the case for remote sensing-based VI regression.

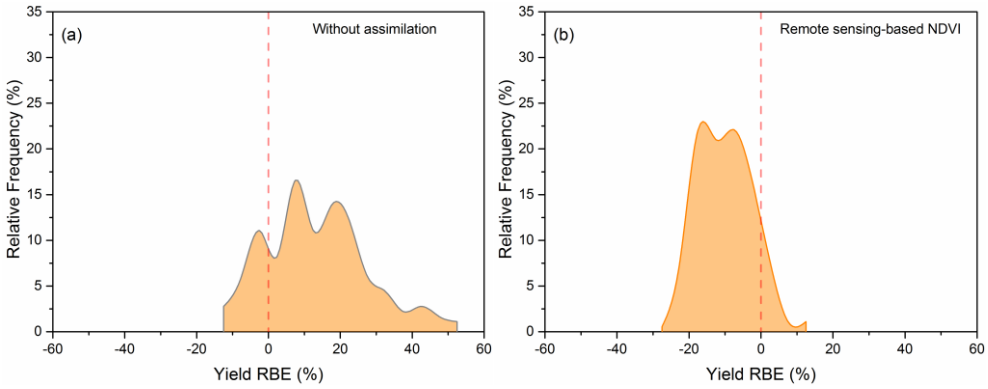

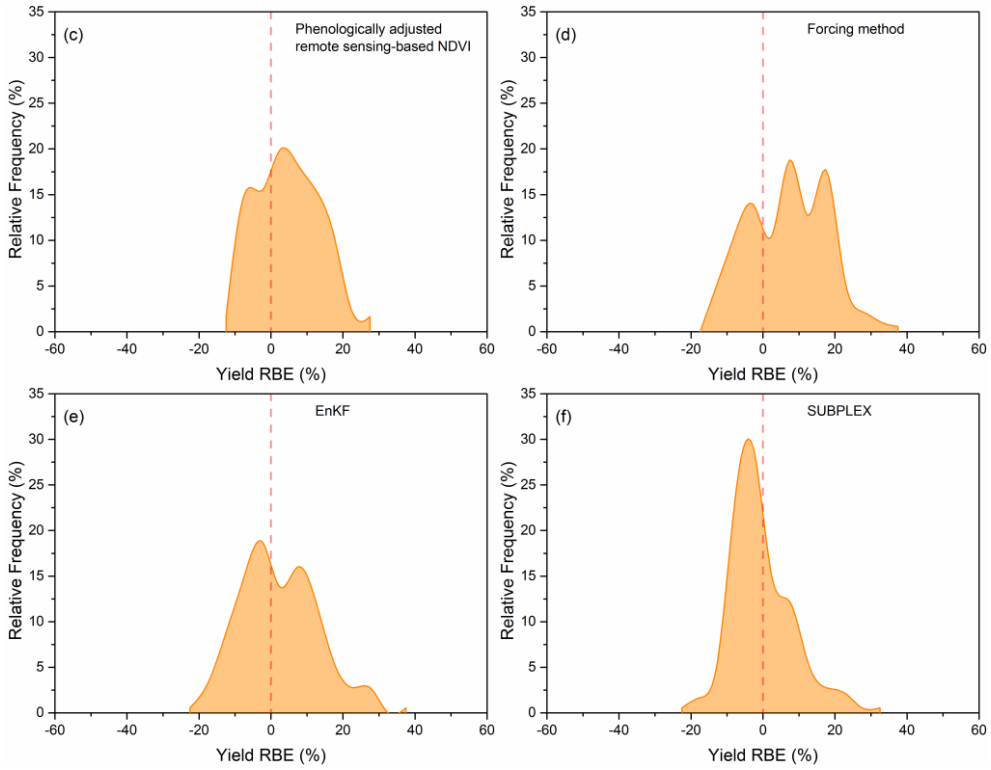

Figure 7–1: Frequency distributions (%) of relative bias error (RBE, %) resulting from different yield estimation methods (2017). Bin size = 5.

1.2. Local-scale jujube fruit yield mapping and significance

The yield variation analysis for local jujube orchards is also an important part of the precision management of these orchards. Based on the proposed method, the jujube fruit yield distribution map of the local agro-ecological zones can be produced (Figure 7–3). The estimated average yield increases from 2016 to 2017, showing the same inter-annual change as the actual yield, this is probably because the jujube fruit yield rose sharply with the increase of tree age. The maps also show that there were annual spatial changes in the different ecological zones. Spatial distribution analysis of jujube fruit yields can help agricultural management departments or fruit farmers to quickly locate low-yield and high-yield areas, and then analyse the causes and economic benefits of yield variation, such as irrigation, fertilization, pruning, and pest control. For yield losses due to orchard management factors, the yield can be increased through technical training and improved management. For some yield declines due to soil structure and characteristics, it may be that these site-specific soils are not suitable for the growth of jujube trees, and it may be a reasonable option to cultivate other jujube varieties or other, more suitable crops to increase economic benefits. Variations in yields may also be caused by meteorological changes. Based on the correlation

analysis of historical meteorological data and yields, the environmental adaptability of tree species can be analysed, and the results can also be used as a reference for screening and cultivating suitable fruit crop varieties. The proposed method combined with higher resolution UAV remote sensing data could be used to assess the yield distribution at a sub-field scale, which would be helpful in improving farm precision management.

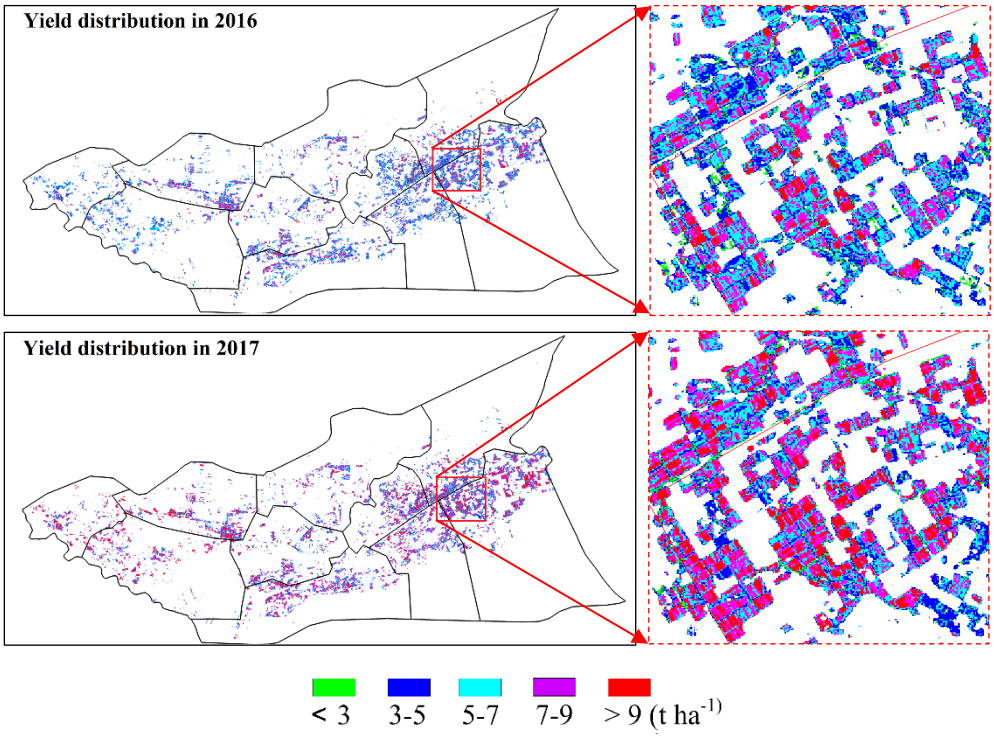

Figure 7–2: Jujube yield mapping for local agro-ecological zones

In addition, local-scale production evaluation is also the basis of regional-scale and national-scale production evaluations. Regional-scale yield estimation has certain reference value for the sale price of jujube fruit and for policy formulation. As mentioned in the introduction section of Chapter 1 (Figure 1−3), the price of jujube fluctuated significantly from 2000 to 2018. The main reason for this may be that the price of jujube fruit is determined by the balance of market supply and demand. According to the classic theory of market economy, if the production of jujube fruit is higher, the supply will be greater, and the price will become lower. Inversely, if its production is lower, the supply becomes smaller, and the price will be higher (Li, 2016). The method proposed in the paper has the potential to be extended to estimate regional-scale jujube fruit yield distributions, which can help government departments to evaluate the distribution of production in different regions. Furthermore, reasonable

price, transportation, and sales strategies will hopefully be formulated to prevent excessive price fluctuations, avoid damaging farmers' enthusiasm and income, and ensure the sustainable development of the jujube industry.

1.3. The limitation of error sources on yield estimation

1.3.1. Uncertainty of input parameters of crop models

When using crop growth models for yield assessment, the uncertainties of input parameters, meteorological driving data, and the simplification of model simulation processes will affect the accuracy of yield estimation (Huang et al., 2019a). In our research, we used local weather station data and the potential growth simulation of the WOFOST model; we did not consider the weather data driving error and the structural error of the model itself and assumed that jujube growth simulations were only affected by the key crop input parameters of WOFOST. Some studies have confirmed that the TDWI parameter strongly influences the initial growth rate of crops and shows a high degree of uncertainty, which can affect the growth rate of the initial LAI and the maximum LAI (de Wit et al., 2012). In this study, tree age mainly affects TDWI. Although SPAN, which determines the rate and timing of leaf senescence, is a characteristic of crop variety, this parameter may be influenced by nitrogen shortage, as well as pests and diseases (Huang et al., 2015), and crop management (de Wit et al., 2012). Yet the WOFOST model cannot simulate the effects of these factors on SPAN (Curnel et al., 2011). Recognizing that tree age and planting density may affect the initial TDWI of jujube trees, and that stress factors and irrigation, fertilization, and pruning management may influence the SPAN value, the effects of these two parameters on the accuracy of the simulated and assimilated yield are mainly considered in our study.

For WOFOST simulation without assimilation, we set a fixed SPAN value which was derived from the calibrated value of the field experiments for different orchards, due to a lack of corresponding local-scale measured data, and set the average TDWI value for the same aged jujube orchards. Results show that the method of inputting the average TDWI for jujube orchards of the same age into the WOFOST model cannot produce optimal simulation accuracy for jujube fruit yields for the 181 orchards, and the uncertainty of inputting TDWI parameters may still be large.

For the remotely sensed VI regression method based on phenological adjustment, we did not correct the simulated TSUM1 parameter (which determines flowering date) due to a lack of accurate observation data from local orchards. In the same situation as TSUM1, the variability of the TSUM2 parameter (which determines the days from flowering to maturity) in different orchards has not been observed and corrected, and the calculated phenotypic deviation may also be introduced into the yield regression model based on remote sensing, thereby influencing the jujube fruit yield estimation accuracy.

For the forcing method, the state variables in the crop model are directly replaced by remotely sensed data (Jin et al., 2018). Tripathy et al. (2013) forced remotely sensed LAI at near to peak vegetative stage into the calibrated WOFOST model to replace simulated LAI to improve wheat yield estimation. The replaced LAI

determined the growth rate of LAI at the next time step. Therefore, it was assumed that the final simulated yield was close to the actual value (Tripathy et al., 2013). We forced different periods of remotely sensed LAI into the WOFOST model and compared the fruit yield estimation accuracy for jujube orchards. Results show that assimilating the LAI from the fruit filling period obtained the highest relative yield estimation accuracy (R2 = 0.59, NRMSE = 11.3%), followed by the early stage of fruit ripening (R2 = 0.54, NRMSE = 11.9%), and the late stage of fruit ripening (R2 = 0.35, NRMSE = 14.1%). LAI during the leaf and shoot development periods show the worst assimilation accuracy, with NRMSE values of 21.6%. The reason for these results may be that jujube fruit yield is highly correlated with the maximum LAI (Yang et al., 2012). Usually, the LAI of the fruit filling and the early ripening periods are closer to the peak vegetative stage, therefore forcing LAI during these periods may result in higher yield estimation accuracy. Existing studies have also shown that the heading LAI has a higher contribution to the improvement of yield estimation accuracy (Huang et al., 2015; Tripathy et al., 2013). Some studies have also confirmed that TSUM1 and TSUM2 may be uncertain at the regional scale (Zhao et al., 2013; Huang et al., 2019b), and the inconsistency of the phenological time of the observed and simulated state variables (phenology shift; Curnel et al., 2011) may lead to a decrease in assimilation accuracy. In practice, the jujube tree age may also affect the actual emergence date, but we did not consider this factor. The deviation of the phenology time between the observed LAI and simulated LAI may also influence the jujube fruit yield estimation accuracy of the forcing method. Therefore, we recommend that when performing forced methods, especially when remote sensing observations are limited, the LAI near the maximum developmental stage is the preferred forcing variable.

For EnKF assimilation, determining and analysing input parameters of the WOFOST model is an important step to improve the accuracy of EnKF assimilation (Huang et al., 2016). Usually, two kinds of methods can be used to generate the ensemble members of simulated LAI, including directly adding a Gaussian perturbation into the modelled LAI (Ma et al., 2013) or adding Gaussian perturbated values to uncertain input parameters (TDWI and SPAN in our research) to simulate the LAI ensemble members (Curnel et al., 2011; de Wit and van Diepen, 2007; Huang et al., 2016). The second method assumes that the uncertainty of crop models comes from the error of key input parameters (Curnel et al., 2011). Referring to existing research results (Curnel et al., 2011; de Wit et al., 2012; Huang et al., 2016) and the characteristics of jujube trees, we assume that the uncertainty of the WOFOST simulation is caused by the input TDWI and SPAN parameters. The two parameters can be treated as Gaussian random variables with the normal distribution centred on the default value (Curnel et al., 2011); in this research we set default values (TDWI = 15 kg ha–1, and SPAN = 50 days), and a standard deviation (5 kg ha–1 for TDWI, 4 days for SPAN). However, the observed TDWI of 55 orchards does not exactly fit the Gaussian distribution, which may also result in a decrease in the assimilation accuracy of EnKF. Assuming that the distribution of SPAN parameters is not a Gaussian distribution, the performance of EnKF may be further reduced. Of course, the spatial distribution of remote sensing observation errors will also affect the

assimilation accuracy of EnKF, which we will cover in the next section. In our research, the difference of phenology time between remotely sensed and modelled LAI (phenology shift) is not considered, which may lead to a decline in assimilation accuracy based on the EnKF strategy (Curnel et al., 2011).

For SUBPLEX assimilation (calibration method), a remotely sensed time series of LAIs were assimilated into the calibrated WOFOST model to correct the key input parameters, here TDWI and SPAN, thereby improving yield estimation. In theory, calibration methods can be used to reduce the accumulation and spread of remote sensing data errors during the assimilation process, which may be better for most applications than updating methods (Jin et al., 2018). Curnel et al. (2011) compared the estimation performance of final grain yields based on a recalibration assimilation method with an EnKF approach. Their results show that a recalibration-based approach is better than EnKF. Our results also indicate that SUBPLEX assimilation provides slightly better jujube fruit yield estimation compared with EnKF. The possible reason for this is that the uncertainty of phenological shift has a greater impact on the assimilation accuracy of the EnKF method than SUBPLEX. In order to test the effect of phenology shift on simulated yield based on SUBPLEX assimilation, the corrected WOFOST model was run for 115 days, 118 days, and 121 days. The results show the estimated yields are 9.039, 9.203, and 9.271 t ha–1, respectively. Obviously, when the phenological time deviation is six days, there is only a relatively small 2.5% yield estimation deviation. The reason may be that the entire simulation curve is shifted overall when phenological time is shifted, so it has little effect on the final estimated yield. The effect of phenological shift on EnKF assimilation was reported by Curnel et al. (2011). For SUBPLEX assimilation, in theory, a larger range of TDWI and SPAN can find a combination of optimal values to ensure that the error of all observed LAIs and simulated LAIs is minimized, but the number of iterations and the computation time is increased. The range of TDWI is derived from the field-measured values of 55 observed orchards. We set an upper limit value for the SPAN parameter (60 days) which is a calibrated value from the potential growth simulation based on field experiments. Considering that this parameter may be affected by various stresses, the SPAN value of different orchards may be lower than the potential value, so we set a possible lower limit of 40 days for 181 orchards. The results show that the corrected TDWIs based on the SUBPLEX assimilation all fall within the range of 5 to 30 kg ha-1, but the SPAN value of 21 orchards may exceed the set SPAN range (Figure 6–9a). The actual SPAN values of the three orchards may be overestimated, while the SPAN of eighteen orchards may be underestimated. We recommend that when performing SUBPLEX assimilation, it is a good choice to increase the SPAN range appropriately so that the corrected SPAN values fall within the actual range. Note that when the SUBPLEX algorithm is run to correct the SPAN parameters, the observed state variables at the end of the growing season are indispensable.

1.3.2. Uncertainty of remotely sensed state variables

The acquisition of remotely sensed vegetation indices or LAI is the basis of remote sensing-based or assimilation methods of yield estimation. Obtaining agronomic variables from remote sensing information largely falls into three categories: pure

empirical methods, mechanistic methods, and contextual methods (Weiss et al., 2020). The empirical method, also known as the regression method, usually applies a calibration empirical relationship to the experimental observations and is therefore limited by the representativeness of the calibration data set. Conditions of acquisition (Epiphanio and Huete, 1995), such as atmospheric conditions, acquisition geometry, crop conditions (Colombo et al., 2003; Gitelson, 2004), and geomorphological context (Matsushita et al., 2007) have an impact on empirical relationships. In addition, the uncertainty associated with remote sensing signals and ground measurements, including the spatial error of the sensor itself and the spatial measurement strategy of the field measurement data, are also considered (Huang et al., 2019a). In our research, these uncertain factors may also be introduced into the remotely sensed NDVI regression method and assimilation process for fruit yield estimation of jujube orchards.

For yield estimation based on NDVI obtained from the Landsat 8 satellite, the number of images available per year is limited due to cloud cover (Whitcraft et al., 2015). It may be difficult to obtain more effective observations for different development stages. Therefore, the best period for determining jujube yield estimation needs to be selected, and this was found to be during the fruit filling period. The phenological length derived from the corrected WOFOST model improved the remote sensing-based yield assessment. However, there is no guarantee that two or more Landsat 8 observations can be obtained during fruit filling periods each year.

For forcing and assimilation methods, the empirical regression model between remotely sensed NDVI and field-measured LAI was fitted to estimate the LAI values of the local orchards, with an error of almost 10%. This error is also accumulated in the assimilation process and reduces the yield estimation accuracy. Empirical methods require a significant amount of time and effort to obtain correction and validation data to establish a good relationship between target agronomic parameters and remote sensing information. Radiative transfer models, such as PROSAIL, are also important methods for obtaining remotely sensed LAI. However, such models require prior knowledge to implement. It is difficult to evaluate which method is better, and different studies have shown that both methods may yield good evaluation results (Jin et al., 2018). The LAI inversion performance of the PROSAIL model for jujube orchards cannot be evaluated due to missing input data that would drive the PROSAIL model. Since our research focuses on local-scale jujube orchards, and the inter-annual variation in local planting structure and spatial heterogeneity is small, using empirical regression models for LAI inversion may also be a good choice.

1.3.3. Uncertainty of assimilation methods

The main goal of this thesis is to develop assimilation methods for the fruit yield assessment of jujube crops at the field scale. Three assimilation methods, including forcing, update (EnKF), and calibration (SUBPLEX) methods, were carried out to reduce the uncertainty of the WOFOST simulation process and to improve yield estimation performance. For forcing methods, the crop model simulation value is directly replaced by the remotely sensed value as a state variable to improve the simulated yield (Yao et al., 2015; Tripathy et al., 2013). The forced method is easy to

operate but, strictly speaking, it does not involve data assimilation methods. If remote sensing can provide high-precision state variables, then good estimates can be obtained (Jin et al., 2018). In our search, a remotely sensed LAI near to maximum leaf development stage was forced into the calibrated WOFOST model to re-simulate the fruit yield for jujube orchards. It is supposed that forcing method may be strongly influenced by the phenological shift. If the phenological shift between the remotely sensed and modelled LAI is large, this approach may have difficulty in obtaining a good estimate. Our research was carried out in a small agro-ecological area (6180 km2) and the phenological bias may not be too large, so an acceptable assessment was obtained. However, when this method is used for regional-scale jujube yield assessment, the phenological development time should be corrected.

For the EnKF method, remotely sensed and simulated LAI errors are assumed to be in accordance with a Gaussian distribution. In our research, the remotely sensed and modelled LAI error may not be completely consistent with a Gaussian distribution, which will also affect the accuracy of yield estimation based on EnKF. Since the time and space of the variances on the modelled LAI and the observed LAI are variable, it is not easy to infer the correct variance. Artificially inflating the observation variance can demonstrate the effect of increased variance on the distribution of normalized innovations (de Wit et al., 2007) and enlarge Kalman gain to reduce the effect of filter divergence (Huang et al., 2016). Phenological shifts (Curnel et al., 2011) are also important factors influencing estimation accuracy.

The SUBPLEX (calibration) method calibrates a set of TDWI and SPAN for each orchard by minimizing the cost function. The relative tolerance for convergence ε is set to the minimum value of the observed and simulated LAI error for all observation points. Although a smaller value of ε may improve the accuracy of assimilation, it may lead to an increase in the number of iterations, which in turn increases the calculation time (Rowan, 1990). The initial step size to compute numerical gradients was artificially set to 0.5 kg ha–1 for TDWI and 1 day for SPAN, respectively. A smaller initial step size may improve the accuracy of yield evaluation, but may also increase the calculation time. In theory, smaller simplex reduction coefficient φ and larger step reduction coefficient ω values can produce smaller objective function values, but the computational time will increase accordingly. The automatic parameter optimization algorithm is also expected to be used to set appropriate SUBPLEX parameters to maintain a balance between assimilation accuracy and computational efficiency. In theory, if there are enough remote sensing observations and the error is small, the calibration method may have high yield estimation accuracy because it can theoretically reduce the accumulation and spread of remote sensing data errors during the assimilation process (Jin et al., 2018). However, the computational efficiency of the calibration method is usually lower than the EnKF assimilation method, and real-time evaluation cannot be achieved (Huang et al., 2019a).

Research results also show that the use of four periods of LAIs yields higher assimilation accuracy than using three periods (Table 6–5). This shows that increasing the number of effective remote sensing observations may improve the accuracy of yield assessment based on the assimilation method. When there are only three

observations, it may be a good choice to assimilate the observations covering major developmental stages.

1.4. Choice of jujube fruit yield estimation methods

In our thesis, both the phenology-adjusted remote sensing-based estimation method (empirical method) and assimilation methods (mechanistic method) achieved fruit yield estimations for jujube orchards with high accuracy. However, just as the limitations of the different methods were analysed above, the application conditions of several proposed methods need to be considered. The advantage of an empirical approach based on remote sensing is its simplicity, but it requires the collection of large amounts of yield and reflectance data, and may lack extrapolation capacity in time and space (Weiss et al., 2020). The purpose of our research is to serve local orchard management. The inter-annual variation of agricultural planting structure and soil structure is very small, so both methods of yield assessment can be considered. However, it should be noted that the proposed methods rely heavily on the number of remote sensing observations. The forcing method is a suitable choice when only a remote sensing image near to the maximum developmental stage is available. Sometimes, in order to perform finer field-scale or sub-field-scale yield analysis, remote sensing satellites with high spatial resolution are required. Since there are usually few remote sensing observations with high-space resolution, the method of forcing a period of remote sensing observation may be suitable. When two satellite images of the main developmental stage are available and apply only to specific regions, the remote sensing-based regression method can be recommended. Although this method lacks a mechanistic description, it is easy to implement and has high operability (Chen et al., 2016). In addition, the regression method without phenological adjustment based on remote sensing has the ability to predict jujube fruit yield three months before harvest. The EnKF (update) and SUBPLEX (calibration) methods can be strongly recommended when multiple remote sensing images from emergence to maturity are available. However, as was found by the results of the above analysis, EnKF may be a suitable choice if the phenological development time is clear, otherwise SUBPLEX may obtain good yield evaluation performance.

As described in Section 2.3 in Chapter 1, other assimilation methods such as PF (Particle Filter), KF (Kalman filter) and 4DVAR (Four-Dimensional Variational Data Assimilation) are often used in remote sensing assimilation. In addition, the Markov Chain Monte Carlo (MCMC) (Gilks et al., 1995) sampling method may have some potential to deal with the uncertainty of the non-Gaussian distribution error in the process of data assimilation (Huang et al., 2019a). A simple decision tree for the selection of data assimilation methods is shown in Figure 7–3. When choosing a data assimilation method, real-time can be used as a first reference. KF, EnKF and PF can be considered as real-time data assimilation methods, which can be extended to within-season estimation (Huang et al., 2019a). Next, whether the observation error is Gaussian can be used as a basis for decision. If observed and simulated errors conform to a Gaussian distribution, EnKF can be preferred under the assumption that the crop model is highly nonlinear. If the crop model is considered to be locally linear, KF may be a good choice. If these errors are not Gaussian, PF may produce a good

estimation performance. 4DVAR, SUBPLEX, and MCMC cannot be considered real-time assimilation methods, and they require consideration of the size of the assimilation time window. For non-sequential assimilation methods, if observed and simulated errors have a Gaussian distribution, 4DVAR and SUBPLEX may be a good choice. If not, MCMC may be a suitable assimilation method. However, MCMC requires more computation time than variational algorithms (Huang et al., 2019a). In conclusion, the selection of assimilation methods should consider factors such as whether they are real-time, the error distribution, phenological shift, and calculation efficiency according to the actual application.

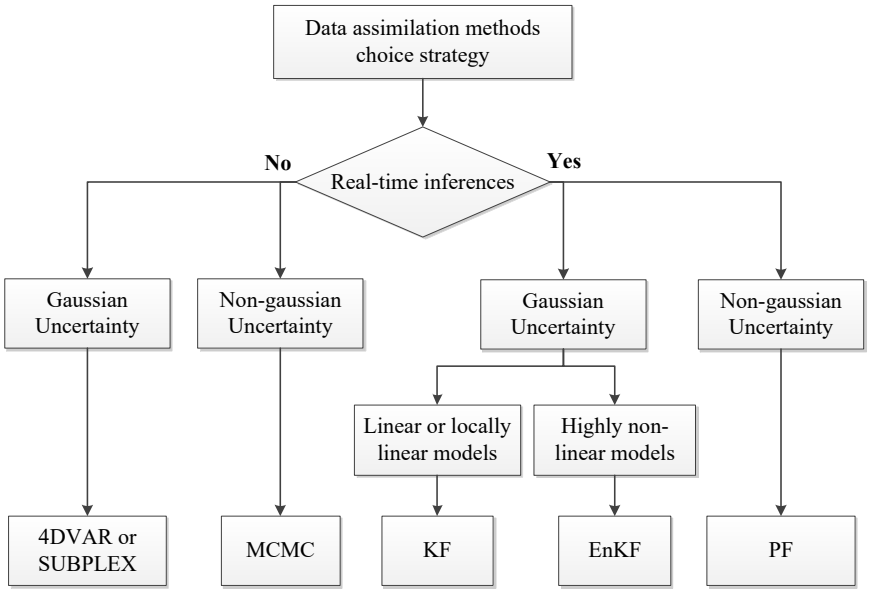

Figure 7–3: Decision tree for the choice of data assimilation methods

2. General conclusions

This study shows that the WOFOST model has potential for use in growth simulation and yield assessment of perennial jujube trees. The results also support that data assimilation technology is a feasible and effective means to realize the coupling of a crop growth model and remote sensing information for jujube fruit yield estimation. The remote sensing assimilation method shows a slightly higher accuracy of jujube fruit yield assessment than the regression method based on the remote sensing vegetation index.

- The jujube growth simulation based on a calibrated WOFOST model was successfully established based on crop, soil, and climatic data measured in field experiments. Note that the growth simulation of fruit trees should consider the tree age, which is one of the key factors in precision simulation. Results show that the calibrated model can not only accurately simulate the biomass of different organs but

also reliably present a number of phenological development stages and superior climate change response under its potential condition. However, the uncertainty of the input parameters of the model affects the accuracy of the yield estimation when the model is applied to different orchards. In the study, although a method that set the fixed (average) TDWI for the same aged jujube orchards was designed to reduce its uncertainty, the estimation error is still large. When using a calibrated WOFOST model at the local scale, this uncertainty should be improved to obtain accurate estimations for jujube fruit yields.

- Remote sensing-based empirical statistical methods can also be considered as a convenient and easy-to-use method of jujube fruit yield assessment. Crop yields are correlated with phenology information, especially the fruit filling days. Therefore, the research also explored an approach using the phenological length of jujube growth to improve remotely sensed estimates of inter-annual variability for jujube fruit yields. Based on the remotely sensed estimation method, the best time for determining jujube yield estimation was found to be during the fruit filling period. The average NDVI for 14th and 15th half-months represents a better performance for yield estimation than other vegetation indices and modelling time, with a higher R2 and lower NRMSE. The potential of integrating the phenology length with Landsat-NDVI for jujube yield estimation was proved, showing a well validated R2 for the two growth seasons. The proposed method may show better performance between years when the fruit filling days differ greatly compared to directly using a remotely sensed VI regression method, which was verified to fit well to jujube yield estimation and mapping one and half months before harvest.
- The remote sensing assimilation method may be more promising for jujube fruit yield assessment. Remote sensing can provide state variables to link crop growth simulations, and has been widely employed to reduce the uncertainty of crop growth models. For jujube trees, the input parameters of the growth simulation may not only be uncertain at local or regional scales, but the uncertainty of tree age and planting density may exist at the field-scale for jujube orchards. In this study, the yield modelling accuracy is enhanced by forcing a single remotely sensed LAI at near to the maximum vegetative development periods from Landsat 8 data into the calibrated WOFOST model. More importantly, the development of a new remote sensing assimilation framework based on the SUBPLEX algorithm obtained better estimation performance than the commonly used EnKF method.
- To summarize, the regression model established directly using the remote sensing vegetation index has the ability of predicting jujube fruit yield three months before harvest. Furthermore, the remote sensing regression method can easily realize the prediction of jujube fruit yield at local and regional scales, which may be beneficial for predicting the price of jujube fruit, formulating transportation and sales strategies to prevent excessive price fluctuations and ensure the sustainable development of the jujube industry. Three yield estimation methods integrated with remote sensing information and a calibrated WOFOST, including forcing, EnKF and SUBPLEX, achieve good performance compared to the simulation without assimilation. In practice, the selection of jujube fruit yield estimation methods is recommended to refer to the number of remote sensing observations, error distribution

and real-time requirements. When only one fruit-filling period of remote sensing observation data is available, the forcing method can be used to improve the simulation state of the model. EnKF and SUBPLEX methods require more remote sensing observations and assume that the observed and simulated errors conforms to the Gaussian distribution. Note that both methods cannot improve the difficulty of non-Gaussian distribution of observed and simulated errors in the assimilation process. Although, the SUBPLEX method exhibits better performance and stability for yield estimation compared to EnKF in this study because the accuracy of the EnKF method is susceptible to phenological shifts, the EnKF assimilation method after phenology time calibration can be recommended for real-time growth monitoring and biomass assessment during the growing season to improve jujube orchard management.

3. Perspectives

3.1. Improvement of jujube fruit yield estimation

For field management of fruit crops, field-scale yield mapping provides benefits for improving agriculture management, such as irrigation, fertilization, pests and disease control, and tree shape pruning strategies. In particular, to target precision farm management, mapping the variation in the field yield can help farmers to find causes of low production. Assimilation technology will play an important role in the operation of fruit yield estimation in agricultural regions, contributing to sustainable agricultural development. In order to further improve the accuracy of jujube fruit yield assessment, the following aspects are worthy of in-depth study:

- Advances in crop growth models: Recently, several model extensions have been implemented to consider crop nutrient dynamics, crop response to critical temperatures (cold and hot), and crop CO_2 assimilation in response to changes in environmental CO_2 levels. Some of these improvements are based on existing methods that have been tested in other models (such as NWHEAT or LINTUL), while others are based on recent developments in international coordination activities, such as the Agricultural Model Intercomparison and Improvement Project (AgMIP; Rosenzweig et al., 2013) and the European MACSUR initiative (Modelling European Agriculture with Climate Change for Food Security). Improvements in the basic theory and process of these models are expected to enhance the simulation mechanism and improve jujube yield estimation accuracy. In addition to the approach proposed in this thesis, an integrated mature nutrient module and water balance module can be expected to further realize the analysis and quantification of jujube water and fertilizer nutrient requirements throughout the growing season, and then guide precision irrigation and precise fertilization.
- Improvement of model input parameter uncertainty: In this thesis, it is supposed that assimilation error comes from the uncertainty of remotely sensed error and key input parameters (TDWI and SPAN). The phenological shift error should be considered which may be affected by factors such as jujube tree varieties and tree age. In future research, the combination of Landsat and Sentinel-2 satellite data is expected to obtain more remote sensing observation information during the main growing season to further correct some key model input parameters, such as TDWI, SPAN,

TSUMEM, and TSUM1, thereby improving the accuracy of jujube fruit yield assessment. In addition, the optimization and correction of CO_2 assimilation parameters and SLATB, which are highly correlated with the jujube tree growth and leaf area index, will also be expected to improve the assimilation accuracy of jujube fruit yield.

- Optimization of remotely sensed state variables: Remote sensing technology is the most promising way to assimilate canopy state variables into crop models and further improve crop yield estimation and management (Jin et al., 2018). The types of satellite data providing remote sensing of terrestrial resources are increasing, and the quality of data has been continuously improved, which strongly supports the research and application of agricultural remote sensing, including the use of Gaofen-1 and Sentinel-2 satellites (Weiss et al., 2020). Due to the characteristics of agriculture itself, aerial remote sensing based on manned aircraft and drones will be an important part of agricultural remote sensing data acquisition. The new Internet of Things based on mobile platforms such as fixed platforms, vehicles, and human-based intelligent terminals will be an important part of agricultural remote sensing data acquisition (Chen et al., 2016). The combination of satellite, aerospace, and ground integrated remote sensing data acquisition systems are expected to achieve more accurate regional, field-scale, and sub field-scale yield estimation. For large-scale jujube yield estimation, the combination of a time series of MODIS and Landsat/Sentinel data based on the proposed methods is worth exploring. For the field scale of local scale yield estimation, the integration of free medium and high spatial resolution satellite data is also expected to improve estimation accuracy, such as Sentinel-1 and 2, Landsat 8, and Gaofen. In addition, high spatial resolution satellites or UAV remote sensing data have the potential to monitor growth information and estimate yield at the sub-field scale. It is worth noting that Sentinel-2 can provide information on chlorophyll concentration, which hopefully can be linked to photosynthetic activity (Croft et al., 2017; Delloye et al., 2018). How to link this information with the simulation process of crop growth models, such as the carbon dioxide assimilation process, is worthy of further exploration.
- Improvement of assimilation methods: A large number of research experiments propose that the combination of variational and filtering algorithms can effectively improve assimilation results, which is an important direction for the research and development of assimilation algorithms (Poterjoy and Zhang, 2014; Zhang et al., 2012, 2009). The MCMC method may be a promising method to reduce the uncertainty of observation error in the assimilation process. These methods are expected to improve the accuracy of jujube fruit yield assessment.

3.2. Construction of regional assimilation systems

The assimilation system is a coupling of crop remote sensing parameters, crop models, and assimilation algorithms. The basic links involved in the application of an assimilation system include a database of regional crops, remote sensing and crop model driving parameters, assimilation algorithm modularization, assimilation result analysis, and ground verification. The following research priorities present some ideas for the construction and operation of crop model assimilation systems.

- Remote sensing plays a decisive role in obtaining the key state variables of crop canopies. An empirical statistical model is a commonly used inversion method for crop canopy state variables (Durbha et al., 2007; Foca et al., 2009; Jin et al., 2013; Huang et al., 2015, 2016). An accurate quantitative description of state variables requires consideration of the sun angle, leaf area density, and leaf angular space distribution, and must have a sufficient number of samples (Curran and Williamson, 1986). Therefore, many scholars have used physical optics to perform inversion studies of canopy state variables (Daughtry et al., 2000; Eitel et al., 2007; Haboudane et al., 2002; Li et al., 2015). The established model needs to be validated according to different application environments and regions. In summary, the quality of regional crop state variables is one of the key factors affecting the results of data assimilation. Therefore, the primary task of establishing a regional crop model assimilation system is to produce and establish a regional crop or state parameters database. This involves a whole set of crop parameters, remote sensing inversion techniques, programs, ground verification, and database establishment.
- It is important to establish and improve the driving database of crop models for the assimilation system. Parameter data such as meteorology, soil, crop varieties, and field management are the basic driving data of the crop model assimilation system (de Wit et al., 2019b). At present, regional meteorological data are obtained by field data interpolation. When the distribution density of meteorological stations is low, the meteorological parameter data obtained by regional interpolation often has large uncertainties, and the results obtained by different interpolation methods often have large differences (Huang et al., 2015). Due to the complexity of the natural environment, soil parameters vary widely in spatial characteristics (spatial heterogeneity) (Jin et al., 2018). Large-scale regional soil parameter data often does not meet the accuracy needs of crop models for assimilation systems. There is an urgent and critical need to establish a more granular regional or local soil parameter database and sharing mechanism for assimilation systems. Differences in data areas such as crop varieties and field management strategies are important factors influencing the results of the estimation. The establishment and improvement of these databases is the basic premise and primary task of the application of the assimilation system.
- It is beneficial for assimilation systems to develop crop growth models based on the results of existing crop models. The existing frameworks, parameterization, and mechanisms of various crop models have their own characteristics. They are usually single-point models. Many crop models have been developed based on the assumption of uniform field growth. However, some limiting factors are likely to occur during the growth process, so the external conditions are beyond the boundaries of the model. Errors from the crop model itself affect the estimation accuracy of LAI, biomass, and yield during region-scale data assimilation (Jin et al., 2018). In the application of regional expansion, the impact of regional terrain, climate, hydrology and other conditions on the agro-ecological environment is not considered. Therefore, it is promising to couple mature regional climate, hydrology, and other models with crop models to improve the regional adaptability of crop models. In addition, it could be worthwhile to combine these models with a remote sensing optical model to realize

the conversion of state variables and spectral reflectance, so that the coupling of the crop model and remote sensing information becomes simpler.

- Research and development of practical and efficient assimilation algorithms needs to be enhanced. In terms of operational applications for the regional scale, the assimilation algorithm should not only fully consider the observations, the initial conditions of the model, and the uncertainty in the simulation process, but also improve the accuracy of the assimilation results. Importantly, it should have higher computational efficiency because it may need to assimilate a large number of observations (Jin et al., 2018).

In short, assimilation technology is an effective means of crop growth monitoring and yield estimation, and has significant application prospects. However, the construction of mature and feasible business systems requires a lot of infrastructure and technical research; such a complex integrated system requires more research workers and departments to coordinate and cooperate.

4. References

Anastasiou E., Balafoutis A., Darra N., Fountas S., Xanthopoulos G., Psiroukis V. and Biniari A., 2018. Satellite and proximal sensing to estimate the yield and quality of table grapes, Agriculture. 8, 94.

Chen, Z., Ren, J., Tang, H., Shi, Y., Leng, P., Liu, J., Wang, L., Wu, W., Yao, Y., Hasiyuya, 2016. Progress and perspectives on agricultural remote sensing research and applications in China. Yaogan Xuebao/Journal Remote Sens. 20, 748–767. https://doi.org/10.11834/jrs.20166214

Colombo, R., Bellingeri, D., Fasolini, D., Marino, C.M., 2003. Retrieval of leaf area index in different vegetation types using high resolution satellite data. Remote Sens. Environ. 86, 120–131. https://doi.org/10.1016/S0034-4257(03)00094-4

Croft, H., Chen, J.M., Luo, X., Bartlett, P., Chen, B., Staebler, R.M., 2017. Leaf chlorophyll content as a proxy for leaf photosynthetic capacity. Glob. Chang. Biol. 23, 3513–3524. https://doi.org/10.1111/gcb.13599

Crow , W.T., Wood, E.F., 2003. The assimilation of remotely sensed soil brightness temperature imagery into a land surface model using Ensemble Kalman filtering: A case study based on ESTAR measurements during SGP97. Adv. Water Resour. 26, 137–149. https://doi.org/10.1016/S0309-1708(02)00088-X

Curran, P.J., Williamson, H.D., 1986. Sample size for ground and remotely sensed data. Remote Sens. Environ. 20, 31–41. https://doi.org/10.1016/0034-4257(86)90012-X

Curnel, Y., de Wit, A.J.W., Duveiller, G., Defourny, P., 2011. Potential performances of remotely sensed LAI assimilation in WOFOST model based on an OSS Experiment. Agric. For. Meteorol. 151, 1843–1855. https://doi.org/10.1016/j.agrformet.2011.08.002

Daughtry, C.S.T., Walthall, C.L., Kim, M.S., De Colstoun, E.B., McMurtrey, J.E., 2000. Estimating corn leaf chlorophyll concentration from leaf and canopy reflectance. Remote Sens. Environ. 74, 229–239. https://doi.org/10.1016/S0034-4257(00)00113-9

de Wit, A., Boogaard, H., Fumagalli, D., Janssen, S., Knapen, R., van Kraalingen, D., Supit, I., van der Wijngaart, R., van Diepen, K., 2019a. 25 years of the WOFOST cropping systems model. Agric. Syst. 168, 154–167. https://doi.org/10.1016/j.agsy.2018.06.018

de Wit, A., Boogaard, H., and Supit I. 2019b. System description of the WOFOST 7.2cropping system model. Wageningen Environmental Research. September, 2019

de Wit, A., Duveiller, G., Defourny, P., 2012. Estimating regional winter wheat yield with WOFOST through the assimilation of green area index retrieved from MODIS observations. Agric. For. Meteorol. 164, 39–52. https://doi.org/10.1016/j.agrformet.2012.04.011

de Wit, A.J.W., van Diepen, C.A., 2007. Crop model data assimilation with the Ensemble Kalman filter for improving regional crop yield forecasts. Agric. For. Meteorol. 146, 38–56. https://doi.org/10.1016/j.agrformet.2007.05.004

Delloye, C., Weiss, M., Defourny, P., 2018. Retrieval of the canopy chlorophyll content from Sentinel-2 spectral bands to estimate nitrogen uptake in intensive winter wheat cropping systems. Remote Sens. Environ. 216, 245–261. https://doi.org/10.1016/j.rse.2018.06.037

Durbha, S.S., King, R.L., Younan, N.H., 2007. Support vector machines regression for retrieval of leaf area index from multiangle imaging spectroradiometer. Remote Sens. Environ. 107, 348–361. https://doi.org/10.1016/j.rse.2006.09.031

Eitel, J.U.H., Long, D.S., Gessler, P.E., Smith, A.M.S., 2007. Using in-situ measurements to evaluate the new RapidEye^{TM} satellite series for prediction of wheat nitrogen status. Int. J. Remote Sens. 28, 4183–4190. https://doi.org/10.1080/01431160701422213

Epiphanio, J.C.N., Huete, A.R., 1995. Dependence of NDVI and SAVI on sun/sensor geometry and its effect on fAPAR relationships in Alfalfa. Remote Sens. Environ. 51, 351–360. https://doi.org/10.1016/0034-4257(94)00110-9

Fleming, A., Schenkel, F.S., Chen, J., Malchiodi, F., Bonfatti, V., Ali, R.A., Mallard, B., Corredig, M., Miglior, F., 2017. Prediction of milk fatty acid content with mid-infrared spectroscopy in Canadian dairy cattle using differently distributed model development sets. J. Dairy Sci. 100, 5073–5081. https://doi.org/10.3168/jds.2016-12102

Foca, G., Cocchi, M., Vigni, M.L., Caramanico, R., Corbellini, M., Ulrici, A., 2009. Different feature selection strategies in the wavelet domain applied to NIR-based quality classification models of bread wheat flours. Chemom. Intell. Lab. Syst. 99, 91–100. https://doi.org/10.1016/j.chemolab.2009.07.013

Gitelson, A.A., 2004. Wide Dynamic Range Vegetation Index for Remote Quantification of Biophysical Characteristics of Vegetation. J. Plant Physiol. 161, 165–173. https://doi.org/10.1078/0176-1617-01176

Gilks, S. Richardson, D. Spiegelhalter, 1995. Markov chain Monte Carlo in Practice.CRC Press (December 1995). http://refhub.elsevier.com/S0168-1923(19)30217-5/sbref0295

Haboudane, D., Miller, J.R., Tremblay, N., Zarco-Tejada, P.J., Dextraze, L., 2002. Integrated narrow-band vegetation indices for prediction of crop chlorophyll content for application to precision agriculture. Remote Sens. Environ. 81, 416–426. https://doi.org/10.1016/S0034-4257(02)00018-4

Huang, J., Sedano, F., Huang, Y., Ma, H., Li, X., Liang, S., Tian, L., Zhang, X., Fan, J., Wu, W., 2016. Assimilating a synthetic Kalman filter leaf area index series into the WOFOST model to improve regional winter wheat yield estimation. Agric. For. Meteorol. 216, 188–202. https://doi.org/10.1016/j.agrformet.2015.10.013

Huang, J., Tian, L., Liang, S., Ma, H., Becker-Reshef, I., Huang, Y., Su, W., Zhang, X., Zhu, D., Wu, W., 2015. Improving winter wheat yield estimation by assimilation of the leaf

area index from Landsat TM and MODIS data into the WOFOST model. Agric. For. Meteorol. 204, 106–121. https://doi.org/10.1016/j.agrformet.2015.02.001

Huang, J., Sedano, F., Huang, Y., Ma, H., Li, X., Liang, S., Tian, L., Zhang, X., Fan, J., Wu, W., 2016. Assimilating a synthetic Kalman filter leaf area index series into the WOFOST model to improve regional winter wheat yield estimation. Agric. For. Meteorol. 216, 188–202. https://doi.org/10.1016/j.agrformet.2015.10.013

Huang, J., Gómez-Dans, J.L., Huang, H., Ma, H., Wu, Q., Lewis, P.E., Liang, S., Chen, Z., Xue, J.H., Wu, Y., Zhao, F., Wang, J., Xie, X., 2019a. Assimilation of remote sensing into crop growth models: Current status and perspectives. Agric. For. Meteorol. 276–277, 107609. https://doi.org/10.1016/j.agrformet.2019.06.008

Huang, J., Ma, H., Sedano, F., Lewis, P., Liang, S., Wu, Q., Su, W., Zhang, X., Zhu, D., 2019b. Evaluation of regional estimates of winter wheat yield by assimilating three remotely sensed reflectance datasets into the coupled WOFOST–PROSAIL model. Eur. J. Agron. 102, 1–13. https://doi.org/10.1016/j.eja.2018.10.008

Jin, X., Kumar, L., Li, Z., Feng, H., Xu, X., Yang, G., Wang, J., 2018. A review of data assimilation of remote sensing and crop models. Eur. J. Agron. https://doi.org/10.1016/j.eja.2017.11.002

Jin, X., Xu, X., Song, X., Li, Z., Wang, J., Guo, W., 2013. Estimation of leaf water content in winter wheat using grey relational analysis-partial least squares modelling with hyperspectral data. Agron. J. 105, 1385–1392. https://doi.org/10.2134/agronj2013.0088

Li, F. 2016. Research on the price formation mechanism of Jujube, China. Ph.d thesis. (In Chinese with english abstract)

Li, Z., Jin, X., Wang, J., Yang, G., Nie, C., Xu, X., Feng, H., 2015. Estimating winter wheat (Triticum aestivum) LAI and leaf chlorophyll content from canopy reflectance data by integrating agronomic prior knowledge with the PROSAIL model. Int. J. Remote Sens. 36, 2634–2653. https://doi.org/10.1080/01431161.2015.1041176

Ma, H., Huang, J., Zhu, D., Liu, J., Su, W., Zhang, C., Fan, J., 2013. Estimating regional winter wheat yield by assimilation of time series of HJ-1 CCD NDVI into WOFOST-ACRM model with Ensemble Kalman Filter. Math. Comput. Model. 58, 759–770. https://doi.org/10.1016/j.mcm.2012.12.028

Matsushita, B., Yang, W., Chen, J., Onda, Y., Qiu, G., 2007. Sensitivity of the Enhanced Vegetation Index (EVI) and Normalized Difference Vegetation Index (NDVI) to topographic effects: A case study in high-density cypress forest. Sensors 7, 2636–2651. https://doi.org/10.3390/s7112636

Poterjoy, J., Zhang, F., 2014. Intercomparison and Coupling of Ensemble and Four-Dimensional Variational Data Assimilation Methods for the Analysis and Forecasting of Hurricane Karl (2010). Mon. Weather Rev. 142, 3347–3364. https://doi.org/10.1175/mwr-d-13-00394.1

Rahman M.M., Robson A. and Bristow M., 2018. Exploring the potential of high resolution worldview-3 Imagery for estimating yield of mango, Remote Sens. 10, 12.

Rowan, T.H., 1990. Functional stability analysis of numerical algorithms. Ph.D. thesis.

Rosenzweig, C., Jones, J.W., Hatfield, J.L., Ruane, A.C., Boote, K.J., Thorburn, P., Antle, J.M., Nelson, G.C., Porter, C., Janssen, S., Asseng, S., Basso, B., Ewert, F., Wallach, D., Baigorria, G., Winter, J.M., 2013. The Agricultural Model Intercomparison and

Improvement Project (AgMIP): Protocols and pilot studies. Agric. For. Meteorol. 170, 166–182. https://doi.org/10.1016/j.agrformet.2012.09.011

Sun L., Gao F., Anderson M.C., Kustas W.P., Alsina M.M., Sanchez L., Sams B., McKee L., Dulaney W., White W.A., et al., 2017. Daily mapping of 30 m LAI and NDVI for grape yield prediction in California vineyards, Remote Sens. 9, 4.

Tripathy, R., Chaudhari, K.N., Mukherjee, J., Ray, S.S., Patel, N.K., Panigrahy, S., Singh Parihar, J., 2013. Forecasting wheat yield in Punjab state of India by combining crop simulation model WOFOST and remotely sensed inputs. Remote Sens. Lett. 4, 19–28. https://doi.org/10.1080/2150704X.2012.683117

Weiss, M., Jaco, F., Duveiller, G., 2020. Remote sensing for agricultural applications: A meta-review. Remote Sensing of Environment, 236, 111402. https://doi.org/10.1016/j.rse.2019.111402

Whitcraft, A.K., Vermote, E.F., Becker-Reshef, I., Justice, C.O., 2015. Cloud cover throughout the agricultural growing season: Impacts on passive optical earth observations. Remote Sens. Environ. 156, 438–447. https://doi.org/10.1016/j.rse.2014.10.009

Yang, W., Gao, J., Xu, C., 2012. The correlation analysis of leaf area index and yield of red jujube. Xinjiang Agricultural Sciences, 49, 1397-1400. (In Chinese with English abstract)

Yao, F., Tang, Y., Wang, P., Zhang, J., 2015. Estimation of maize yield by using a process-based model and remote sensing data in the Northeast China Plain. Phys. Chem. Earth 87–88, 142–152. https://doi.org/10.1016/j.pce.2015.08.010

Zhang, F., Zhang, M., Hansen, J.A., 2009. Coupling ensemble Kalman filter with four-dimensional variational data assimilation. Adv. Atmos. Sci. 26, 1–8. https://doi.org/10.1007/s00376-009-0001-8

Zhang, F., Zhang, M., Poterjoy, J., 2012. E3DVar: Coupling an Ensemble Kalman Filter with Three-Dimensional Variational Data Assimilation in a Limited-Area Weather Prediction Model and Comparison to E4DVar. Mon. Weather Rev. 141, 900–917. https://doi.org/10.1175/mwr-d-12-00075.1

Zhao, Y., Chen, S., Shen, S., 2013. Assimilating remote sensing information with crop model using Ensemble Kalman Filter for improving LAI monitoring and yield estimation. Ecol. Modell. 270, 30–42. https://doi.org/10.1016/j.ecolmodel.2013.08.016

Author's publications related to this thesis

1. **Tiecheng Bai**, Tao Wang, Nannan Zhang, Youqi Chen * and Benoit Mercatoris *. 2020. Growth simulation and yield prediction for perennial jujube fruit tree by integrating age into the WOFOST model. *Journal of Integrative Agriculture.* 19(3): 721-734. https://doi.org/10.1016/S2095-3119(19)62753-X
2. **Tiecheng Bai**, Zhang Nannan, Benoit Mercatoris*, Youqi Chen *. 2019. Jujube yield prediction method combining Landsat 8 Vegetation Index and the phenological length. *Computers and Electronics in Agriculture*. 162: 1011-1027. https://doi.org/10.1016/j.compag.2019.05.035
3. **Tiecheng Bai**, Nannan Zhang, Benoit Mercatoris* and Youqi Chen*. 2019. Improving Jujube Fruit Tree Yield Estimation at the Field Scale by Assimilating a Single Landsat Remotely-Sensed LAI into the WOFOST Model. *Remote sensing*. 11(9), 1119. https://doi.org/10.3390/rs11091119
4. **Tiecheng Bai,** Shanggui Wang, Wenbo Meng, Nannan Zhang, Tao Wang, Youqi Chen and Benoit Mercatoris*. 2019. Assimilation of Remotely-Sensed LAI into WOFOST Model with the SUBPLEX Algorithm for Improving the Field-Scale Jujube Yield Forecasts. *Remote Sensing.* 11(16), 1945. https://doi.org/10.3390/rs11161945